AN INVESTIGATION OF THE INITIAL STAGES OF THE DEPOSITION OF LEAD AND THALLIUM ON SILVER CATHODES

A Thesis submitted for the degree of

Doctor of Philosophy

in the University of Southampton.

By Brian Thomas B.Sc.

October 1976

CONTENTS

UNIVERSITY OF SOUTHAMPTON

ABSTRACT

FACULTY OF SCIENCE

CHEMISTRY

Doctor of Philosophy

AN INVESTIGATION OF THE INITIAL STAGES OF THE DEPOSITION OF LEAD AND THALLIUM ON SILVER CATHODES

by Brian Thomas

The underpotential deposition of lead and thallium monolayers onto polycrystalline and single crystal silver electrodes has been investigated with conventional electrochemical and reflectance spectroscopic techniques.

Careful chemical polishing of the electrode surfaces was necessary to remove the distorted layer left by alumina polishing.

The voltammetry behaviour of the polycrystalline electrode was shown to be a composite of the various single crystal structures in its surface. In the thallium system, it was possible to form two monolayers at an underpotential but only one in the lead system. In the absence of significant anion adsorption, the monolayer deposition process was dependent on the orientation of the substrate and consisted of two stages; an initial adsorption process in which the favourable, high co-ordination, sites on the electrode were occupied, followed by a phase transformation and crystal growth process until a complete layer was formed.

With the majority of common anions, diffusion processes prior to lattice incorporation were the slowest step in the crystal growth process. With lead deposition from a citrate complex the electron transfer/lattice incorporation step was sufficiently slow to obtain direct evidence for the participation of two-dimensional nucleation steps in the monolayer formation.

The first monolayer of thallium and the single monolayer of lead was shown to be a close packed layer in all cases, distorted to an extent depending on the substrate structure. In the case of thallium, these distortion effects were also seen in the formation of the second layer.

The effect of anion adsorption in both systems was investigated and shown to be an important factor in determining the nature of the deposition characteristics. Lead monolayers on the {110} substrate could catalytically decompose perchloric acid electrolytes to a product which markedly reduced the rate of the lattice incorporation step in subsequent deposition.

The overpotential deposition of lead was investigated on the same substrates. Monolayer formation was an essential precursor to thicker deposits. The effects of substrate orientation were still important in determining the growth kinetics of the bulk deposit. In nucleation pre-pulse experiments, evidence for nuclei orientation effects was obtained.

ACKNOWLEDGEMENTS.

I would like to thank the following:

My supervisor, Dr. A. Bewick, for the benefit of his knowledge and experience.

Kodak Ltd. for the award of a European Fellowship and Professors Hills and Fleischmann for instituting the scheme.

My friends, both in the laboratory and outside, for constant encouragement, advice and kindness.

CHAPTER ONE: METAL DEPOSITION.

1.0 INTRODUCTION.

The majority of the work described in this Thesis is concerned with the underpotential deposition of metals, i.e. deposition occurring at more positive potentials than that of the deposited metal/metal ion electrode. The widespread belief that such processes were adsorption phenomena has resulted in few attempts being made to relate them to the relatively familiar events occurring in overpotential deposition and consequently surveys of earlier work in the two areas must be treated separately.

This chapter presents a brief review of the principal conclusions derived from studies of the initial stages of overpotential metal deposition in the present century.

1.1 EARLY CONCEPTS.

To the extent that Faraday's[1] early studies relating the quantity of charge passed to the amount of metal deposited can be regarded as metal deposition, this area constitutes one of the oldest areas of experimental electrochemistry.

The earliest ideas relating to the growth of crystals (e.g. metals and salts) were concerned with a 2-dimensional nucleation, layer by layer growth mechanism suggested by Kossel[2] and developed by Stranski[3] (1927). In this theory an ideal crystal face grows by the formation of 2-dimensional nuclei which are not stable unless they have a certain critical size, related in an inverse manner to the supersaturation (overvoltage). Nucleation is followed by expansion of the nucleus over the entire face, by incorporation of atoms at the peripheral growth steps. The growth of a second plane cannot occur until a fresh nucleus is formed and consequently the deposit is built up from layer upon layer of 2-dimensional crystal planes each formed from a single nucleus. The nucleation probability involves an activation energy governed by the work of formation which is inversely proportional to the supersaturation. This

implies that growth becomes insignificant below a certain supersaturation which is about 50%. The Kossel-Stranski model assumed that charge transfer between electrode and ion took place on a plane site followed by the surface diffusion of the resulting 'ad-atom' to the growing centre where incorporation at a high co-ordination site (e.g. a kink site) could occur. The role of surface diffusion as a rate-determining step in electro-deposition was emphasized by Brandes[4] (1929), however Erdey-Gruz and Volmer[5] (1931) deduced an equation relating current density to over-potential with the assumption that 2-dimensional layer formation was rate determining. These workers advocated the direct discharge of an ion at a growing centre rather than on a plane site.

Subsequent experiments[6] revealed growth rates in many systems at supersaturations well below those expected to produce nucleation (25-50%) in divergence with the classical theory of crystal growth and a new mechanism was sought to explain these results. Burton, Cabrera and Frank[7] introduced the concept of emergent screw dislocations (1949) into the model for crystal growth and it was shown that self-perpetuating steps resulting from such dislocations could account for growth at low super-saturations. This would obviate the necessity for nucleation in such systems provided that the dislocation density was not too low or the deposition current density too high. Soon after, Steinberg[8] observed growth spirals on electro-deposited titanium and subsequently many examples were found and this was thought to support the spiral mechanism of crystal growth. However a large number of crystals were found (not necessarily metals) possessing no features of this type and doubts concerning the universal applicability of the theory were expressed.[9] Fleischmann and Thirsk[10] suggested that the calculated frequency factors used in the calculation of 2-dimensional nucleation rates at a given supersaturation might be in error; the 3-D. rates were much greater than those calculated and it seemed possible that there could be a similar disparity between the

theoretical and actual rates of 2-D. nucleation. Bewick et al.[11] illustrated the importance of 2-D. nucleation in the growth of calomel deposits on mercury. Subsequently many examples of this type were found in anodic film formation on this substrate. However, this substrate is atypical in that the lack of surface structure prevents the possibility of screw dislocations determining the growth kinetics. Until comparitively recently no evidence was available to suggest that metals grew by the 2-D. nucleation of perfect crystal planes and the screw dislocation mechanism was generally accepted in this case.

Calculations by Bockris and Conway[12] indicated that the direct deposition from solution onto growing centres , i.e. the Volmer mechanism, would be improbable on account of the activation energy for the various possible elementary processes and the picture of deposition and charge transfer at a plane site followed by surface diffusion of the resulting ad-atoms to the points of incorporation on step lines, the 'indirect mechanism', was generally accepted. Estimates of the ad-atom concentration at the reversible potential, were made by several groups[13] but there was wide divergence in the values obtained and this was attributed to the different methods of surface preparation employed. More recently several workers have questioned the validity of explaining the results of such experiments in terms of ad-atom concentrations.[14] It was shown that a direct Volmer mechanism involving no surface diffusion and hence ad-atoms, would produce similar experimental results (see sec. 1.4 of this chapter).

Progress in the understanding of metal deposition in the last ten years or so, is best illustrated by considering systems in which the metal deposited is identical with the substrate material separately from those involving deposition onto a foreign substrate (e.g. Pb on Ag, Ag on C).

1.2 DEPOSITED METAL AND SUBSTRATE IDENTICAL.

Undoubtedly the most significant studies in this category are those of the Bulgarian school,under Budevski.[15] These workers studied deposition

of silver from 6M $AgNO_3$ solution onto silver single crystal electrodes prepared in a special way such that the surface configuration could be one of three types;

a) a dislocation free plane with an atomically smooth surface.

b) a dislocation free plane with a monatomic step of known length.

c) a stepped plane with a known uniform step density.

The electrode preparation involved the growth of a single crystal wire in a narrow capillary (150μm) under the influence of superimposed alternating and direct voltages.

These dislocation free electrodes enabled the classical, Kossel/Stranski model of electrodeposition involving growth of perfect crystal planes by 2-D nucleation, to be realised experimentally for the first time. The dislocation density on normal substrates is usually sufficiently high to obviate the need for nucleation.

Experiments on dislocation free planes gave the following results:

At constant current ($\sim$ 0.5mA cm^{-2}) the overvoltage rises to 7-12mV and shows periodic oscillations which are due to formation of 2-D nuclei. The overvoltage rises rapidly to the critical value on switching on. As the nucleus expands over the surface, there is first a fall in the overvoltage and then a rise in accordance with the variation in the length of the monatomic step. When this reaches the edge of the electrode, the overvoltage rises again to the critical value and the process restarts. The period of oscillation and the current density give the thickness of the layer (monatomic).

In potentiostatic experiments, potentials up to $\sim$ 7mV leave the cell non conducting whereas at 8-12mV there is a strong oscillatory current corresponding to nucleation. In double potential step experiments, if the first pulse is long enough for nucleation to occur at that potential, the

current continues in the second (lower overpotential) pulse until the new plane has completely covered the face. The experimental current-time transients vary from test to test and these can be simulated from purely geometrical considerations for a nucleus of specified shape arising at a specified distance from the edge of a circular face, with the assumption that the current is proportional to the length of the growing edge.

Although calculations by Bockris and Conway[12] suggested that the direct deposition mechanism was unlikely on account of the high activation energy associated with it, other workers have shown that this is not necessarily the case[16]; the theoretical treatment appears to be rather complicated and uncertain. Budevski et al.[17] have shown that the direct transfer mechanism plays a predominant role in the deposition of silver on dislocation free silver electrodes and in this case the contribution of surface diffusion was negligible.

Fischer and co-workers[18] have stressed the role of inhibition as a general phenomenon in electrodeposition. Studies involving copper deposition onto mono and polycrystalline copper substrates, in the presence of inhibitors, indicated that the lattice planes in the growth layers are formed via 2-dimensional nuclei.

Many other examples of studies in this category of metal deposition (i.e. deposited metal and substrate identical) in conjunction with those described above allow the following generalisations to be made:

1. A relatively high density of crystal imperfections i.e. growth sites in the substrate surface permits the deposition reaction to occur without a nucleation overvoltage and the charge transfer reaction takes place directly on these growth sites e.g. kinks and steps. Nucleation may become significant at high deposition rates.

2. When the density of crystal imperfections is relatively low or zero the formation of 2-dimensional nuclei is the rate determining step at low

overvoltages and can be considered the initial step.

1.3 DEPOSITION ONTO FOREIGN SUBSTRATES.

These systems are capable of yielding most information about the nucleation process as substrate lattice extension at dislocations, case 1. above, is not normally possible.

Studies in this category can be conveniently divided into two groups,

a) systems involving the direct formation of three-dimensional nuclei onto the bare substrate with a considerable nucleation overpotential (50-100mV),

b) systems involving the formation of a complete monolayer of the deposited metal prior to any subsequent 3-dimensional growth (which occurs at small overpotentials, 0-15mV depending on concentration).

This categorical distinction has frequently been ignored or misunderstood with the result that the present understanding of such deposition processes is somewhat primitive compared to that of systems where the deposited metal and substrate are identical.

Category b) relates to the systems which show underpotential-deposition (U.P.D.). This is a phenomenon in which a complete monolayer of the deposited metal can be formed at potentials more positive than the reversible potential of the deposited metal/metal ion electrode.

U.P.D. is very common on noble metal substrates (e.g. platinum gold and silver) but several questions pertaining to the nature of the monolayer (e.g. its structure and state of charge) are still unresolved despite extensive investigations by many research groups. This topic is the central theme of this thesis and is considered in detail in Chapter 2.

The uncertainty associated with many published studies of metal deposition onto foreign substrates (i.e. those not specifically aimed at investigating U.P.D.) is due to the fact that the possible formation of an

initial monolayer and the effect of this on subsequent nucleation, in potential step experiments, has been ignored. Although the deposition of a monolayer prior to the bulk is readily apparent in linear potential sweeps, this is not the case in potential step experiments and to date it has not been conclusively established whether monolayer formation always occurs (in those systems which show U.P.D. that is) as an initial step in the electro-deposition process even when the potential is sufficiently high for 3-dimensional growth to occur.

Kaischev[19] and co-workers have investigated the deposition of iron, silver, lead and mercury onto monocrystalline platinum substrates with a view to confirming the validity of the Volmer equation for the initial formation of 3-dimensional nuclei;

$$J = A.\exp(-\Delta G_{crit}/kT) = A.\exp(-S/\eta^2)$$

where,
$$S=8\pi.\gamma_{n-v}^{3}.V_m^{2}/3kTz^{2}.F^{2}$$

with, J = rate of 3-dimensional nucleus formation.

γ_{n-v} = specific free surface energy of the interface between nucleus and electrolyte phase.

V_m = mole volume of nuclei.

The other symbols have their usual significance.

Although the results showed that the logarithm of the nucleation rate was inversely proportional to the square of the overpotential in agreement with theory, the significance of this conclusion is in doubt as the electrodes were not free from oxide films at the potential where metal deposition occurred and in addition, silver, lead and mercury all form underpotential monolayers on platinum[31,32] (lead and mercury form underpotential alloys in fact) and this was totally ignored. The overpotential necessary for nucleation to occur in these systems was of the order of 100mV which is suggestive of 3- rather than 2-dimensional nucleation, however these

systems are unusual in that most most metal deposition systems involving U.P.D. show very small overvoltages for nucleation (usually < 10mV). Presumably the surface oxide film was complicating the behaviour which Kaischev attributed solely to 3-dimensional nucleation.

The importance of the presence of monolayer deposits in the subsequent nucleation and growth of thicker deposits was pointed out by Vermiliyea in 1963[20] with reference to anodic films (e.g. oxides and salts) but this idea has rarely been applied to the deposition of metals.

The most obvious examples of category a) systems are those involving deposition onto vitreous carbon substrates. No underpotential monolayer formation is discernible and bulk deposition is usually associated with large overvoltages (typically of the order of 100mV) which probably represents a true 3-dimensional nucleation overpotential. The deposition kinetics of several of these systems have been studied by Harrison et al.[21] There are relatively few examples of metal deposition onto foreign substrates which involve neither U.P.D. or alloy formation and to date these have not been investigated kinetically.

In concluding this section, it seems essential to stress the importance of resolving the question of the role played by metal monolayers in electro-deposition on foreign substrates. This topic is considered further in Chapter 2.

1.4 MODELS OF ELECTROCRYSTALLIZATION AT THE ATOMIC LEVEL.

This topic has been very adequately reviewed elsewhere[22] and will be treated here very briefly.

1.4(a) THE ADATOM MODEL.

This model has been treated extensively although conclusive experimental verification has never been achieved. In it, adatoms arrive at the metal surface by diffusion and electrochemical reaction to the step line where they are incorporated into the lattice. The step lines arise from inherent imperfections in the substrate such as screw dislocations

and do not advance significantly during the measurement.

In a potentiostatic pulse experiment, starting from the equilibrium potential, the theory has been fomulated exactly for two cases;

a) when the equilibrium concentration of adatoms is maintained at the edge and the rate of incorporation and the reverse reaction at the step line are both fast;

b) when equilibrium is not maintained and the rate of removal of adatoms at the step line is slow.

In addition the theory has been developed for A.C. and galvanostatic experiments.[33]

For case a) above, neglecting bulk diffusion, the equation relating the steady state current to the overvoltage can be written as,[17]

$$i = i_{o(ad)}\{\exp\alpha zF\eta/RT - \exp-(1-\alpha)zF\eta/RT\}\lambda_o/x_o\tanh(x_o/\lambda_o) \qquad (1.1)$$

where λ_o, termed the surface diffusion penetration, is given by,

$$\lambda_o = (zFD_sC^o_{ad}/i_{o(ad)})^{\frac{1}{2}} \exp-\alpha zF\eta/2RT$$

where, D_s = surface diffusion coefficient.

C^o_{ad} = equilibrium concentration of adatoms.

$i_{o(ad)}$ = exchange current density of ions in solution with adatoms.

x_o = ½.average step distance.

When $\lambda_o >> x_o$, 1. reduces to the Butler-Volmer relation and the reaction is controlled by the rate of charge transfer. When $\lambda_o << x_o$, 1. becomes

$$i = i_{o(ad)}\{\exp\ \alpha zF\eta/RT - \exp-(1-\alpha)zF\eta/RT\}\lambda_o/x_o$$

In this case the current is strongly influenced by the step density and

surface diffusion plays a predominant rôle.

1.4(b) DIRECT DEPOSITION MODEL.

This was suggested for the first time by Volmer[5] and the charge transfer is assumed to occur directly at a step or a kink.

Neglecting bulk diffusion, the equation relating the steady state current to overvoltage is given by,[23]

$$i = i_{o(st)} 2r_o L\left[\exp\{\alpha zF\eta/RT\} - \exp\{-(1-\alpha)zF\eta/RT\}\right] \qquad (1.2)$$

where, $L = 1/2x_o$ = the total length of growth steps per unit area,

$i_{o(st)}$ = exchange current density of ions in solution with atoms on a step or a kink,

r_o = atomic radius in the crystal lattice.

Experimentally no clear distinction can be made between 1.1 and 1.2; at low overpotentials the 'apparent' exchange current density obtained from the slope of the current-overvoltage plot, is given by

$$i_o = (RT/zF)\frac{di}{d\eta}$$

therefore in the case of the surface diffusion mechanism, replacing $2x_o$ by $1/L$

$$i_o = i_{o(ad)} 2L\lambda_o \tanh(1/2L\lambda_o$$

or in the case of direct transfer

$$i_o = i_{o(st)} 2r_o L$$

In the latter case, i_o is proportional to L irrespective of the step density. For indirect transfer, i_o is proportional to L for small step densities ($2L\lambda_o < 1$). For higher step densities, i_o becomes independent of L and the reaction is controlled by the rate of charge transfer. This result illustrates the impossibility of distinguishing between the two mechanisms from steady state measurements. However, the use of high

frequency impedance measurements[30] can lead to such a distinction. Budevski et al.[23] have shown, with silver electrodes of known step density, that it is possible to calculate the quantities, $i_{o(ad)}$ and $i_{o(st)}$. It was found that $i_{o(st)}$ exceeded $i_{o(ad)}$ by almost three orders of magnitude, contradicting the calculations of Bockris and Conway.[12]

1.4 (c) NUCLEATION AND GROWTH MODELS.

In the adatom model, metal growth takes place by incorporation of material at the step lines created by screw dislocations; this model is appropriate for the deposition of a metal on a substrate of the same material or the later stages of deposition onto a foreign substrate. Reference has already been made to the fact that deposition can also involve nucleation processes; these will be important in,

a) the initial stages of metal deposition onto foreign (inert) substrates,

b) metal growth on substrates of the same material which possess few dislocations,

c) growth at specific sites on electrodes of the same material (dendrite formation).

The nucleation and growth model has been extensively developed for two limiting cases,

1. rate control by the rate of mass transfer,

2. rate control by charge transfer occurring when material is incorporated at the periphery of a growing centre.

In addition the case of joint control by the rate of surface diffusion and charge transfer has been considered.[24]

The rate of formation of nuclei can be described [25] by a single exponential rate law i.e.

$$N_t = N_o(1-\exp\{-At\}) \qquad (1.3)$$

where,

N_t = total number of nuclei at time t.

N_o = total number of available nucleation sites.

A = nucleation rate constant.

Two limiting cases of this equation are possible depending on the value of A. If A is large, all the sites are converted to nuclei virtually instantaneously and,

$$N_t = N_o \qquad (1.4)$$

This situation is described as instantaneous nucleation and is most likely to hold on surfaces posessing significant microstructure. When A is small,

$$1-\exp\{-At\} \simeq At$$

therefore,

$$N_t \simeq AN_o t \qquad (1.5)$$

A nucleation situation of this type is described as progressive and would occur, for example, on a surface free from microstructure.

The limiting cases of rate control, stated above, will now be described.

1.5 (a) NUCLEATION AND GROWTH MODEL: RATE CONTROL BY CHARGE TRANSFER.

This situation is commonly encountered in the growth of salt and oxide films (especially on mercury) where the slow step is incorporation of material at the periphery of the growing centres. In this case a substantial amount of information may be gained about lattice building

rates and (in the case of progressive nucleation) nucleation rates.

Fleischmann and Thirsk[25] have formulated the current-time relationships for the potentiostatic growth of two and three-dimensional nuclei, using simple geometrical arguments. Considering the case of two-dimensional growth; for a single cylindrical nucleus, the area on which deposition takes place increases with time and the current is given by,

$$i = \frac{2zF\pi Mhk^2t}{\rho} \qquad (1.6)$$

where,

k = rate constant governing crystal growth.

h = height of the centres.

M = gram molecular weight of the deposited material.

ρ = density of the deposited material.

In the case of instantaneous nucleation, N_o growth centres are formed and the total current is given by,

$$i = \frac{2zF\pi Mhk^2t}{\rho} \times N_o \qquad (1.7)$$

whereas for a progressive nucleation system,

$$N_t = N_oAt$$

and,

$$i = \frac{2zF\pi Mhk^2t^2}{\rho} \times N_oA \qquad (1.8)$$

In the later stages of crystal growth the individual growth centres overlap and the peripheral length available for deposition decreases with time. Provided that the overlapping is random, the statistical problem of coalescence may be solved algebraically by application of the Avrami theorem.

The complete equations for two-dimensional layer growth, including overlap are,

$$i = \frac{zF\pi hAk^2t^2}{\rho} \exp -\frac{\pi M^2Ak^2t^3}{3\rho^2} \qquad (1.9)$$

for progressive nucleation.

and,

$$i = \frac{zF\pi MN_o k^2 t}{\rho} \exp \frac{-\pi M^2 N_o k^2 t^2}{\rho^2} \qquad (1.10)$$

for instantaneous nucleation.

Three-dimensional nucleation and growth can be treated similarly, although in this case the problem of overlap is more difficult. Three-dimensional deposits formed from successive two-dimensional layers have also been considered theoretically[26] and can be observed experimentally e.g. in the growth of calomel deposits on mercury.[11]

1.5 (b) NUCLEATION AND GROWTH MODEL: RATE CONTROL BY MASS TRANSFER.

This situation is very common in metal deposition, and transport processes, either on the surface or in the solution, prior to the growth step, control the rate of the reaction. The case of two-dimensional layer formation will be considered first.

1. Diffusion zones limited to individual nuclei.

The growth of a single two-dimensional nucleus, expanding at a rate determined by the flux, was originally considered by Frank.[27] The hemi-cylindrical diffusion zone is concentric to the nucleus and the radius at time t, R_t, is given by,

$$R_t = \theta(Dt)^{\frac{1}{2}} \qquad (1.11)$$

where θ is a constant which depends on,

$$\frac{(c^* - c^o)M}{\rho}$$

where,

c^* = concentration in bulk of solution.

c^o = concentration at surface.

D = diffusion coefficient.

For the potentiostatic growth of a two-dimensional layer from N_o nuclei formed instantaneously, the i-t relationship is given by,

$$i = q_{mon}\pi\theta^2 D.\exp(-\pi\theta^2 D N_o t) \qquad (1.12)$$

where,

q_{mon} = monolayer charge.

This function is plotted out in Fig. 1.1.

For progressive nucleation,

$$i = q_{mon}\pi\theta^2 DAt.\exp\left(\frac{-\pi\theta^2 DAt^2}{2}\right) \qquad (1.13)$$

This function is plotted in Fig. 1.2

2. Overlap of the individual diffusion zones.

This situation is likely to arise when a large number of nuclei are formed initially and the individual diffusion zones soon overlap, the rate of growth being controlled by planar diffusion perpendicular to the surface. The mathematical treatment was formulated by Astley, Harrison and Thirsk.[28]

Assuming a linear Langmuir isotherm and Nernst equilibrium at the growing patches, the expression relating current and time is given by,

$$i = \frac{zFA'C^*D^{\frac{1}{2}}}{\pi^{\frac{1}{2}}t^{\frac{1}{2}}} - \left\{\left(\frac{zFA'^2C^{*2}D}{m}\right)\left(\exp\frac{-zF\eta}{RT}\right) \times \exp\left[\frac{C^{*2}DA'^2t}{m^2}\left(\exp\frac{-2zF\eta}{RT}\right)\right] \times \operatorname{erfc}\left[\frac{C^*D^{\frac{1}{2}}A't^{\frac{1}{2}}}{m}\left(\exp\frac{-zF\eta}{RT}\right)\right]\right\} \qquad (1.14)$$

where,

A' = area of electrode (cm^2)

D = diffusion coefficient ($cm^2\ s^{-1}$)

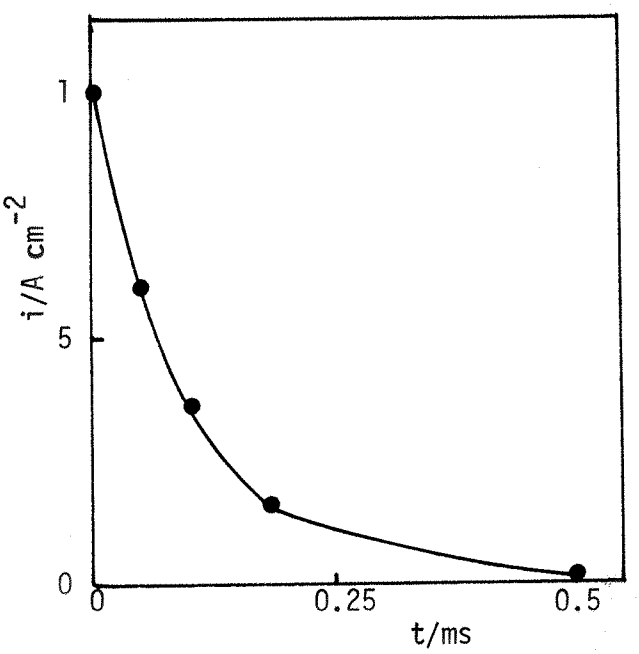

Fig. 1.1 Plot of equation 1.12 for the growth of a two-dimensional layer controlled by diffusion, with instantaneous nucleation.[22]

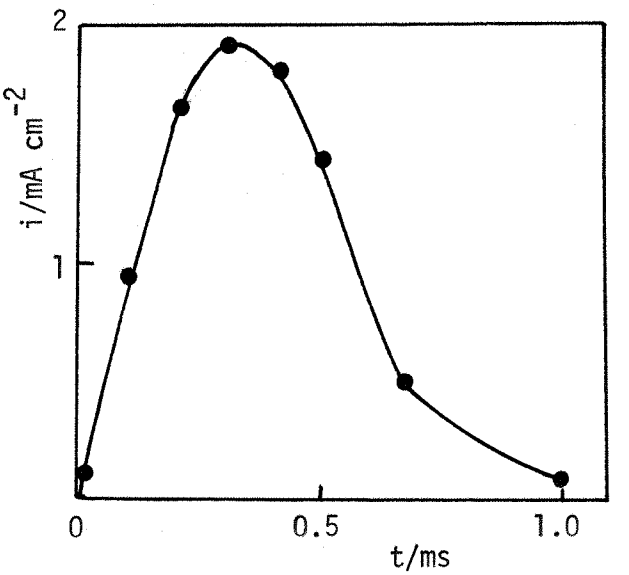

Fig. 1.2 Plot of equation 1.13 for the growth of a two-dimensional layer controlled by diffusion, with progressive nucleation.[22]

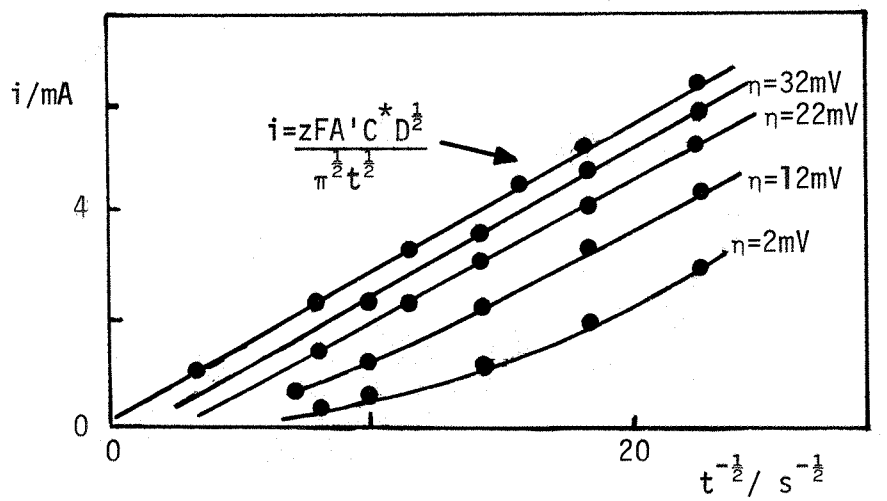

Fig. 1.3 Plot of equation 1.14 at different overpotentials for the growth of a two-dimensional layer, controlled by planar diffusion.[28]

C^* = concentration in the bulk of the solution (mol cm^{-3})

m = number of moles in a monolayer of area A'

The other symbols have their usual significance. Plots of i versus $t^{-\frac{1}{2}}$ for this expression are shown in Fig. 1.3 as a function of overpotential. At short time these plots are linear and of constant slope equal to,

$$\frac{zFA' C^* D^{\frac{1}{2}}}{\pi^{\frac{1}{2}}}$$

This equation was applied to the experimental results for the underpotential deposition of lead and thallium on polycrystalline silver in an attempt to show that nucleation processes were occurring in this situation. Although a certain amount of agreement with the above equation was found, the result could not be regarded as conclusive as similar i-t transients could arise from the deposition of a simple adsorbed layer with no nucleation, (see Chapter 4).

3. Fixed diffusion zone.

Two-dimensional nucleation and growth with a fixed diffusion zone has also been considered theoretically and compared with the experimental results for nickel monolayer deposition, from a thiocyanate complex, onto mercury.[29] Examples of current-time transients for this system are shown in Fig. 1.4. At low overpotentials an unsymmetrical peak is seen in the transient. In this case, the diffusion zones surrounding the nuclei are narrow and lattice building is to some extent rate determining. At higher overpotentials, only a falling transient is observed and corresponds to the case of wide diffusion zones and rate control predominantly by surface diffusion. A graphical simulation of the growth of two-dimensional surface diffusion zones indicated that there was a change from progressive to instantaneous nucleation with increasing potential of growth. This affect was ascribed to the rapid decrease at higher potentials of the adatom concentration due

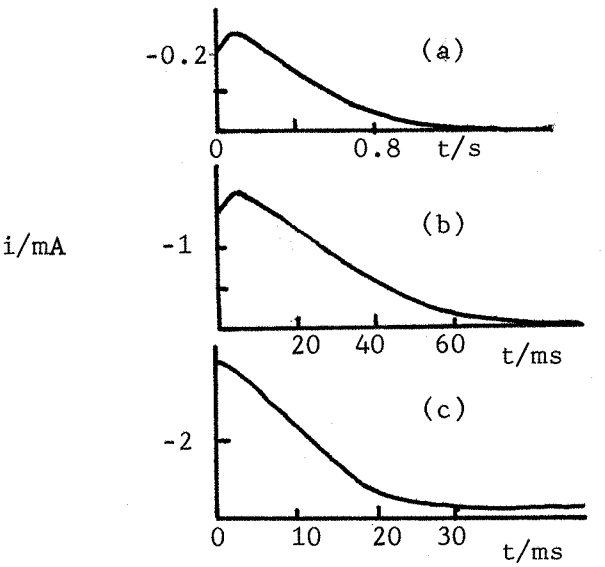

Fig. 1.4 Typical cathodic i-t transients for the solution, 0.1M $Ni(NO_3)_2$/ 0.1M KSCN/ 2.2M KNO_3. Area of mercury surface was 0.055cm^{-2}. Potentials (a) -600mV (b) -640mV (c) -670mV vs. S.C.E. The transients show the effect of comparable rates of lattice growth and surface diffusion.

to rapid extension of the diffusion zones.

The initial stages of three-dimensional growth, from hemispherical nuclei, has also been treated taking into account the outward movement of the metal surface.[30]

The relationships obtained before overlap has occurred are,

$$i = \frac{zF\rho N_o \pi\theta'^3 D^{3/2} t^{1/2}}{M} \qquad (1.15)$$

for instantaneous nucleation, and

$$i = \frac{zF\rho(\pi\theta'^3 DA^{3/2})\frac{2}{3}t^{3/2}}{M} \qquad (1.16)$$

for progressive nucleation. (θ' is a constant).

This brief review has shown that systems with totally different nucleation and growth laws can result in identical i-t relationships; this ambiguity makes an unequivocal determination of the particular growth law followed in a given situation,difficult, unless further tests are carried out.

CHAPTER TWO: UNDERPOTENTIAL METAL DEPOSITION.

2.0 INTRODUCTION.

In this chapter, studies of U.P.D. will be divided into two groups; the historical aspects are illustrated with studies up to ∿ 1960 and following a description of available experimental methods, the extent to which several problems concerning the nature of U.P.D., have been solved, will be illustrated with studies from 1960 up to the present time. Following a survey of reflectance spectroscopic studies of metal deposition, sections on other aspects of U.P.D., the relevance of U.P.D. to overpotential growth and a discussion of the scope of this project conclude the chapter.

2.1 HISTORICAL ASPECTS.

The first studies[34-37] of the deposition and dissolution of very small amounts of metals on inert substrates were made with radioactive tracers. In general, the deposition of fractions of monolayers was observed to occur at a certain undervoltage with respect to the equilibrium potential for the deposition of the bulk phase. To explain this behaviour, Haissinsky[38] suggested that a small number of lattice sites on the electrode would have such high adsorption energies for metal atom deposition as to be equal to the substrate work function, while the rest would be associated with adsorption energies smaller than this. He showed that the width of a typical deposition curve,in volts, corresponded to a reasonable value for the range of adsorption energies on a heterogeneous surface. According to this explanation, irrespective of the electrode material, deposition of a given element would always begin at the same potential. However it was shown later that the initial deposition behaviour of fractional monolayers was very sensitive to the electrode material.

Rogers and co-workers studied the deposition of traces of radioactive silver onto platinum.[39,40] The observed underpotential deposition was interpreted on a thermodynamic basis by developing the concept of

Herzfeld[41] which stated that the activity of a monolayer deposit should vary with the fraction of surface covered e.g.

$$a_{m(s)} = f_{m(s)} \times Z/Z_o$$

where, $a_{m(s)}$ = activity of metal in a fractional monolayer

$f_{m(s)}$ = activity coefficient of metal deposit

Z_o = no. of moles amounting to one monolayer deposit on the electrode

Z = no. of moles of metal deposited.

Mills and Willis[42] in a study of the U.P.D. of lead and thallium on gold and lead on gold, using a galvanostatic technique showed that the magnitude of the underpotential effect (underpotential shift) was larger on gold than on silver and that the results were highly dependent on the nature of the metal being deposited and the state of the electrode surface. These workers concluded that the nature of the underpotential deposit could not be a 2-dimensional crystal plane, as an overpotential for the formation of the bulk phase was observed.

During the last decade or so, many attempts have been made to resolve the physico-chemical nature of underpotential monolayers employing electrochemical, radioactive tracer and optical techniques. The next section gives details of the main experimental methods which have been used in the study of U.P.D. together with a comprehensive list of all the systems studied by the various techniques.

2.2 EXPERIMENTAL METHODS.

(a) THIN LAYER CELLS.

Schmidt and co-workers have been the most prolific of the research groups studying U.P.D. and were the first to use potentiostatic techniques in linear sweep voltammetry experiments. The majority of the work was

accomplished using thin layer cells of two designs.

The first type of cell, which was in use by these workers up until 1969 [43-45], was of the so called 'chamber type'. The potential of the working electrode was slowly varied in a linear manner and the current-potential behaviour recorded. The set-up was such that only a limited amount of reducible cation (the depolariser) was available for the electrode reaction. This was enclosed in the electrode chamber which was isolated against diffusion from the other solution.

More recently a different type of thin layer cell has been employed [46] which contains 4 electrodes, a) working b) generator c) reference d) counter. The electrolyte volume between a) and b) (separated by about 50μm) constitutes the thin layer. Both working and generator electrodes are polarised potentiostatically at different potentials and that of the former is varied in a linear manner between defined start and end potentials. The generator is a reversible electrode for the ion species being reduced at the working electrode i.e. for a metal ion reduction,a reversible metal/metal ion electrode.

Integration of the current flowing in the working electrode circuit gives the charge flowing. This may be a function of,

a) capacitive effects due to metal ion adsorption,
b) faradaic processes occurring at the electrode e.g. metal ion reduction.

The generator electrode, which is kept at a fixed potential maintains a constant concentration of the metal ion being reduced in the thin layer (according to the Nernst equation) such that any concentration changes due to metal ion ad- or desorption on the working electrode are compensated for. Integration of the currents flowing in the generator circuit corresponds directly to measurement of the fraction of surface covered by the deposited metal species.

The advantage of this technique, is that the surface coverage-potential isotherm is measured independently of the charge-potential isotherm , so that any process apart from metal ion adsorption contributing to the current flowing in the working electrode circuit, can be detected by comparison of the two isotherms. Some examples of this technique will be given below. In addition, it is possible to place grid electrodes between the working and generator to measure potentiostatically the fluxes of different ionic species.

However, the fact that reversible generator electrodes exist for only a few systems and that the high impedance of the cell prohibits its use for pulse measurements, limits the versatatility of this method. Two examples of the use of this technique will now be given.

LEAD ON POLYCRYSTALLINE GOLD.

For this system[47] it is found that the currents flowing in the working and generator circuits, as a function of potential, are equal in magnitude indicating the occurrence of no other process apart from metal ion adsorption/reduction taking place at the working electrode. The linear sweep voltammetry exhibits several peaks below the reversible potential. Schmidt attributed these to different adsorbed states, in particular the species responsible for the comparatively sharp peak observed, was thought to be adsorbed further away from the electrode than the metal deposited at more positive potentials.[48] This system will be referred to again in section 2.4 (a).

LEAD ON POLYCRYSTALLINE SILVER.

This system[49] has been investigated in chloride media and in this case the current-potential curves for the generator and working electrodes show significant differences. In the lower underpotential range, the charge flowing in the working electrode circuit was equivalent to greater than two electrons flowing per Pb^{2+} deposited. These results were inter-

preted by co-desorption and co-adsorption of chloride ion respectively.

2.2(b) LINEAR SWEEP VOLTAMMETRY.

This technique has been used in the present study and needs no further explanation. It is capable of giving useful thermodynamic and kinetic results rapidly, however it does not possess the advantage of the thin layer cell mentioned previously and the ellucidation of the processes occurring in underpotential systems which show several peaks in the voltammetry, cannot be made with any certainty unless combined with additional techniques e.g. potential step measurements.

2.2(c) ROTATING RING DISC.

This method has been employed by Bruckenstein and co-workers[50] in the study of several underpotential systems. The ring electrode can detect electroactive species being generated at the disc and those retained. By this means, surface coverage isotherms can be constucted as for the thin layer cell, but the method is not so straightforward.

2.2(d) PULSE MEASUREMENTS.

Conventional potential step methods, to date have only been used by Astley et al.[28] in a study of the deposition of lead and thallium onto silver. They are however, very powerful tools for the investigation of the possible participation of two-dimensional growth steps, as opposed to adsorption, in the underpotential region, and for that reason have been extensively used in the work described in this Thesis.

Galvanostatic pulse measurements have been employed by Schultze[51] to ellucidate the kinetics and thermodynamics of Cu^{2+} 'adsorption' on polycrystalline platinum. However the results were complicated by the disturbing processes of hydrogen and oxygen ad/desorption.

Lorenz and co-workers[52] have applied multi-channel pulse galvanostats in a study of the kinetics of Cu^{2+}, Ag^{+}, Pb^{2+} and Tl^{+} deposition on polycrystalline and single crystal gold substates. An initial equilibrium

state in the underpotential region is fixed potentiostatically, a galvanostatic pulse is then applied such that the charge flowing does not exceed 1μC cm^{-2} and the potential deviations from the initial value are a few mV.. Attempts were made to simulate the experimental potential -time transients using a model which considered charge transfer and surface diffusion as possible rate determining steps in the deposition process.

2.2 (e) RADIOACTIVE TRACER METHODS.

This technique has been mainly applied by Bowles[53] in a study of thallium and copper deposition on platinum. The electrolyte contains a radioactive isotope of the metal being deposited (∿ 1μM) and its activity can be monitored by a Geiger counter tube immersed in the solution. Metal deposition results in the level of activity changing depending on the change in concentration of radioactive material in solution. In this way coverage isotherms can be constructed as a function of potential.

2.2 (f) OPTICAL METHODS.

For the *in situ* characterisation of an electrode surface, optical spectroscopy is one of the most versatile of available physicochemical methods. Two optical techniques have been employed in the study of U.P.D.,

a) specular reflectance spectrocopy,[54]
b) ellipsometry.[55]

SPECULAR REFLECTANCE SPECTROSCOPY.

This technique has been employed in the present work and is discussed more fully in section 2.4 and 3.6 (b) but for the sake of completeness a brief description is given here.

In this method light, specularly reflected from an electrode surface is monitored in order to detect changes in intensity due to the electrochemical process taking place on the electrode surface. As absolute reflectivities are difficult to determine, it is usual to measure the change in reflectivity, ΔR, between defined states of the electrode. For

example, if the electrode potential was modulated with a square wave-form, the reflectivity change measured would correspond to the difference in reflectivity of the electrode at the two potentials of the modulation. It is advantageous to employ some form of modulation to the electrode potential as this enables one to use a correlation technique to greatly increase the sensitivity. In the present work signal averaging has been used which enables changes in surface coverage at the sub-monolayer level to be readily detected.

A comprehensive survey of the studies of U.P.D. employing reflectance spectroscopy is given in section 2.4 together with some studies of metal deposition on semi-conductor substrates.

ELLIPSOMETRY.

This is a reflectance method in which polarised monochromatic light is reflected obliquely from the electrode surface and the polarisation state of the reflected beam is measured as the relative phase retardation, Δ and amplitude attenuation, $\tan\psi$. From these measurements the complex refractive index of the interfacial region can be calculated. To date this technique has only been used to study one underpotential system, lead on gold[56] (sec. 2.4 (a)).

2.3 THE NATURE OF UNDERPOTENTIAL MONOLAYERS AND THE MECHANISM OF THE DEPOSITION PROCESS.

The earliest studies of U.P.D., involving radiotracer measurements have already been described. Subsequent work using the techniques described in section 2.2 can be best described by considering the following questions.

1. Why does U.P.D. occur?
2. What is the state of charge of the species within the monolayer?
3. Does the layer consist of adsorbed species or is it a crystal plane?
4. What is the origin of the multi-peaks observed in the linear sweep

voltammetry of many U.P.D. systems?

The conclusions derived from optical studies of U.P.D. will be considered separately in section 2.4.

2.3 (a) THE RAISON D'ÊTRE OF U.P.D.

Apart from the conclusions reached by the early workers in this area mentioned in section 2.1, three theories have been put forward to account for the occurrence of U.P.D. The first was due to Schmidt and Gygax,[44] who assumed the deposition process produced adsorbed neutral atoms on the electrode. The experimental current-voltage curves obtained in a thin layer cell could be reproduced theoretically by coupling an appropriate adsorption isotherm to the bulk diffusion conditions. If a Langmuir isotherm was chosen the calculated curves showed a pre-peak before the bulk deposition process whereas a linear isotherm predicted only a single peak due to bulk deposition.

The second theory (Astley, Harrison and Thirsk)[28] assumed that the underpotential monolayer consisted of a two-dimensional crystal plane epitaxially fitted to the substrate. Large differences in the lattice parameters of substrate and deposited metal were thought to preclude U.P.D. in certain systems e.g. cadmium on lead, whereas a similarity of crystal structure and lattice parameters would lead to underpotential deposition. These ideas did not gain widespread acceptance as the opinion was widely held that U.P.D. was an adsorption rather than a crystal growth process. This will be discussed in detail in section 2.3 (c).

The most recent theory to explain the origin of U.P.D. was put forward by Gerischer, Kolb and Przasnyski[57] and their model has gained support from most workers in the field. They investigated 22 systems in which U.P.D. occurred and it was found that the potential difference between monolayer and bulk deposition peaks was closely related to the difference in work function of substrate and deposit. They assumed this

work function difference to be a measure of the difference in electronegativities between a substrate atom and a deposited atom to which it is bonded. Partial electron transfer arising from this electronegativity difference would give an ionic contribution to the bond energy enabling the first layer to be deposited at an underpotential. The correlation between underpotential shift and work function differences is quite good suggesting that the electronegativity difference is a major factor in determining the onset of U.P.D. The theory gives no explanation for the multi-peak nature of certain systems e.g. Pb on Au and in such cases the most anodic peak shift was used in the correlation; nor does it consider the possible importance of structural effects. It would be expected that the detailed structures of substrate and deposit and their epitaxial relationship would become as important as the electronegativity difference in determining the course of the deposition process. These matters will be referred to again in the results section.

A slight modification to this theory has been suggested by Vijh[58] in view of the fact that several couples, notably associated with bismuth, tin and lead electrodes do not give U.P.D. despite the existence of work functions equal to those in systems which do. He argues that for U.P.D. to occur, the electrode surface atoms must posess significant 'd' character and that the heat of adsorption of the metal atom on a given substrate as calculated from the Pauling-Eley equations, must be exothermic. The electrode metals Pt, Au, Ag and Cu have percentage 'd' characters of 44, 36, 36 and 36% respectively and all of these substrates sustain U.P.D. whereas the metals Bi, Sn and Pb, which have a clear cut 'sp' nature, do not. Vijh correlated underpotential shifts with heats of adsorption and the resulting plot was similar to the $\Delta U_p/\Delta\Phi$ plot of Gerischer et al. Metal couples involving Bi, Sn and Pb were not considered on the plot because of the absence of 'd' character in these elements.

Gerischer's work function theory predicts the existence of a

small partial charge (10-20%) on the underpotential adatoms. This topic is considered in the next section.

2.3 (b) THE STATE OF CHARGE OF THE MONOLAYER.

This question has been considered in detail by Vetter and Schultze.[59] These authors define a quantity, γ, the electrosorption valency, which depends on geometrical factors, a partial charge transfer coefficient, λ, dipole factors and a capacitive term.

γ is defined by,

$$\gamma = \frac{-1}{F}\left[\frac{\partial q_m}{\partial \Gamma_{ad}}\right]_{\Delta\psi}$$

where, q_m = electrode charge,

Γ_{ad} = surface concentration of specifically adsorbed substance,

$\Delta\psi$ = potential difference of the compact double layer.

Whilst the quantity γ, is measureable experimentally, examples are given below, the partial charge transfer coefficient, λ, has never been determined although several authors, whilst claiming to measure λ, have in fact measured γ.

A determination of γ can be made by the independent measurement of q_m (by coulometry) and the coverage isotherm Γ_{ad}. This is readily achieved with the thin layer technique, ring disc electrodes and radiotracer methods.

Electrosorption valencies have frequently been obtained for underpotential deposits on platinum. For the system, Tl on Pt, Bowles[53] found γ values ranging from 0.22 to 0.6 depending on θ_{Tl}. Similar values were obtained by Schmidt.[59]

The U.P.D. of Cu on Pt was investigated by Schultze[51] using several techniques. At low coverages $\gamma \sim 2$ was obtained but as $\theta \to 1$, γ decreased to

1.4. Low values of γ were thought to arise from the mainly electro-static adsorption of ions with a small partial charge transfer.

Schmidt et al. have investigated several systems on gold and silver electrodes e.g. Cu on Au,[60] Pb on Au,[60] Tl on Ag.[44] In all cases γ was found to be equal to z, the charge on the cation being reduced. Bismuth deposition on gold[59] however was found to give a coverage dependent γ value. The deposition of lead on gold has already been referred to.

In cases where γ values approximately equal to z are obtained, it seems plausible that the adsorbed metal atom would be only slightly charged and bonded to the surface by a covalent bond with a small partial ionic character. It should be stressed however, that to date no actual experimental determination of the partial charge on an adsorbed species, has been achieved.

2.3 (c) THE STRUCTURE OF THE MONOLAYER: ADSORBED ATOMS OR A CRYSTAL PLANE?

Before the completion of the work described in this Thesis, the identification of underpotential metal monolayers as either an adsorbed layer of neutral or partially charged atoms, or a 2-dimensional crystal plane, had not been proved for either case. The majority opinion however, was that the metal layers consisted of adsorbed atoms rather than 2-dimensional islands formed by nucleation and growth but this was based on the lack of any firm evidence for the existence of the latter rather than conclusive proof for the presence of the former. This section presents a cross segment of views relevant to this topic.

Schmidt and co-workers originally defined[44] the monolayer as consisting of neutral atoms, the deposition of which at an underpotential was governed by a Langmuir isotherm. More recently, they have used the term 'cation adsorption' to describe U.P.D., and have treated it in an analogous manner to the specific adsorption of anions.[49,61] Although this appears to be a change of the original definition it is clear that Schmidt et al. do not imply that the charge flowing when U.P.D. takes place, is

purely capacitive which would be the case if only specific adsorption of cations was involved. Indeed in a recent paper[52], Schmidt and Lorenz considered charge transfer being rate determining in 'metal ion adsorption' which clearly implies the participation of a Faradaic process. It would seem therefore, that this term, when used by Schmidt, Lorenz and co-workers applies only to the initial stage of the deposition process before any Faradaic charge transfer has taken place, (the distinction between capacitive and Faradaic charge cannot be achieved experimentally at present making it impossible to determine the partial charge of the adsorbate). Nevertheless this method of nomenclature has caused confusion and in some cases[57] has been interpreted literally as implying the Presence in the inner Helmholtz plane of cations bearing the full ionic charge.

To support the idea of underpotential deposits existing as adsorbed layers, Schmidt has provided no conclusive evidence. Instead, the fact that deposition (in most systems) occurs over a wide range of potential, which is consistent with an adsorption isotherm, the activity of the deposit varying with coverage, was considered sufficient evidence for the lack of any phase formation processes occurring. It is questionable whether deposition of a monolayer as a crystalline phase would occur at a single potential and consequently whether deposition over a range of potentials excludes this possibility. Changes of state can be of several types[62] and it is quite common e.g. in second order transformations such as spinodal decompositions, for the phase transition to occur over a range of whatever variable is causing the transformation.

Lorenz and co-workers[63] have argued that the fact that the measured charges in many underpotential systems correspond just to a monolayer is strong evidence for the lack of crystallization processes taking place which would be more dependent on pretreatment of electrodes and the purity of solutions. It is difficult however, to reconcile this with fact as any

coincidence between experimental charges and those calculated from adsorption models must be dependent on the roughness factor chosen to represent the electrode surface and also, in the case of polycrystalline electrodes, the number and type of different single crystal grains present in the surface, as the number of adsorption sites depends on crystal orientation. Roughness factors have rarely been determined in U.P.D. studies and no attempt has ever been made to quantify the crystal structures present in the surface of polycrystalline electrodes. Consequently, in view of these uncertainties 'calculated' monolayer charges, for a particular electrode, will always be associated with a certain amount of error and Lorenz's point cannot be substantiated. In addition, the surface coverages corresponding to a complete adsorbed layer are dependent on whether the adsorbed atoms are restricted to interstitial sites between the surface atoms in the electrode or whether a close packed structure is adopted independent of the substrate structure.

Vetter and Schultze[59] have discussed the electrosorption valencies of the 'adsorbed state' in U.P.D. and consider these systems analogous to those in which specific anion adsorption or adsorption of neutral organics takes place. Most recently, Schultze[64] has attempted to explain the linear sweep voltammetry for the deposition of various metals on gold single crystals in terms of ordered structures in analogy to those observed in the vapour phase deposition of metals. In this study certain systems gave very sharp voltammetry peaks e.g. Pb on Au{111} and Cu on Au{100} and to explain these in terms of (Frumkin) adsorption isotherms, it is necessary to use positive interaction parameters. The validity of this procedure will be considered in the results section.

The most positive suggestion that nucleation and growth was involved in the formation of underpotential metal monolayers was made by Astley, Harrison and Thirsk.[28] These workers considered such systems to be analogous to those in which monolayers of mercury salts can be formed at

potentials negative to the reversible potential for the bulk salt, e.g. in the formation of Hg_2HPO_4 the first monolayer occurs approximately 40 mV negative to the thermodynamic reversible potential and is formed by 2-dimensional nucleation and growth processes. Astley *et al.* investigated lead and thallium U.P.D. on polycrystalline and a single crystal {111} silver substrate with potential step techniques. To characterise the monolayer as a 2-dimensional crystal phase, a rising current-time transient with a peak containing a monolayer charge, should be observed (see chapter 1). However this will only result if the incorporation of material into the growing centres is rate determining. In the systems investigated a falling transient was observed which plotted out to give $i \propto t^{-\frac{1}{2}}$ with a positive intercept on the $t^{-\frac{1}{2}}$ axis. This was interpreted as resulting from the instantaneous formation of a very large number of nuclei, due to surface roughness, restricting the rising portion to very short times preventing the observation of a peak. These results were shown to be consistent with a model involving direct deposition from solution, the concentration of ions at the interface being controlled by the Nernst equation and a linearised Langmuir isotherm. However the transients obtained could equally well result from the formation of adsorbed metal layers and cannot be regarded as definitive proof for the existence of the monolayer as a crystalline phase, perhaps, rather proof of the former.

Bowles and Cranshaw[65] investigated the U.P.D. of tin on platinum with *in situ* Mossbauer spectroscopy. The results showed that the deposit was remarkably similar to metallic tin and could not have been obtained from a layer of discrete adatoms. This conclusion is not necessarily applicable to all U.P.D. systems however.

Adzic *et al.*[66] in a reflectance spectroscopic investigation of the U.P.D. of lead on gold concluded that the final state of the monolayer was a crystalline deposit; an ellipsometric investigation of the same system produced similar conclusions. These results will be discussed more fully

in section 2.4 (a).

In conclusion, it seems that the present uncertainty with regard to the nature of underpotential monolayers is in part due to the lack of potential pulse studies. These are capable of yielding the most kinetic information about the deposition process and under favourable circumstances permit a clear distinction between adsorption and crystal phase formation, to be made.

2.3 (d) THE ORIGIN OF MULTI PEAK LINEAR SWEEP VOLTAMMETRY.

In the linear sweep voltammetry of many U.P.D. systems, notably on gold substrates, the deposition and stripping takes place over two or three distinct potential regions, giving the voltammogram a multi peak structure, e.g. Pb on Au,[66] Tl on Au.[67] In some cases, e.g. Pb on Pt,[68] Sn on Ag,[69] the various peaks have been shown to result from the formation of various alloys between substrate and deposited metal. However, when this does not occur, the interpretation has taken various forms.

Schmidt and co-workers consider the various peaks to arise from different adsorbed states[47] whereas Breiter[70] in a voltammetric study of U.P.D. of copper on polycrystalline platinum associated the multiple stripping peaks with bulk copper, thin copper patches and adsorbed atoms. Bowles,[53] in a radiotracer study of the same system, attributed the peaks to dissolution from different crystal faces.

Recently, there have been several studies of U.P.D. on single crystal substrates.[63,64,66,71] Lorenz[71] found for the deposition of thallium on single crystals of silver, no dependence of the deposition peak potential on orientation (only a single deposition peak was observed) but the charge associated with the deposition was found to increase in the order,

$$Q_{\{100\}} > Q_{\{110\}} > Q_{\{111\}}$$

which was explained by a superlattice model of adsorption. This system has

been reinvestigated in the present work and the results are reported in chapter 4. In contrast, Adzic et al.[66] found the L.S.V.'s for the deposition of lead on single crystals of gold were markedly dependent on orientation but the total charge for each crystal face was identical. No attempt to correlate the single crystal voltammetry with that of the polycrystalline sample was made. Schultze and Dickertmann,[64] in a comprehensive voltammetry study of Cu, Bi, Pb, Tl and Sb deposition on gold single crystals also found a pronounced effect of substrate orientation on the peak structure, with each crystal face giving more than one deposition peak. The various peaks were thought to arise from different adsorbed states.

2.4 REFLECTANCE SPECTROSCOPIC STUDIES OF METAL DEPOSITION.

(a) UNDERPOTENTIAL DEPOSITION.

The first reported application of specular reflectance spectroscopy (S.R.S.) to study U.P.D., was that by Takamura et al.[72] in 1969. These workers recorded the reflectance change, using a multiple reflection technique, corresponding to the formation of monolayers of lead and cadmium on gold electrodes. Monolayer deposition caused comparatively large changes in reflectivity (several %), moreover the sign of the change was wavelength dependent.

Shortly afterwards, McIntyre and Kolb[73] reported results for the U.P.D. of silver on platinum. These workers were able to obtain adequate sensitivity using only a single reflection by employing more sophisticated electronic techniques than used by Takamura et al. This work showed that the reflectance change caused by the deposition of a silver monolayer was opposite in sign to that predicted by computer calculations, made using the optical constants for bulk silver but any thicker films produced reflectance changes in agreement with theory. These results were interpreted as being due to the anomalous optical properties of thin metal films.

Takamura et al.[74] studied the U.P.D. of lead, cadmium and copper on

gold. The wavelength dependence of the magnitude and sign of $\Delta R/R$ was explained on the basis of the difference in wavelength dependence of the reflectivity of the bulk metals.

Deposition of silver on gold was also studied by Takamura et al.[75] Films of up to 50nm were investigated and it was shown that the agreement between experimental and calculated wavelength dependencies of $\Delta R/R$ improved with increasing thickness of the deposit. A linear dependence of the reflectance change on the amount of charge passed up to the formation of two atomic layers, was demonstrated and such anomalous optical behaviour for monolayer films as reported by McIntyre and Kolb, was not observed.

Kolb et al.[76] have obtained reflectance-wavelength plots for the deposition of thallium, lead and copper on polycrystalline gold electrodes and, from these, optical constants of the monolayers were calculated. The supposed similarity between these constants and those of gold was interpreted as being due to the measured reflectance changes being principally determined by changes in the gold surface optical properties rather than absorption processes in the metal monolayer. They assumed the partial ionic character of the adatom-substrate bond would produce an enhanced electro-reflectance effect in the gold and this would be the major factor determining the observed reflectance changes, with a smaller effect from absorption processes in the monolayer superimposed on the E.R. spectrum, (the electro-reflectance{E.R.} effect is the change in reflectivity of a surface produced by changes in the electron concentration). This interpretation can be disputed however, as the optical constants obtained by Kolb are approximately as close to those of the bulk metal as they are to gold and in the case of lead, much closer. In addition, the experimental reflectance changes are larger than those calculated from the bulk optical constants and it is difficult to reconcile this fact with Kolb's interpretation. It is possible that his model is meant to apply only to wavelengths near the interband transition of gold where E.R. effects are

large although this is not made clear

Recently, both Takamura et al.[77] and Adzic et al.[66] have again studied the U.P.D. pf lead on gold with a view to explaining the several well defined peaks observed in the linear sweep voltammetry of this system. Takamura simultaneously recorded reflectance-potential and current-potential plots over a wide variety of wavelengths; the latter were electronically intergrated to give charge-potential information and this was correlated with the reflectance data to give reflectance-charge plots corresponding to the monolayer deposition process. At wavelengths remote from the inter-band transition of gold, the relationship between these two quantities was approximately linear for all the deposition peaks but the slope of the plot was slightly different for each peak. The wavelength dependence of the reflectance change for each of the 4 deposition peaks observed in the voltammetry was determined and compared with that expected for a lead monolayer having bulk optical properties. Agreement was best for the most cathodic of the underpotential deposition peaks, but the most anodic peak gave poor agreement. This was assumed to be due to the very strong interaction of the metal adsorbed at the most anodic potentials, with the substrate. They concluded that the U.P.D. of lead on gold was a multi-stage process, each step corresponding to a more dense monolayer packing structure on top of the substrate and that the optical properties of each successive structure gradually approached those of bulk lead.

Adzic, Cahan and Yeager[66] in a similar study of the system, used evaporated, polycrystalline and single crystal gold substrates, although the latter were not employed in optical experiments. The nature of the voltammetry on the single crystal electrodes was shown to be markedly dependent on orientation but no explanation was given for this nor were these results incorporated in the conclusions reached for the polycrystalline behaviour. Their voltammetry on evaporated gold was similar to that of previous workers on this system, yet the most cathodic deposition peak

appeared to be much sharper than was normally found (in a later paper Yeager attributes this to the evaporated gold surface having mainly a {111} orientation; this single crystal also gave a very sharp peak at the same potential). This peak was also found to give a different reflectance-charge behaviour than those at more anodic potentials. This optical effect and the remarkable sharpness of the voltammetry peak prompted Adzic et al. to suggest that it corresponded to a phase transition from a partially ionic to a crystalline layer of lead. The charge associated with the sharp peak was thought to result from the complete neutralisation of the ionic species adsorbed at more anodic potentials and the two separate processes occurring were expressed as follows,

more anodic process $$Pb^{2+}_{(soln)} + (2-y)e^- \rightleftarrows Pb^{y+}_{(ads)} \qquad (1)$$

more cathodic process $$Pb^{y+}_{(ads)} + ye^- \rightleftarrows Pb_{(ads)} \qquad (2)$$

This explanation was challenged by Schmidt and Wüthrich[61] on the basis that their data for lead'adsorption' on gold, obtained with the twin electrode thin layer technique, did not reveal any deviation from a linear relation between the amount of lead adsorbed and the charge passed through the electrode, at the potential corresponding to the sharp peak. This difference in interpretation will be considered in a later section, in the light of results reported from the present work.

More recently, an ellipsometric investigation of the same system was undertaken by Horkans, Cahan and Yeager.[56] The potential and wavelength dependence of the complex refractive index of the(partial) monolayer was determined. The results indicated that the 2 main current peaks in the voltammetry curves were associated with surface states neither of which had optical properties resembling those of bulk lead. However the optical properties of the lead film deposited at the potential of the more cathodic

current peak { (2) in the above equations } were more typically metallic. (higher values of ε'' than those of lead deposited at more anodic potentials). This evidence was thought to substantiate that from the previous reflectance and voltammetric study, indicating that initially the lead ions are adsorbed with a partial charge transfer, which, at more cathodic potentials, undergo a transition into lead patches of predominantly metallic character.

In view of the various interpretations of the nature of the reflectance change associated with U.P.D., it is worthwhile summarising the position.

Although there is general agreement that the interaction between the substrate and the underpotential deposit will result in a modification of the former's optical properties, opinions differ as to the mechanism of this modification. The viewpoint of Kolb and co-workers has already been mentioned. The modification of the substrate optical properties is thought to arise from the partially ionic character of the metal adatoms increasing the free electron concentration in the substrate surface layer, thereby producing an enhanced electro-reflectance effect. However, at wavelengths where the electro-reflectance of gold tends to zero, Kolb argues that absorption effects in the monolayer would contribute a much greater fraction to the observed reflectance change.

Yeager and co-workers[66] also assume the strong interactions between monolayer and substrate would result in substantial changes in the complex refractive index of the gold surface but they do not postulate any enhanced electro-reflectance effects: adsorption processes in the monolayer itself are also thought to be important but these will be affected by the interaction with the substrate.

Takamura and co-workers explain their results simply on the basis of absorption processes in the monolayer which, at low coverages, will be affected by the interaction with the substrate.

2.4 (b) METAL DEPOSITION ON SEMI-CONDUCTOR SUBSTRATES.

In addition to work on metal substrates, Kolb and co-workers[67,78] have studied deposition onto compound semi-conductor electrodes. These have received increasing attention in recent years on account of their utility in electrode kinetics.[79]

Reduction of a compound semi-conductor results in the deposition of metal atoms from the lattice onto the surface of the semi-conductor. However, in a cathodic scan, hydrogen evolution normally begins anodic to the potential where reductive deposition commences. Consequently conventional electrochemical techniques involving measurement of current and/or voltage yield little information about the lattice reduction process as this is masked by the hydrogen evolution current. In such cases however, S.R.S. constitutes an extremely sensitive and selective tool as the reflectance changes associated with gas evolution processes are very much smaller than those resulting from metal deposition which can therefore be studied in isolation from interfering (gas producing) reactions. Moreover the large differences in the optical properties of the semi-conductor substrate and the metal film deposit results in such large reflectivity changes on deposition that fractions of a monolayer may easily be detected (this also applies to many metal deposition processes on metal substrates.)

To date, metal deposition onto zinc oxide has been studied in some depth and this will be illustrated here with the example of zinc deposition.

ZINC DEPOSITION ON ZINC OXIDE.

Zinc deposition may be affected by either cathodic decomposition of the semi-conductor lattice or by reduction of zinc ions in solution. It was found that, whereas the reflectivity change associated with the former process was always positive, that resulting from the latter mode of deposition depended on the zinc ion concentration. For example, at Zn^{2+}

levels of 5×10^{-5}M, the sign of $\Delta R/R$ was always positive for the deposition process, (i.e. metal deposition caused an increase in reflectance). Non metallic optical properties were sustained for two to three monolayers whereas thicker films had optical characteristics typical of a bulk metal ($\varepsilon < 0$). Similar results were found for metal deposited directly from the semi-conductor lattice. However, the deposition associated with Zn^{2+} concentrations of 5×10^{-4}M resulted initially in a decrease in reflectivity, which at more cathodic potentials (in a sweep experiment) or longer times (in a pulse experiment) became an increase. This latter type of behaviour indicated that metallic optical properties were not achieved until films of several monolayers thickness had been deposited.

These interesting results were interpreted as being due to the higher three-dimensional nucleation rates in the solution of higher zinc concentration resulting in rough films with an island structure, whereas the lower deposition rates obtained with the more dilute metal ion solution were thought likely to produce much smoother, island free films with more typically metallic optical properties.

2.5 OTHER STUDIES INVOLVING U.P.D.

Recently several studies have been devoted to the catalytic effect of underpotential metal monolayers. Adzic and Despic found that the presence of foreign metal monolayers on gold could substantially increase the rate of the Fe^{2+}/Fe^{3+} redox couple.[80] This was interpreted as being due to the change in the work function of the substrate by the foreign adatoms; such effects have been well established in gas phase studies.

Watanabe and Motoo[81] found that the presence of gold atoms could enhance the rate of oxidation of formic acid on platinum. In a more detailed study of the same reaction, Adzic *et al.*[82] considered the effect on the oxidation rate of cadmium, thallium, bismuth and lead monolayers on gold.

A seventy fold increase in the rate was observed on lead monolayers, with the other metals giving somewhat lower enhancement factors. This effect was thought to be mainly attributable to the decreased rate of hydrogen adsorption as compared to that on platinum surfaces. This would prevent the formation of the main poisoning species ($\dot{C}\ddot{O}H$) by a reaction which involves adsorbed hydrogen.

2.6 THE RELEVANCE OF U.P.D. TO THE BULK DEPOSITION PROCESS.

Recently there have been attempts to correlate the underpotential monolayer formation with the subsequent electrocrystallisation of the bulk deposit. Klapka[83] suggested that the presence of an adsorbed metal monolayer might promote the formation of nuclei in the overpotential region. Astley et al.[28] found no difference in the growth kinetics of bulk lead on silver if the monolayer was preformed or not. The fact that U.P.D. occurs in so many of the systems involving metal deposition onto a foreign substrate prompted Lorenz[63,84] to suggest that it could be considered as the regular initial stage in such electrodeposition processes. In addition, Lorenz argued that the low (< 10mV) overvoltages required for the initiation of bulk growth suggested the formation of two rather than three-dimensional nuclei in this potential region. Kolb et al.[57] have attributed the fact that the optical properties of thin metal deposits formed on top of underpotential monolayers reach those of the bulk metal at much lower thicknesses than evaporated films, to the monolayer promoting the growth of subsequent deposits in regular layers rather than three-dimensional islands

To date however it has not been conclusively established if the formation of the metal monolayer is an essential precursor to the growth of thicker deposits. Indeed, many studies involving bulk electrocrystallisation on platinum substrates have ignored completely the possibility of an initial monolayer formation.[19] Clearly it is crucial to establish the role, if any, played by the metal monolayer in subsequent growth steps as this would give greater insight into the nucleation process occurring in such

systems.

In this context it seems relevant that Vermilyea[20] in a 1963 review on anodic film formation discussed* the implications of the expression relating the radius of the critical nucleus, $r^{\times}$, (that which has maximum energy) to the relevant surface energy parameters, which is

$$r^{\times} = \frac{a\sigma_3}{-a\Delta G_v - (\sigma_2 + \sigma_3 - \sigma_1)}$$

where,

a = height of patch,

ΔG_v is the free energy change per unit volume accompanying the formation of the film,

σ_1, σ_2 and σ_3 are the free surface energies of the electrode-solution, electrode-film and film-solution interfaces respectively.

If $\sigma_2 + \sigma_3 - \sigma_1 = \Delta\sigma$, is negative, $r^{\times}$ becomes positive even for somewhat positive values of ΔG_v, i.e. when the bulk phase is unstable. He argued that this would imply the electrode should be covered with a monolayer of reaction product at a potential more negative than the equilibrium potential for the reaction* and that this would provide a surface where subsequent deposition could occur with little overpotential. Calculations using typical values of σ_1, σ_2 and σ_3 suggested that most metals should be covered with monolayer (anodic) films below the equilibrium potential. The scarcity of reliable experimental data at the time however, prevented Vermilyea from supporting these calculations with experimental evidence. Subsequent work on anodic film formation, reviewed by Harrison and Thirsk[22], revealed many examples of this type of behaviour however.

---

*Bewick et al.[11] had also reached the same conclusion somewhat earlier.

Fleischmann and Thirsk's review[25] 'Metal Deposition and Electrocrystallisation' dating from the same period as Vermilyea's article omitted any mention of U.P.D. of metals and the relevance of metal monolayer formation in the electrodeposition process.

2.7 THE SCOPE OF THE WORK DESCRIBED IN THIS THESIS.

This chapter has shown, despite the extensive studies of U.P.D. by several groups, there are several central problems which are still unresolved. These relate principally to the nature of the layer (adsorbed or crystalline), the interpretation of multi-peak linear sweep voltammograms, the origin of reflectance changes associated with U.P.D. and the relevance of monolayer growth to the overpotential deposition process.

The aim of this project was to attempt to provide satisfactory solutions to these outstanding problems. The degree to which this has been achieved is considered at the end of this Thesis.

Two underpotential systems have been selected for study; thallium on polycrystalline and single crystal silver and lead on the same substrates. In addition, the kinetics of the overpotential deposition of lead on silver single crystals have also been investigated. Silver posesses advantages over platinum and gold for electrochemical and optical work in that, unlike gold, no interband transitions occur in the visible part of the spectrum which complicate the interpretation of optical results. U.P.D. on platinum is invariably complicated by hydrogen and oxygen co-adsorption processes, moreover the ease of oxide formation limits the stability of single crystal surfaces.

The techniques employed are linear sweep voltammetry, potential step, constant current potential decay and modulated reflectance spectroscopy.

CHAPTER THREE: EXPERIMENTAL TECHNIQUE.

3.0 INTRODUCTION

The experimental work described in this Thesis can be divided into two categories;

a) Conventional electrochemical experiments e.g. linear sweep voltammetry and potential step measurements.

b) Optical experiments employing modulated reflectance spectroscopy.

A description of the apparatus and techniques involved in both categories of experiments will be given in this chapter together with the methodology associated with the preparation of electrodes, solutions and glassware etc.. Finally a description of the experimental procedure adopted in each type of measurement will be given.

3.1 THE ELECTROCHEMICAL CONTROL EQUIPMENT

Three electrode optical cells were used throughout the work and will be described later. All potential programming of the working electrode was supplied from a potentiostat (types used were Chemical Electronics models V 150/1.5A, TR70/2A or a Hi-Tek Instruments model DT 2101) in conjunction with a Chemical Electronics waveform generator (type RB1). This latter instrument provided either,

a) a ramp type voltage output for linear sweep voltammetry,

or b) single or double potential steps.

In voltammetry, cell currents were recorded as voltages on an XY recorder (types Bryans 26000 or Hewlett Packard 7015A).

The oscilloscopes employed for the observation of current-time transients or other functions to rapid to be recorded directly onto an XY recorder were Tektronix 547 or 5030. Permanent records of such transients were obtained using a Hi-Tek Instruments signal averager (type AA1) in conjunction with an XY recorder. The mode of operation of the averager will be described in the optical section of this chapter.

Integration of current-time information was achieved using an integrator (constructed in these laboratories) with an analogue output.

3.2 THE OPTICAL EQUIPMENT.

The basic optical experiment consisted of measuring the reflectance changes which occurred at the working electrode as its potential was scanned in a linear manner in the deposition potential region. The experimental principles have already been mentioned but the particular method adopted in this work will now be described.

Although the reflectance changes associated with the formation of lead or thallium monolayers on silver are typically of the order of a few percent, this value is not sufficiently high to permit the direct recording of the reflectance-potential/time profile resulting from linear potential scans in the U.P.D. region, as noise, both random and periodic, will distort the true optical response. The periodic noise is almost entirely 50 Hz resulting from residual mains ripple on the direct voltage applied to the lamp. Provided the optical cell is enclosed in a darkbox, 50 Hz noise pick-up from other sources of light e.g. indicator lamps on equipment, is negligible. Random noise results from the photodetector, changing levels of background light intensity in the immediate environment of the optical detector (these are also negligibly small inside a dark-box) or possibly, fluctuations caused by the electrochemical process itself. To record a signal of high signal/noise ratio, it is necessary to eliminate these two sources of noise. The well known method of signal averaging has been employed here. This technique relies on the fact that the time average resulting from the superposition of a number of (in this case) reflectance -potential sweeps each of which has random and periodic noise associated with it, will be the true optical response devoid of any noise. This statement is valid provided that any periodic noise on the reflectance signal is not time locked to the repitition rate of the linear sweeps (e.g. as would be the case if the beginning of each sweep coincided with the same point on the 50 Hz mains sine wave). On each cycle of the signal, the averager samples the signal input at fixed time intervals, converts the

sampled voltages into digital form and stores the information in a memory having one location for each sample (256 locations in all). This sampling process is repeated a preset number of times, 'n'; a trigger signal from the waveform generator ensures that the samples are taken at equivalent points on each cycle. Each new sample is added algebraically to the value already accumulated in the memory location, so that the final value stored is equal to 'n' multiplied by the average value of the sample taken at that point. If one assumes the electrochemical process itself produces no random fluctuations in the signal level, the signal content of each sample point is constant, and therefore its contribution to the value stored will increase linearly with 'n'. However, as 'n' increases, the average value of the noise will approach zero.

The overall signal to noise improvment, $(SN)_n$, is given by

$$(SN)_n \propto n^{\frac{1}{2}}$$

Typically in the optical experiments described here, the value of 'n' used was 32 or 64. A similar number of repetitions was employed for recording current-time transients in the U.P.D. region.

A block diagram of the optical apparatus is shown in Fig. 3.1. The light source employed was a 200W Hg-Xe arc (Engelhard-Hanovia 901-B1) mounted in a steel housing (Oriel Optical Corp. 6165) fitted with a virtually vibration free fan. The housing was also fitted with a U.V. grade 35mm aperture f1.0 fused silica condensing lens assembly. The lamp power supply consisted of a high stability D.C. unit constructed in these laboratories which supplied 9 amps at 22 volts, with a current ripple in operation of less than 0.1%.

The light from the lamp was focused on the entrance slits of the monochromator (Bauch and Lomb High Intensity Model) fitted with a U.V.-visible diffraction grating (range 200 to 700nm). In practise a wavelength range of 300 to 600nm was used. At wavelengths longer than 500nm an optical filter was employed to remove unwanted 2nd. order diffracted

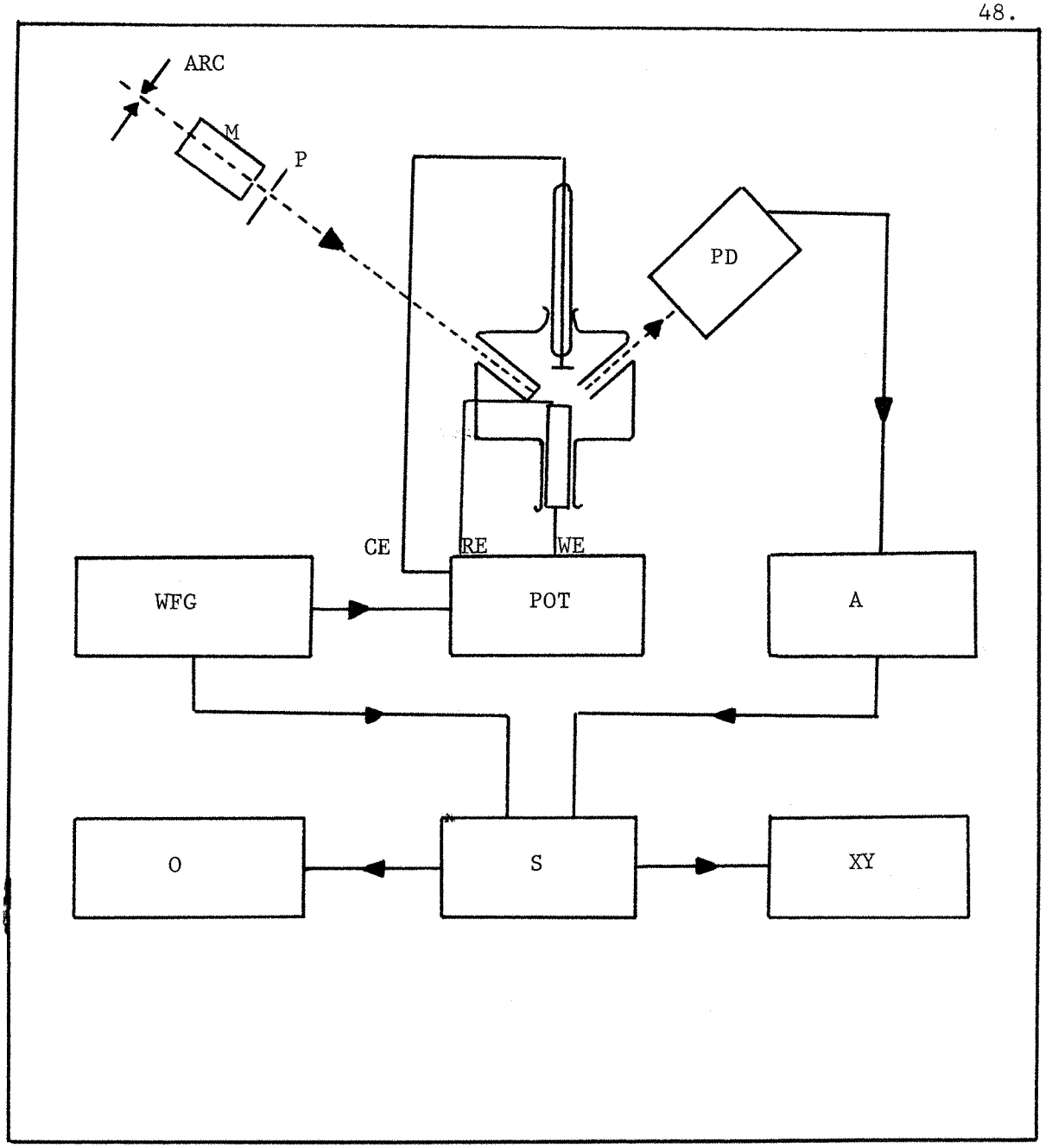

Fig. 3.1. A block diagram of the optical apparatus.

ARC = Arc lamp.

M = Monochromator, P = Polarizer.

PD = Photo-detector, CE = Counter electrode.

RE = Reference electrode, WE = Working electrode.

WFG = Waveform generator, POT = Potentiostat

A = Amplifier, O = Oscilloscope,

S = Signal averager, XY = XY recorder.

beams.

The monochromatic beam was then polarised parallel or perpendicular to the plane of incidence at the electrode surface using a U.V.-visible plastic polariser (Polarisers Ltd. type HNP'B) and then focused onto the working electrode with a 25mm. diameter f.1.0 Spectrosil lens (Thermal Syndicate Ltd.). A similar lens focused the reflected light onto the photo--detector which was a vacuum photodiode (EMI 9715QB). This was connected directly to a current follower constructed using Philbrick-Nexus 1009 operational amplifiers. Feedback resistors could be selected in the range 10K ohm to 1M ohm depending on the intensity of light reaching the detector. Typically a value of 0.1M ohm was used.

The output from the photodiode was amplified with a low noise differential amplifier and then fed into the input of the signal averager (Hi-Tek Instruments AA1). The voltage output of the photodiode could be read simultaneously on a D.V.M..

All the optical components were mounted on a single optical bench, apart from the photodiode and its collimating lens, which were mounted on a second optical bench perpendicular to the first one. This arrangement was possible because an angle of incidence of 45^{o} was used throughout the work. The optical benches were bolted onto a heavy wooden table which rested on inflated rubber inner tubes to curtail vibrational effects.

The position of the optical cell could be adjusted in the three translational modes by means of knurled thumb screws such that a precise alignment of the working electrode with the incident light beam was possible.

A large light-proof box enclosed all the optical components, except for the lamp and monochromator, in order to exclude ambient light.

3.3 THE ELECTROCHEMICAL CELL

The optial cell was used for all measurements, whether optical or not. This is shown in Fig. 3.2. An angle of incidence of 45^{o} was used throughout the optical work as this minimised optical effects due to structural changes

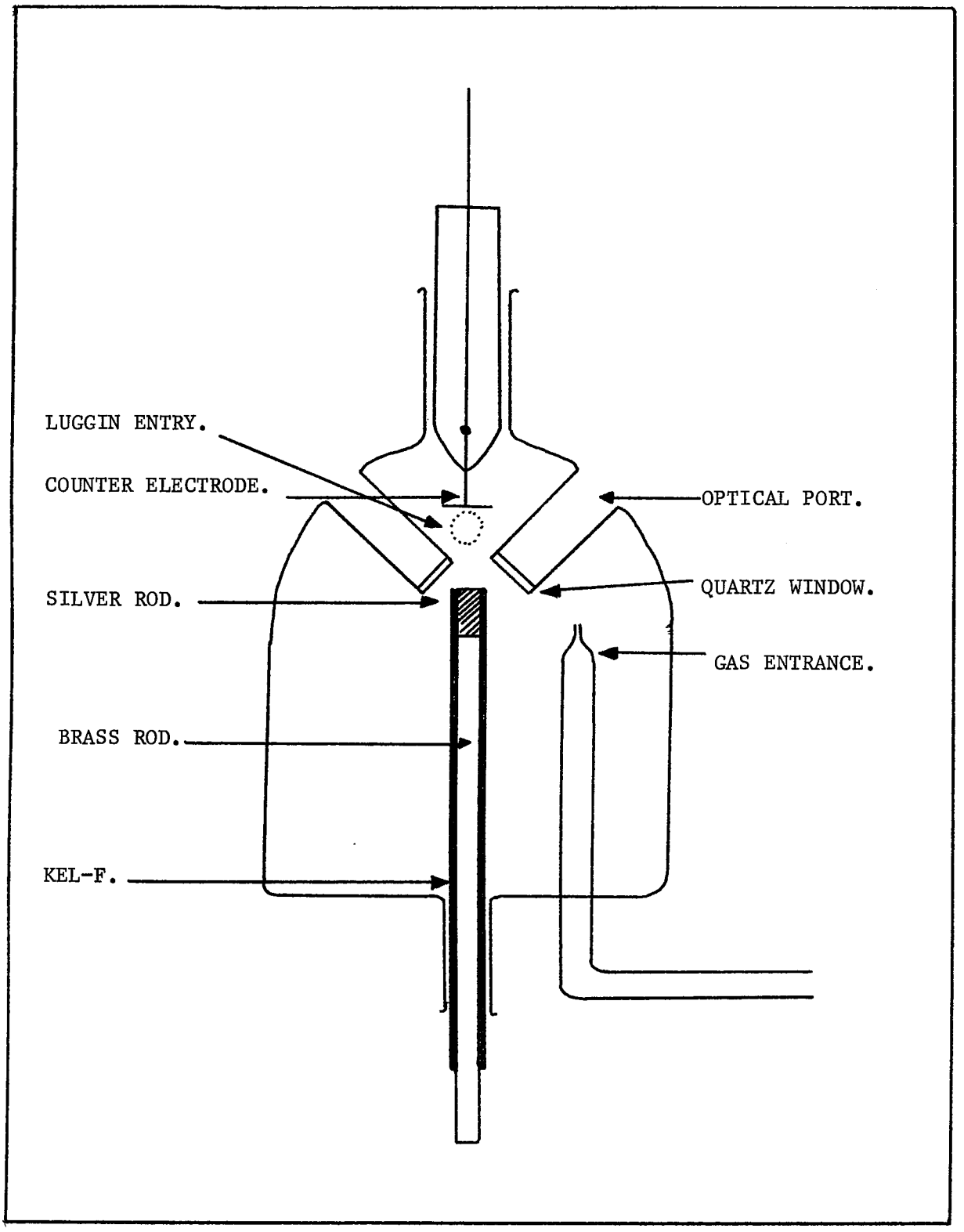

Fig. 3.2. The optical cell. The gas exit and Luggin capillary are not shown.

in the double layer (e.g. changes in water concentration or specific ion adsorption).

The cell was composed entirely of glass except for the optical windows which were 1cm diameter Spectrosil discs; these were inset into the cell to minimize the optical path length. The working electrode and Luggin capillary were positioned in syringe barrels such that optimum placement for the incident light beam could be accomplished. The counter electrode was a platinum disc of area $\sim 1cm^2$ positioned parallel to the working electrode.

The working electrodes were small cylinders of polycrystalline (Johnson-Mathey 99.9999%) or single crystal silver (Metals Research Ltd. 99.9999%), 5-6mm diameter. These were sealed into Kel-F rod such that only the top surface of the metal cylinder was exposed to the solution. Great care was taken to ensure that no leakage occurred around the side of the metal crystal. This was achieved by cooling the cylinder of silver in liquid nitrogen before mounting in the hollow Kel-F rod (drilled for a tight fit at room temperature) which had been placed in boiling water so that insertion of the metal cylinder was facilitated. The subsequent expansion of the metal and contraction of the plastic housing ensured a very tight fit. Electrical contact was made via brass soldered to the silver cylinder. Occasionally a vitreous carbon working electrode was used which was constructed in a similar way. The reference electrode which was housed at the end of a Luggin capillary was either a saturated calomel(S.C.E. Radiometer K401) or lead or thallium wires sealed into glass holders.

3.4 PREPARATION OF SOLUTIONS AND GLASSWARE.

Prior to use all glassware was soaked in a mixture containing equal volumes of concentrated nitric and sulphuric acids to remove any traces of grease, then it was rinsed thoroughly in tap water, singly distilled and finally triply distilled water. The latter was prepared by slow distillation from a weakly alkaline solution of $KMnO_4$ and then

from a solution containing a trace amount of ortho-H_3PO_4. All solutions were made up from Analar grade chemicals (without further purification) in triply distilled water. Prior to each experiment the solutions were deaerated inside the cell by purging with a stream of oxygen-free nitrogen, for about 25 minutes.

3.5 ELECTRODE PREPARATION.

The importance of electrode surface preparation cannot be over-stressed in connection with metal deposition work and this point will be illustrated in the next chapter. The surface preparation procedure finally adopted for the silver electrodes (both polycrystalline and single crystal) was the result of investigating a number of other methods. The criteria used to judge the success of each method was based on the best reproducibility of the experimental data and the clearest delineation of the various features on the voltammetric and optical characteristics. The polishing process consisted of two stages, the first mechanical and the second chemical.

Firstly, the silver electrodes were polished on selvyt cloths impregnated with alumina. Initially a 5μ grade is used and then progressively smaller particle sizes down to 0.3μ, until the electrode had a mirror-like appearance free from scratches or other blemishes. These mechanical polishing steps were always performed manually rather than on a polishing machine, which was less convenient to use. Before each experiment, the electrodes were chemically polished using a modified version of a process described by Soderberg.[85]

First, the electrode was immersed in a mixture containing equal volumes of NaCN solution (21g dm^{-3}) and 20 volume H_2O_2, for about 3s (or less if gas evolution occurred), followed by exposure to the air until gas evolution occurred on the surface. The electrode was then re-immersed in the $NaCN/H_2O_2$ mixture for about two seconds and then

immersed in another (purely) NaCN solution (37.5 g dm^{-3}) until gas evolution ceased. This cycle was repeated about 10 times or until a highly reflecting homogeneous surface was obtained. The appearance of the polycrystalline silver was that of a mosaic with grain boundaries plainly visible whereas the single crystal surfaces were featureless. This polishing process, like most of its type, required a considerable amount of practise before consistent results were obtained.

Examination of the electrode surface with X-ray emission spectroscopy revealed no contaminating elements except very minute particles of alumina, but these were very few in number (on the sample investigated only one particle of alumina was found in an area of $\sim 0.25 cm^{-2}$).

The amount of silver dissolved in the chemical polishing process was very small. Indeed, over a period of use of two years, during which time the crystals would have been chemically polished several hundred times each, the length of the crystals had decreased by only 20% (1mm) and much of this would have been removed in the mechanical stage of the polishing process. Such small dissolution rates are a prime requisite of chemical polishing processes used in the preparation of expensive single crystals.

The vitreous carbon electrode was mechanically polished in an identical manner to the silver electrodes.

After polishing the working electrodes were thoroughly washed, first in flowing tap water, then singly and finally triply distilled water before being placed in the cell.

3.6 EXPERIMENTAL PROCEDURES.

a) NON OPTICAL EXPERIMENTS.

The types of non optical experiment used were,

1. Linear Sweep Voltammetry (L.S.V.).

2. Single, double and triple Potential Step measurements.

3. Constant current, Potential decay experiments.

1. LINEAR SWEEP VOLTAMMETRY.

An investigation of the linear sweep voltammetry behaviour exhibited by a particular electrode/solution combination was the prelude to all experiments, both optical and non-optical. In many cases it constituted the whole experiment. The appearance of the voltammogram was a direct indication of the nature of the electrode surface and consequently could be used to assess the degree to which the chemical polishing step had been successful in producing a well defined crystal plane (in the case of single crystals). For any particular system, repeated linear sweep experiments were performed before any additional measurements were made in order to establish an arbiter to which all future voltammetry could be referred. Optical or potential step measurements were only made if the linear sweep voltammetry was identical or very close to the accepted arbitrary standard, which was the clearest delineation of the voltammetric features. The procedure described here for L.S.V. is that which was finally adopted after trying a number of slightly different approaches. It enabled a given solution/electrode combination to be used for a whole days experiments without any deterioration in the results over this period.

Firstly, the cell complete with working electrode (not yet freshly chemically polished) was rinsed thoroughly in tap, singly distilled and triply distilled water. Then the cell was rinsed with the solution being used and finally filled with it. This was followed by deaeration with a rapid stream of nitrogen (scrubbed by a vanadous ion mixture), for about 25 minutes. During this process the working electrode was polarised at a potential slightly positive to that where U.P.D. began. At the end of the deaeration period, the working electrode was removed from the cell and chemically polished as described earlier and after thorough

rinsing was placed back in the cell. The process of polarising the electrode during the gas purging acted as a mild pre-electolysis method and impurities were removed from the solution. That this was the case could be seen by carrying out voltammetry with the electrode at the end of the degassing period, without chemical polishing, when markedly inferior results were obtained.

Voltammetry experiments would then be carried out in the normal way; the potential being cycled continually and sweeps recorded when necessary at a variety of sweep speeds.

2. POTENTIAL STEP MEASUREMENTS.

Single and double potential steps could be applied to the working electrode with the RB1 waveform generator.A pulse train was usually employed with the metal dissolution pulse about ten times the length of the deposition ones, to ensure steady state conditions.

All experiments in the overpotential region were done with a Hi-Tek Instruments potentiostat as it posessed extremely good potential stability which was necassary for this part of the work. This potentiostat was a two channel instrument and the potential applied to the working electrode could be switched from channel A to channel B by electronic or manual triggering. This facility, in conjunction with the double potential step available from the waveform generator enabled triple potential step experiments to be performed.

If the potential steps were of sufficient duration and the current did not vary rapidly with time, the transient was recorded direct-onto an XY recorder with a time base supplied from a signal averager. When this was not possible, the averager was used to store and average the current transient which could then be played back onto a recorder.

3. CONSTANT CURRENT, POTENTIAL DECAY EXPERIMENTS.

Potential/time decay curves were obtained in the following manner,

a) the working electrode was potentiostated at about 20mV anodic to the bulk reversible potential of thallium or lead for several seconds;

b) the potentiostat was switched out of curcuit to open curcuit the electrode;

c) the electrode was connected to a known anodic leak and its potential plotted onto an XY recorder as a function of time.

In each case the decay rate was sufficiently slow for the potentials to approximate closely to equilibrium values.

3.6 (b) OPTICAL EXPERIMENTS.

The experiments performed were:

1. Reflectance-potential sweeps as a function of wavelength.
2. Reflectance-time transients as a function of wavelength.
3. Simultaneaous recording of reflectance-potential and charge-potential sweeps as a function of wavelength for construction of reflectance-charge plots.

1. REFLECTANCE-POTENTIAL SWEEPS.

Firstly, the voltammetry was checked as already described and if satisfactory the cell was aligned with the optical beam. The sweep speed was adjusted until the time interval of a single return linear sweep was equal to,

256× time per sample.

The reflectance-potential characteristic was then averaged until a noise free signal was obtained (the output of the signal averager being monitored continuously on an oscilloscope). The reflected light intensity associated with the metal (film free) electrode would be measured on a D.V.M., this gave R_o. This procedure would be repeated at other wavelengths and the data used to construct a reflectance spectrum associated with monolayer deposition as described in the results section.

The quantity $\Delta R/R$ is here defined as,

$$\frac{\Delta R}{R} = \frac{R_\theta - R_0}{R_0}$$

where, R_θ is the reflectivity of the film covered electrode.

R_0 is the reflectivity of the bare electrode.

2. REFLECTANCE-TIME TRANSIENTS.

The reflectance-time transient associated with a potential step would be measured; the time per sample on the averager being determined by the length of the deposition transient.

3. CORRELATION PLOTS.

These involved correlating the measured reflectance change associated with metal deposition, with the corresponding charge passed. Normally this was done for reflectance-potential sweeps only. At a given wavelength, a reflectance-potential sweep would be obtained as described above. Then an equivalent charge-potential sweep would be recorded directly by electronically integrating the current flowing with an integrator with analogue output. A reflectance-charge plot could then be constucted by taking reflectance and charge values at equal potential intervals. Although the reflectance and charge values were recorded at slightly different times, this was not a source of error as the results showed no variation with time provided the potentiostat showed no significant drift (less than 1mV) during the interval. Great care was taken to ensure that this was the case. In some cases, where the reflectance changed very rapidly in a narrow range of potential, it was essential to use a transistorised potentiostat for potential control as these had lower drift characteristics than the valve models.

CHAPTER FOUR: UNDERPOTENTIAL DEPOSITION OF THALLIUM ON SILVER.

4.0 INTRODUCTION.

This chapter begins with a description of how a conventional surface preparation technique for silver, was shown to be unsatisfactory. Voltammetry results for chemically polished polycrystalline and single crystal electrodes are presented and based on these, a tentative mechanism will be proposed for the underpotential deposition process. Optical, potential step and potential decay results are discussed in connection with the proposed scheme. Finally the effect of anions, pH and thallium ion concentration are considered.

4.1 OPTICAL AND ELECTROCHEMICAL BEHAVIOUR OF MECHANICALLY POLISHED POLYCRYSTALLINE SILVER ELECTRODES.

The surface preparation methods available for silver range from purely mechanical methods (e.g. with alumina or diamond paste) to mechanical methods followed by a chemical or electrochemical polishing step. The evidence available in the literature suggested electrochemical polishing methods were unreliable in producing a contamination free surface.[86] Chemical polishing methods were rare and the most generally satisfactory method of surface preparation seemed to be alumina polishing. In view of the fact that previous optical studies of U.P.D. on gold and platinum substrates had used electrodes polished in this way, the initial experiments were performed with alumina polished electrodes.

Fig.4.1 shows a linear sweep voltammogram for thallium deposition onto a mechanically polished polycrystalline silver electrode, from a sulphate base electrolyte. The familiar pair of peaks around -520mV (vs. S.C.E.) are associated with the formation and dissolution of the thallium monolayer. A small peak on the rise in current due to the onset of bulk deposition can also be seen and could possibly represent the formation of a second monolayer. This voltammogram is very similar to that obtained by Lorenz[63,71,84] on polycrystalline and single crystal samples of silver, polished in

Fig. 4.1. L.S.V. for thallium deposition on mechanically polished polycrystalline silver.

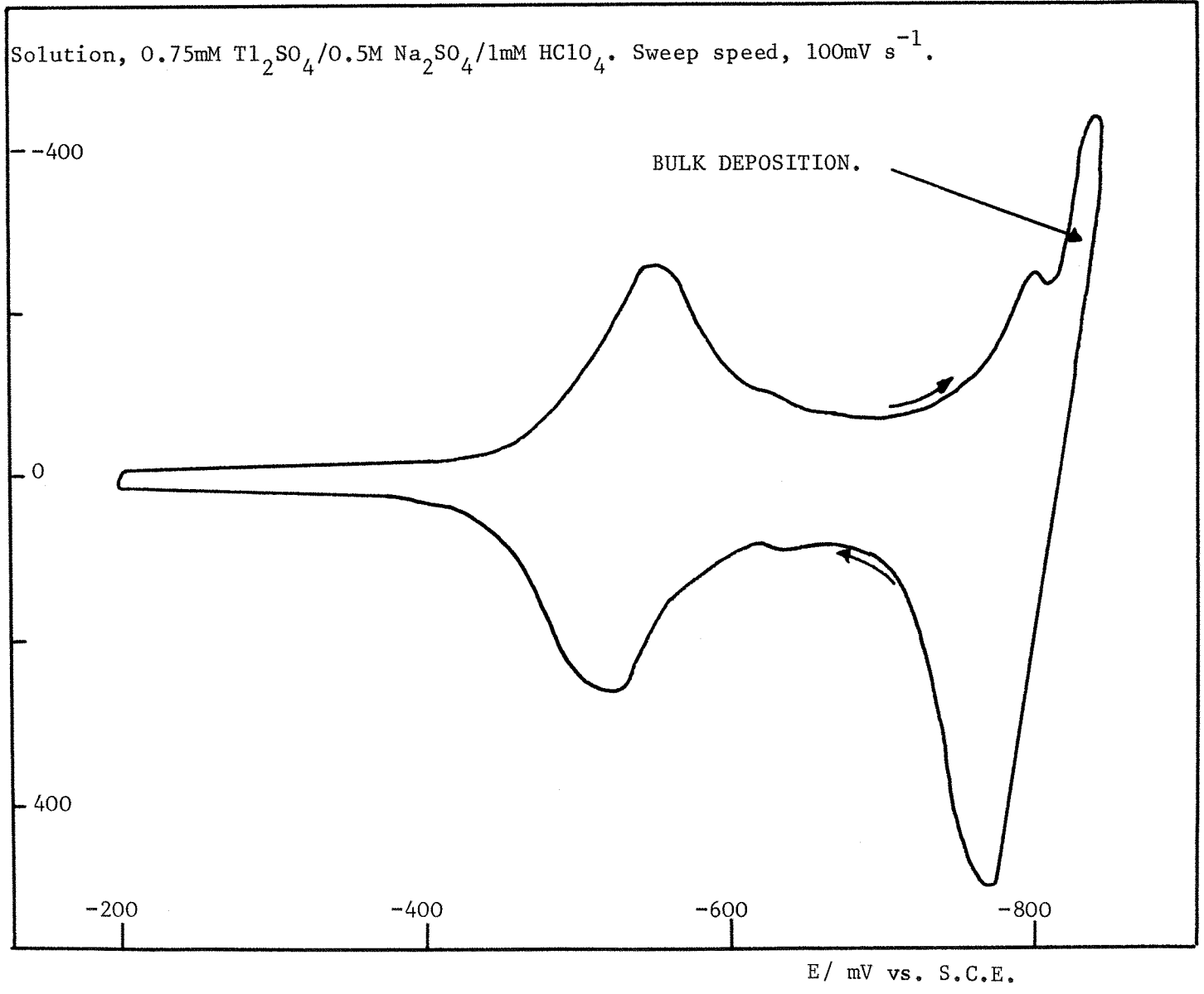

an identical manner to the method used here.

One of the initial aims of this project was an investigation of the optical properties of thin metal films. The reflectance variation associated with the metal deposited in a linear sweep experiment is shown in Fig.4.2 (a) (in the unfolded format) together with the associated linear sweep voltammogram. It is seen that, although monolayer formation produces the expected (from calculations using the optical constants of bulk thallium) decrease in reflectance, bulk deposition causes an immediate increase in reflectance which changes to a decrease after the deposition of a certain amount of metal. On the reverse sweep, this decrease continues until the reversible potential is reached. At this point the optical sweep shows a remarkable peak structure which fits exactly with the bulk stripping peak in the voltammetry. This type of behaviour would not be expected from the optical model normally used to represent the deposition process.[87] Experiments showed that the length of time the electrode was polished and the grade of alumina used in the final step were important in determining the nature of the optical sweep. Similar results were obtained from electrodes polished with diamond paste.

In view of the dependence of the optical results on the exact details of the polishing process, it seemed likely that residual surface roughness was the main factor causing the anomalous optical behaviour. Silver is a relatively soft metal and it is possible that alumina polishing was producing a highly distorted surface region with no well defined crystallographic features. An electron diffraction study of mechanically polished single crystals of silver showed that surfaces polished with 0.1μ alumina were considerably distorted[88] (0.3μ was the finest grade employed in the present work). A perfect crystal structure could only be obtained by lightly chemically etching the mechanically polished surface.

The optical effects of a rough silver surface have been discussed by Beaglehole et al.[89] They found that when light is reflected from a rough

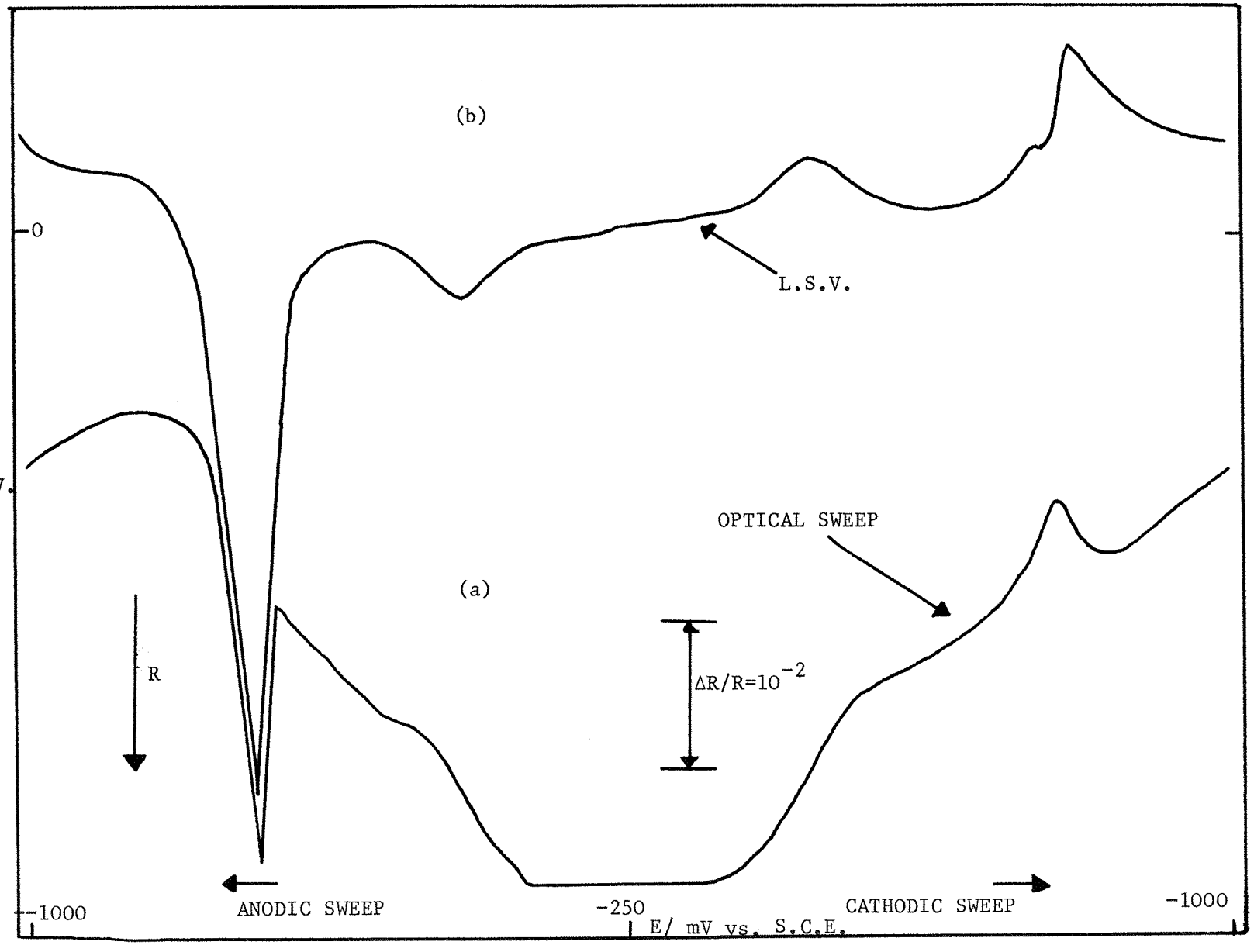

Fig. 4.2(a) Optical sweep for thallium deposition on a mechanically polished polycrystalline silver electrode. Solution, 2mM $TlNO_3$/0.5M $NaClO_4$/10mM $HClO_4$. Sweep speed 250 mV s^{-1}. λ = 440nM. Parallel polarisation. (b) the L.S.V. corresponding to (a).

surface, the beam comprises both specular and scattered components and also that surface currents may be excited and dipoles introduced across pits and bumps on the surface. It was shown that the difference in reflectivity between a rough and a smooth silver surface, reached a maximum at 380nm, a wavelength very close to that where the unusual behaviour observed in the reflectance-potential sweeps of the present work, is most predominant. This seemed to confirm the idea that surface roughness problems were giving rise to the anomalous optical behaviour. Previous optical studies of U.P.D. on gold and platinum [72-76] did not show the same effects of mechanical polishing as seen here presumably because the greater hardness of these metals resulted in much less surface deformation

Chemical polishing or etching methods are capable of removing the distorted surface layers left by mechanical polishing. However difficulty was encountered in finding a method which gave consistent results. The process used by Schmidt and co-workers [90] in their work on silver electrodes was found to give the optical behaviour expected of a metal deposition system but reproducibility was poor. The technique eventually adopted was that described in the experimental section. When a certain amount of practise had been acquired in its use, it was found to give extremely reproducible optical and voltammetry results. A reflectance-potential sweep obtained on a polycrystalline electrode polished in this way, is shown in Fig.4.3. It is free from the peculiarities resulting from surface roughness evident in Fig. 4.2 (a). In fact the chemically polished electrodes were completely free from problems of this nature except in a small wavelength region around 360nm where surface plasmon excitation [91] can occur.

4.2 LINEAR SWEEP VOLTAMMETRY BEHAVIOUR OF CHEMICALLY POLISHED POLYCRYSTALLINE SILVER.

Fig.4.4 shows a L.S.V. obtained using a polycrystalline electrode polished as described in the experimental section. In contrast to the L.S.V.

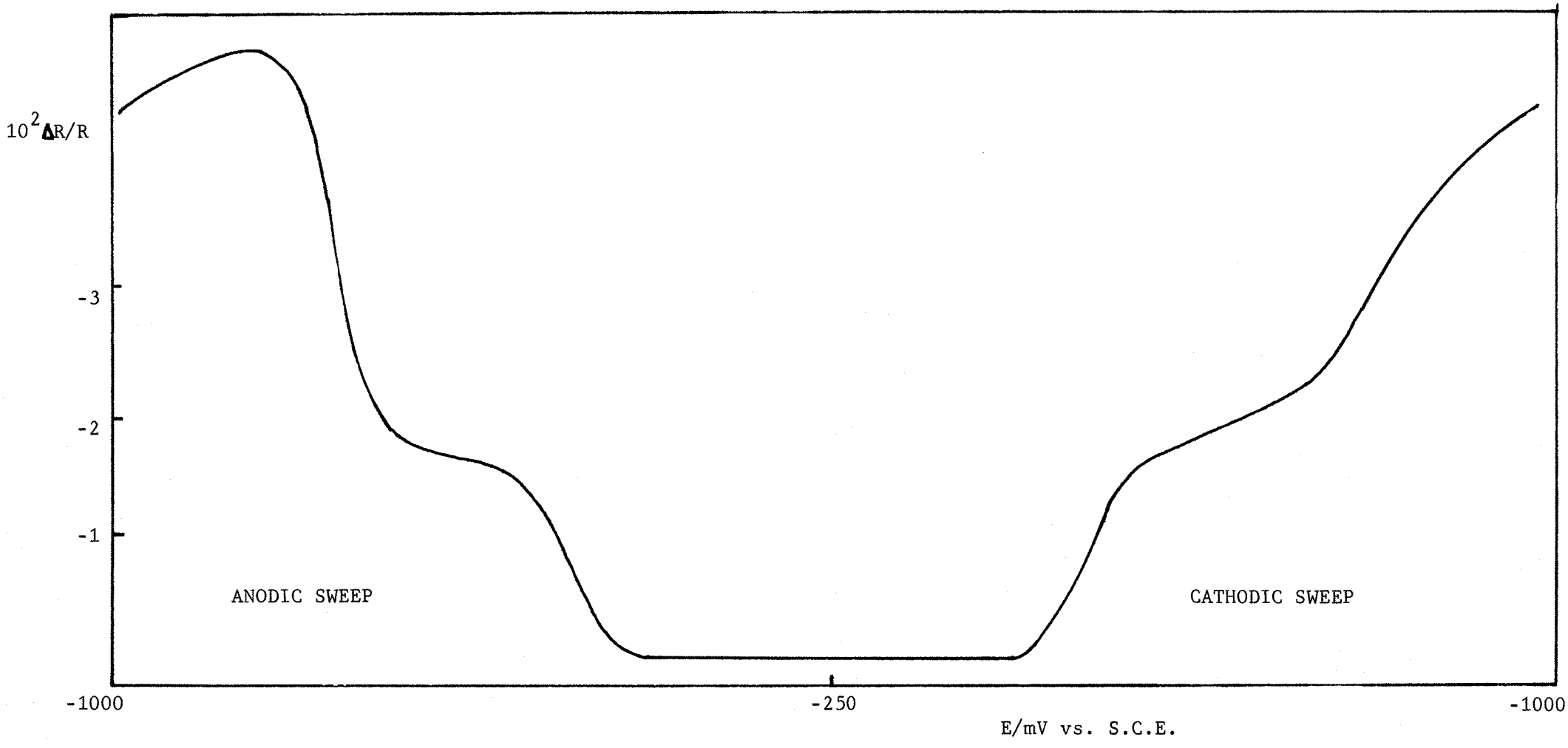

Fig. 4.3 Typical optical sweep (in the unfolded format) for thallium deposition on a chemically polished, polycrystalline silver electrode. Wavelength, 570nm; solution, 0.5mM Tl_2SO_4/ 0.5M Na_2SO_4/ 1mM $HClO_4$; sweep speed, 250mV s^{-1}; parallel polarisation.

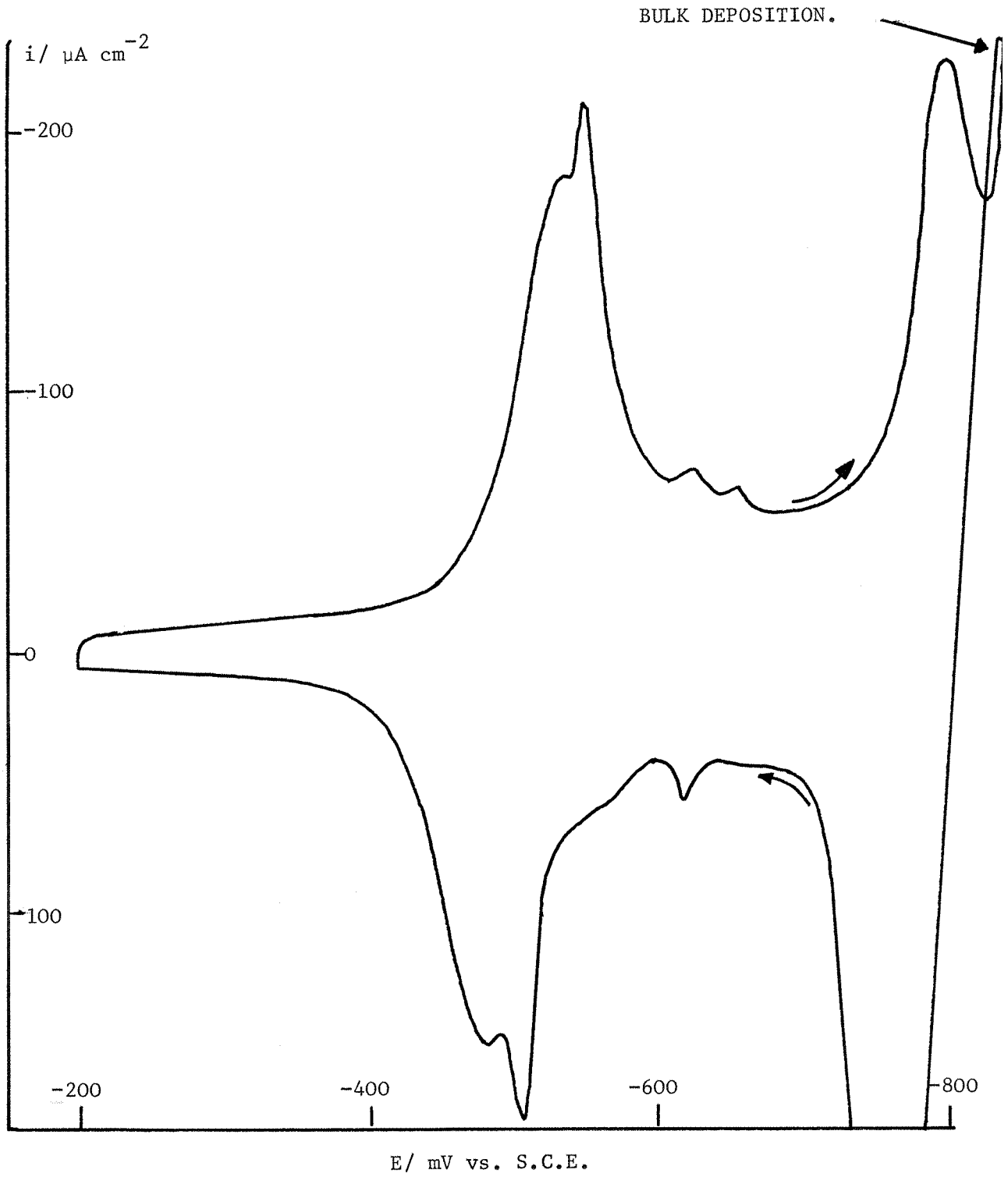

Fig. 4.4. L.S.V. for thallium deposition on chemically polished polycrystalline silver. Solution, 0.75mM Tl_2SO_4/0.5M Na_2SO_4/1mM $HClO_4$. Sweep speed, 100mV s^{-1}.

shown in **Fig.** 4.1, fine structure can be seen in the vicinity of both the monolayer deposition and stripping peaks. In addition the resolution of the second monolayer peak and the beginning of bulk deposition is more well defined. The details of the fine structure were very reproducible and voltammetry carried out in the absence of any thallium ion showed currents flowing due to double-layer charging only until hydrogen evolution occurred. The fact that the optical behaviour of the chemically polished was similar to that expected from calculations also made it very unlikely that a contaminating surface film was present on the electrode surface.

The most likely explanation for the fine structure illustrated in Fig. 4.4 is that the underpotential deposition process is influenced by the crystallographic orientation of the substrate. A polycrystalline metal is an aggregate resulting from many single crystals or grains meeting at grain boundaries. These grains would belong to a variety of different lattice planes which would determine the atomic arrangement at the surface. The polycrystalline electrode would therefore possess a variety of sites with different adsorption energies for the adatoms which are thought to be involved in the underpotential process. This would be reflected in the voltammetry by the presence of more than one deposition (or stripping) peak for the first monolayer, as seen in Fig. 4.4. If this explanation for the observed fine structure was correct it would be expected that voltammetry carried out on single crystals would be dependent on orientation. As mentioned already the results of Adzic et al.[66] for lead deposition onto single crystals of gold showed such effects (as does the work of Schultze et al.[64] published after the completion of the present work), but the results were not very well defined and no explanation was given. It is possible that in this case the electrochemical polishing procedure used was not very successful in providing a well defined surface free from mechanical damage.

4.3 LINEAR SWEEP VOLTAMMETRY BEHAVIOUR OF CHEMICALLY POLISHED SINGLE CRYSTAL ELECTRODES.

L.S.V.'s for the three single crystals, {110}, {100} and {111} are shown in Fig. 4.5. The exact potentials of the peaks and their shape are dependent on sweep speed, thallium ion concentration and whether the anions in the system are specifically adsorbed to any significant extent but the essential characteristics remain the same except that voltammograms obtained for thallium deposition on the {100} face, show an additional peak at sweep speeds greater than $\sim$ 40mV s^{-1}, as shown in Fig. 4.6. The deposition peak potentials are tabulated in Table 4.1. Each of the single crystals shows a characteristic, well resolved (except on the {110} plane) peak structure which is very reproducible. Before the interpretation of these results is considered in detail, a discussion of the possible factors which could give rise to multi-peak U.P.D. voltammetry on single crystals, will be given.

(a) The various peaks in the voltammetry could correspond to different adsorbed states. Two factors could give rise to such behaviour;

1. If all the adsorption sites on the electrode are assumed to be equivalent, each peak could correspond to a different ordered structure on the surface. Such structures have been observed in the gas phase adsorption of foreign metal atoms onto noble metals, using L.E.E.D. techniques.[92]

2. If the polishing process was not entirely successful in producing a single crystal plane, the slight polycrystalline nature of the surface would result in multi-peak voltammetry if it is assumed that the adsorption energies associated with a particular crystal structure are very different.

(b) If it is assumed that U.P.D. produces a crystalline rather than an adsorbed layer on the electrode, the peaks could correspond to different

TABLE 4.1

CRYSTAL FACE	A_1/mV	A_2/mV	A_3/mV	B/mV	STARTING POTENTIAL OF A_1/mV
{110}	-532	-585	-	-737	-444
{110}	-535	-644	-	-785	-452
{111}	-507	-536	-587	-755	-482

Variation of first and second monolayer deposition peak and deposition starting potential with crystal face. Solution and sweep speed as in Fig.4.5

TABLE 4.2

CRYSTAL FACE	CHARGE PASSED UP TO POINT X /μC cm^{-2}	CHARGE PASSED UP TO POINT Y /μC cm^{-2}	SURFACE ATOM CONCENTRATION /ATOMS cm^{-2}
{110}	196±6	325±6	8.5×10^{14}
{100}	198±5	320±10	12.1×10^{14}
{111}	196±6	324±7	13.9×10^{14}

Charge values for the first and second monolayers on the various crystal faces (double layer charge subtracted, no correction for surface roughness) The table also shows the surface atom concentrations of the Ag crystal planes.

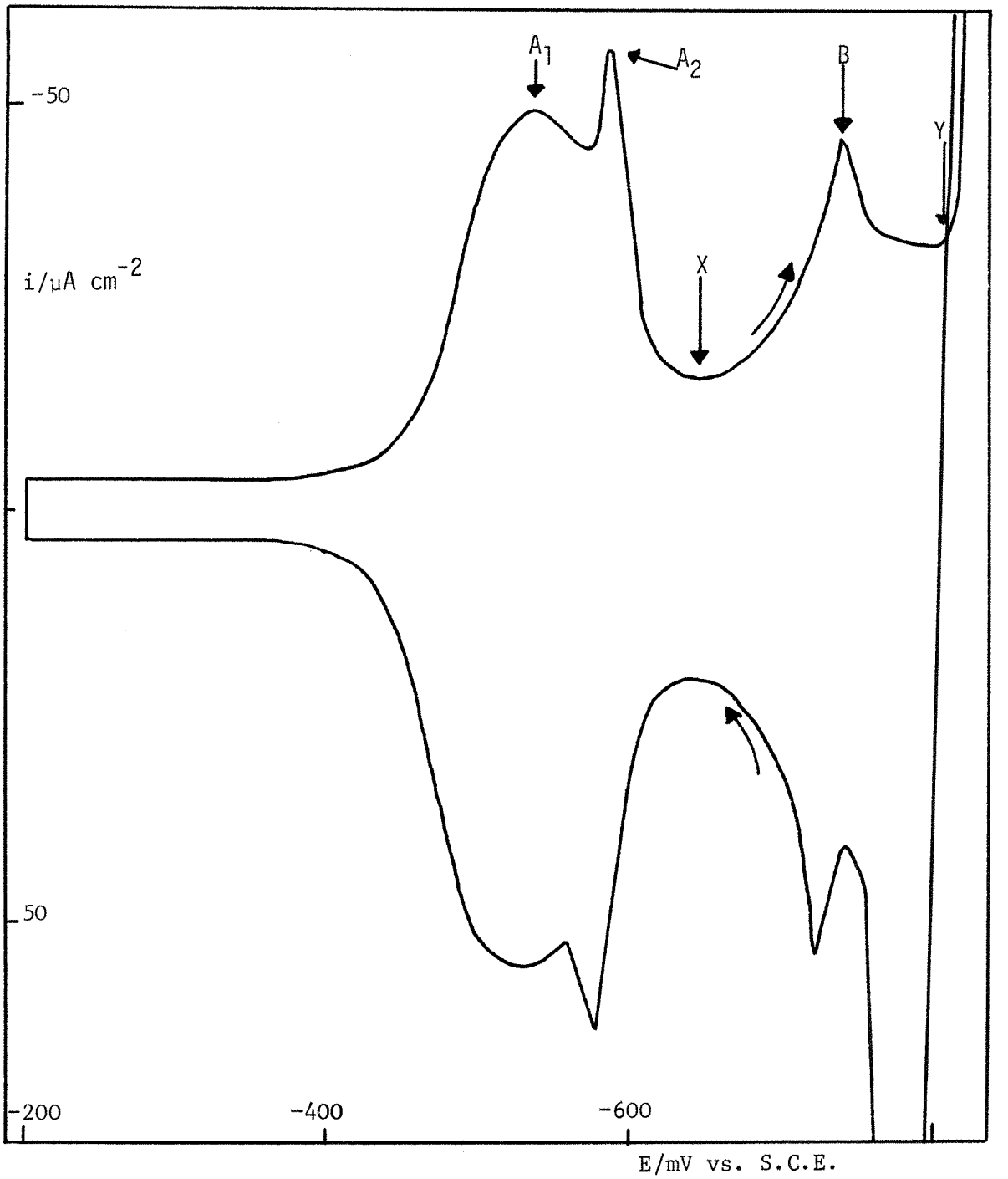

Fig. 4.5(a) L.S.V. for thallium deposition on the {110} plane of silver. Solution, as in Fig.4.4. Sweep speed, 30mV s^{-1}.

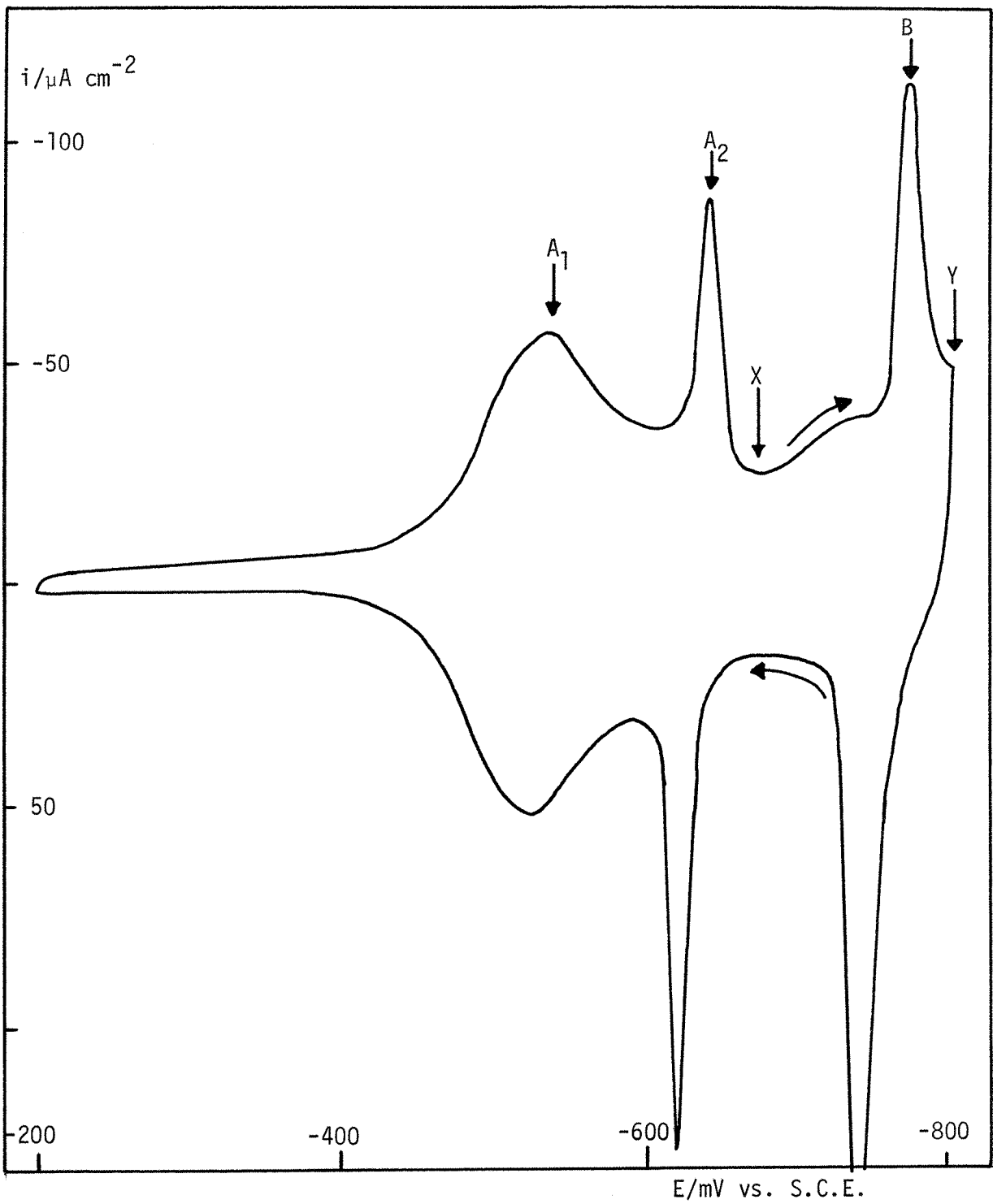

Fig. 4.5(b). L.S.V. for thallium deposition on the {100} plane of silver. Solution, as in Fig. 4.4. Sweep speed, 30mV s^{-1}.

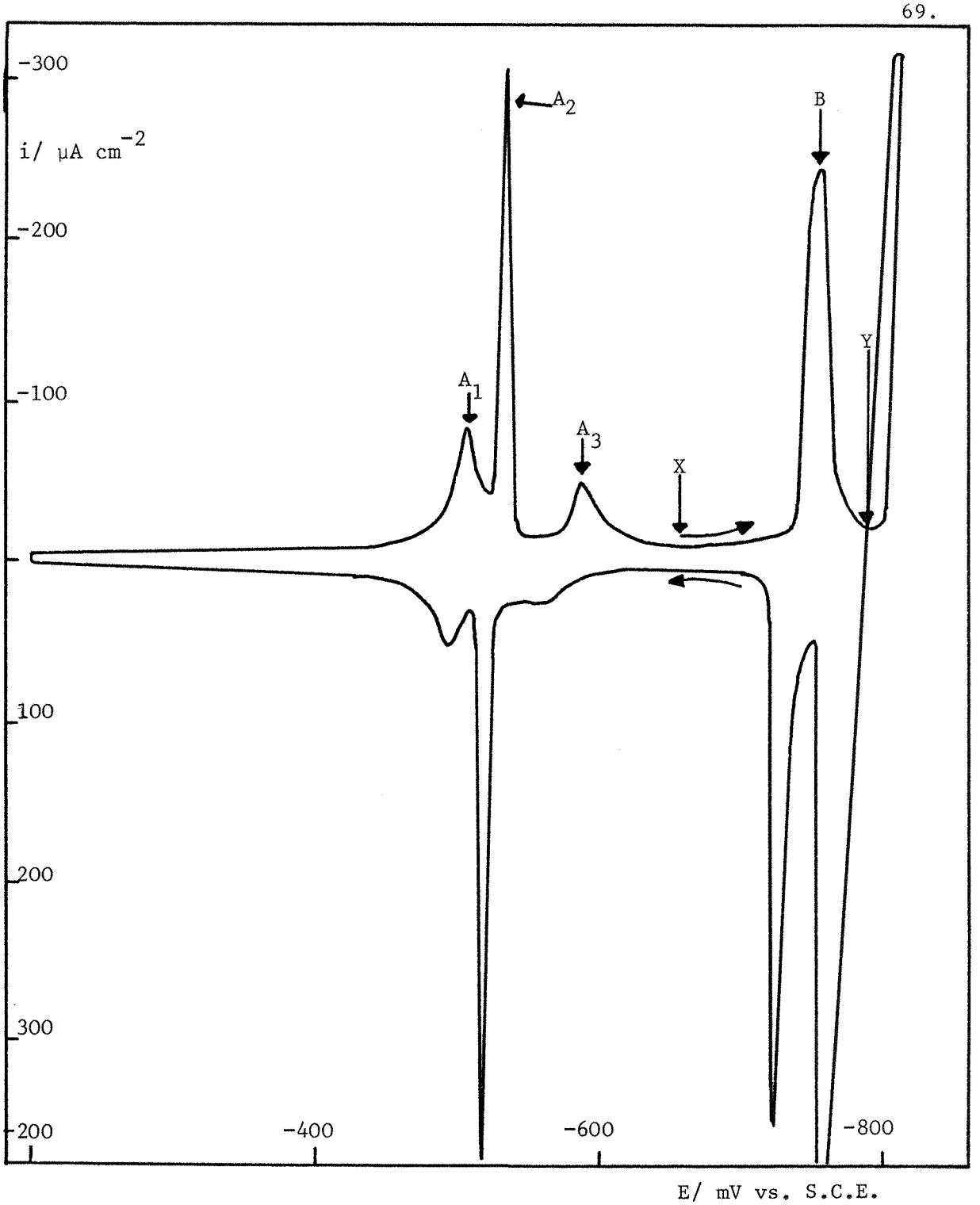

Fig. 4.5(c). L.S.V. for thallium deposition on the {111} plane of silver. Solution, as in Fig.4.4. Sweep speed, 30mV s^{-1}.

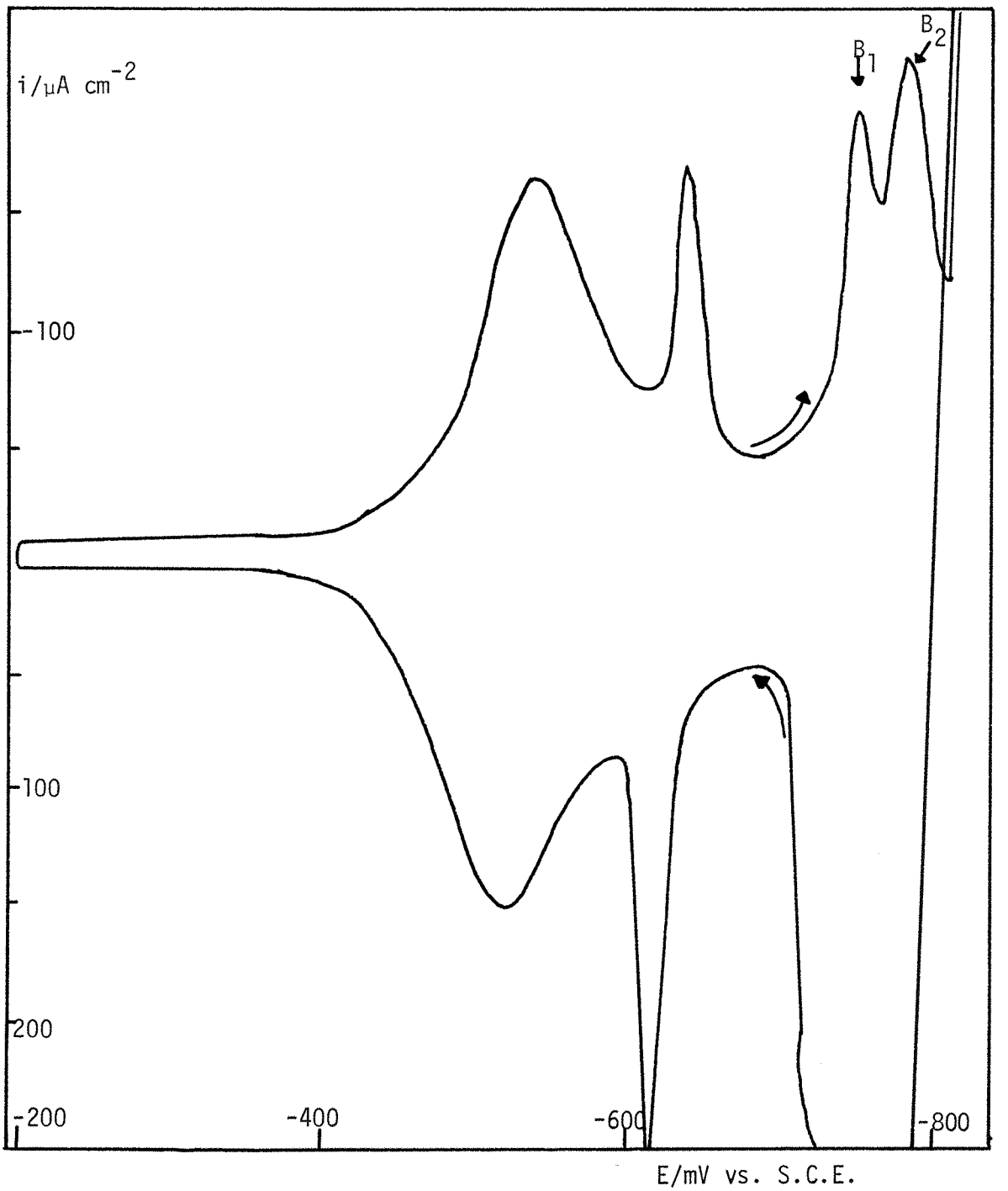

Fig.4.6 L.S.V. for thallium deposition on the {100} plane of silver. Solution, as in Fig.4.4. Sweep speed, 100mV s^{-1}.

phase structures. A discussion of the distinction between an adsorbed layer and a crystalline layer is given later.

(c) An initial adsorption stage later transforming to a crystal growth process could also explain such voltammetry. Again, mechanisms of this type have been observed in gas phase deposition onto metals.[93] Adzic et al.[66] postulated such a transformation process to explain their voltammetry results on polycrystalline gold but supplementary evidence was not provided.

(d) Deposition of partial monolayers on top of each other could produce such results.

Alloy formation can be discounted in this system at room temperature.

Possibility (d) can be discussed in connection with the measured charge values at various potentials in the linear sweep. These are tabulated in Table 4.2 for the points marked X and Y on the voltammograms. The fact that underpotential deposition can only take place by virtue of the interaction between deposit and substrate makes it improbable that any three-dimensional structure would begin to form before the two-dimensional layer (whether adsorbed or crystalline) was complete. The point marked X in Fig4.5(a) to (c) was chosen as representing the completion of the first thallium monolayer. The measured charges up to this point are identical on all crystal faces and if it is assumed that a close packed structure is formed, the experimental and calculated charges for such a model agree when a surface roughness factor of 1.22 is used. Such a low value for the roughness parameter is typical of chemically polished surfaces. One can conclude that deposition at more negative potentials than point X, up to the reversible potential is associated with a second monolayer formation. Again, the charge measured up to point Y (this being the point just before the onset of bulk deposition) is almost independent of orientation but is slightly lower than expected for two complete close packed layers, however the voltammetry suggests the second layer is not quite complete.

Possibility (a) is unlikely as the observed voltammetry was very reproducible which would probably not be the case if more than one lattice plane was exposed by the polishing process. In addition, other chemical polishing techniques gave identical results; reproducibility was much poorer though; (Confirmation of the essential unique nature of the surface structure of each single crystal has come recently from the results of other workers*; Lorenz,[94] using a set of commercial single crystals polished in an identical manner to the method used here, found identical behaviour to that shown in Fig.4.5 (a) to (c). Also, dislocation free silver single crystals produced by the method of Budevski et al., which need no surface preparation, also gave identical results. Kolb[95] has shown that a thin film of silver deposited epitaxially on mica, which has a {111} structure, gives identical voltammetry to the {111} crystal used in the present work. These results show that the orientation of the single crystal surfaces produced by the chemical polishing process was essentially perfect.).

There remains the possibility that the observed voltammetry is caused by different adsorbed states, different crystalline states or a combination of both adsorbed and crystalline states.

There are a number of simple diagnostic criteria which can be applied to voltammetry in order to distinguish between a purely adsorbed layer of metal and a crystalline phase layer. Perhaps the simplest is the separation between opposite peaks in a linear sweep experiment. For a purely adsorbed layer of metal atoms, assuming the scan rate is sufficiently slow for the reaction to achieve equilibrium, the peaks would be exactly opposite each other,[96] whereas for a crystalline phase layer, the onset of the stripping process should not occur until the potential is equal to or more positive than that at which deposition commences (the exact separation between the starting potentials of stripping and deposition would depend on the magnitude of any nucleation overpotentials).

The results show that the pair of peaks marked A_1 in the figures

* Results obtained since the publication of the work in this chapter.

show a separation of $\leq$ 5mV at a sweep speed of 10mV s^{-1} and can be regarded as being mutually opposite. The peaks marked A_2 however, as well as being much sharper than the A_1 peaks, exhibit the characteristic of crystalline phase peaks described above, i.e. even at very low sweep speeds there is a characteristic asymmetry about the zero current axis. This is especially well defined on the {111} plane and to a slightly lesser extent on the {100} but the {110} A_2 peak seems to behave much more like an adsorbed layer peak. The same criteria can be applied to the second monolayer peaks, B. In all cases a characteristic separation between the anodic and cathodic peaks is seen with the same sequence of clarity as found for the A_2 peaks.

The variation of peak currents with sweep speed is another useful diagnostic tool which can be applied to the voltammetry. For an adsorption reaction controlled by the number of available sites on the electrode, peak currents should vary linearly with sweep speed.[96] The results show that, in all cases, the peak current of A_1 follows this relationship (see Fig. 4.7) whereas the shapes of peaks A_2 and B are much more sensitive to sweep speed and current is proportional to $\beta^{<1}$, (β = sweep speed), the peaks becoming less sharp at the higher sweep speed. However the application of this voltammetry rule is only strictly valid for sweep speeds greater than 100mV s^{-1} and some of the sweep speeds used here are above this value.

Another feature of the voltammetry which can be discussed in connection with the distinction between an adsorbed layer and a crystalline plane is the peak sharpness. The peaks A_2 and B (especially on the {111} plane) are much sharper than those normally associated with an adsorption process e.g. for the deposition of a monolayer of adsorbed species, the expected half peak width for a Langmuir isotherm is 90mV/z.[64] For a peak sharper than this, one has to assume some degree of attraction between the adsorbed species and a Frumkin isotherm is then applicable, the degree of atomic interaction being reflected in the interaction parameter. It is impossible to explain such a sharp peak as seen on the {111} face by an

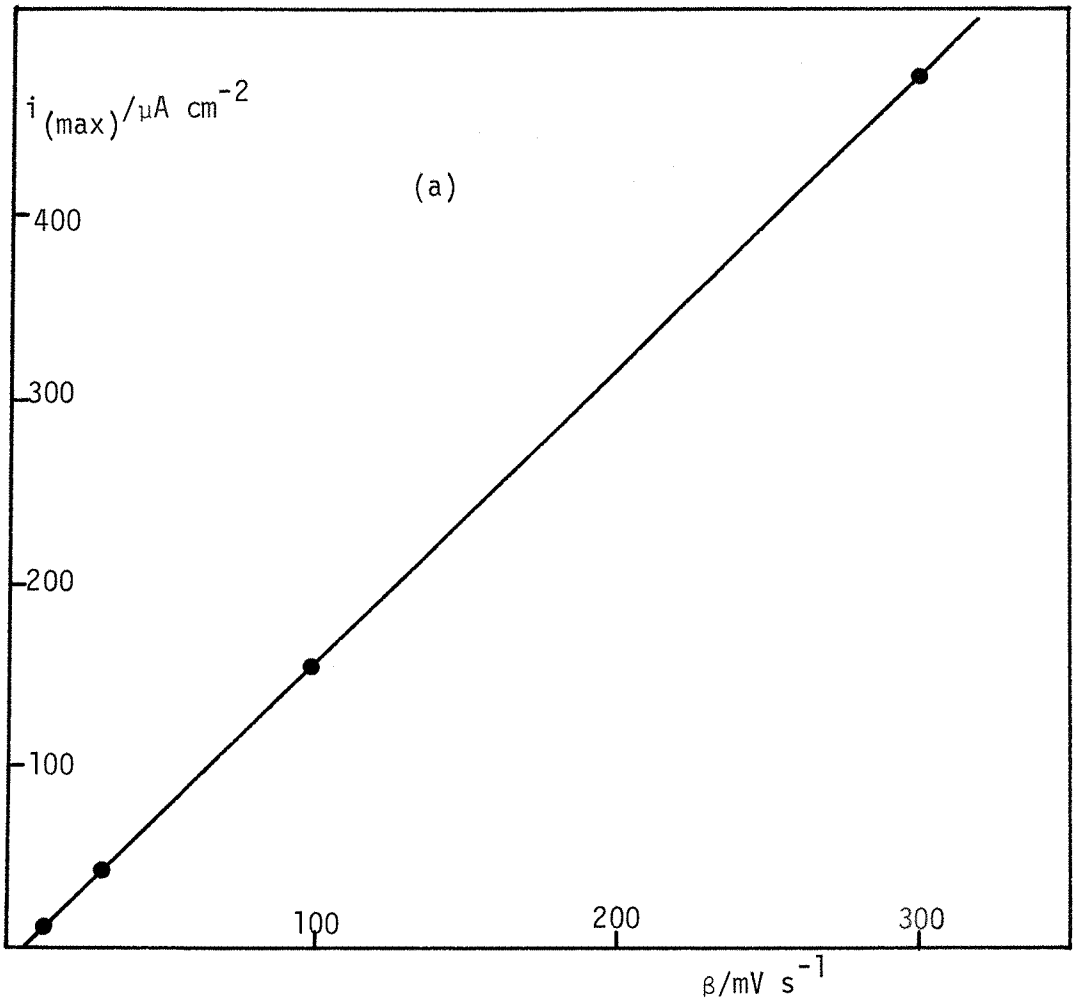

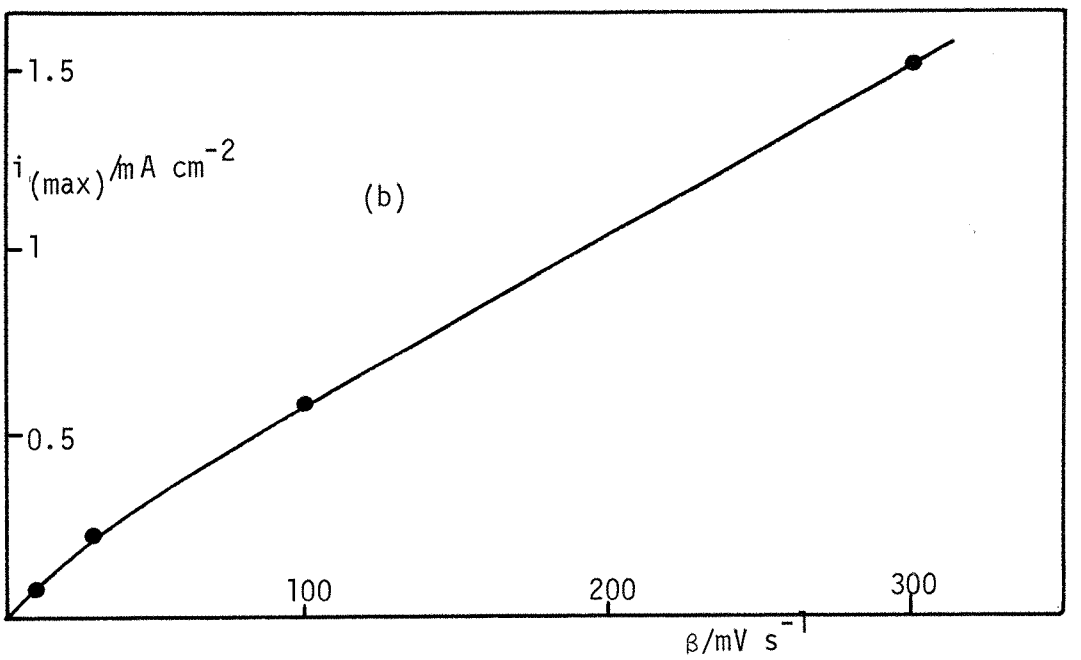

Fig. 4.7 Plot of $i_{(max)}$ vs. sweep speed (β) for, (a) peak A_1, (b) peak A_2, on the {111} face of silver. Solution, as in Fig. 4.4.

adsorption isotherm unless one uses an unreasonably high value for the interaction parameter; (It should be noted however, that Gerischer has shown[57] the half peak width to be markedly dependent on $\Delta\Phi$ and hence ΔU_p. This would imply that systems with smaller underpotential shifts have to described by Frumkin isotherms with increasing interaction parameters. This point was not considered in a recent paper by Schultze and Dickertmann[64] who investigated a number of systems on gold single crystals). In any case, the distinction between a crystalline and an adsorbed layer with a large interaction parameter is questionable. It seems more realistic to define the properties of the deposits formed in the underpotential region with respect to the interaction parameter necessary to describe a particular voltammetry peak by a Frumkin isotherm. Peaks with low or negative values (indicating repulsion) could then be ascribed to the deposition of a purely adsorbed species whereas sharp peaks associated with high values of the interaction parameter could be ascribed to the formation of a layer with mainly crystalline properties. Peaks associated with intermediate values would seem to be related to deposits with the properties of both adsorbed and crystalline layers. It should be stressed that a crystal plane formed from an adsorbed layer by a phase transformation process, need not necessarily involve two-dimensional nucleation as the initial step.[62,102] If the phase transformation is of the homogeneous type i.e. involving compositional fluctuations which grow in intensity until they eventually yield the equilibrium phase, nucleation does not occur. Examples of transformations of this type are most common in the gaseous phase but there are also examples in liquid and solid state transformations. It is possible to define the nature of metal monolayers, as crystal planes, without recourse to arguments involving nucleation processes and in the present case, where an appreciable amount of adsorption takes place before

phase transformation, the homogeneous mechanism may be a viable route. The growth of crystalline deposits preceeded by no adsorption e.g. the formation of the bulk deposit, must involve a preliminary nucleation step (except where growth occurs at existing dislocations).

A heterogeneous transformation[62] involves nucleation and growth. Small volumes of the product phase or nuclei, often assumed to be identical in structure and composition to the transformation product, form first.

The first-order transformation from an adsorbed layer to a crystalline phase should occur at a single potential. However, such factors as surface heterogeneity or a variation in the activity of the deposit with the fraction of surface covered could result in a much broader voltammetry peak and the transformation would be second rather than first-order. The sharpness of the A_2 peak on the {111} face indicates a first-order transformation. On the {110}face however, the transformation seems to occur over a much wider potential range and is characteristic of a second-order or continuous transition. The {100} face results fall between these two extremes. A discussion of the possible factors which could cause a variation in activity as the monolayer phase is deposited is given in a later section of this chapter.

The tentative conclusions derived from the voltammetry results can be summarised as follows:

1. Peak A_1 in all cases seems to represent a metal adsorption process. No information can be obtained on the state of charge of the deposited species.
2. The A_2 peaks do not show the characteristics of an adsorption reaction and especially in the case of the {111} and {100} planes, the assymmetry with respect to the potential axis and the sharpness of the peaks, are more typical of a crystal growth process.

3. Peak B is associated with the growth of a second monolayer and shows the same characteristics, mentioned in 2. above, as the A_2 peaks.

Linear sweep voltammetry however is not a sufficiently diagnostic tool that one can distinguish between adsorbed and crystalline states with absolute certainty. Such a distinction can be made however, under favourable circumstances, by the use of potential-step techniques as the shape of the resulting current-time transient can give an insight into the kinetics of the reduction process. The type of transient expected for the deposition of an adsorbed layer or a crystal plane (by two-dimensional nucleation and growth), can be calculated and compared with experiment. Before the results of the potential-step experiments are given, the optical effects of the underpotential deposition process will be discussed.

4.4 OPTICAL MEASUREMENTS.

The possible origins of the reflectance changes associated with U.P.D. have already been discussed. It was shown that the major factor determining the reflectance change was most likely associated with absorption processes in the metal film and at wavelengths where the optical characteristics of the substrate change dramatically, these absorption processes in the monolayer would be strongly perturbed on account of the necessary electronic interaction between electrode and deposit.

Fig. 4.8 shows an example of the variation of the relative reflectivity change $\Delta R/R$ with potential. These optical effects are more readily interpreted in terms of the associated electrochemical process if correlated with charge rather than potential. Fig. 4.9 shows such reflectance-charge plots for the three monocrystalline electrodes used in the present work. Before discussing these results in detail, the sign and magnitude of the observed reflectance changes can be compared with values calculated on the basis of different types of process being responsible for

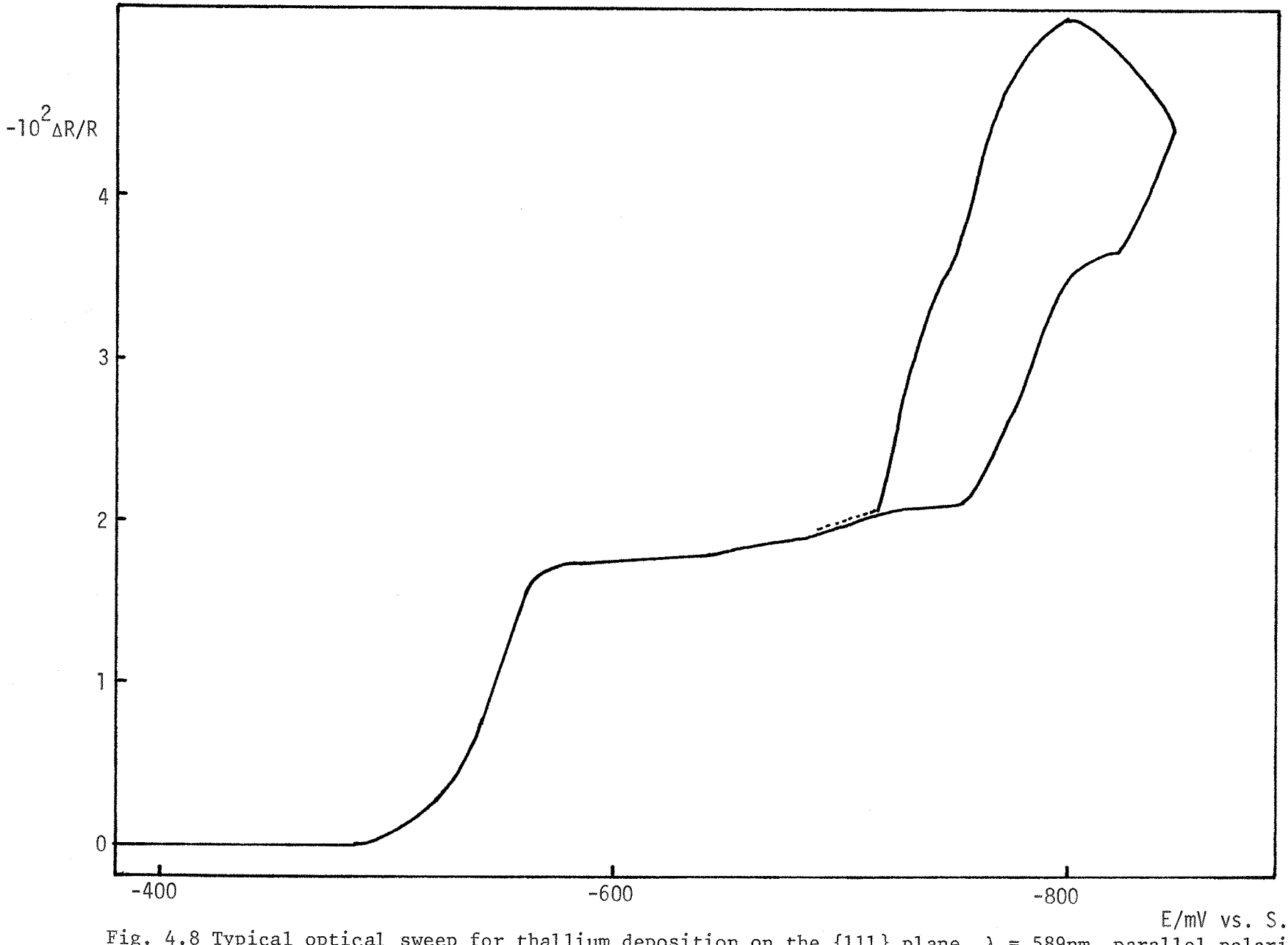

Fig. 4.8 Typical optical sweep for thallium deposition on the {111} plane. λ = 589nm, parallel polarisation. Solution, as in Fig. 4.5; sweep speed, 180mV s^{-1}.

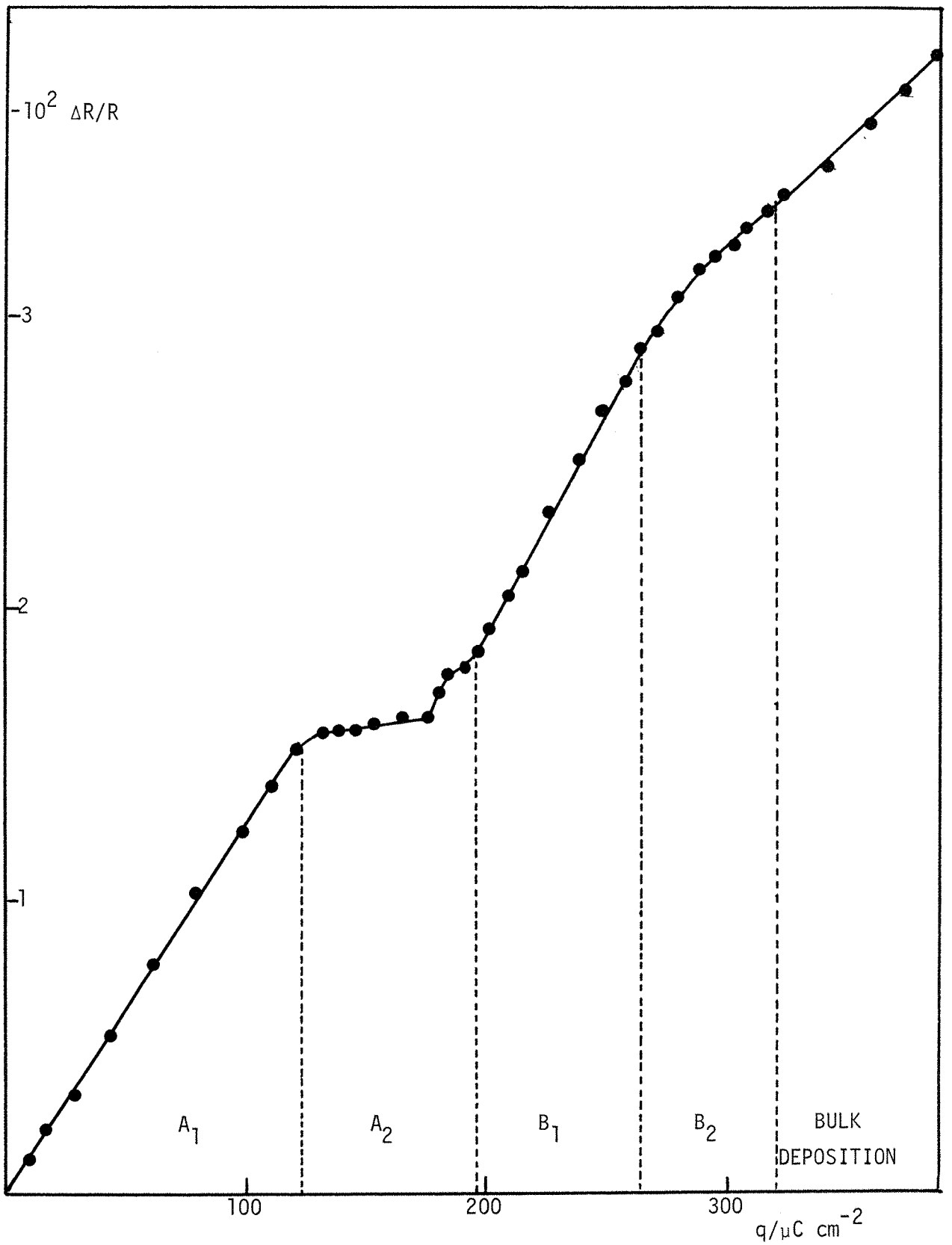

Fig. 4.9 (a). Plot of ΔR/R against charge q for thallium deposition on the {100} face of silver. λ = 589nm, parallel polarisation. Solution and sweep speed as in Fig. 4.8.

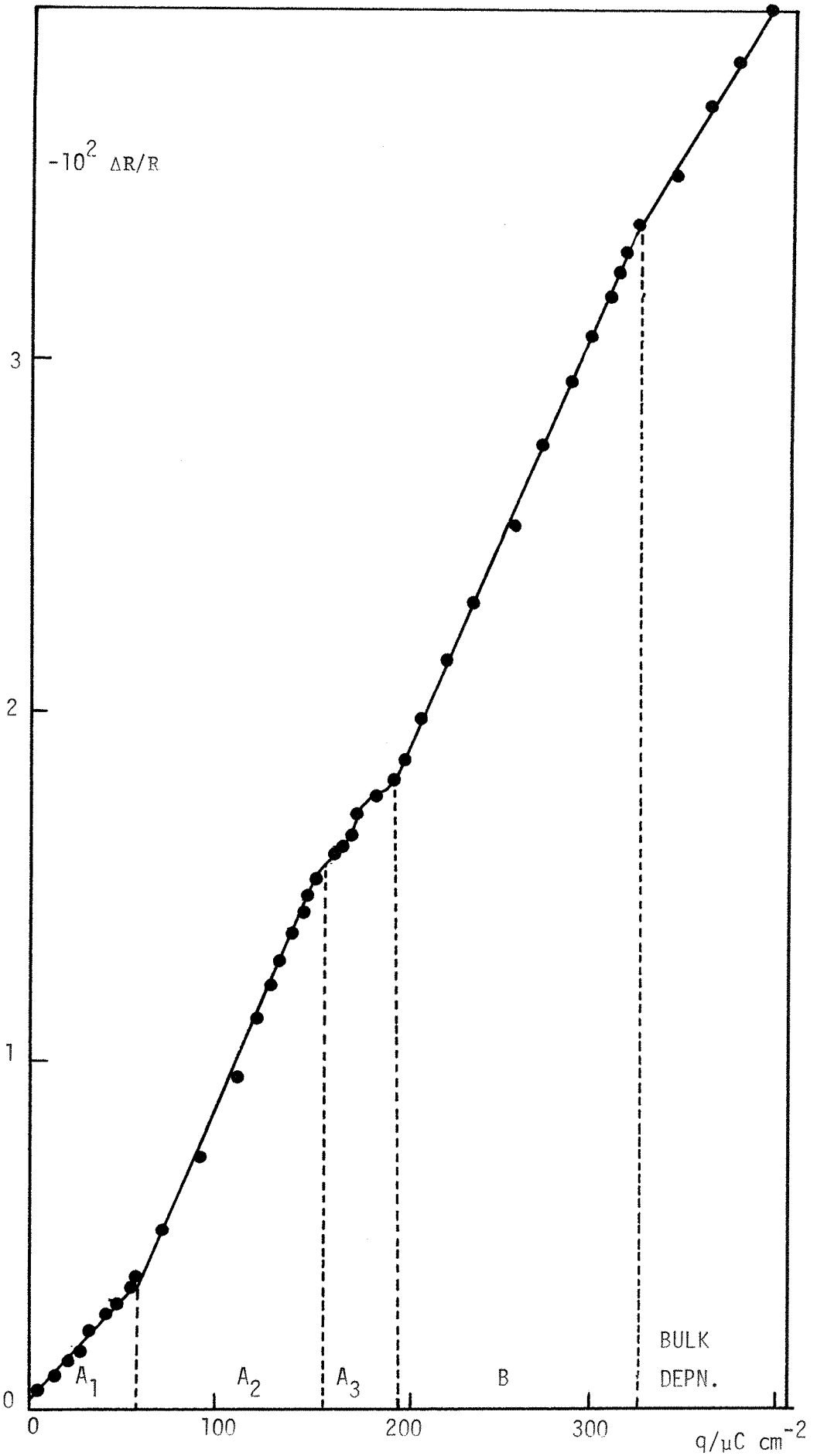

Fig. 4.9 (b). {111} orientation, otherwise as Fig. 4.9(a).

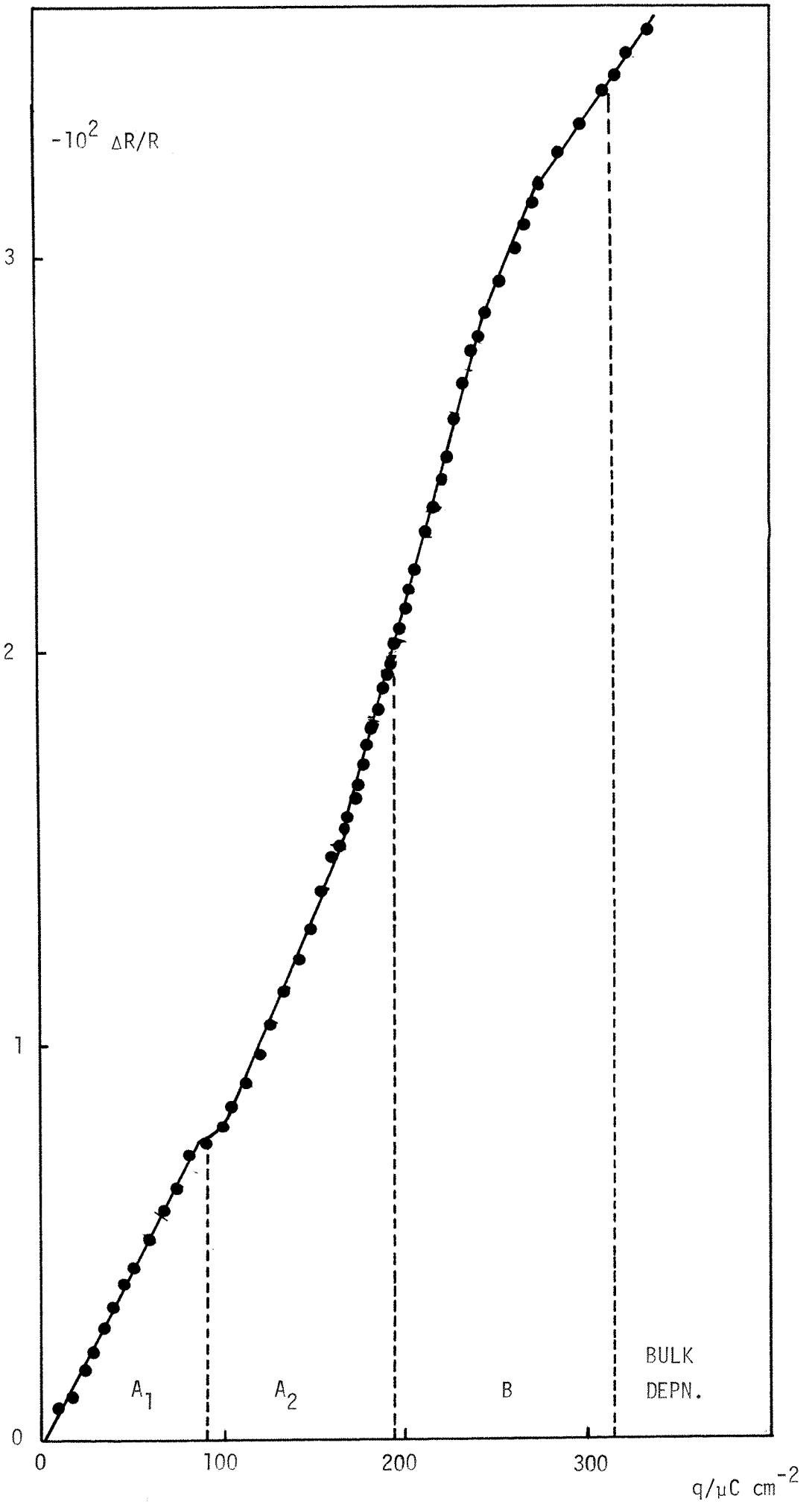

Fig. 4.9 (c). {110} orientation, otherwise as Fig. 4.9 (a).

the reflectance changes.

The measured changes are so large ($\sim$ 2% in reflectivity for monolayer coverage) that optical effects from the solution side of the double layer can be neglected, (i.e. contributions from the diffuse double layer and from solvent and anion adsorption). There remain two effects to be considered, the electroreflectance (ER) effect from the metal substrate and the optical contribution from the deposited thallium layer. Thus the relative change in reflectivity can be written as,

$$\frac{\Delta R}{R} = \frac{1}{R}\left(\frac{\partial R}{\partial q}\right)_{\theta} \Delta q + \frac{1}{R}\left(\frac{\partial R}{\partial \theta}\right)_{q} \Delta\theta$$

where q is the surface charge density on the electrode and θ is the fraction of surface covered by thallium. The magnitude of the ER coefficient $\left(\frac{\partial R}{\partial q}\right)_{\theta}$ can be seen from the slope of the optical characteristics at potentials anodic to thallium deposition, (see Fig. 4.8). This slope is comparatively small. This conclusion is confirmed by other measurements[97] of the ER effect on silver which give a value for $^{1}/_{R}\left(\frac{\partial R}{\partial q}\right)$ of about $3 \times 10^{-5} \mu C^{-1}\ cm^{2}$ in the wavelength range 400nm to 700nm. The ER contribution to $\frac{\Delta R}{R}$ can be shown to be negligible at these wavelengths even if an unreasonably large value is assumed for Δq. If the deposited atoms are assumed to have a 20% ionic character, then Δq will be about $40 \mu C\ cm^{-2}$ for a monolayer and $^{1}/_{R}\left(\frac{\partial R}{\partial q}\right)_{\theta} \Delta q$ is $+1.2 \times 10^{-3}$ whereas the measured $\frac{\Delta R}{R}$ values are about -2×10^{-2}. Thus neither the sign nor the magnitude of the reflectivity changes are consistent with an ER effect. Moreover the possibility that the underpotential monolayer consists of adsorbed cations can be firmly ruled out as this situation would predict a positive reflectance change[76]; the experimental values are negative at all wavelengths longer than 325nm (see Fig. 4.10). These conclusions are at variance with those of Kolb et al.[76] but as stated already, their interpretation of the optical data is questionable.

For results to be obtained which were undistorted by large optical

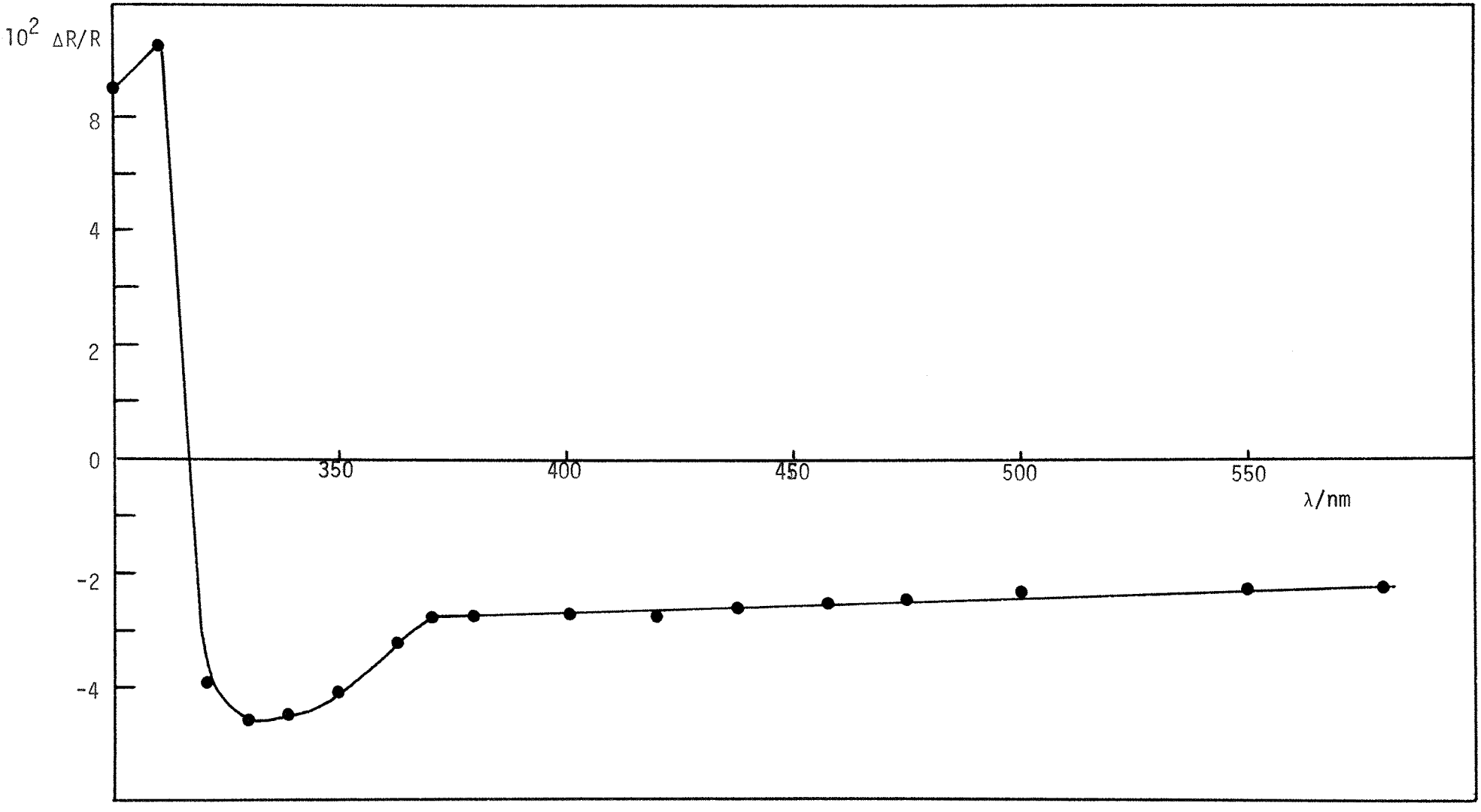

Fig. 4.10. Reflectance spectrum for the deposition of a monolayer of thallium on polycrystalline silver. Solution, 0.5mM Tl_2SO_4/ 0.5M Na_2SO_4/ 1mM $HClO_4$. Sweep speed, 250mV s^{-1}. Parallel polarisation.

changes in the substrate, wavelengths greater than 390nm had to be employed. Below this value the effects of surface plasmon excitation (360-380nm) and bulk plasma resonance (320nm) caused marked effects in the reflectance-charge plots as shown in Fig.4.11, presumably due to the greater contribution of the substrate to the overall optical change.

Inspection of the reflectance-charge plots in conjunction with the corresponding voltammograms, shows that almost all the features seen on the voltammetry curves reveal themselves as changes in the gradient of the optical plots. It is particularly notable that the process associated with peak A_2 on the {100} face, causes very little reflectance change at this wavelength despite the fact that it spans 60-70μC cm^{-2} of charge. A similar effect is observed, although to a smaller extent with peak A_3 on the {111} face.

Before considering the detailed interpretation of Fig.4.9 it is necessary to discuss the factors which could influence the nature of the reflectance-charge plots. It can be shown[54] that for the deposition of a monolayer of atoms $\frac{\Delta R}{R}$ is proportional to the effective thickness $\bar{d}$, of the film, where,

$$\bar{d} = \frac{1}{A}\sum_{i}^{n} d_i \delta A_i$$

where d_i is the local thickness and δA_i is the area of an island of film on the substrate of area A. $\bar{d}$ will be proportional to θ, the fraction of surface covered, and hence to q. This model assumes the optical constants of the film and substrate remain unchanged as θ varies from 0 to 1 which would imply no interactions between the atoms in the layer. If ER effects are ignored it can be seen that changes in the gradient of a reflectance-charge plot could be due to two factors:

1) variations in the partial charge (electrosorption valency) of the deposited metal atoms;

2) changes in the optical constants of the deposited metal atoms.

If changes in optical constants are neglected, it is clear that a transition from deposition of a partially charged state to a neutral state would produce a decrease in the gradient of the plot as the amount of charge flowing per atom deposited would be greater. From Fig. 4.9 it is seen that in all cases, the transition from the second monolayer region to bulk deposition causes a decrease in the slope as would be expected if under-potential deposition involved partial discharge whereas bulk deposition requires complete discharge. However, if there is any change in the nature of the monolayers as θ varies from 0 to 1, e.g. from a layer of adsorbed atoms to a crystal plane with more typically metallic properties, it would be expected that a change in optical properties would result. The results for each crystal face will now be considered separately.

4.2 (a) THE {100} ORIENTATION.

The deposition associated with peak A_1, which on the basis of voltammetry results alone has been ascribed to an adsorption process, produces a linear variation of $\Delta R/R$ with q which implies that up to surface coverages corresponding to 125μC cm^{-2}, there is no appreciable change in the electrosorption valency nor in the optical properties of the layer. The optical effect of peak A_2 is more complicated and is wavelength dependent. The slope of the plot in this region is always markedly less than in the region of A_1 and at the wavelength shown it is practically zero. It has already been speculated that on each crystal face, the A_2 peak corresponds to a crystal growth process. On the {100} face, where there seems to be a large amount of adsorption (125μC cm^{-2}) a phase growth process would involve a considerable rearrangement of the existing adsorbed layer as well as extra deposition to form a complete crystalline monolayer. It can be envisaged that such a reorganisation process would produce a sudden reduction in the electrosorption valency as the bonding to the substrate is reduced. It is not possible to predict the optical change

associated with such a process but on charge arguments alone it is clear that it would result in a substantial decrease in the slope of the reflectance-charge plot since not all of the charge would be the result of additional deposition, a considerable amount would be caused by redistribution.

The second monolayer region can also be divided into two segments with the first having a slope very similar to that associated with peak A_1 (these reflectance-charge plots are constructed from voltammograms run at sweep speeds where the presence of two distinct peaks in the second monolayer region, was apparent (see Fig. 4.6). The second segment has a lower slope which merges into the bulk deposition line, the gradient of which remains constant for films up to 5nm at least (thicker films have not been investigated). This result suggests that the formation of the second monolayer also involves the transformation of an adatom layer into a crystal plane.

4.2(b) THE {111} ORIENTATION.

Peaks A_1 and A_2 in the voltammetry both produce linear reflectance-charge plots of markedly different slope. The increase in gradient of the A_2 region compared to that of the A_1 region must be related to a change in optical constants, as higher surface coverages would be expected to favour a reduction in the electrosorption valency and lead to a decrease in the reflectance-charge slope. Transformation to a crystal plane (peak A_2) occurs at a lower value of charge (50-60μC cm^{-2}) compared to the {100} orientation (120-130μC cm^{-2}) and will mainly involve further thallium deposition to form a complete crystal plane whereas on the {100} face there would seem to be much less deposition and a considerable redistribution of charge due to the decrease in electrosorption valency for the atoms already present on the surface; consequently the reflectance-charge slopes will be much higher in the former case. Peak A_3 does not produce a linear slope and

it is difficult to speculate on the nature of this peak at this stage; it seems possible that some slight rearrangement of the crystal structure takes place.

The linear sweep voltammetry in the second monolayer region reveals only a single sharp peak and the corresponding optical effect is a linear variation of $\Delta R/R$ with q until bulk deposition begins. This suggests that the formation of the second layer involves two-dimensional nucleation and growth from the outset.

4.2(c) THE {110} ORIENTATION.

The various features on the voltammetry are not so well defined on this plane as on the other two and correspondingly the reflectance-charge plot is less easy to divide into segments. A change in slope occurs after about 90μC cm^{-2} of charge have passed, following a short region of low slope. The transition occurs at a point where the peak A_2 would be expected to begin. This peak is again reasonably sharp suggesting a phase transformation at this point. The corresponding optical behaviour lies between that seen for the {111} and {100} faces. Further changes in slope in the reflectance-charge plot occur at 170μC cm^{-2} and 250μC cm^{-2} which probably correspond to the formation of the second monolayer by adsorption followed by transformation into a crystal plane (although in Table 4.2 the end of the first monolayer was taken as point X, which occurs at a slightly higher charge value than 170μC cm^{-2}, the broadness of the second monolayer peak makes its starting point difficult to define exactly).

Based on evidence from voltammetry and optical experiments, a model has been proposed for the occurence of phase transformation processes during deposition on all three crystal faces. These seem to take place both in the first and second monolayer regions except in the case of the {111} orientation when the second layer appears to form as a crystal plane from the outset. The results from the potential-step experiments will now be

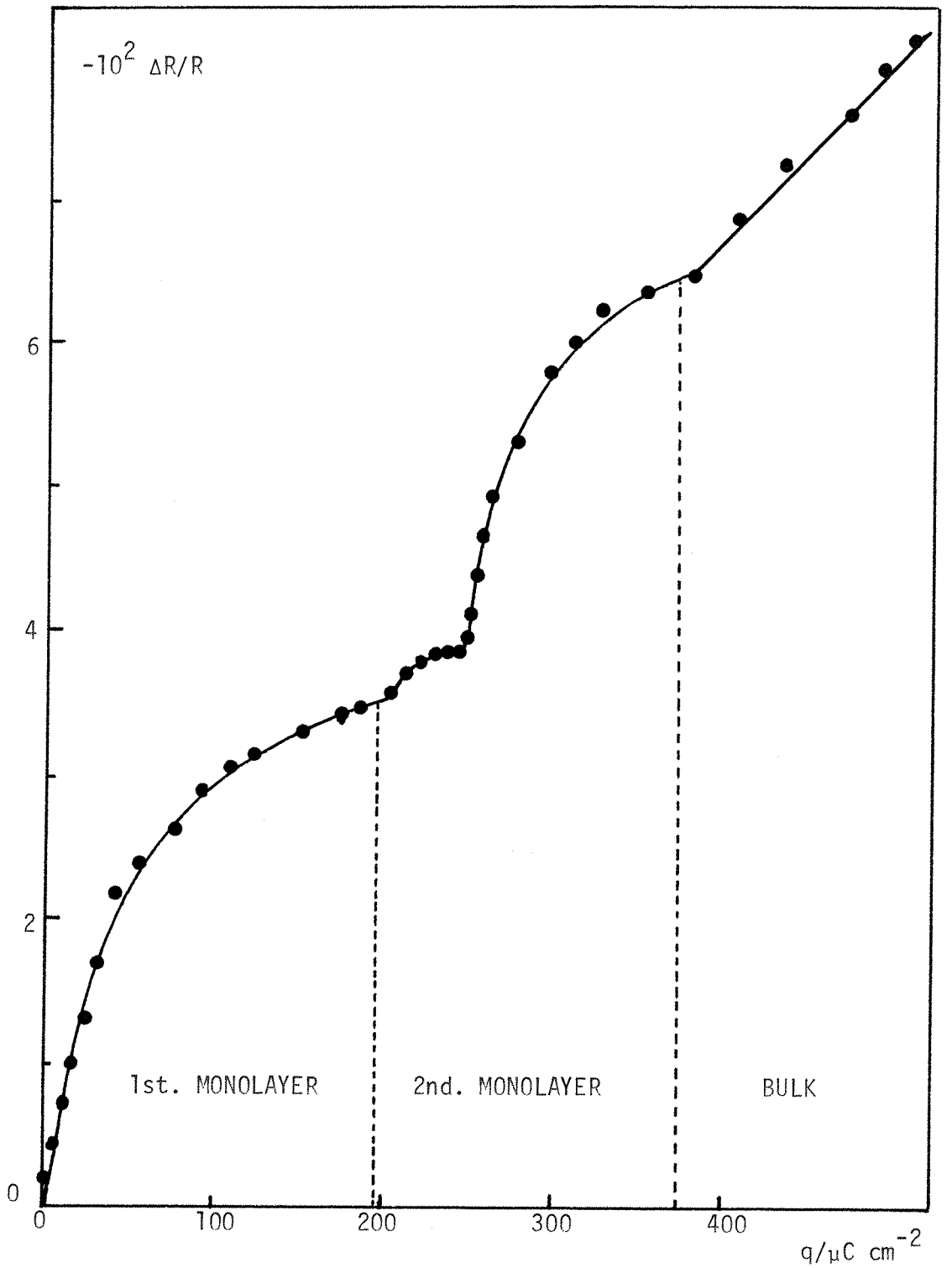

Fig. 4.11. Plot of ΔR/R against q for thallium deposition on the {100} face of silver at a wavelength where surface plasmon effects occur. λ = 380nm, parallel polarisation. Solution and sweep speed, as in Fig. 4.8.

discussed in connection with the proposed model.

4.5 POTENTIAL STEP MEASUREMENTS.

(a) RESULTS.

Pulsing into the potential region of peak A_1 on all faces produced a falling transient of characteristic shape, as shown in Fig. 4.12 for the {111} face. These transients had the following characteristics:

(1) For all three crystals, the initial part of the transient followed an $i \propto t^{-\frac{1}{2}}$ relationship. On the {100} face this was maintained throughout the majority of the transient but the i vs. $t^{-\frac{1}{2}}$ plots for the {111} and {110} faces developed curvature at longer times.

(2) The initial linear portion of the i vs. $t^{-\frac{1}{2}}$ plot extrapolates to intersect the $t^{-\frac{1}{2}}$ axis at positive values.

Examples of i vs. $t^{-\frac{1}{2}}$ plots, for all crystal faces, are shown in Fig. 4.13.

Pulsing to potentials more negative than the A_2 peak potential in all cases, produced a change in the shape of the transient which is best described by reference to the transient obtained pulsing to a potential just anodic to that where the second monolayer formation begins.

{111} FACE.

Pulsing into the A_2 region immediately results in the initial part of the transient coming under planar (limiting) diffusion control. At longer times, a sudden rapid decrease in the current flowing occurs, giving the transient a characteristic 'kink' shape. Examples of this are shown in Fig. 4.14.

{100} FACE.

In the A_2 region at short times the current falls rapidly to a value well below the planar diffusion limiting current and the transient shows a well defined hump as shown in Fig. 4.15. The charge associated with

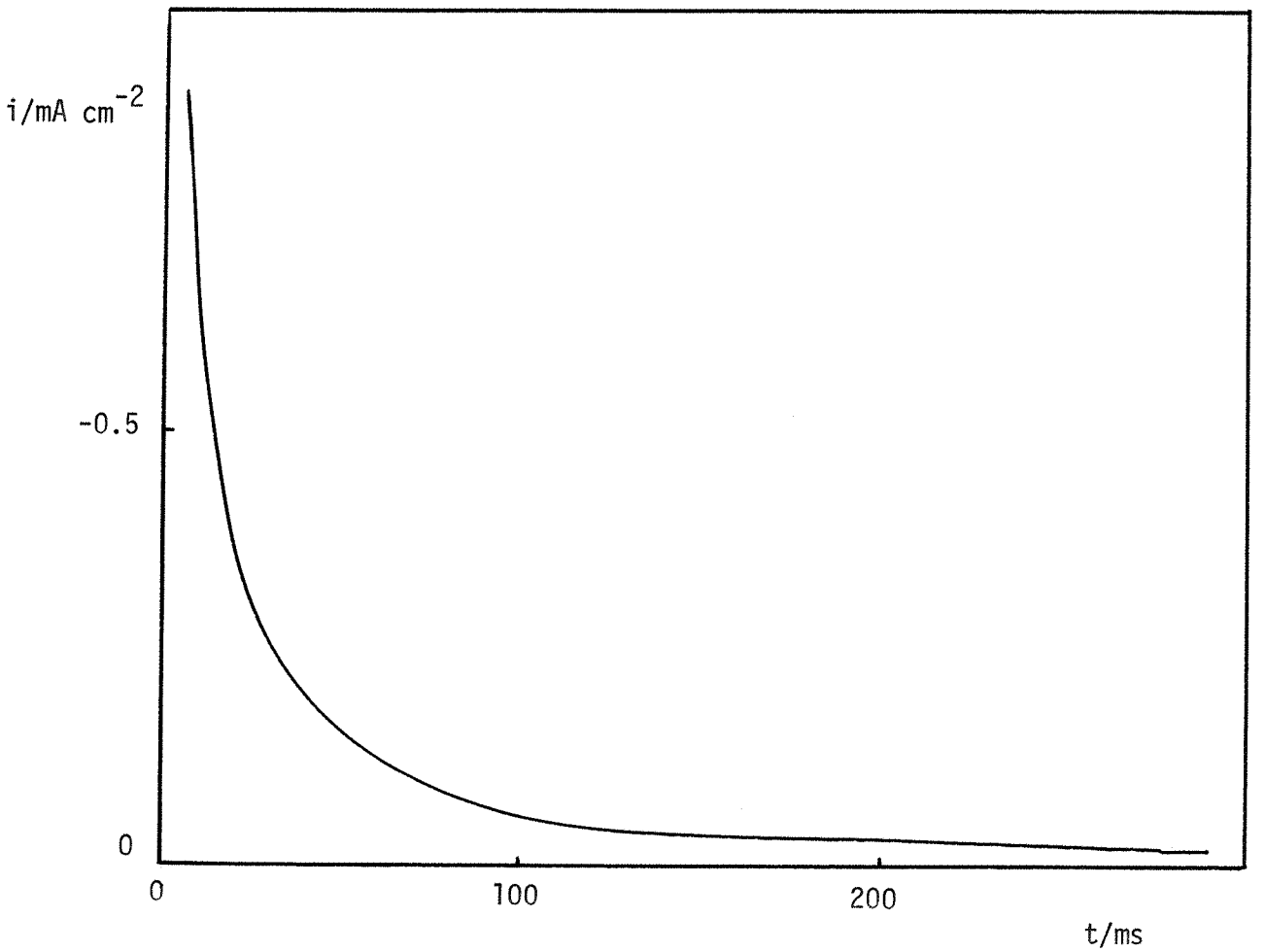

Fig. 4.12. i-t transient for thallium deposition (adsorption region) on the {111} plane of silver for a potential step from -200mV to -522mV (vs. S.C.E.). Solution, 0.5mM Tl_2SO_4/ 0.5M Na_2SO_4.

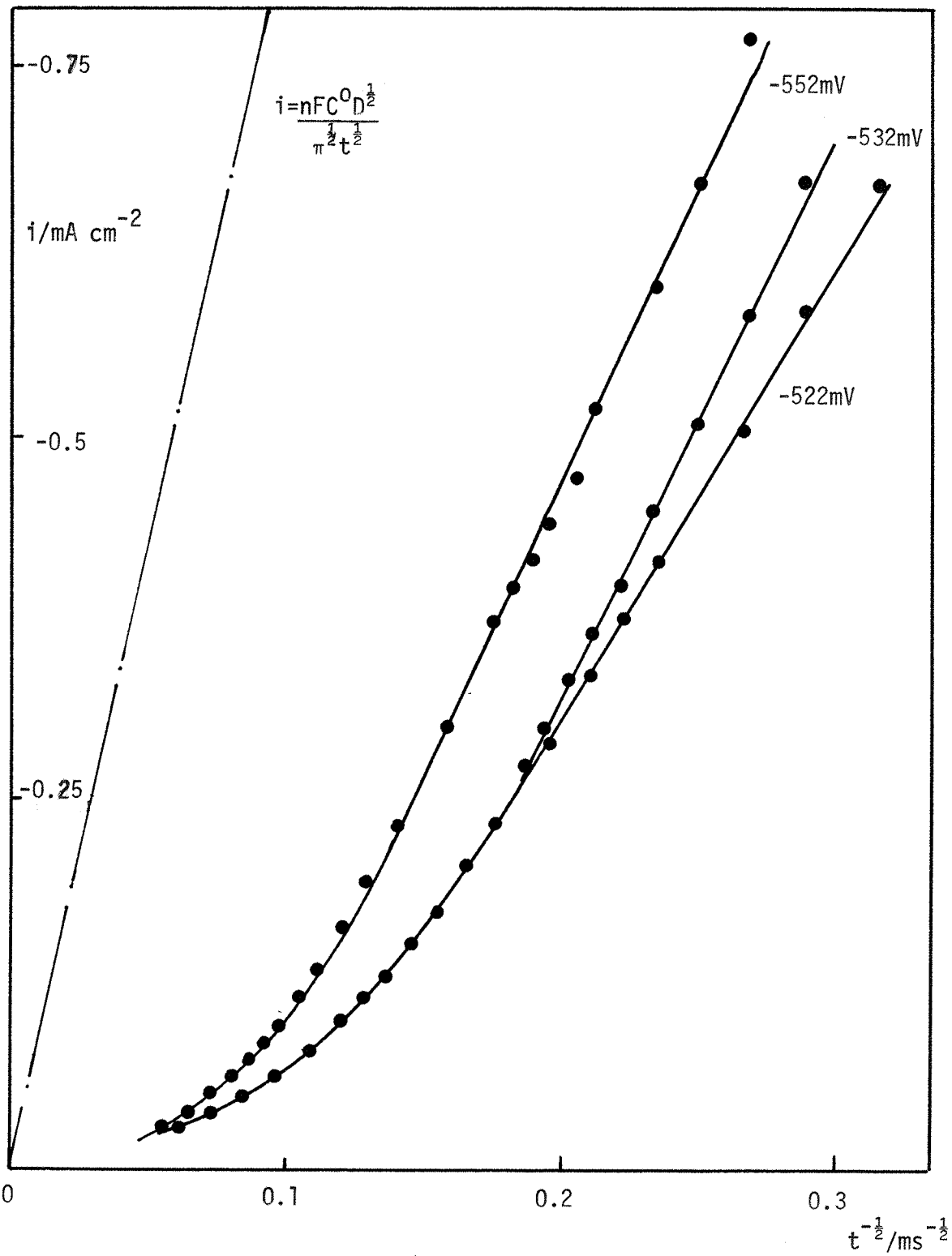

Fig. 4.13 (a). Plot of i vs. $t^{-\frac{1}{2}}$, for thallium deposition on silver{111}, for potential steps from -200mV to the potentials shown (vs. S.C.E.). Solution, 0.5mM Tl_2SO_4/ 0.5M Na_2SO_4.

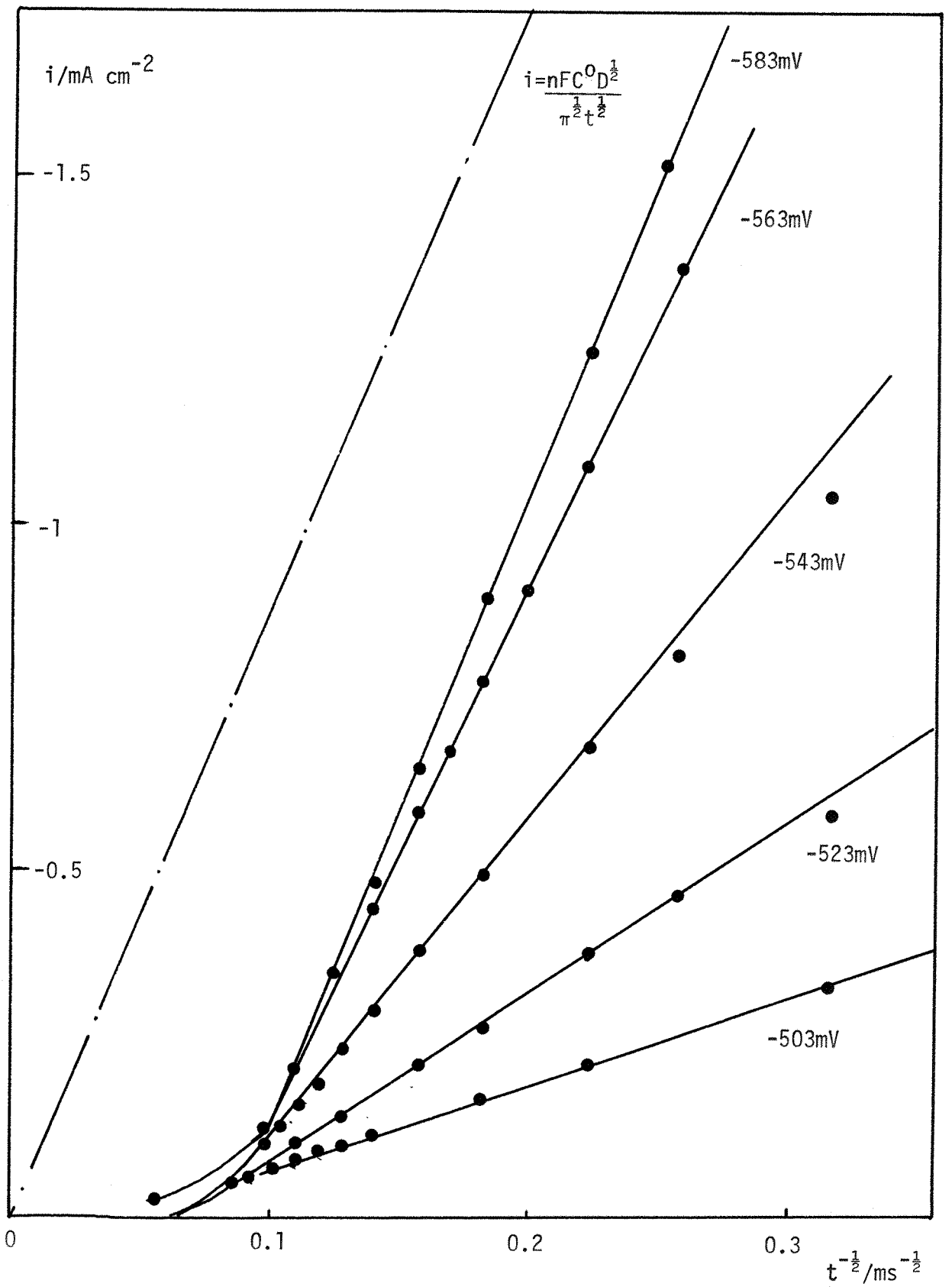

Fig. 4.13 (b). Plot of i vs. $t^{-\frac{1}{2}}$, for thallium deposition on silver{100}, for potential steps from -200mV to the potentials shown (vs. S.C.E.). Solution, 0.5mM Tl_2SO_4/ 0.5M Na_2SO_4.

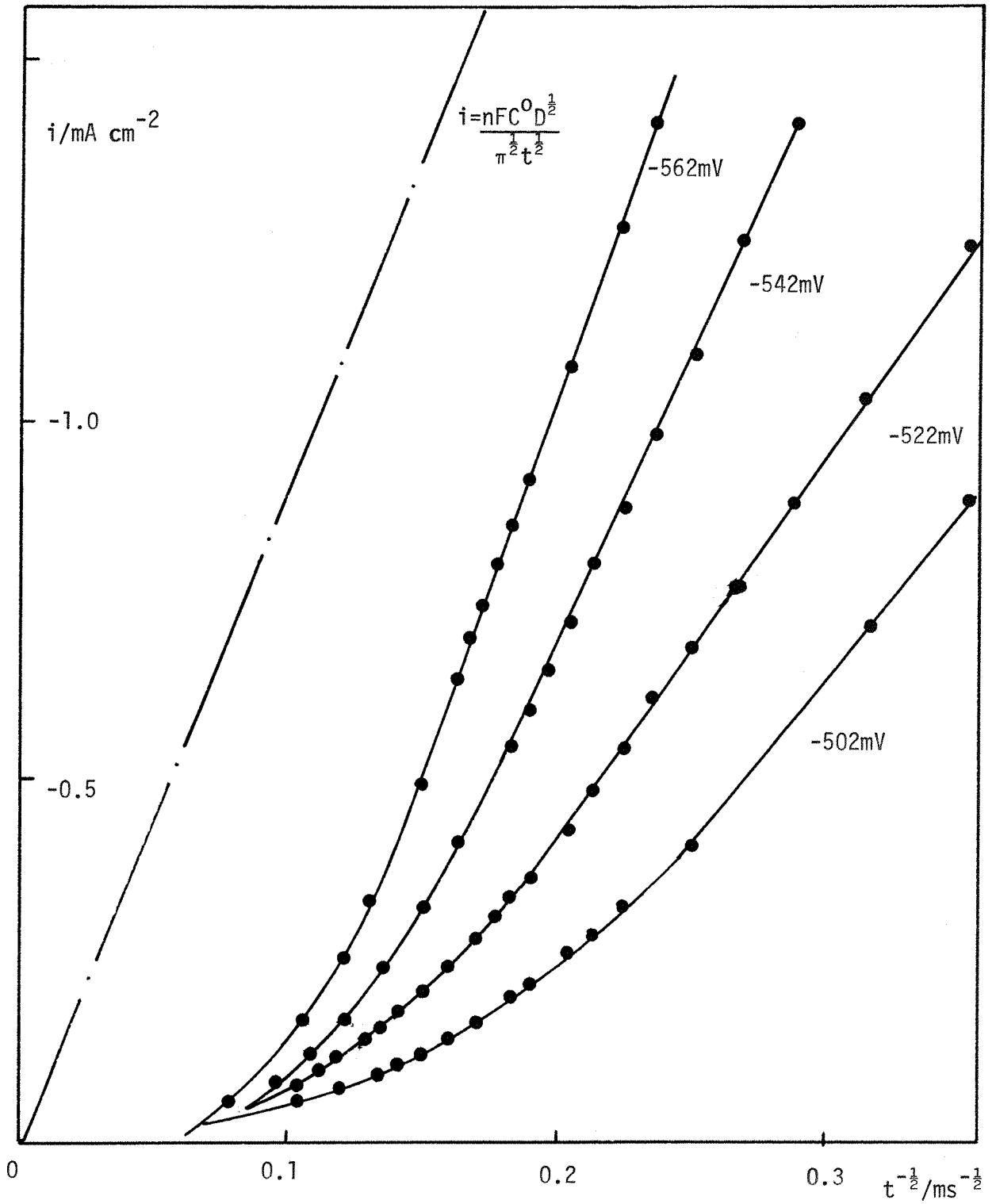

Fig. 4.13 (c). Plot of i vs. $t^{-\frac{1}{2}}$ for thallium deposition on silver{110}. Other details as in Fig. 4.13 (a).

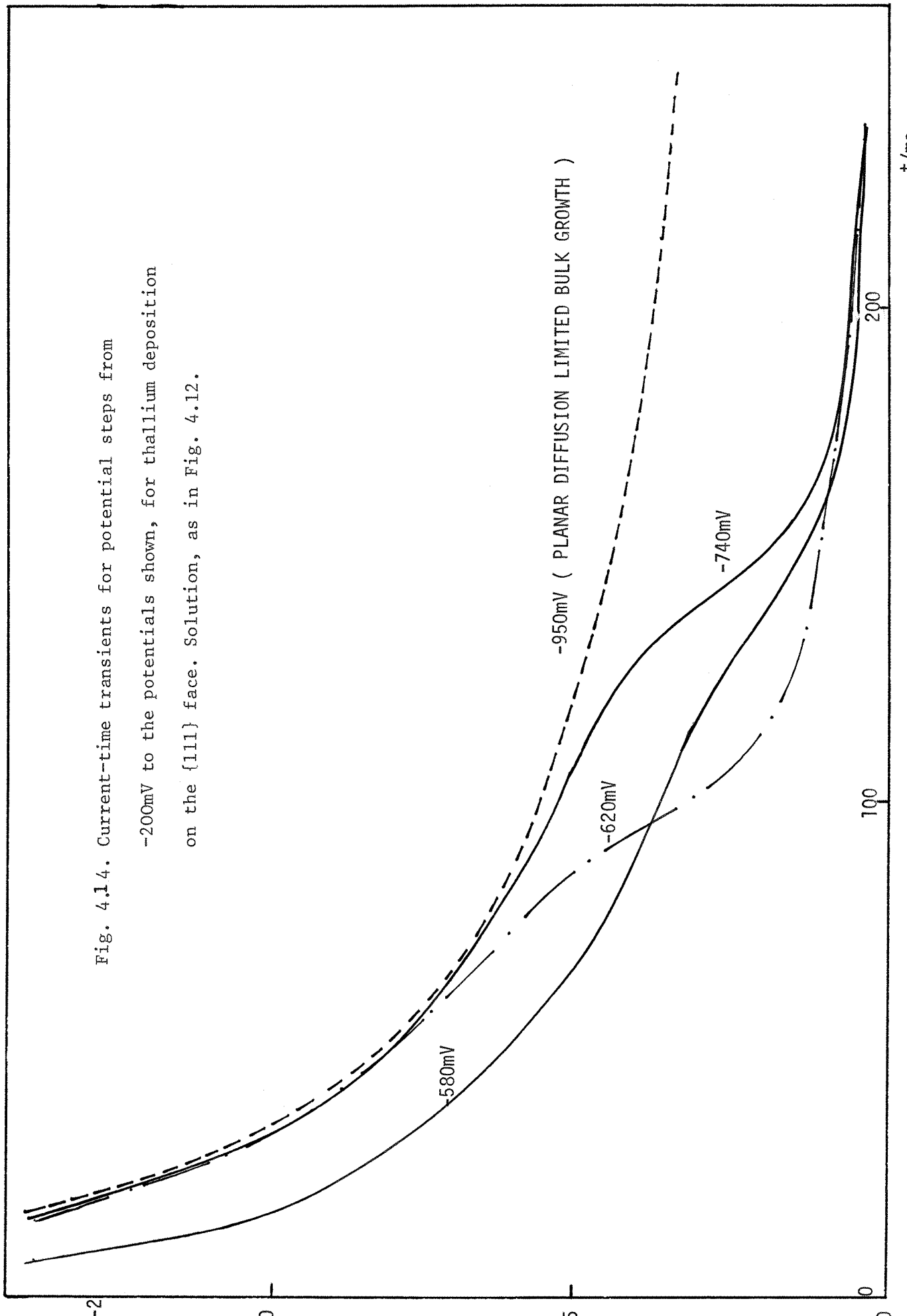

Fig. 4.14. Current-time transients for potential steps from -200mV to the potentials shown, for thallium deposition on the {111} face. Solution, as in Fig. 4.12.

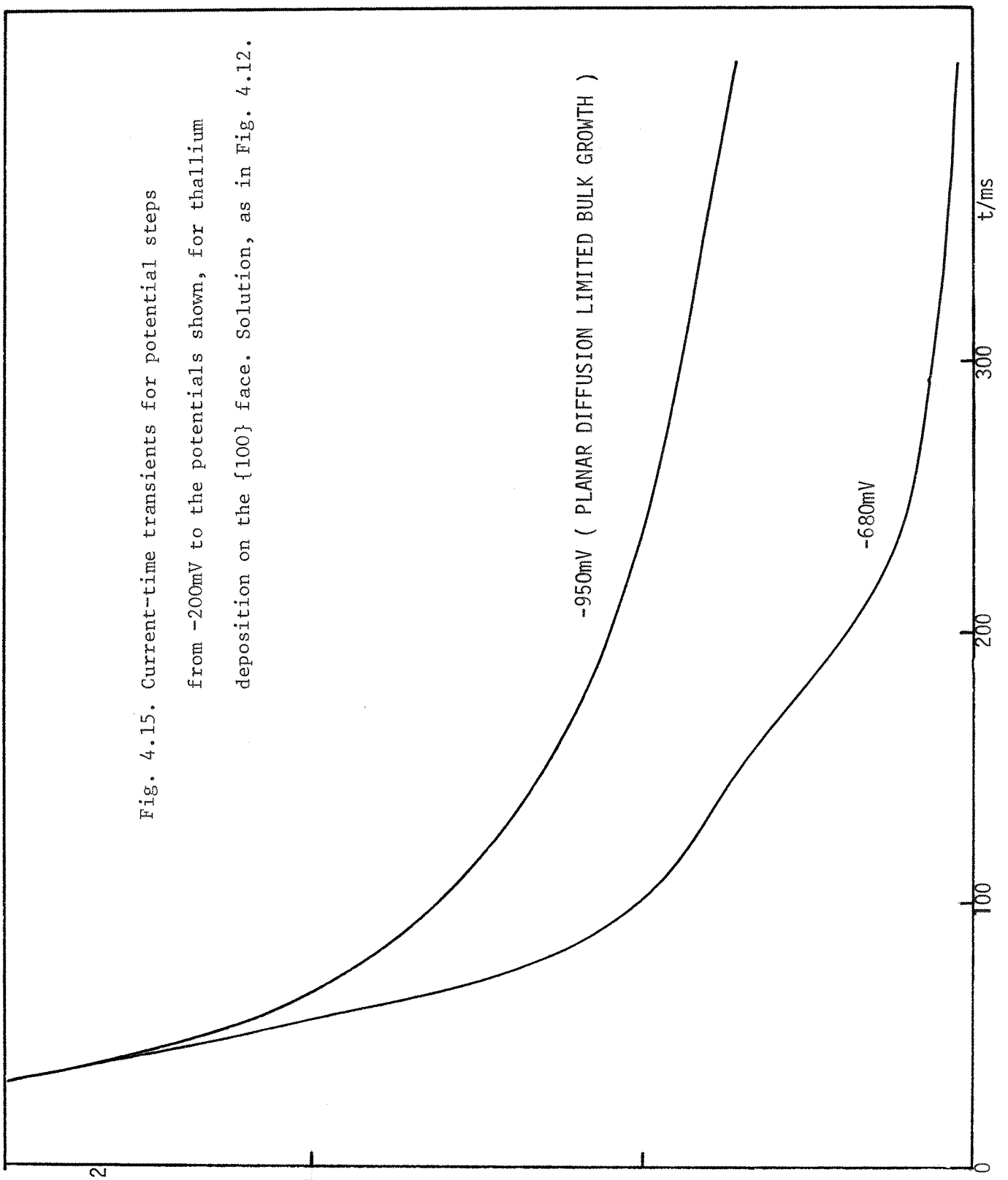

Fig. 4.15. Current-time transients for potential steps from -200mV to the potentials shown, for thallium deposition on the {100} face. Solution, as in Fig. 4.12.

this feature is 60-70μC cm^{-2}. A plot of i vs. $t^{-\frac{1}{2}}$ for this potential region is shown in Fig. 4.16.

{110} FACE.

At short times, the transients are under limiting planar diffusion control but then the current drops below this limiting value and the transient develops a slight hump, similar to, although not as well defined as, that found on the {100} plane. The charge associated with this feature is approximately 85-90μC cm^{-2}. Fig. 4.17 shows an i vs. $t^{-\frac{1}{2}}$ plot in this region.

Pulsing to potentials in the second monolayer region from a potential positive to that where any deposition occurs produces the following results.

{111} FACE.

At short times the shape of the transient is identical to that obtained by pulsing into the A_2 region of potential i.e. a diffusion limited falling transient with a rapid decrease from this value. At longer times however, an additional feature develops on the end of the transient which, depending on small variations in surface preparation, appeared either as a well defined peak, as shown in Fig. 4.18 or a pronounced hump.

{100} FACE.

Again the initial part of the transient (corresponding to the first monolayer formation) was identical in shape to that obtained at more positive potentials. At longer times a second hump developed corresponding to the second monolayer formation; this occurred at a magnitude of current well below the diffusion limiting value.

{110} FACE.

The transient initially showed a falling section with kink which at longer times was followed by a second falling segment.

These potential-step measurements can now be discussed in connection

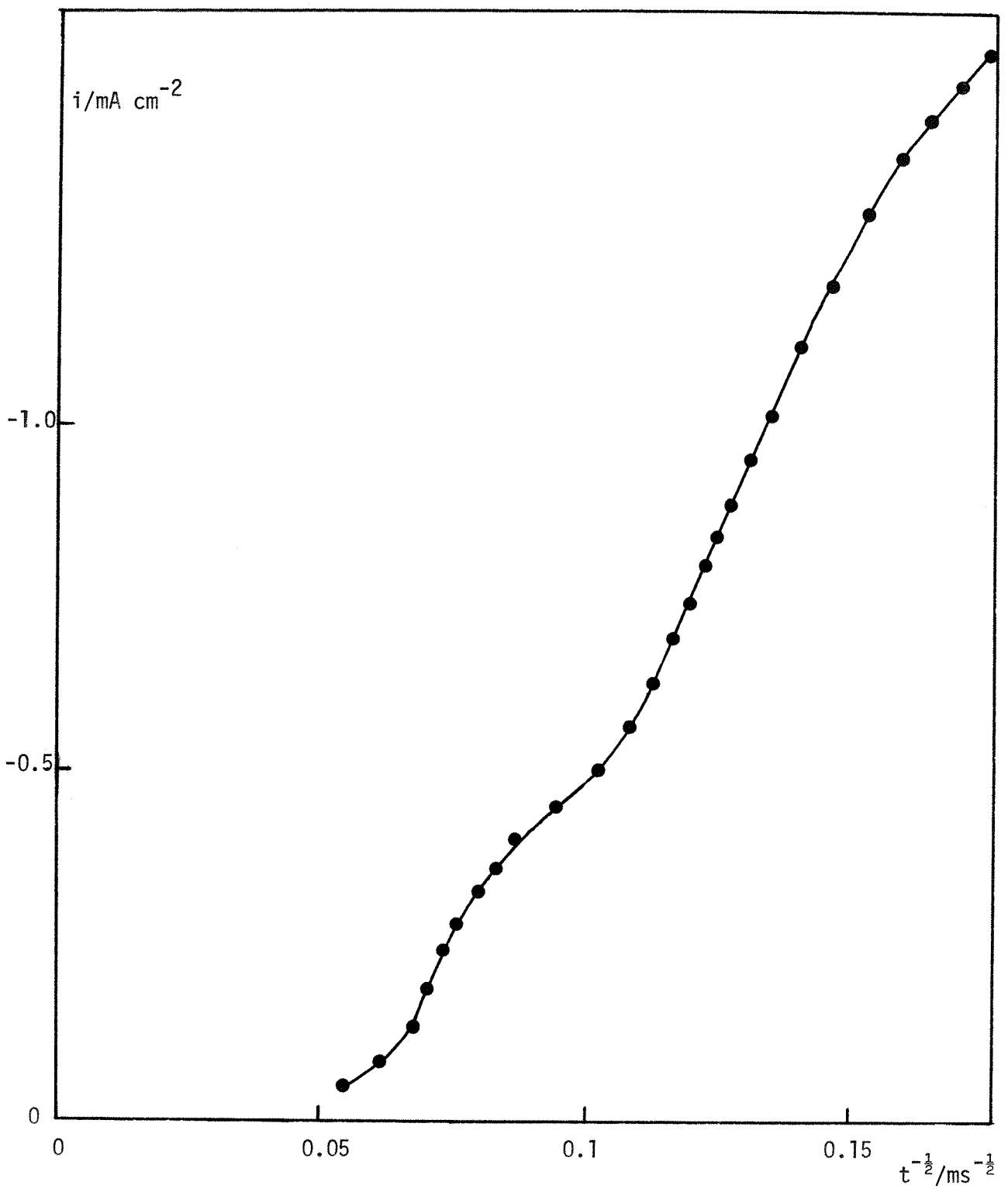

Fig. 4.16. Plot of i vs. $t^{-\frac{1}{2}}$ for a potential step from -200mV to -683mV for thallium deposition on the {100} face. Solution, as in Fig. 4.12.

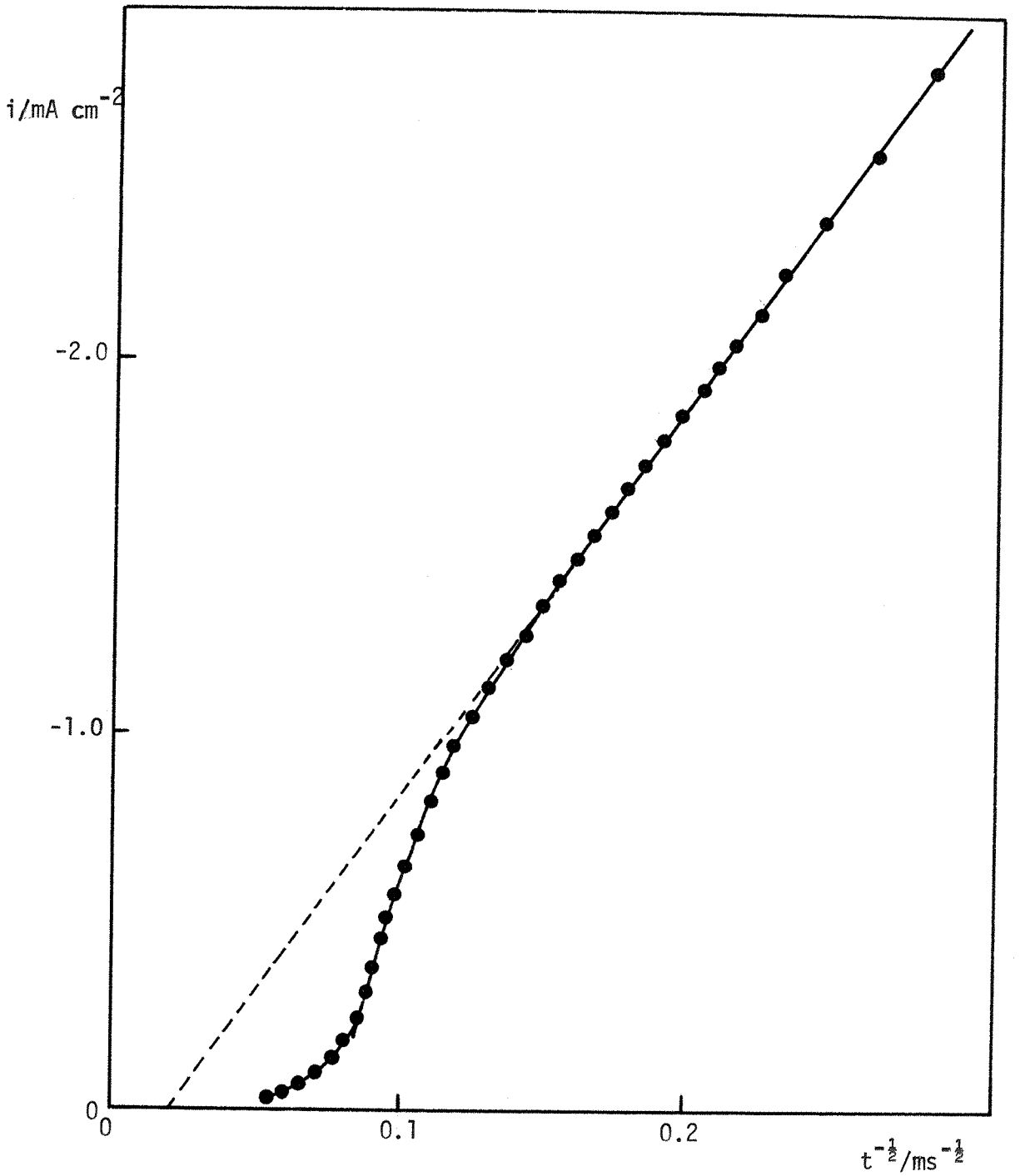

Fig. 4.17. Plot of i vs. $t^{-\frac{1}{2}}$ for a potential step from -200mV to -665mV, for thallium deposition on the {110} face. Solution, as in Fig. 4.12.

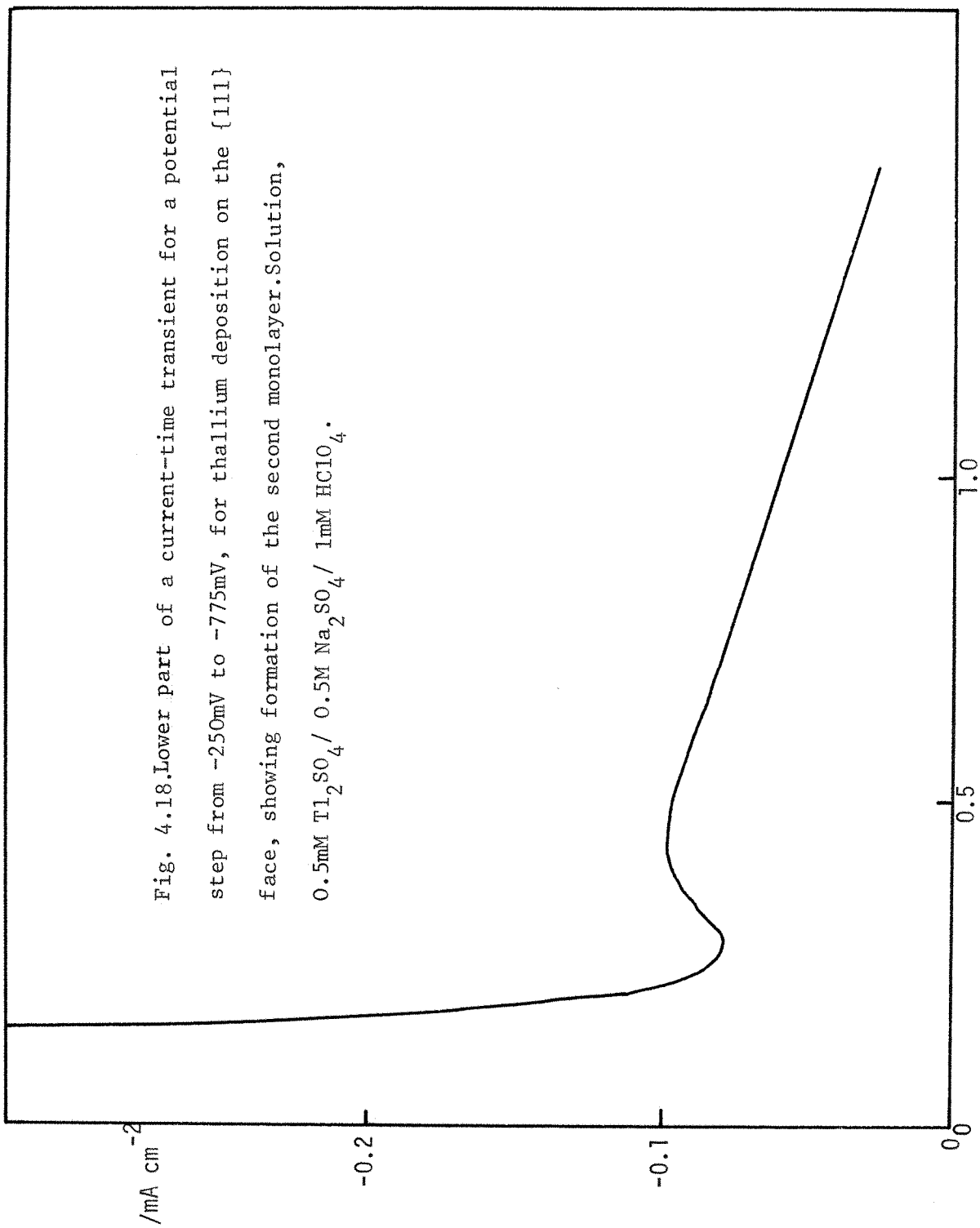

Fig. 4.18.Lower part of a current-time transient for a potential step from -250mV to -775mV, for thallium deposition on the {111} face, showing formation of the second monolayer.Solution, 0.5mM Tl_2SO_4 / 0.5M Na_2SO_4 / 1mM $HClO_4$.

with the model proposed for the U.P.D. process, based on the voltammetry and optical results.

4.5 (b) DISCUSSION: ADSORPTION REGION.

The dominating feature of the i-t transients on all crystal planes in this region of potential, is the linear relationship between i and $t^{-\frac{1}{2}}$ for the initial part of the transient.

The adsorption of neutral atoms on an electrode has been treated by Delahay.[98] In his treatment, it is assumed that the adsorption process is so rapid that it is controlled by the rate of planar diffusion and the surface concentration Γ is related to the volume concentration at the electrode surface, $C_{x=o}$, by the adsorption isotherm, i.e.

$$\Gamma = \frac{\Gamma_m . C}{a + C} \qquad (4.1)$$

where Γ_m is the surface concentration for maximum coverage and 'a' is a parameter which is characteristic of the isotherm. The adsorption isotherm can be linearized and hence,

$$\Gamma = KC \qquad \text{with} \quad K = \Gamma_m/a \qquad (4.2)$$

By a method involving Laplace transforms, the relationship between the concentration C and C^o (bulk concentration) is given by,

$$C = C^o\left[1 - \exp\left(\frac{x}{K} + \frac{Dt}{K^2}\right)\operatorname{erfc}\left(\frac{x}{2D^{\frac{1}{2}}t^{\frac{1}{2}}} + \frac{D^{\frac{1}{2}}t^{\frac{1}{2}}}{K}\right)\right] \qquad (4.3)$$

$$\therefore \quad \frac{dC}{dx} = -\frac{C^o}{K}\exp\left(\frac{x}{K^2} + \frac{Dt}{K^2}\right)\operatorname{erfc}\left(\frac{x}{2D^{\frac{1}{2}}t^{\frac{1}{2}}} + \frac{D^{\frac{1}{2}}t^{\frac{1}{2}}}{K}\right)$$

$$+ C^o\exp\left(\frac{x}{K} + \frac{Dt}{K^2}\right)\frac{2}{2D^{\frac{1}{2}}t^{\frac{1}{2}}\pi^{\frac{1}{2}}}\exp\left(-\frac{x}{2D^{\frac{1}{2}}t^{\frac{1}{2}}} + \frac{D^{\frac{1}{2}}t^{\frac{1}{2}}}{K}\right)^2 \qquad (4.4)$$

$$\therefore \quad \left(\frac{dC}{dx}\right)_{x=o} = -\frac{C^o}{K}\exp\frac{Dt}{K^2}\left(\operatorname{erfc}\frac{D^{\frac{1}{2}}t^{\frac{1}{2}}}{K}\right) + \frac{C^o}{\pi^{\frac{1}{2}}D^{\frac{1}{2}}t^{\frac{1}{2}}}\exp\left(\frac{Dt}{K^2}\right)\exp\left(\frac{-Dt}{K^2}\right) \qquad (4.5)$$

$\therefore$ by Fick's first law,

$$i = zFD\left(\frac{dC}{dx}\right)_{x=o}$$

$$= zF\left[-\frac{DC^o}{K}\exp\left(\frac{Dt^2}{K^2}\right)\operatorname{erfc}\left(\frac{D^{\frac{1}{2}}t^{\frac{1}{2}}}{K}\right) + \frac{C^oD^{\frac{1}{2}}}{\pi^{\frac{1}{2}}t^{\frac{1}{2}}}\right] \qquad (4.6)$$

This equation is identical to that derived by Astley et al. for the case of metal deposition in which the diffusion zones of each nucleus rapidly overlapped and the rate of the reaction was controlled by diffusion perpendicular to the surface. Plots of i vs. $t^{-\frac{1}{2}}$ for this equation were shown in Fig. 1.3 , at short times the slopes are of constant gradient equal to, $\frac{zFC^oD^{\frac{1}{2}}}{\pi^{\frac{1}{2}}}$, independent of η . Before the overpotential is high enough for the limiting diffusion controlled current to be achieved, the plots show a characteristic intercept on the $t^{-\frac{1}{2}}$ axis and they also develop curvature at longer times.

The experimental i vs. $t^{-\frac{1}{2}}$ plots, in the adsorption region, are in reasonable agreement with the predictions of this formula, except that the linear slope is not completely independent of potential. This is most marked on the {100} face but is also true to a lesser extent on the {111} and {110} faces. Such potential dependencies of the gradient may be caused by the partial charged nature of the adsorbed atoms; on the basis of the results from optical experiments, this would be expected to be most pronounced on the {100} face.

4.5 (c) DISCUSSION: CRYSTAL GROWTH REGION.

If the potential step is increased to include the region of peak A_2, an additional feature develops on the transients. The results for each

face will now be discussed separatly.

{111} FACE.

At potentials more negative than that of the A_2 peak, the majority of the deposition comes under limiting planar diffusion control. This rapid increase in the deposition rate compared to that found in the adsorption region would be expected on account of the extreme sharpness and relatively high current density associated with A_2. Unfortunately this prevents conclusive proof for the participation of crystal growth steps being obtained from the transient, as the observed kink would automatically result from the rapid decrease in current away from the planar diffusion limited value as the monolayer approached saturation. Such a transient only presents conclusive proof for crystal growth via two-dimensional, to the extent that it is argued that such a sharp peak as A_2 could only arise from the deposition of a crystalline phase rather than an adsorbed layer. It has been mentioned already that a distinction between a crystalline layer and an adsorbed layer with a high interaction parameter is questionable. In this case, there is no doubt that the final form of the first monolayer on the {111} plane is a close packed crystalline monolayer. What is not proved,however, is that two-dimensional nucleation steps are occurring as the initial stage in the crystallisation process or whether some homogeneous phase transition is taking place.

It is possible that more information about the nature of the crystallisation process could be obtained by removing the diffusion limiting constraint from the current-time transient by increasing the thallium ion concentration. The effect on the voltammetry of this concentration variation will be discussed in section 4.10. For the present purpose, the only relevant difference between the voltammetry in 50mM Tl_2SO_4 and 0.75mM Tl_2SO_4/ 0.5M Na_2SO_4 is the virtual absence of the adsorption peak A_1 (on the {111} face) in the more concentrated solution, i.e. the voltammetry shows two sharp cathodic peaks corresponding to the first and second

monolayer formation respectively.

Fig. 4.19 shows an example of a current-time transient obtained by pulsing to a potential slightly more negative than the first monolayer peak potential for a 50mM Tl_2SO_4 solution. The kink seen in the results for 0.75mM Tl_2SO_4 solutions is absent because the thallous ion concentration is now too high for the initial part of the transient to be controlled by planar diffusion to the electrode. The rate of current fall off is virtually linear with time. This type of behaviour is similar to that obtained from deposition of nickel monolayers onto mercury[24] from a thiocyanate complex where the surface diffusion of ad-atoms to growing centres was the slowest step in the deposition process; in this case, at lower potentials the transient posesses a rising section on account of the lower lattice building rate. In the present case, for thallium deposition from concentrated solutions, the basic shape of the transient is not altered by potential except that the current increases and the time scale contracts as the potential is made more negative. This suggests that lattice building rates are rapid compared to surface diffusion processes at all potentials and under these circumstances no direct information about the growth process can be obtained. However the fact that the experimental transients are very similar to those obtained in a system where crystal growth is known to be taking place strongly suggests that they do represent a crystal growth process rather than adsorption.

Double pulse experiments in the concentrated solutions, with the first pulse to a potential just prior to the second monolayer formation and the second pulse to the reversible potential produced a transient of the type shown in Fig. 4.20. These results show that, at this concentration, the rate of the second monolayer phase formation is also dominated by surface diffusion.

Single potential steps into the second monolayer region, in more dilute (0.5mM Tl_2SO_4) thallous ion solutions can produce a rising transient

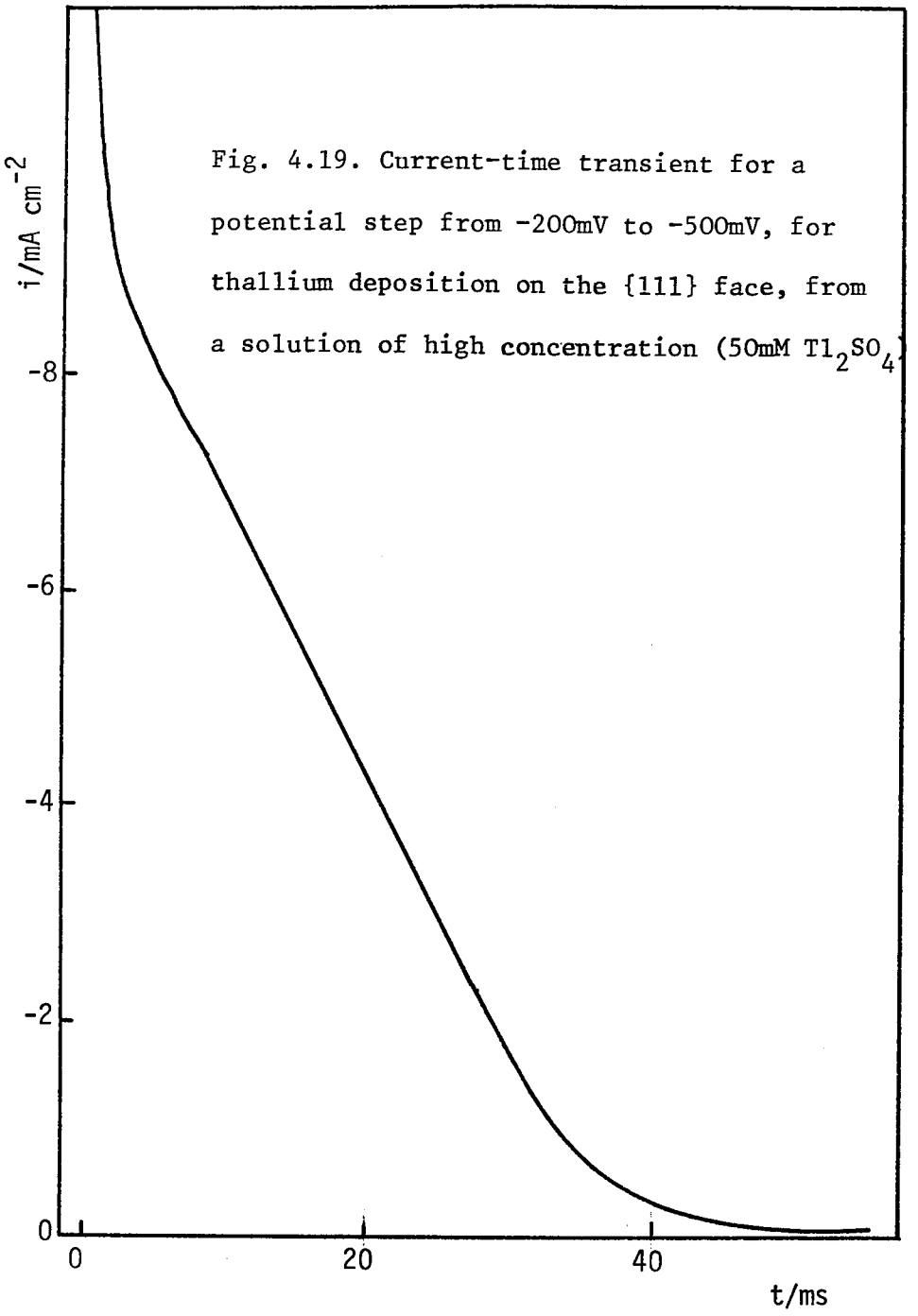

Fig. 4.19. Current-time transient for a potential step from -200mV to -500mV, for thallium deposition on the {111} face, from a solution of high concentration (50mM Tl_2SO_4)

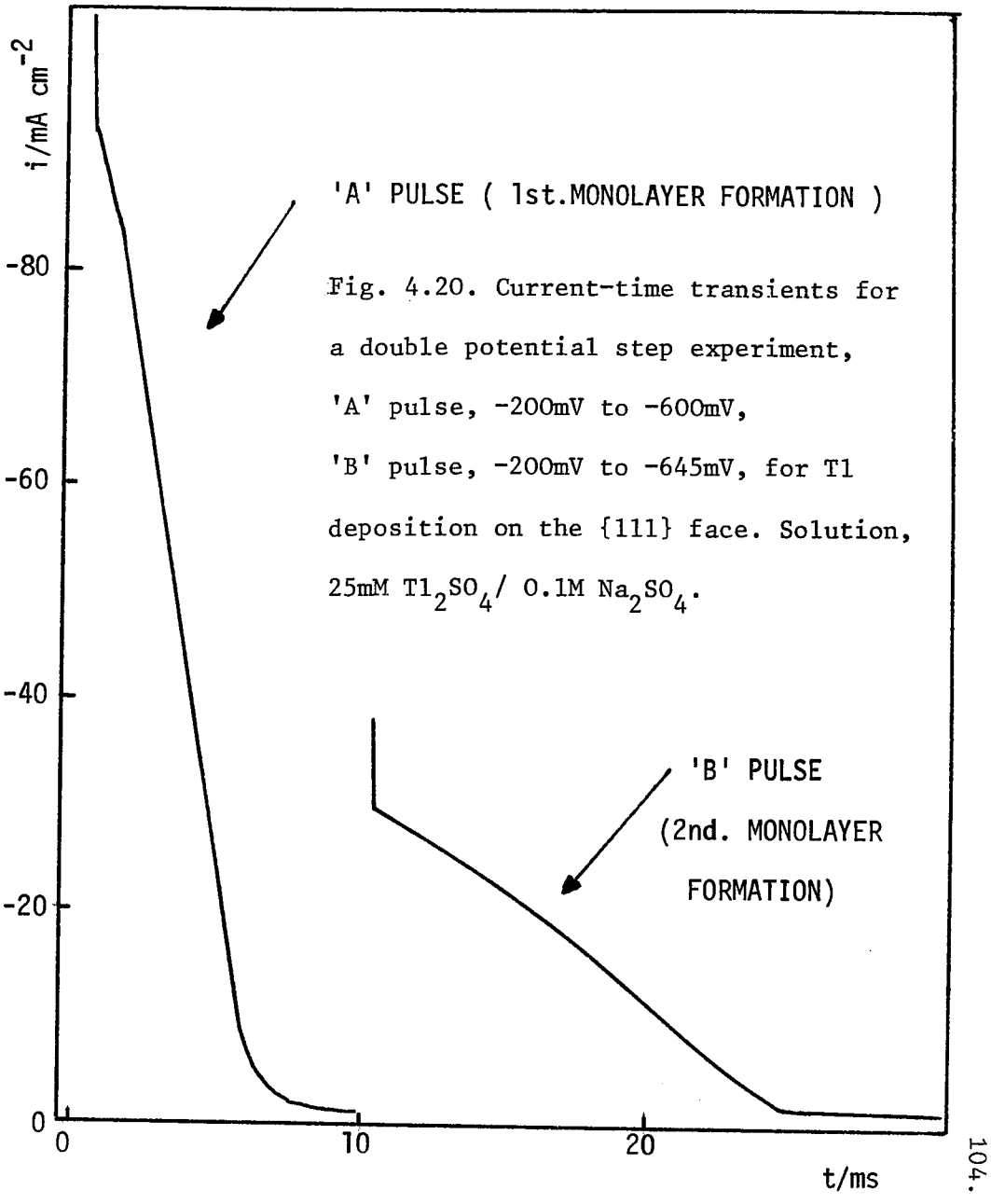

Fig. 4.20. Current-time transients for a double potential step experiment, 'A' pulse, -200mV to -600mV, 'B' pulse, -200mV to -645mV, for Tl deposition on the {111} face. Solution, 25mM Tl_2SO_4/ 0.1M Na_2SO_4.

as was shown in Fig. 4.18. This rise is preceeded by a falling transient with kink, corresponding to the first monolayer formation. A rising transient of this nature could arise from two-dimensional nucleation processes taking place in the formation of the second layer. Another possibility is that the rise in current is caused by an increasing flux of material to the surface; this situation would result if the rate of the first monolayer formation dropped to a sufficiently low value to allow the surface concentration of Tl^{+} to relax back towards the bulk value. In this case the peak in the transient would arise through diffusion processes. The decay from the planar diffusion limited current, for the first monolayer formation at this potential, occurs at a current density of 700μA cm^{-2} and a time of 130ms. The current density, i_{max}, associated with the second monolayer peak in Fig. 4.18, is 97μA cm^{-2} and this occurs at a time of 450ms. These figures show that i_{max} cannot be limited by bulk diffusion processes, as the experimental value is much lower than could be obtained, even assuming the rate of formation of the first monolayer did not fall off significantly. The peak would seem to arise therefore, through overlap processes in the crystallisation of the second layer. The sensitivity of the peak shape to surface preparation, also suggests that it is caused by two-dimensional nucleation and growth.

{100} FACE.

The relatively large potential interval between the A_1 and A_2 peaks on this plane, results in the adsorption process coming under limiting planar diffusion contol (i.e. $C_{surface} = 0$) at short times, before the A_2 peak potential is reached. However this enables a more direct indication of crystal growth to be observed on the transients from potential steps into the A_2 region, as the latter stages of the adsorption process are sufficiently slow to reduce the current flowing, to a value well below the diffusion limited one and consequently, the subsequent rearrangement and crystal growth processes, assuming rate control by lattice incorporation, will contribute an increase in current with time and can be seen as a distinct

hump on the falling transient, rather than the rapid decrease from the planar diffusion limited value, as seen on the {111} face. The fact that a hump, rather than a well defined rising transient is seen, can be attributed to the relatively small amount of charge (70-80μC cm^{-2}) associated with the A_2 peak on this face. Moreover, the optical results strongly suggest that much of this charge is associated with redistribution rather than extra deposition; this would reduce the tendency for the current to increase with time on account of any increase in the peripheral area of the growing centres especially if the lattice building rate was at all limited by preceeding diffusion processes, as seems to be the case on the {111} plane.

At more negative potentials, in the second monolayer region, the i-t transients show a second hump corresponding to crystal growth processes in the second layer formation. The absence of a well defined peak, as seen on the {111} plane, is almost certainly attributable to the prior adsoption step, indicated by the voltammetry and optical results. Double potential step experiments were not helpful in providing increased delineation of the crystal growth process occurring in the formation of either the first or second monolayers.

It is interesting that the chronological order of events in the overall deposition process of the two monolayers seems to be identical whether occurring as a result of a potential step to, say, the reversible potential for the bulk deposition process, or from a linear sweep to the same potential. This is confirmed by Fig. 4.21, which shows a reflectance -charge plot obtained as a result of a potential-step from a potential where no deposition occurred, to a value in the overpotential region. It is virtually identical to the plot obtained from a linear sweep experiment over a similar potential range (shown in Fig. 4.9). These results confirm that the formation of the thallium monolayers is an essential precursor to the deposition of thicker films. This point will be taken up again in Chapter 6.

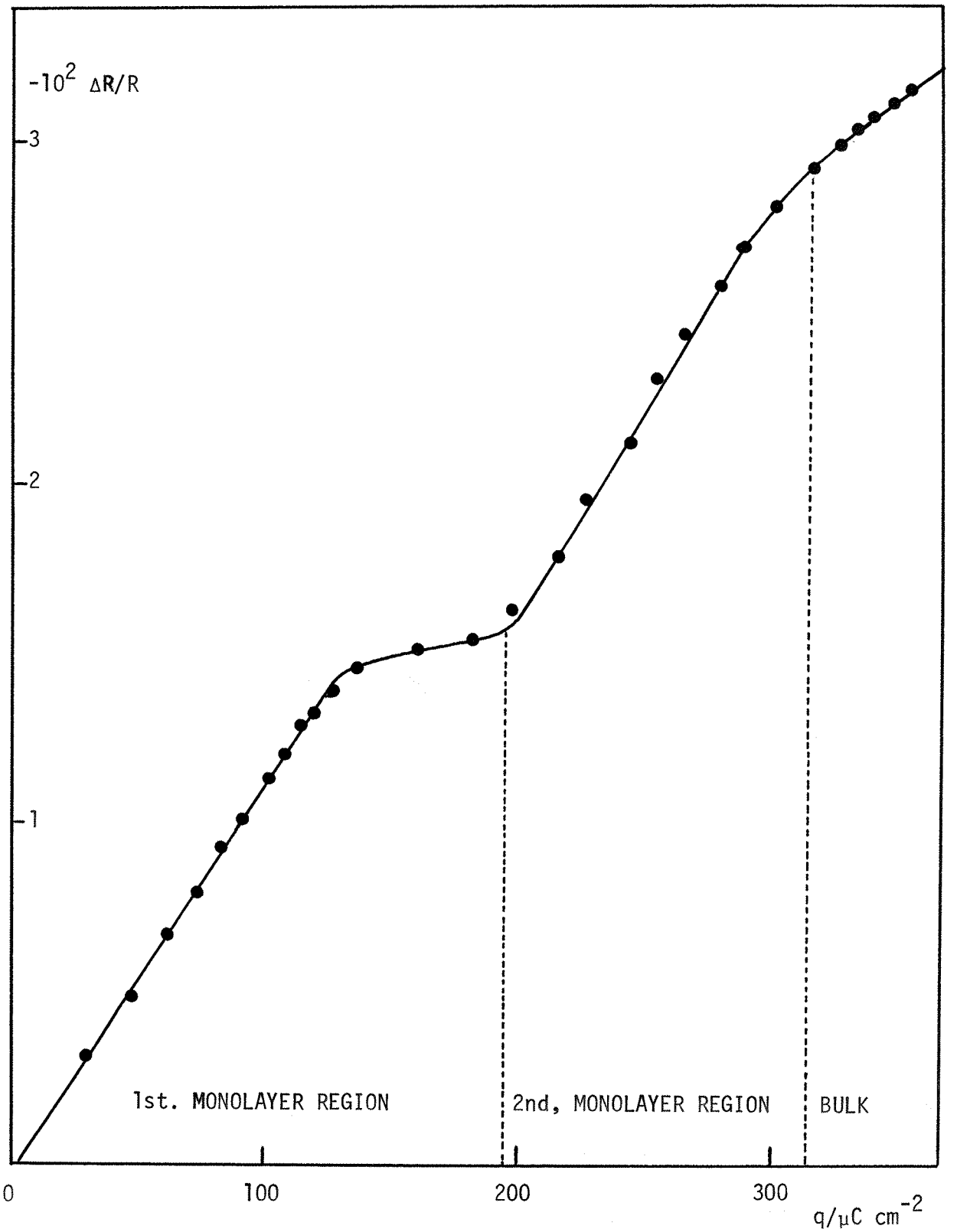

Fig. 4.21. Plot of ΔR/R against charge q for thallium deposition on the {100} plane of silver for a potential step from -400mV to -913mV (vs. S.C.E.). λ = 589nm, parallel polarisation. Solution, 0.75mM Tl_2SO_4/ 0.5M Na_2SO_4/ 1mM $HClO_4$.

{110} FACE.

The A_2 peak on this face is not only mixed up with the adsorption peak A_1 but is also less sharp than the phase peaks on the other two crystal faces. However a sharp peak would only result if the activity of the deposited phase was independent, or only slightly dependent, on the fraction of surface covered. The validity of this condition is discussed later. It is sufficient to mention however, that the'open' structure of the {110} substrate would seem to prevent the deposition of a foreign metal on top of it whose activity was largely independent of the amount deposited.

Potential steps into the A_2 region do produce a slight hump on the transient but this is not as well defined as that on the {100} plane. The $i\text{-}t^{-\frac{1}{2}}$ plots in this range, however, show similarities to those from the {100} plane.

The difficulty of separating the adsorption and phase transformation processes on this plane would seem to be responsible for the poor definition of both the optical and potential step results. By analogy with the results from the other two crystal faces, the fact that a slight hump occurs in the i-t transient,suggests the occurrence of crystal growth processes.

Potential steps into the second monolayer region produce only a falling transient on the end of that shown for steps into the A_2 region and no information can be obtained about the occurrence of crystallisation steps.

The combined evidence from the potential sweep, potential step and optical experiments, shows conclusively, for the first time, that the formation of two-dimensional crystal planes is an important feature in the underpotential deposition of metals. These systems do appear therefore, to be somewhat analogous to those in which crystalline monolayer salt films

are formed, at underpotentials, on mercury; in these cases however, the shifts involved are relatively small (<50mV). Unfortunately, in the present case, the occurrence of two-dimensional nucleation steps as the initial stage of the crystal growth process, cannot be proved unequivocally as the i-t transients are dominated by diffusion processes.

4.6 THE SUPERLATTICE MODEL FOR ADSORPTION.

Before considering the nature of the crystalline phases formed in more detail, it is interesting to compare the surface coverages at which phase transformation occurs on the different crystal faces. These values, given as measured charges for the first monolayer transformation, are shown in Table 4.3, column 1. Column 2 gives the values corrected for surface roughness, using the factor of 1.22 obtained earlier and they show that the closest packed crystal plane, the {111}, adsorbs the least amount of metal.

These results can be explained by assuming that the adsorption of thallium atoms occurs on the interstitial sites between the surface silver atoms, leading to the formation of a superlattice. Such structures are well known from L.E.E.D. investigations of gas phase adsorption phenomena[99]. A scaled representation of the superlattice model, for each orientation, is given in Fig. 4.22.

It should be pointed out at this stage, that this model was first proposed by Lorenz et al.[63,71,84] to explain their results for the deposition of thallium onto monocrystalline silver electrodes. However, linear sweep voltammograms obtained by these workers, on each of the single crystals, were qualitatively identical to Fig. 4.1 but the charge values associated with the monolayer deposition peak, were dependent on orientation. The fact that several different (mechanical and electrochemical) polishing methods gave very similar results and the very marked dependence of the monolayer charge values on sweep speed[84], indicates that surface preparation and/ or solution purity, were inadequate in their case. It is possible that

TABLE 4.3

CRYSTAL FACE	AMOUNT OF CHARGE PASSED BEFORE PHASE CHANGE OCCURS IN 1st MONOLAYER. /μC cm^{-2}	CORRECTED VALUES OF CHARGE, ASSUMING A ROUGHNESS FACTOR OF 1.22. /μC cm^{-2}	VALUES OF CHARGE FROM SUPERLATTICE MODEL OF LORENZ. /μC cm^{-2}
{110}	91	75	68
{100}	125	102	96
{111}	60	50	53

Values of the charge at which the phase transition occurs in the first monolayer region together with values calculated from the superlattice model, assuming all favourable adsorption sites have been filled.

It is, in fact possible to have a higher concentration of deposited atoms on the {111} plane than that shown in the above Table: this was not considered by Lorenz though.

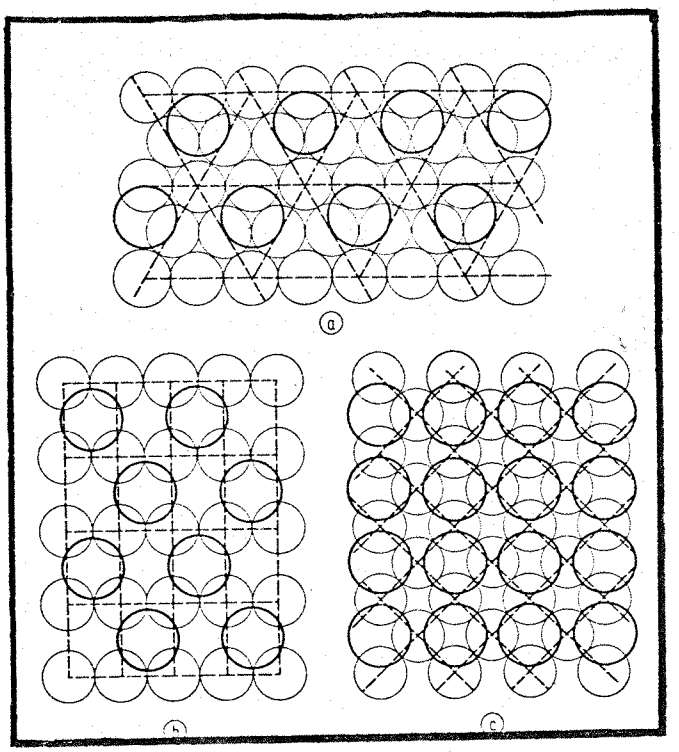

Fig. 4.22 Lorenz' superlattice model for the adsorption of thallium on different crystal planes of silver, (a) {111} orientation (b) {110} orientation (c) {100} orientation.

the epoxy electrode housing material was contaminating the solution. Any agreement between their monolayer charges, and those expected from the superlattice model must be fortuitous. Mechanical polishing of the single crystals used in the present work, produced voltammograms identical to Fig. 4.1 in all cases,but unlike the results of Lorenz et al., the charge values were virtually independent of orientation.

Charge values calculated from the superlattice model are also shown in Table 4.3. It can be seen that there is good agreement between the experimental values of charge, corrected for surface roughness, and those calculated from the superlattice model. This stongly suggests that the adsorption process proceeds until all the favourable adsorption sites are occupied. It is important to stress however, that if the points at which phase transformation occurs, represent true thermodynamic potentials, they are not determined by the number of adsorption sites available on a particular orientation but principally by the energy of interaction of the close packed monolayer phase, with the surface crystal plane of the electrode. In the present case, for the {111} and {100} orientations, the adsorption sites do appear to be fully occupied before phase transformation occurs; on the {110} plane however, the transition seems to occur before the adsorption sites are completely filled. It is perfectly feasible for crystal phase formation to occur before any, or only a small amount, of adsorption has taken place, provided that the negative free energy change associated with this process is more favourable than that associated with adsorption.

Table 4.1 shows the potential at which the adsorption process starts on the different crystal planes. It can be seen that deposition starts at considerably lower potentials on the {110} and {100} planes, than on the {111}. It is likely that deposition will be most favoured when an adsorbed atom can interact with the greatest number of atoms in the substrate. This can be illustrated with Fig. 4.23 which shows the atomic

arrangements on the surface of each crystal. A silver atom on the surface of the {110}, {100} and {111} planes will have respectively, 5, 4 and 3 closest neighbours, In the {110} case, 4 neighbours are in the same plane as each other and the 5th is in the plane below.A thallium atom is slightly larger than a silver atom and consequently could not interact equally with 5 silver atoms in the {110} surface and so the adsorption sites on this plane would only be slightly more favourable than those on the {100} plane. The deposition starting potentials shown in Table 4.1 would therefore seem to reflect the differences in adsorption energy for a thallium atom on the different crystal planes.

It is interesting to note that these structural effects on the adsorption energy appear to greatly outweigh the effects of differences in the ionic contribution to the bonding due to variations in the work function with crystal orientation. The point of zero charge values for the {111}, {100} and {110} faces of silver are -690mV, -910mV and -1010mV (vs. S.C.E.) respectively.[100] If the work function values are correlated with these in the usual way,[101] then the underpotential deposition should commence at the most cathodic potential on the {110} face and the least cathodic potential on the {111} face, whereas the experimental data, Table 4.1, are completely opposite to this. Moreover, the magnitude of the differences between these starting potentials are very much smaller than would be expected from the slope of the plot obtained by the treatment of Gerischer et al.[57], e.g. a measured difference of + 38mV between the values for the {111} and {110} planes compared with a calculated difference of -140mV on this treatment.

4.7 THE SECOND MONOLAYER FORMATION.

The voltammetry peak structure in the region of the second monolayer is also dependent on the substrate orientation although not to the same extent as the first layer. This suggests that the effects of the substrate

structure are still important even though charge values indicate that the final form of the first monolayer is a close packed thallium layer in all cases. This behaviour can be explained with reference to Fig. 4.23 showing the hard sphere models of the different crystal faces. After formation of the first monolayer on the {111} face, the surface will consist of a close packed thallium layer on a close packed silver surface, there are no particularly favourable sites for adsorption and nucleation and crystal growth of the second layer, starts directly.

In contrast, crystal phase formation of the second monolayer on the {100} and {110} planes (in the latter case, there is no firm evidence for it), is preceeded by an appreciable amount of adsorption and it is possible to envisage the existence of special adsorption sites for these two orientations, similar to those in the underlying silver surface. A number of thallium atoms in the close packed first layer will lie above the specially favourable sites for adsorption on the silver substrate and could possibly move down slightly into the silver surface to occupy these sites. This process would create adsorption sites in the first layer for the second layer and by this means the structure of the underlying substrate would be partly reproduced in the first close packed thallium layer without greatly affecting the number of atoms in the layer (the latter quantity being almost identical for the three orientations).

4.8 EFFECT OF SUBSTRATE ORIENTATION ON THE CRYSTALLINE PHASE PROPERTIES OF THE DEPOSIT.

The fact has already been pointed out, that the deposition of a monolayer phase of constant activity, should occur at a single potential. If the growth process involves a rearrangement of an existing adsorbed layer, as is the case here, one is concerned with a phase transformation as well as a crystal growth process. A 'first order' phase transformation process would occur at a single potential, however a'second order' or

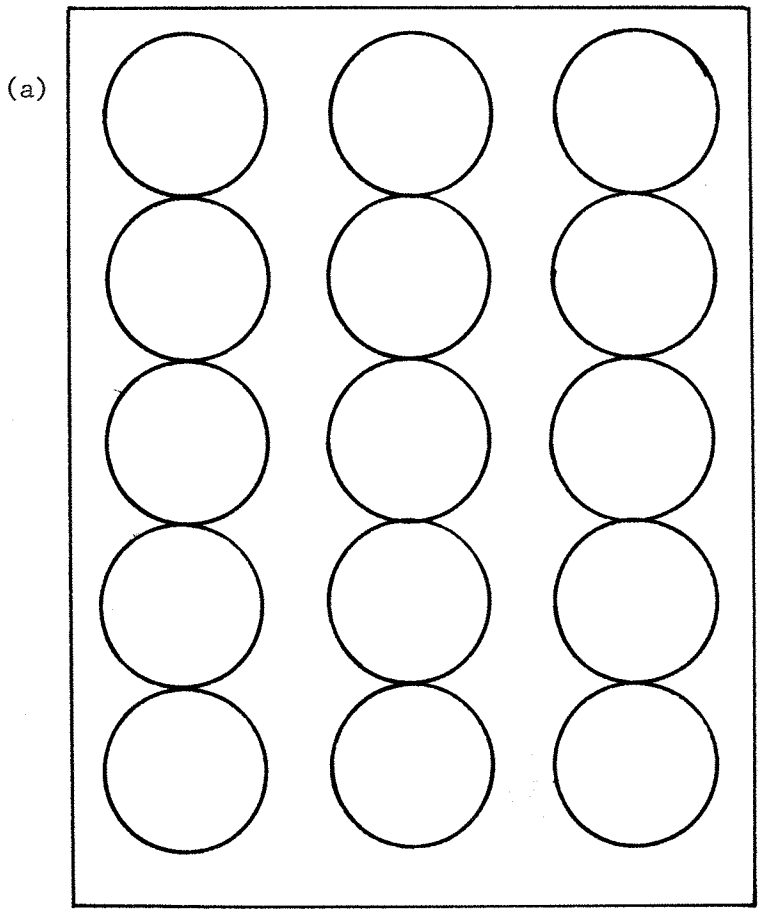

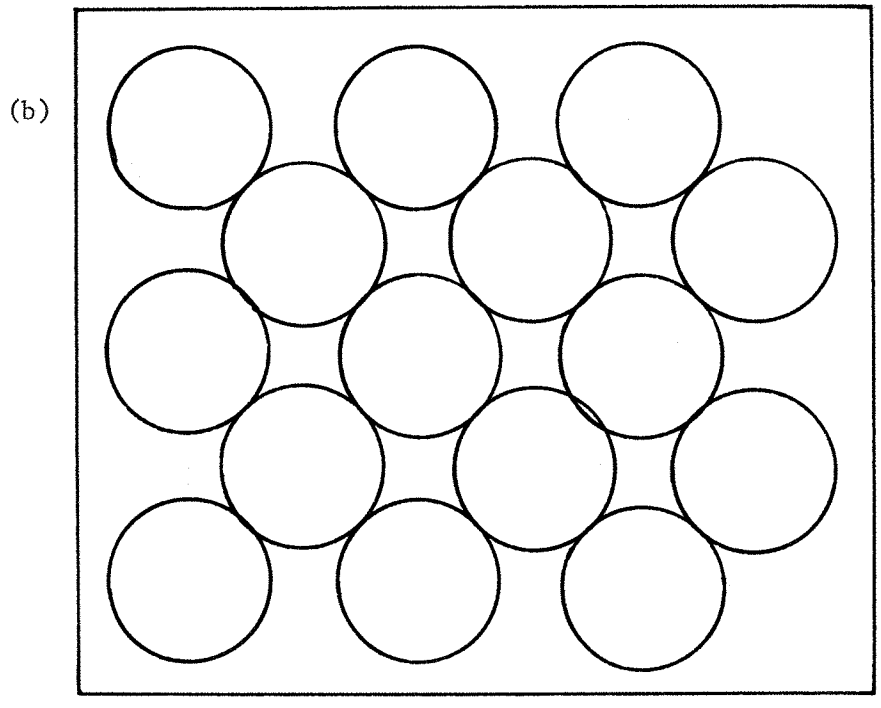

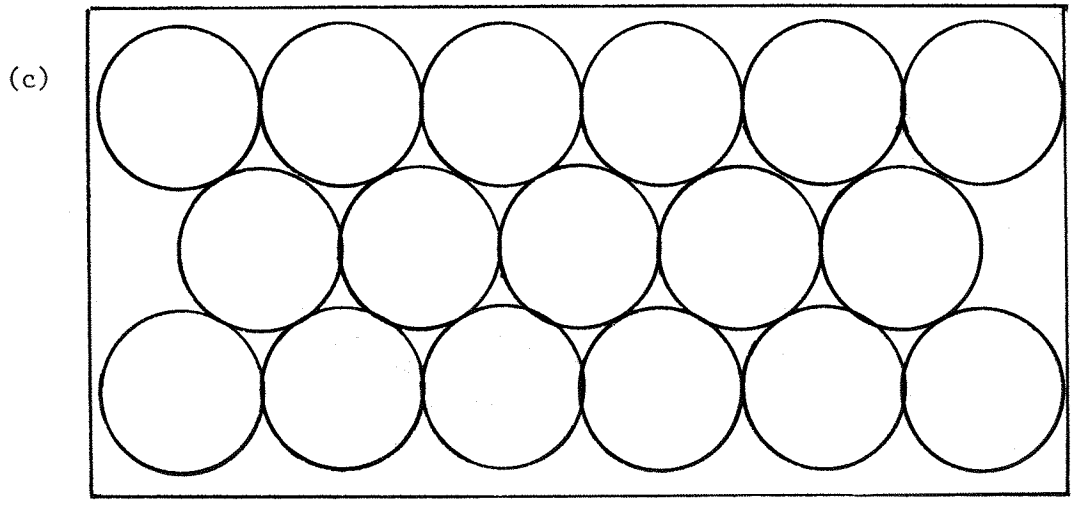

Fig. 4.23 The arrangement of atoms at different crystal faces of silver, (a) {110} (b) {100} (c) {111}

'continuous' transition, i.e. one whose rate depends on the extent of the transformation, would occur over a range of potential. Many examples[102] of first and second order transformations, involving adsorbed gas layers on solid metals, are available but comparatively little information has been published about such processes occurring in the liquid phase. Much of the earlier work in this area is suspect on account of poor surface definition. The same criticism would seem to apply to much of the published work on underpotential deposition.

Another factor which could cause the crystal phase deposition to occur over a range of potential, is electrode surface heterogeneity. The extent of this in the present case must be reasonably small, as identical voltammetry results were obtained on dislocation free micro-electrodes and also epitaxially deposited silver films ({111} orientation).

The effect of substrate orientation on the properties of the crystalline phase will now be considered more closely. The results from the potential decay experiments, shown in Fig. 4.24, will be used in this discussion. In each case, these plots show regions of slow decay in the range of potential previously assigned to crystal plane formation and removal, although these are hardly discernible for the {110} orientation. In particular, for the {111} orientation, these regions are very sharply defined plateaux indicating that the corresponding monolayers are well defined phases, which show only a small activity change over a wide range of surface coverage. This behaviour contrasts strongly with earlier assumptions concerning the nature of underpotential monolayers, i.e. it was assumed that the activity of the deposit was a linear function of the fraction of surface covered.

It is interesting to consider why the phase layers formed on each single crystal should have markedly different properties. Fig. 4.24 shows that for the {110} face the phase layer seems to have an activity which varies considerably with surface coverage, in marked contrast to the {111}

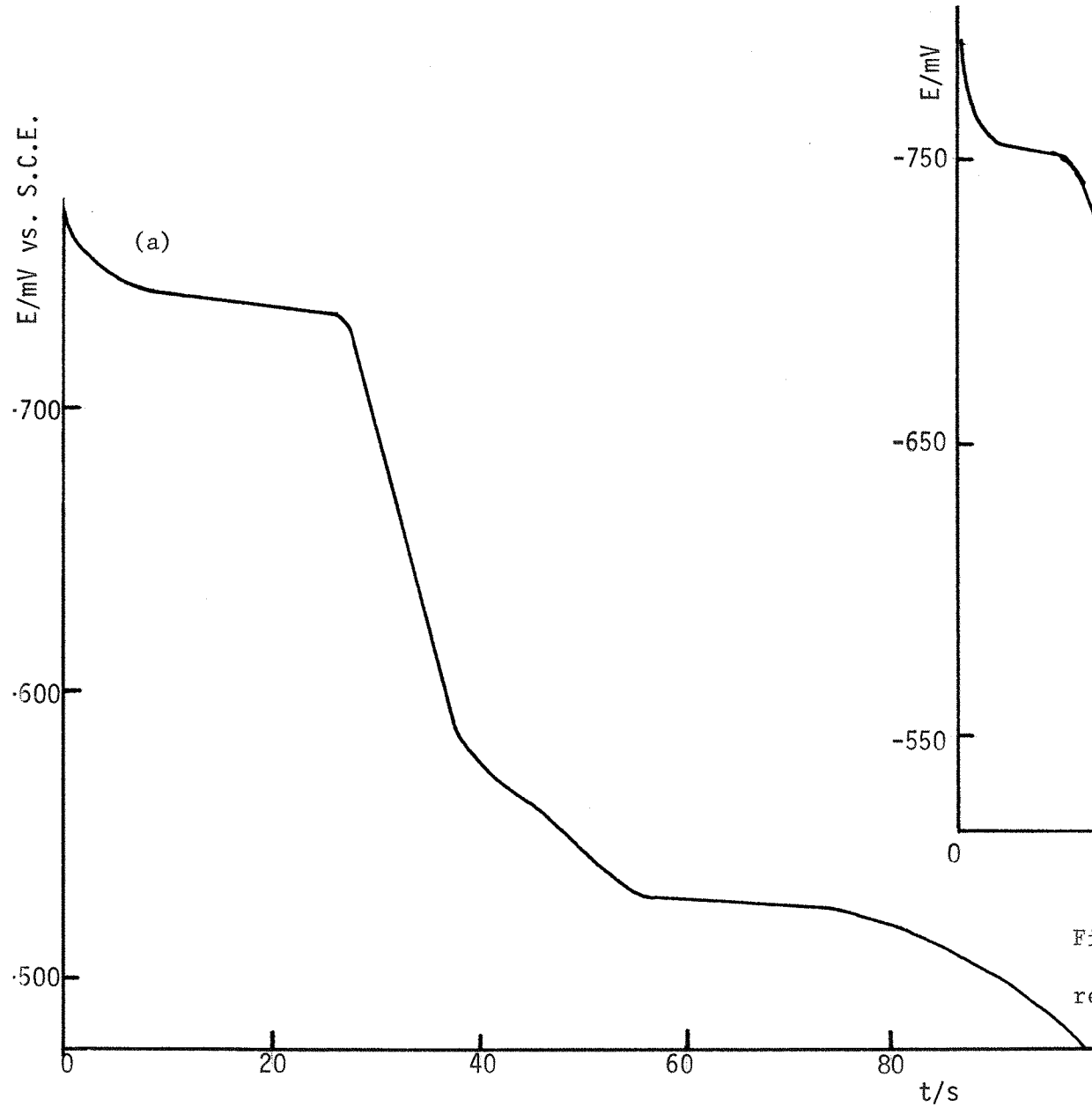

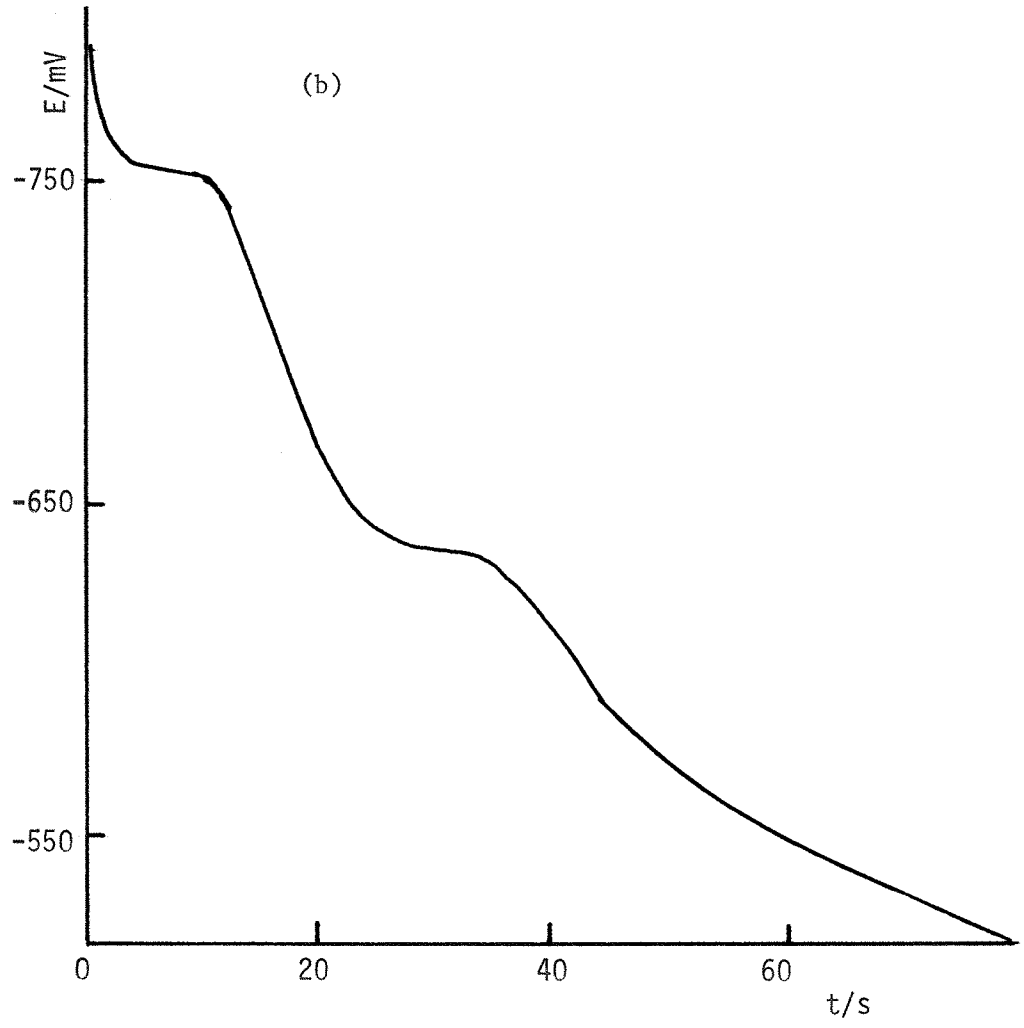

Fig. 4.24. Potential/time decay curves for thallium removal from silver electrodes of different orientation. (a) {111} face. (b) {100} face. Solution, as in Fig.4.5

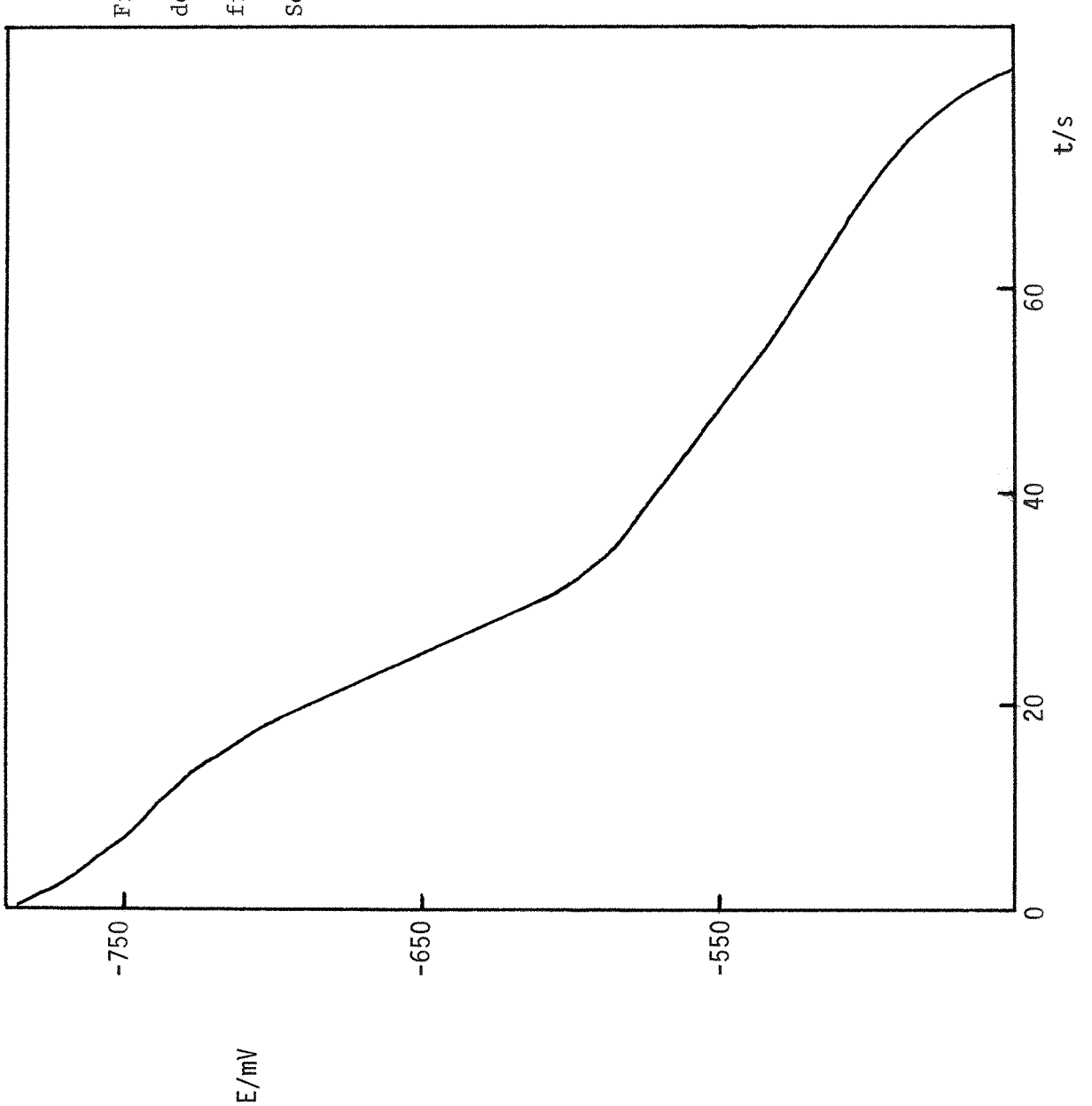

Fig. 4.24(c). Potential/time decay curve for thallium removal from the {110} plane of silver. Solution, as in Fig. 4.5.

face. The {100} face results fall between these two extremes. The reason for this difference is almost certainly due to the distortion of the monolayer structure by the structure of the substrate as discussed above.

Although charge measurements indicate that the complete (first) monolayer exists as a close packed layer in all cases, this will be distorted to an extent depending on the substrate structure. For the {110} orientation, which is the least densely packed of the three crystals used, this distortion would be greatest and moreover would be expected to decrease with increasing surface coverage as the monolayer structure becomes progressively less able to be moulded by the substrate. This would result in a coverage dependent activity, as found experimentally. However, for the {111} substrate, its close packed surface layer presents a relatively flat profile for the depositing monolayer phase and comparatively little distortion would be expected.

The features found in Fig. 4.24 correlate well with the voltammetry in that very sharp peaks are found on the {111} orientation, whilst the {110} crystal produces quite broad phase peaks. However, in voltammetry experiments, the sharpness of a phase peak increases with decreasing sweep speed until a limiting peak width is obtained. This effect is caused by the relatively slow rate of the phase formation process rather than the activity/coverage relationship varying with sweep speed. Any kinetic influence on Fig. 4.24 can be ignored as these results were recorded at sufficiently slow stripping rates for such effects to be absent.

It is interesting to compare these results with those predicted from the theory of Gerischer et al.[57] relating underpotential shifts to the work function difference between the substrate and the deposited metal. These workers used data obtained with polycrystalline electrodes to illustrate their correlation,which showed no distinction between adsorption and crystal phase formation and consequently the significance of the potentials used is not clear. It has already been shown that this correlation

does not hold for the potentials at which the onset of adsorption was observed; these were, in fact, in the reverse order to that predicted. However, it would seem most reasonable to apply the correlation to the crystalline phase formation potentials, since the work functions are properties of crystalline phases; it would be expected that the underpotential shifts of the phase peaks in the voltammograms would provide an accurate test of the Gerischer thoory. Although, for the {110} orientation, Fig. 4.24 (c) does not provide a simple value for the equilibrium phase potential (first monolayer), a value can be estimated fairly accurately from the voltammetry, as the equilibrium phase potentials for the other two faces coincide with the start of the phase peak in the voltammetry. The mean phase potentials for the first thallium monolayer, on the different orientations, are tabulated in Table 4.4.

The work function theory predicts the underpotential shift on the {111} plane to be 140mV larger than on the {110} (these figures were calculated assuming the work function of the monolayer phase to be independent of the substrate which is justifiable as the phase structure on all faces seems to be close packed). These calculated values give better agreement with the experimental values in Table 4.4, than was found for the adsorption potentials. The difference between the {111} and {100} planes is similar to that expected from theory but the {110} potential appears in the wrong position in the sequence. Such a disagreement is to be expected since the theory takes no account of the epitaxial relationships between the substrate and the deposit and the way in which these govern the interactions between them and affect the structure of the deposited phase layer. It seems that a model incorporating such interactions is needed. A complete simulation of a close packed thallium or lead layer on top of the different silver faces, involving lattice distortion effects, would be difficult. Nevertheless it seems probable that, neglecting monolayer lattice distortion, the amount of overlap between a close packed

TABLE 4.4

CRYSTAL FACE	THALLIUM PHASE POTENTIAL (1st. MONOLAYER)/mV
{111}	-523
{100}	-633
{110}	-571

Table showing the phase potential of the thallium monolayer (1st.) on the different crystal planes. Solution, as in Fig. 4.5.

TABLE 4.5

CRYSTAL FACE	AMOUNT OF FREE SPACE /%
{111}	9.5
{100}	21.2
{110}	44.6

Table showing the variation in the amount of free space at the surface, for the different silver orientations.

layer of thallium and the various crystal faces of silver, would be highly dependent on the packing density in the surface of the substrate, i.e. maximum overlap would occur with a monolayer on top of the most densely packed silver lattice (the {111}) and the smallest overlap with the least densely packed lattice (the {110}). It is probable that maximum overlap between monolayer phase and substrate would favour phase formation at the most anodic potential, i.e. whilst lattice energy is gained by forming a crystal plane, it is important not to lose too much bond energy by sacrificing interactions with the substrate. Table 4.5 gives the amount of'free'space at the surface of each single crystal, calculated from a hard sphere model. These figures would predict a phase potential/orientation sequence with the same order as that obtained from the work function theory. It would appear therefore, that the deformation of the close packed monolayer phase on the {110} surface increases bonding with the substrate sufficiently to allow phase formation to occur at a more anodic potential than would be expected if no distortion occurred. This would also be accompanied by the loss of a certain amount of lattice energy associated with the formation of a close packed plane. This would occur to a much smaller extent on the {100} surface.

It is evident from these results, that any model which successfully describes quantitatively the variations of underpotential shift with different metal couples, must consider structural interactions in addition to work function differences.

4.9 THE EFFECT OF ANIONS, pH AND THALLIUM ION CONCENTRATION.

In addition to the studies in sulphate solutions, thallium deposition from perchlorate, fluoride, acetate and chloride base electolytes, has been investigated. The results showed that, provided the system anion is not extensively specifically adsorbed on the electrode (ClO_4^-, F^-, SO_4^{2-} and CH_3COO^- fall into this category) the qualitative features of the

linear sweep voltammetry were identical in all cases. However, the results from solutions containing an ion e.g. chloride, which does undergo specific adsorption on the electrode, were markedly different. L.S.V.'s for thallium deposition from chloride ion solutions, are shown in Fig. 4.25 for the three crystal faces. It is clear that the chloride ion has a pronounced effect on the mechanism of the U.P.D. process and the simple pattern observed, e.g. in sulphate ion solutions, is no longer followed.

The underpotential shift, ΔU_p, (the potential difference between the stripping peaks of monolayer and bulk deposits)) is considerably smaller than that found in sulphate and perchlorate solutions etc.. For example, for the first monolayer phase peak on the {111} face, ΔU_p at 30mV s^{-1} in the solution 0.75mM Tl_2SO_4/ 0.5M $NaClO_4$/ 10mM $HClO_4$ is 267mV. whereas in 0.32mM Tl_2SO_4/ 0.3M KCl/ 1mM $HClO_4$, ΔU_p is 193mV. The magnitude of the underpotential shift is a function of the difference in strength between the chloride ion interactions with silver or thallium and also of the way in which the silver-thallium interaction is modified by the presence of adsorbed chloride on the thallium.

It would be expected that the substrate silver would have a greater affinity for chloride ion adsorption than the thallium (being the more electronegative metal). This effect alone would cause the effective electronegativity difference and hence the underpotential shift, to decrease (i.e. more energy is lost breaking silver-chloride bonds than is gained forming thallium-chloride bonds). In addition, any reduction of the $\delta+$ charge on the thallium atoms through bonding with the chloride ions, would also reduce the strength of bonding with silver.

Many previous studies of U.P.D. have been carried out in chloride ion solutions but the present results show that the behaviour obtained in this medium, is complex even on single crystals.

Although the L.S.V. results from the solutions containing anions

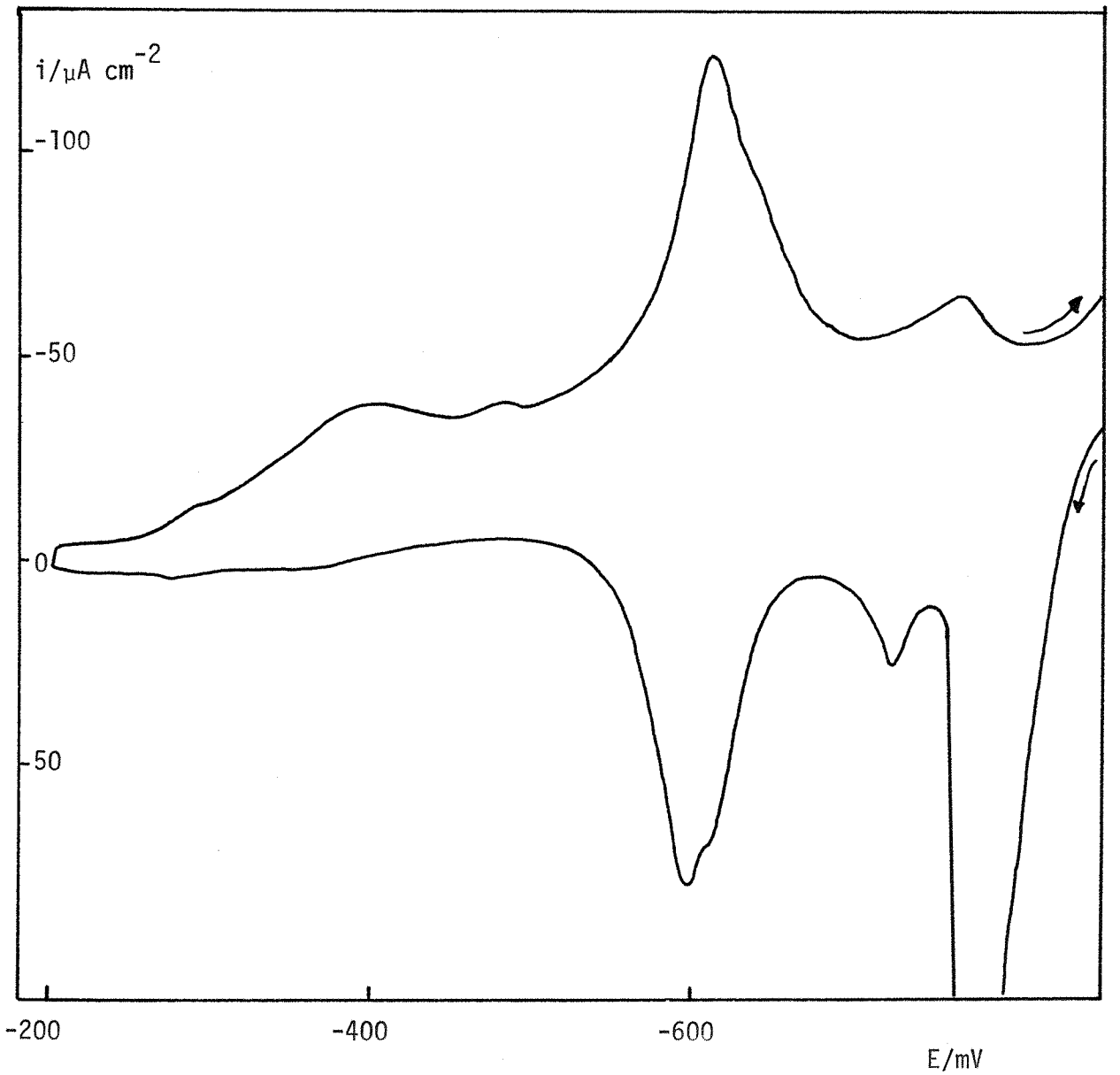

Fig. 4.25 (a). L.S.V. for thallium deposition on the {110} plane of silver from a chloride containing electrolyte. Solution, 0.32mM Tl_2SO_4/ 0.3M KCl/ 1mM $HClO_4$. Sweep speed, 30mV s^{-1}.

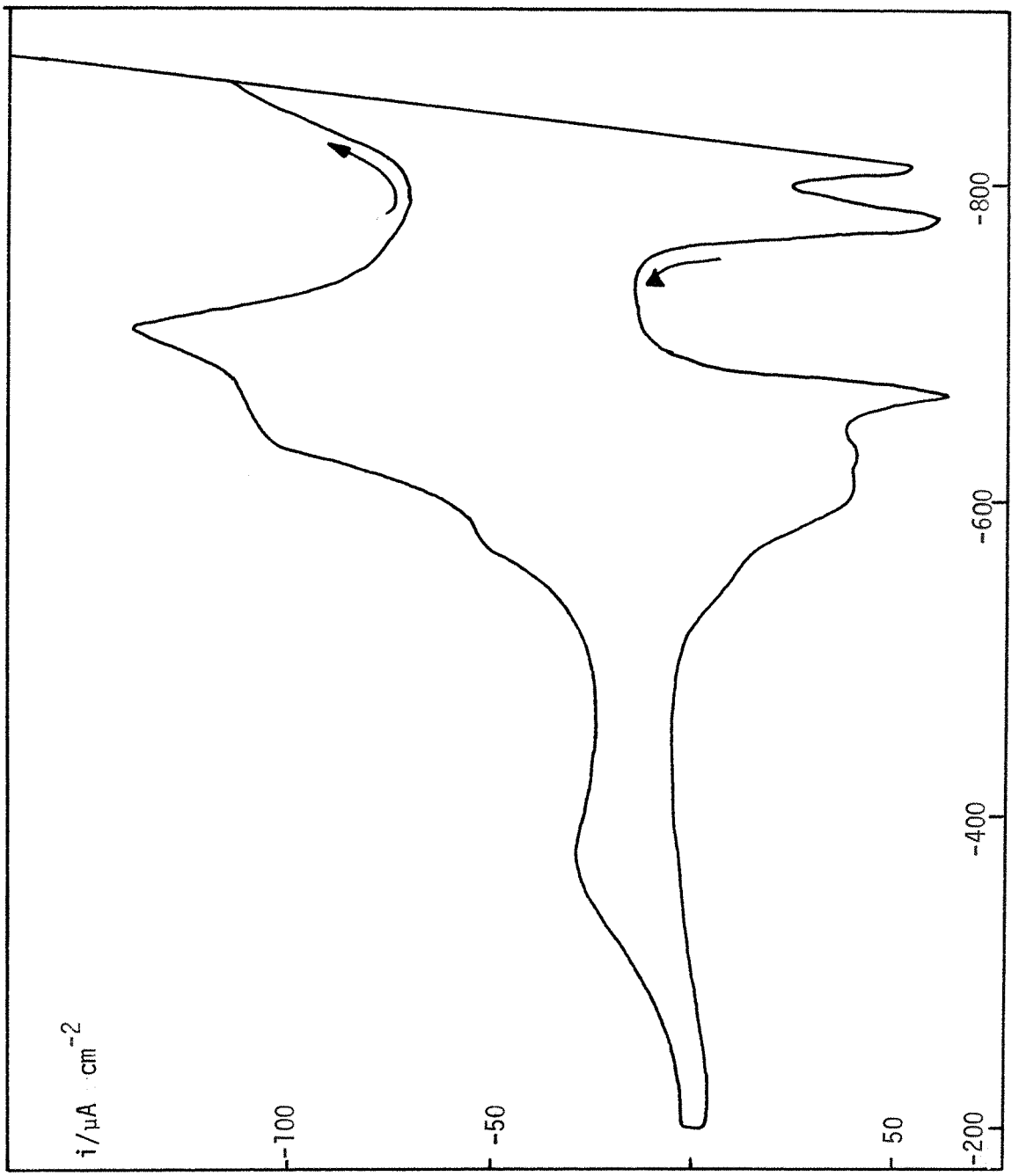

Fig. 4.25 (b). L.S.V. for thallium deposition on the {100} plane of silver from a chloride containing electolyte. Otherwise as Fig. 4.25 (a).

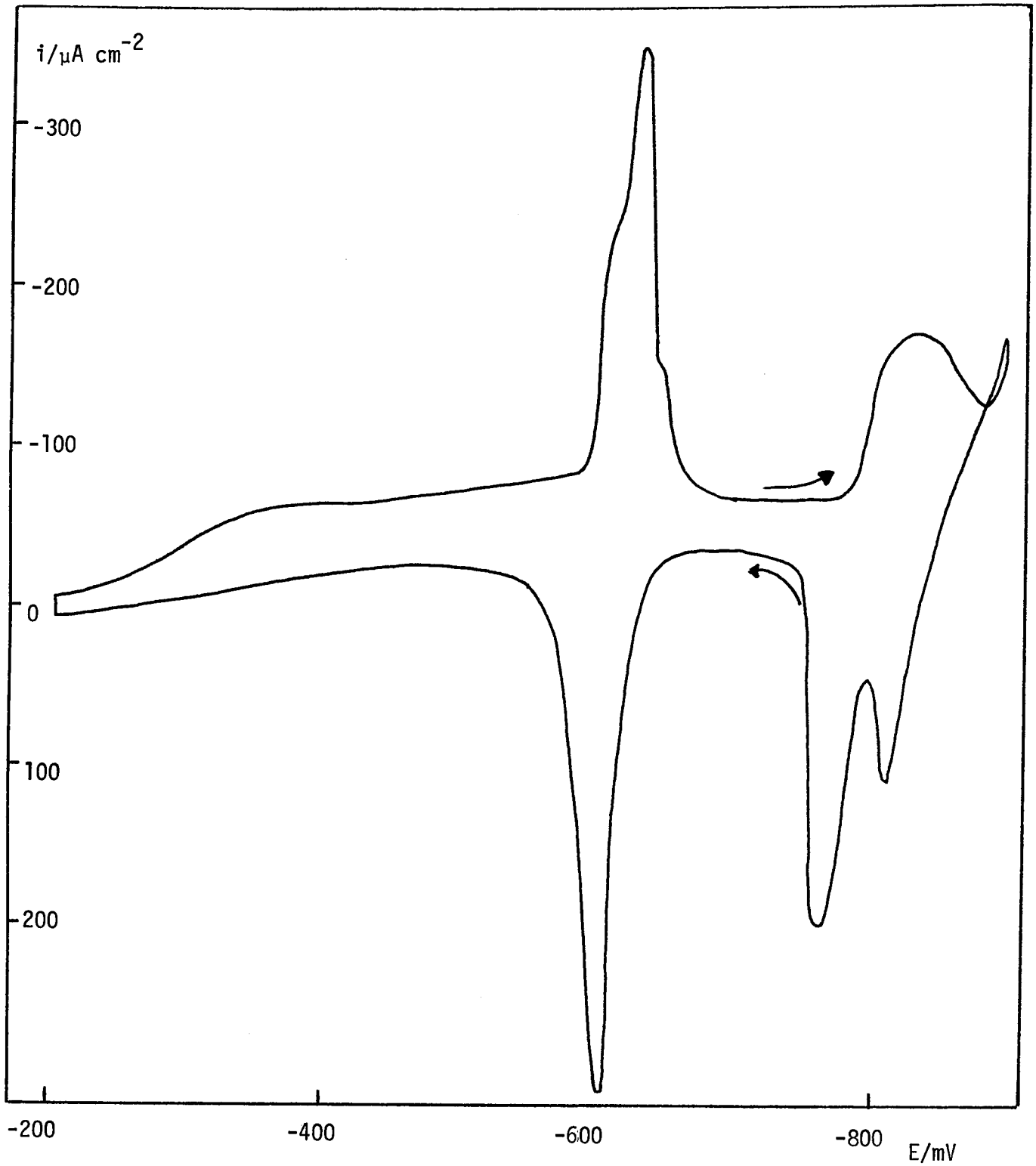

Fig. 4.25 (c). L.S.V. for thallium deposition on the {111} plane of silver from a chloride containing electrolyte. Solution, as in Fig. 4.25 (a). Sweep speed 30mV s^{-1}.

which are not extensively specifically adsorbed on the electrode (ClO_4^-, SO_4^{2-}, F^- and $CH_3CO_2^-$) were qualitatively identical to each other, there were small quantitive differences; these were:

1. For a constant total thallium concentration of 1.5mM, the bulk reversible potentials and hence the potentials of the underpotential peaks, varied with the anion, depending on the actual activity of a thallium ion in the different solutions. Any complexing between the anion and thallium ions would reduce the activity of the latter and correspondingly move the deposition peaks to more cathodic potentials. For example, see Table 4.6. The E_r (i.e. E_{Tl/Tl^+}) value obtained in perchlorate solutions is identical to that obtained from the Nernst equation assuming the thallium ion activity to be equal to the bulk concentration of thallium. This implies that virtually no complexing takes place between thallium and perchlorate ions. However, in sulphate ion solutions, the complexing is such as to reduce the effective thallium ion activity to 4.1×10^{-4}. The complex responsible for this effect is presumably $Na_2SO_4.3Tl_2SO_4$, which has been reported in Tl_2SO_4/Na_2SO_4 solutions.[103]

2. The underpotential shifts of the various peaks varied slightly depending on the nature of the anion, e.g. the ΔU_p values, for the A_2 peak on the {111} face, vary as shown in Table 4.7. The effect of specific ion adsorption on underpotential shift, has already been discussed. These results suggest that the tendency of the perchlorate ion to specifically adsorb, was somewhat less than that of the other anions, but it is generally accepted that the fluoride ion has a lower tendency for adsorption than the perchlorate ion. However, a comparison of the extent of specific adsorption based on the ΔU_p values alone is only valid provided that the ratio of the quantity,

$$\frac{\text{fraction of electrode surface covered by anion}(\theta=0)}{\text{fraction of deposit surface covered by anion } (\theta=1)}$$

TABLE 4.6

ANION	$CH_3CO_2^-$	ClO_4^-	F^-	SO_4^{2-}
E_r/mV	-769	-746	-755	-779
SOLUTION COMPOSITION	A	B	C	D

Variation in E_r for different base electrolyte anions, for a total thallium ion concentration of 1.5mM. Solution compositions, as shown below.

A = 1.5mM $Tl(CH_3CO_2)$/ 0.5M $Na(CH_3CO_2)$/ 0.1M CH_3CO_2H

B = 0.75mM Tl_2SO_4/ 0.5M $NaClO_4$

C = 1.5mM TlF/ 0.2M NaF/ 3.5mM HF

D = 0.75mM Tl_2SO_4/ 0.5M Na_2SO_4/ 1mM $HClO_4$

TABLE 4.7

ANION	$CH_3CO_2^-$	ClO_4^-	F^-	SO_4^{2-}
ΔU_p/mV	249	254	245	244

The variation in underpotential shift (here defined as E_r - cathodic peak potential) for the A_2 peak on the {111} plane, depending on the nature of the base electrolyte anion. Solution compositions, as in Table 4.6. The ΔU_p values were measured at a sweep speed of 30mV s^{-1}.

is constant for all anions (θ=fraction of surface covered by deposited metal). If, for example, this ratio was higher for fluoride than for perchlorate, even though the absolute amount of specific adsorption of fluoride might be less than that of perchlorate, the ΔU_p value would be greater in the latter solution.

3. The difference in ΔU_p values between sulphate ion and perchlorate ion solutions, should be reflected in the measured charge values corresponding to coverage by one or two monolayers, as this quantity is sensitive to anion ad/de-sorption processes. The average values measured for the {111} face, at 100mV s^{-1} (the charge values were virtually independent of sweep speed when $1<\beta<300$mV s^{-1}) as a function of anion, are shown in Table 4.8. These figures substantiate the conclusions based on ΔU_p values. They show that the roughness factor already quoted, from the results in sulphate ion solutions, i.e. 1.22, was a composite of both a genuine roughness factor and a factor due to anion effects. For example, in perchlorate ion solutions, the apparent roughness factor, i.e.,

$$\frac{\text{experimental monolayer charge (for close packed thallium layer)}}{\text{calculated charge for a close packed thallium layer}}$$

$$= 1.14$$

Hence, it is important to use an apparent roughness factor appropriate to the anion being used, in calculations involving charge values.

Apart from the effects already mentioned, it would appear that, provided the base electrolyte anion is not specifically adsorbed on the electrode or deposit to any great extent, the underpotential deposition mechanism is independent of the nature of the anion.

4.9(b) pH EFFECTS.

Acid concentrations of 0.001M and 0.01M $HClO_4$ have no effect on the voltammetry or potential step results. At concentrations as high as 0.1M, hydrogen adsorption/evolution processes begin to occur before the

TABLE 4.8

ANION	$CH_3CO_2^-$	ClO_4^-	SO_4^{2-}
CHARGE VALUE UP TO POINT X /μC cm^{-2}	198	184	196

Variation of the cathodic charge (double layer charging subtracted),for the first monolayer on the {111} plane, with base electrolyte anion. The values were obtained from linear sweeps at 100mV s^{-1}.

deposition process begins; however, the much higher hydrogen overpotential on thallium as opposed to silver, prevents hydrogen evolution once a significant quantity of metal has been deposited. Apart from this effect, varying the solution pH appears to have no effect on the deposition mechanism.

4.9(c) CONCENTRATION EFFECTS.

The effect on the voltammetry of varying the thallium ion concntration has also been investigated on the {100} and {111} planes. The solution composition used for these experiments was, xmM Tl_2SO_4/ 0.1M Na_2SO_4, where the value of x was in the range 0.75 to 25mM.

On the {100} face, at all concentrations the appearance of the voltammetry was as shown in Fig. 4.5(b). On the {111} face however, the adsorption peak A_1 virtually disappeared at high thallium ion concentrations. The quantitative differences in the voltammograms on the two crystal faces have been examined by measuring the underpotential shift of the A_1 and A_2 peaks as a function of concentration and hence reversible potential (here the underpotential shift is defined as E_r - cathodic peak potential). A plot of ΔU_p vs. E_r for the A_1 and A_2 peaks on the two crystal faces is shown in Fig. 4.26. It is seen that a linear relationship exists between these two quantities in all cases, with the shifts decreasing with increasing thallium ion concentration. Such a concentration dependence has not been reported before, indeed Gerischer et al.[57] stated that the underpotential shift would be insensitive to concentration changes.

The explanation for such an effect is probably related to anion adsorption. It has already been shown that such a process can result in a considerable reduction in the underpotential shift. In the present case, as the thallium ion concentration is increased, the reversible potential and hence the underpotential peaks, move in a positive direction. This results in the monolayer deposition process starting with progressively higher positive charges on the substrate and hence an increasing influence

of anion specific adsorption should be noticed. This situation would result in a gradual reduction in the underpotential shift values as anion adsorption becomes progressively more favourable, for the reasons already discussed in 4.9(a).

It should be noted however, that an additional factor has to be taken into account when the thallium ion concentration is changed. The effective electronegativity or work function of the substrate is dependent on its potential and therefore, for a deposition reaction with increasing metal ion concentration, the effective electronegativity of the substrate will increase as the reversible potential moves more positive. For the adsorption part of U.P.D., when only discrete ad-atoms are present on the surface, the variation in surface charge, for a given metal coverage, with increasing metal ion concentration, should be restricted to the substrate only. Hence the apparent electronegativity difference between the two metals will increase (the substrate being the more electronegative element) and correspondingly the underpotential shift should increase. In the present case of thallium deposition, it would seem that the anion adsorption effects outweigh the effect of increasing electronegativity differences. However, with the U.P.D. of lead on silver it is found that the underpotential shifts associated with both the adsorption and crystal phase peaks show no dependence on the lead ion concentration. In this system therefore, the electronegativity factor must have an equal and opposite effect to anion adsorption.

It is interesting to note that the increased underpotential shifts which would result from the greater apparent electronegativity differences between substrate and deposit at higher metal ion concentrations, should be restricted to the adsorbed layer only. For the crystalline phase layer, the surface charge would most likely reside in the monolayer rather than on the substrate as is the case for the adsorbed layer. This effect would increase the electronegativity of the deposit and hence the apparent electronegativity

differences would decrease. This would predict a reduction in the underpotential shift values at higher metal ion concentrations.

Clearly there are several factors which have to be accounted for in a rigorous treatment of underpotential shift. The correlation of Gerischer et al. is only reasonable when applied over a wide range of metal ion couples.

The disappearance of the A_1 peak on the $\{111\}$ face, at higher metal ion concentrations suggests that the adsorption sites on this plane are no longer available. It is possible that this peak represents adsorption at sites associated with surface defects rather than the three co-ordinate planar sites as assumed up till now. It will be shown in Chapter 5 that these defect sites are the most favourable for anion adsorption.

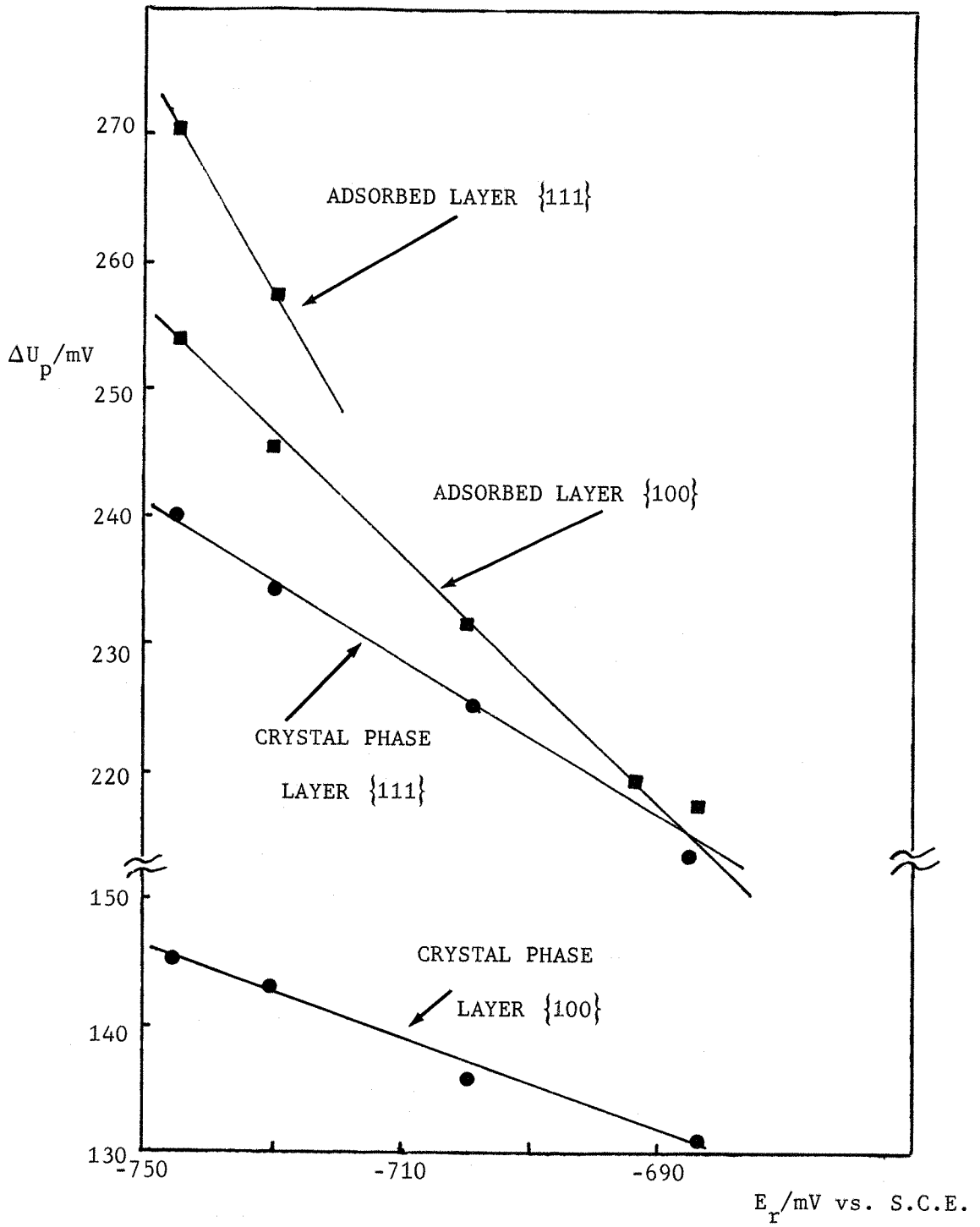

Fig. 4.26 Plot of underpotential shift vs. reversible potential for the A_1 and A_2 peaks on the {111} and {100} faces. Solution, xmM Tl_2SO_4/ 0.1M Na_2SO_4, where x was in the range 0.75 to 25.

CHAPTER FIVE: UNDERPOTENTIAL DEPOSITION OF LEAD ON SILVER.

5.0 INTRODUCTION.

The mechanism observed for the U.P.D. of thallium on silver, i.e. adsorption/phase transformation-crystal growth, needs to be tested in other systems before a general rule can be stated; in particular, more information on the nucleation process occurring, is needed. Lead deposition on silver is a suitable system as alloy formation does not occur and the underpotential shifts involved, although smaller than those observed in the thallium system, are of sufficient magnitude for the component steps in U.P.D. to be resolved.

A previous study of this system[49], in chloride ion media, using mechanically polished silver electrodes, indicated that anion ad-/desorption processes were occurring simultaneously with metal deposition/dissolution. Consequently, the effect of anions is reported in detail in this chapter, together with pH dependent effects.

5.1 U.P.D. OF LEAD ON POLYCRYSTALLINE SILVER.

The same conclusions with regard to mechanically polished electrodes, i.e. voltammetry with no fine structure and anomalous optical behaviour, found for thallium deposition, are equally applicable to the lead results.

The L.S.V. for lead deposition on chemically polished, polycrystalline silver, from a perchlorate ion electrolyte, is shown in Fig. 5.1. Again, a large amount of fine structure is visible corresponding to deposition on the different crystal faces present in the polycrystalline surface. However, in this case the amount of metal deposited at an underpotential is restricted to a single monolayer.

5.2 U.P.D. OF LEAD ON SINGLE CRYSTAL SILVER.

The following systems have been studied in detail on single crystal silver:

$$x\text{M PbO} / 0.5\text{M } HClO_4$$

$$(\ 0.001<x<0.05\ )$$

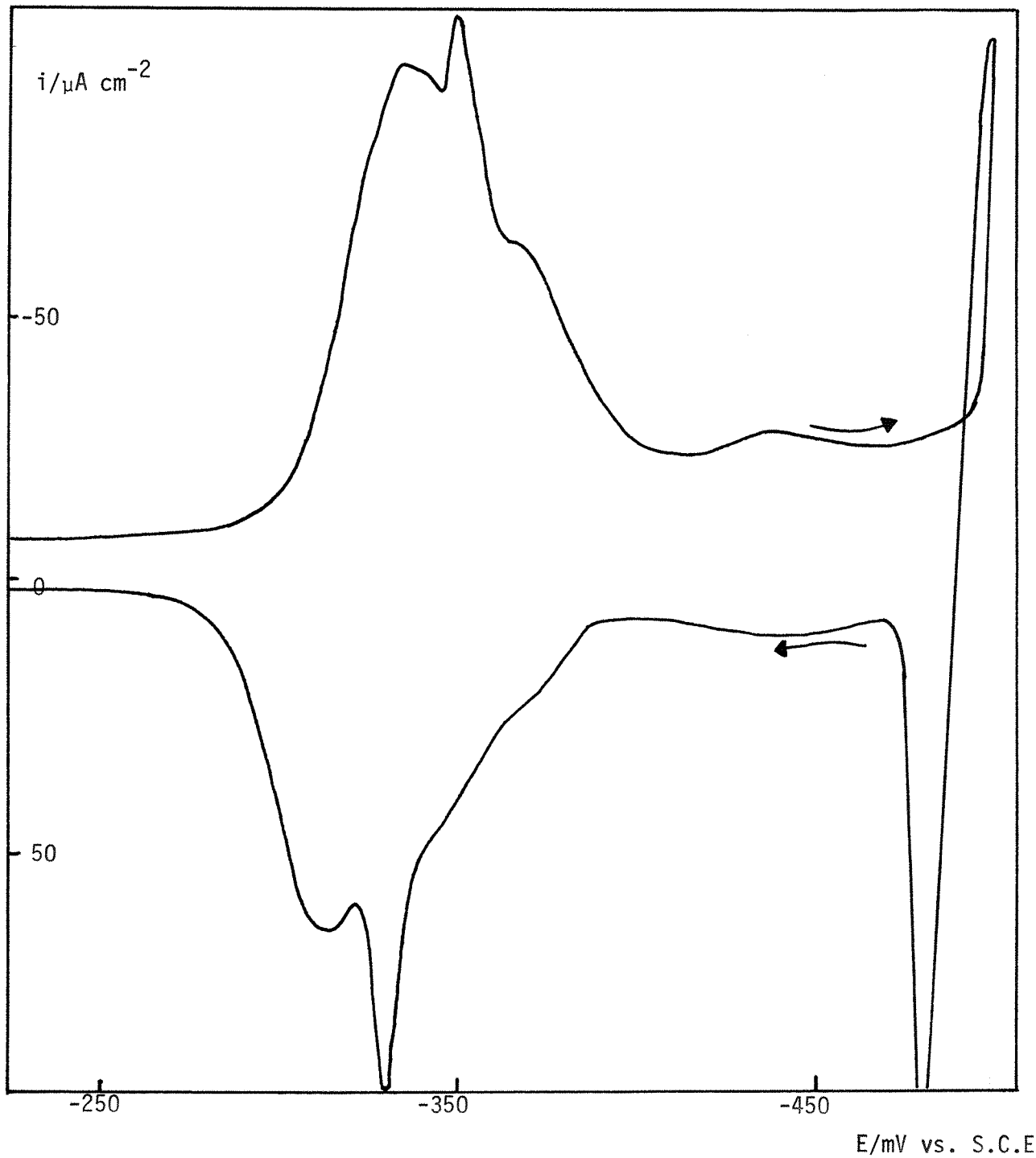

Fig. 5.1. Linear sweep voltammogram for lead deposition on a chemically polished polycrystalline silver electrode. Solution, 1mM $Pb(ClO_4)_2$/ 0.5M $NaClO_4$/ 1mM $HClO_4$. Sweep speed, 10mV s^{-1}.

xM PbO/ yM $HClO_4$/ 0.5M $NaClO_4$

(x = 0.05, y = 2x or 0.011)

xM $Pb(CH_3CO_2)_2$/ 0.5M $Na(CH_3CO_2)$/ yM CH_3CO_2H

($0.0015<x<0.1$, $0<y<0.1$)

0.001M $PbCl_2$/ 0.3M KCl/ 1mM $HClO_4$

0.003M $Pb(CH_3CO_2)_2$/ 0.1M citric acid/ 0.2M NaOH/ 0.5M $NaClO_4$

In addition to this, several other solution compositions were used occasionally and these will be referred to when necessary.

Such a wide variation in solution composition and concentration was necessary to understand all the variables affecting the deposition. This illustrates the increased complexity of this system relative to the thallium behaviour, where anion and pH effects were relatively unimportant.

Firstly, the similarities and differences to the thallium system will be illustrated with results from 5mM PbO/ 0.5M $HClO_4$. The perchlorate anion, on account of its low tendency for specific adsorption, should allow the deposition behaviour to be most readily observed independent of anion effects. This oxide/acid combination has been commonly employed as a medium for the U.P.D. of lead onto gold.[64,72,74,77]

5.3 RESULTS FROM 5mM PbO/ 0.5M $HClO_4$

L.S.V.'s for the three single crystals, recorded at a sweep speed of 30mV s^{-1}, are shown in Fig. 5.2. The results obtained for the {111} and {100} faces were independent of whether the potential scan was repetitive or single. This was not true for the {110} face however. That shown in Fig. 5.2 is the result of a single potential scan and is most appropriate for the present purpose of comparing the results obtained for lead deposition with those expected for an adsorption/phase transformation mechanism.

The cathodic peak potentials on the different crystal planes,

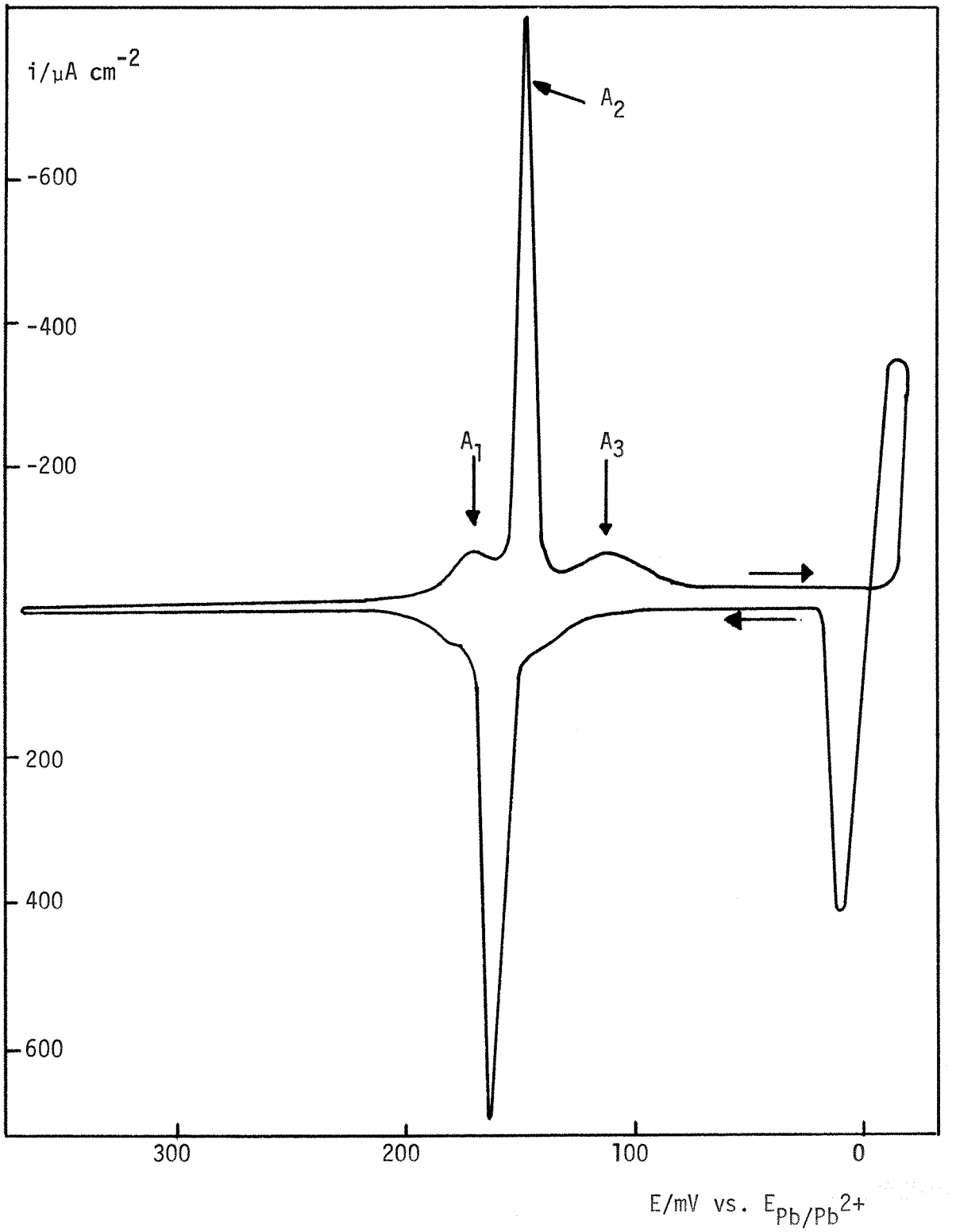

Fig. 5.2(a). L.S.V. for lead deposition on the {111} face of silver. Solution, 5mM PbO/ 0.5M $HClO_4$. Sweep speed, 30mV s^{-1}.

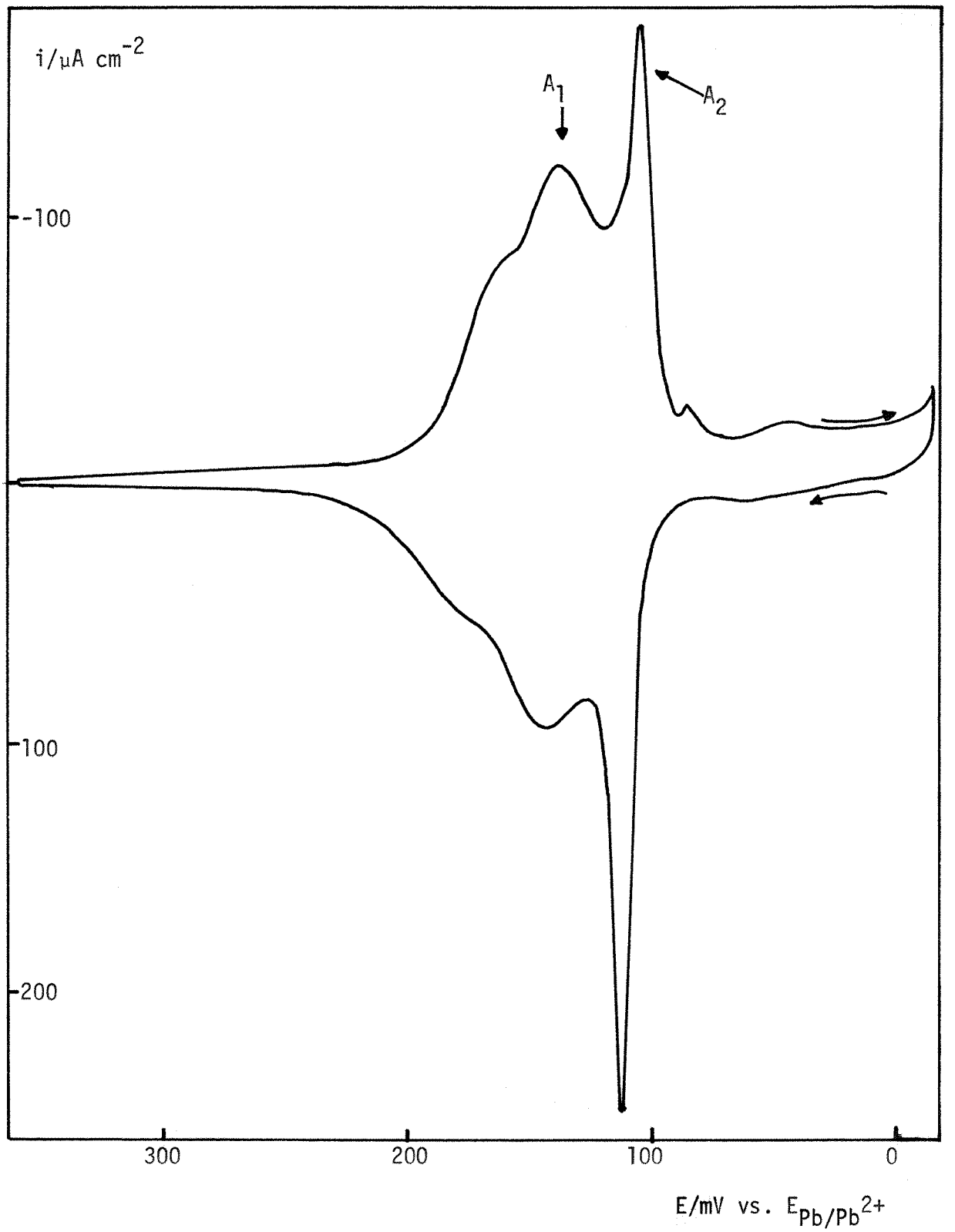

Fig. 5.2(b). L.S.V. for lead deposition on the {100} face of silver. Solution, as in Fig. 5.2(a). Sweep speed, 30mV s^{-1}.

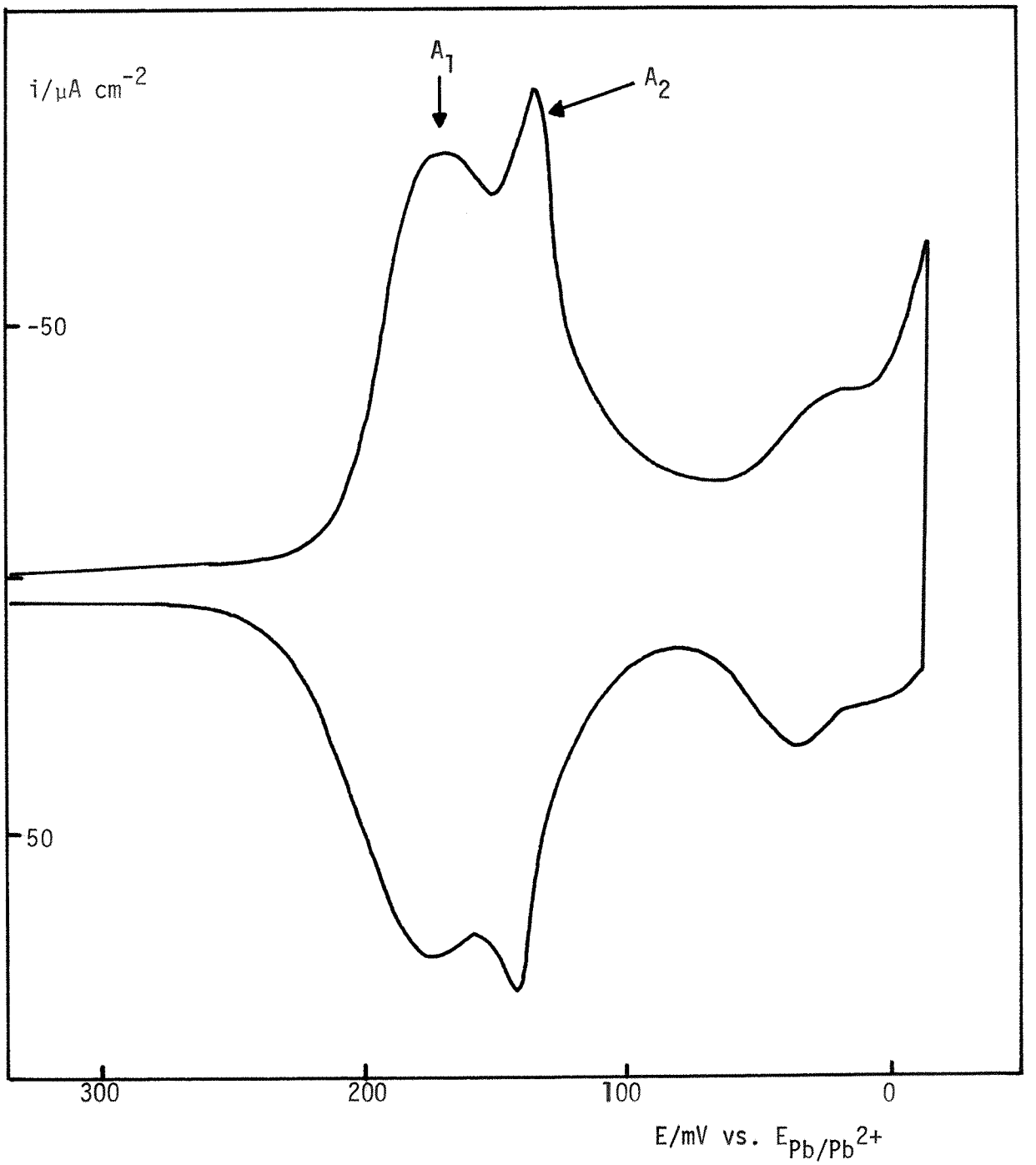

Fig. 5.2(c). L.S.V. for lead deposition on the {110} face of silver. Solution and sweep speed,as in Fig. 5.2(a). This result was obtained from a single potential scan only (see text).

TABLE 5.1

CRYSTAL FACE	A_1/mV	A_2/mV	A_3/mV
{110}	+167	+133	-
{100}	+139	+106	-
{111}	+170	+148	+108

Table showing peak potentials for lead deposition on different faces of silver. Solution, 5mM PbO/ 0.5M $HClO_4$; sweep speed, 30mV s^{-1}. Potentials are with respect to $E_{Pb^{2+}/Pb}$

TABLE 5.2

CRYSTAL FACE	AMOUNT OF 'q' PASSED UP TO BULK DEPSN. /μC cm^{-2}	AMOUNT OF 'q' CONTAINED IN A_1 PEAK /μC cm^{-2}	VALUE OF 'q' WITH ROUGHNESS FACTOR OF 1.1 /μC cm^{-2}	VALUE OF 'q' FROM SUPER-LATTICE MODEL /μC cm^{-2}
{111}	334±4	20-30	18-27	106
{100}	337±3	∿205	186	192
{110}	383±6	∿162	147	136

Table showing various charge values (double layer charging subtracted) for lead deposition on different faces of silver. Solution, 5mM PbO/ 0.5M $HClO_4$; sweep speed, 30mV s^{-1}.

are given in Table 5.1.

The results for each crystal face will now be discussed separately.

{111} FACE

In analogy to the thallium system, the cathodic scan shows three peaks, A_1, A_2 and A_3, in the U.P.D. region,which have the following characteristics:

1. The size, and therefore charge associated with, the A_1 and A_3 peaks, was dependent on surface preparation but the variations always affected A_1 and A_3 to the same extent. The A_1 charge was always less than 50μC cm^{-2} (subtracting double layer charging).

2. A_2, like its thallium counterpart on this orientation, was remarkably sharp and shows a characteristic asymmetry with the corresponding anodic peak. Fig. 5.3 shows just the cathodic part of a potential scan at 10 mV s^{-1} in this system. This gives a better idea of the sharpness of the A_2 peak and its size relative to A_1 and A_3 (at higher sweep speeds the X-Y recorder could not follow the A_2 peak exactly).

The total cathodic charge (see Table 5.2) flowing before bulk deposition occurred was 334±4μC cm^{-2} (subtracting double layer charging). The calculated value for a close-packed lead monolayer (rPb = 1.75Å) is 302μC cm^{-2}. Division of these two quantities yields an 'apparent' roughness factor of 1.11 which compares favourably with the value of 1.14 obtained from thallium deposition from a perchlorate electrolyte.

By analogy with the thallium results, the peak A_2 must correspond to a crystal growth process.

Lorenz' superlattice model would predict a charge of 106μC cm^{-2} (≡ 117μC cm^{-2} with a surface roughness factor of 1.1) associated with an adsorption process on this plane, and as pointed out in chapter 4, this does not correspond to occupation of all possible sites. As stated already,

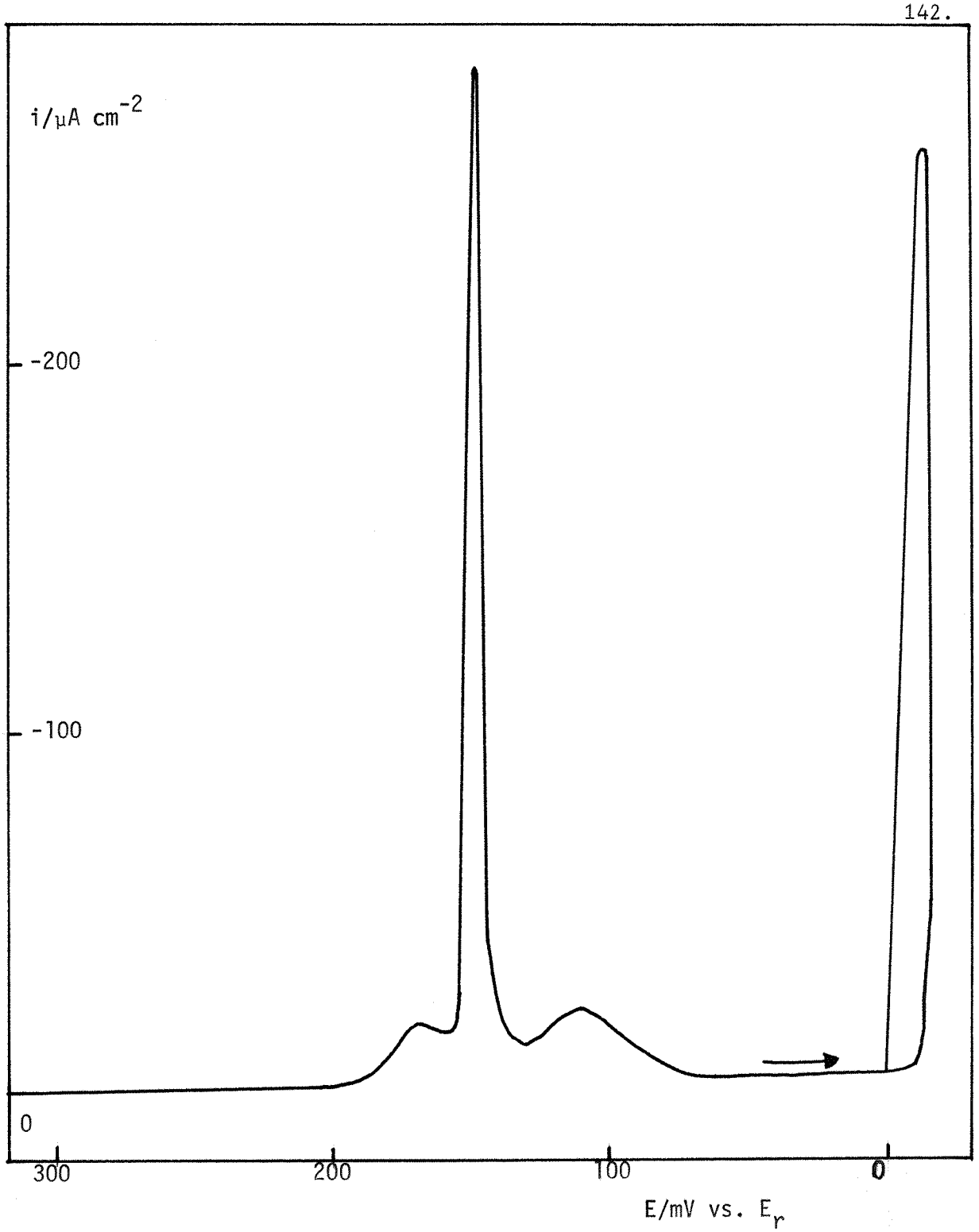

Fig. 5.3. The cathodic part of an L.S.V. for lead deposition on the {111} face. Solution, as in Fig. 5.2(a). Sweep speed, 10mV s^{-1}.

the measured A_1 charge values are dependent on surface preparation but, in any case, are much less than this value and typically of the order of 20 to 30μC cm^{-2}. The most reasonable explanation for a peak associated with such a low charge value is that it corresponds to adsorption occurring at defect sites, e.g. steps, kinks etc. on the electrode surface. This would explain the variation with surface preparation. The normal three co-ordinate adsorption sites are not sufficiently favourable to be filled before the formation of a two-dimensional crystal plane becomes thermodynamically possible. The planar adsorption sites on the {110} plane are possibly similar in energy to kink sites on the {111} plane. It will be seen that a considerable amount of adsorption takes place in the former case. Experiments on dislocation free {111} surfaces should be virtually free of the A_1 peak.

On account of the correlation in relative size between A_1 and A_3 in different experiments, it would seem that the latter peak is also associated with the defect sites in the electrode. For a dislocation free surface, a two-dimensional crystal plane should be deposited over a very narrow range of potential and only a single voltammetry peak would be seen. However, surfaces possessing a finite number of dislocations, would have favourable adsorption sites (peak A_1), but these would prevent the complete surface being covered by a perfect, dislocation free, crystal plane. In the present case, the charge corresponding to A_2 would seem to be associated with crystal plane formation on the largely dislocation free parts of the electrode surface, whereas A_3 represents completion of surface coverage, associated with growth centres around dislocation sites.

VOLTAMMETRY ON THE {100} FACE

The voltammetry on this face shows two main peaks on the cathodic scan, A_1 and A_2, with a shoulder on the former. The shoulder only becomes

apparent at sweep speeds lower than 50mV s^{-1}. At higher scan rates, A_1 appears as a single peak with no fine structure. In addition, the resolution of this feature was markedly dependent on surface preparation. In some cases, it was hardly visible (see Fig. 5.4.).

The adsorption/phase transformation/crystal growth model would predict two voltammetry peaks with the more cathodic of these being sharp, corresponding to the crystal growth process and associated with an amount of charge equal to the difference in calculated charges (multiplied by the roughness factor) between a close packed monolayer and a superlattice structure appropriate to the {100} orientation. The calculated charges for the superlattice model of adsorption were given in Table 5.2 together with values calculated from a surface roughness factor of 1.1. The amount of charge associated with A_1, given in Table 5.2, is an average value from optical (section 5.4(b)) and current integration measurements. The calculated superlattice and experimentally measured charges are in good agreement, implying that peak A_1 represents a simple adsorption process where all favourable sites on the electrode are filled. This is in exact analogy with the thallium results on the same crystal face. The sharpness of the A_2 peak confirms its crystal growth character, and it corresponds to complete coverage of the surface by a close packed monolayer.

A complication in the results for lead deposition on the {100} face, compared to the thallium case, is the presence of the shoulder on the adsorption peak, A_1. The dependence of the resolution of this shoulder on surface preparation, similar to the A_1 peak on the {111} orientation, would suggest that it was associated with special surface sites which were not typical of the majority, i.e. planar adsorption sites. The explanation for the apparent ability to separate between adsorption at kink and step sites and adsorption at planar sites, in this case, whilst no such distinction was apparent on the same face for thallium deposition, must be

attributed to the difference in the energy of interaction between a lead atom with silver atoms at a kink site being greater than the corresponding difference for a thallium atom. That this is the case can be seen from the A_1 peak potential for lead and thallium deposition on the {100}and {110} faces (see Table 5.1 and 4.1). In the thallium case, the difference in potentials for the A_1 peak on the {110} and {100} faces, is 3mV whereas in the lead case, the difference is 28mV. In addition, the underpotential shift values for lead are considerably lower than for thallium and so a difference in peak potentials of 28mV, is relatively more significant in the U.P.D. of lead than it would be for thallium. The planar adsorption sites on a {110} surface are somewhat analogous to kink sites on the{100} surface and therefore the 28mV (eqiuvalent to 5.4KJ mol^{-1}) difference in peak potentials is a rough measure of the difference in the interaction energies of lead atoms at kink sites and planar sites on the 100 surface (this arguement takes into account both the work function and structural effect on peak potential values) (the charges involved at the A_1 peak potential on the {100} and {110} faces are very similar). In the case of thallium deposition, this difference in interaction energy is considerably smaller (0.29KJ mol^{-1}) and consequently no separation can be seen in the results from the {100} face.

VOLTAMMETRY ON THE {100} FACE.

As mentioned already, the nature of the voltammetry on the {110} face was dependent on whether the potential was scanned continuously in a cyclic manner or not. This effect was most pronounced at high sweep speeds (greater than 75mV s^{-1}) and is discussed in section 5.10). The voltammogram shown in Fig. 5.2 was the result of a single potential sweep.

On the cathodic scan, three peaks are observed before bulk deposition commences. By analogy with the thallium system, A_1 and A_2 would seem to represent adsorption and phase transformation/growth respectively. The relative shape of these peaks is very similar to that found for thallium

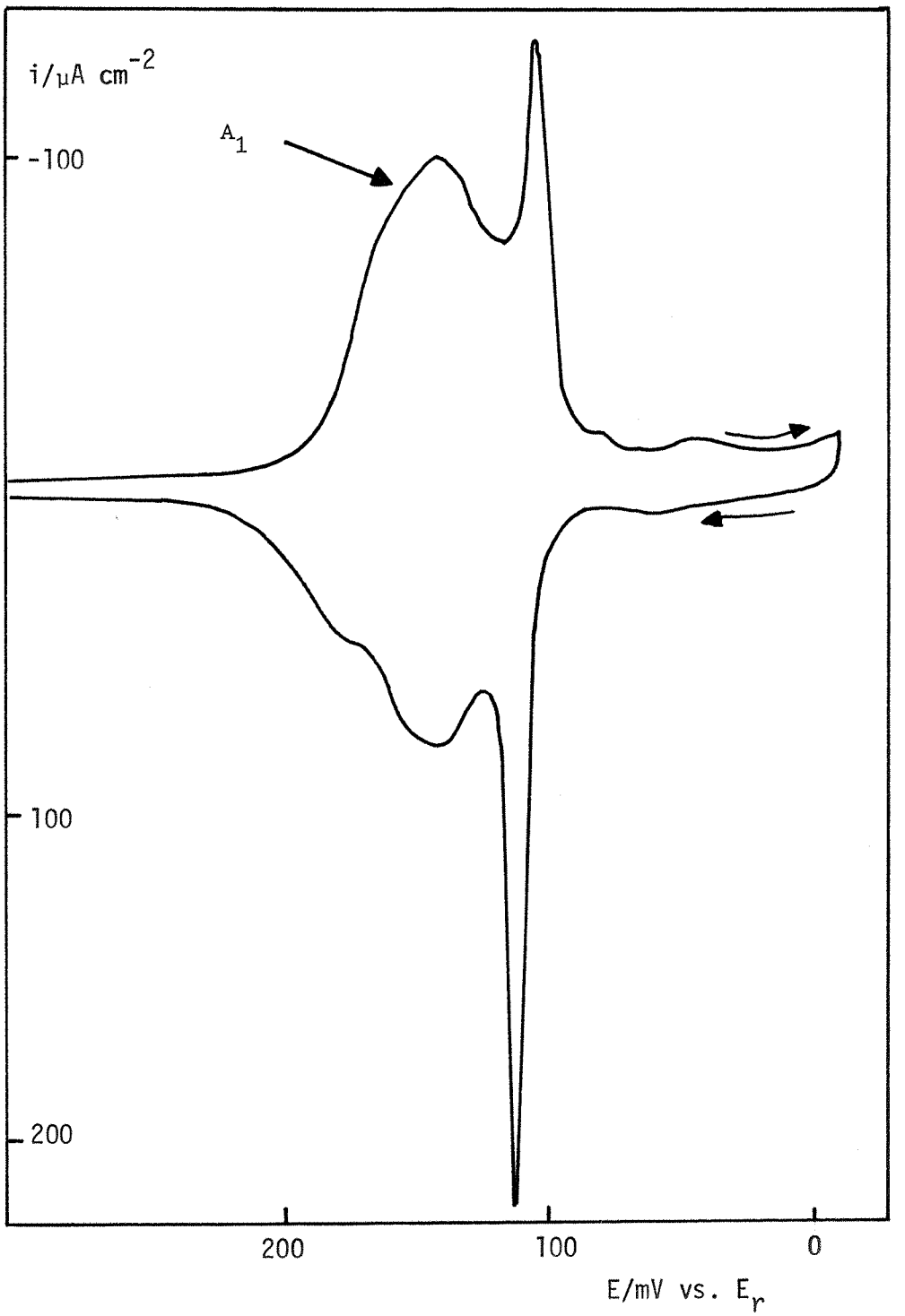

Fig.5.4. An example of an L.S.V. for lead deposition on the {100} face, in which the appearance of the shoulder on the adsorption peak (A_1) is not very apparent. Solution and sweep speed, as in Fig. 5.2(a).

deposition on the same crystal face and moreover the charge associated with A_1 (see Table 5.2) is in good agreement with the value calculated from the superlattice model, when a surface roughness correction is made. This finding supports the conclusion that adsorption proceeds until all the favourable sites are occupied.

On the {111} and {100} faces, surface defect sites, associated with a higher co-ordinating ability than planar sites, seemed to be influencing the observed voltammetry and causing some slight variation between different polishings of the electrode. No such effects are discernible on the {110} face and the A_1 peak shows no shoulder associated with adsorption at specially favourable sites created by dislocations etc.. This would be expected on account of the planar sites on this crystal face being particularly favourable for adsorption and the difference in co-ordination of a lead atom adsorbed at a planar site or at a kink site, would be small and hence such effects as were observed on the {100} plane will be absent.

The total charge passed before the onset of bulk deposition on this face is approximately 383μC cm^{-2}, which is somewhat higher than expected for a close packed layer (330μC cm^{-2}). This can be attributed to the presence of the third peak,B, which would seem to represent deposition occurring on top of the close packed lead monolayer. On the {111} and {100} faces, there was no evidence for the formation of a second monolayer, whereas in the present case, a significant amount of deposition of a second layer occurs. This result can be explained by the distortion of the first close packed layer by the structure of the substrate, as already explained in connection with the thallium results. On the {110} face, the 'open' structure of the substrate must produce a considerable amount of distortion in the structure of any close packed layer deposited on top of it and hence the latter will possess some very favourable adsorption sites. In the present case it would seem that this structural effect is responsible

for the possibility of depositing some lead in a second layer, at the favourable sites, on top of the first layer. Electronegativity differences may also play a part but the structural factor would seem to be the most important. The close packed lead monolayers associated with the {111} and {100} planes do not provide a sufficiently distorted surface for any adsorption to occur on top of them (there is a hint of this on the {100} plane however).

The voltammetry observed at other lead oxide concentrations in perchloric acid, is identical with that shown in Fig. 5.2.

5.3(b) POTENTIAL STEP RESULTS IN THE 5mM PbO/ 0.5M $HClO_4$ SYSTEM.

The results for thallium deposition, from potential step experiments, have already been described in detail. As the results from various concentrations of PbO in 0.5M $HClO_4$ were exactly analogous to these results, they will be presented here only briefly.

On the {111} face, in dilute solutions (e.g. 1mM PbO/ 0.5M $HClO_4$) the high current density associated with A_2 produces an i-t transient with the first part under limiting planar diffusion control and at long times, a rapid decrease from this value as the monolayer approaches saturation. An example is shown in Fig. 5.5. In more concentrated solutions, the characteristic kink is eliminated from the transient, as the planar diffusion limiting constraint is removed and surface diffusion becomes important. A transient obtained from 50mM PbO/ 0.6M $HClO_4$ is shown in Fig. 5.6. As with thallium, it would appear that diffusional processes, either on the surface or in solution, are slower than the charge transfer/lattice incorporation processes and no rising transients can be observed.

On the {100} face, pulsing into the region of A_1 produces a falling transient of the type shown in Fig. 4.12 for thallium deposition. In the

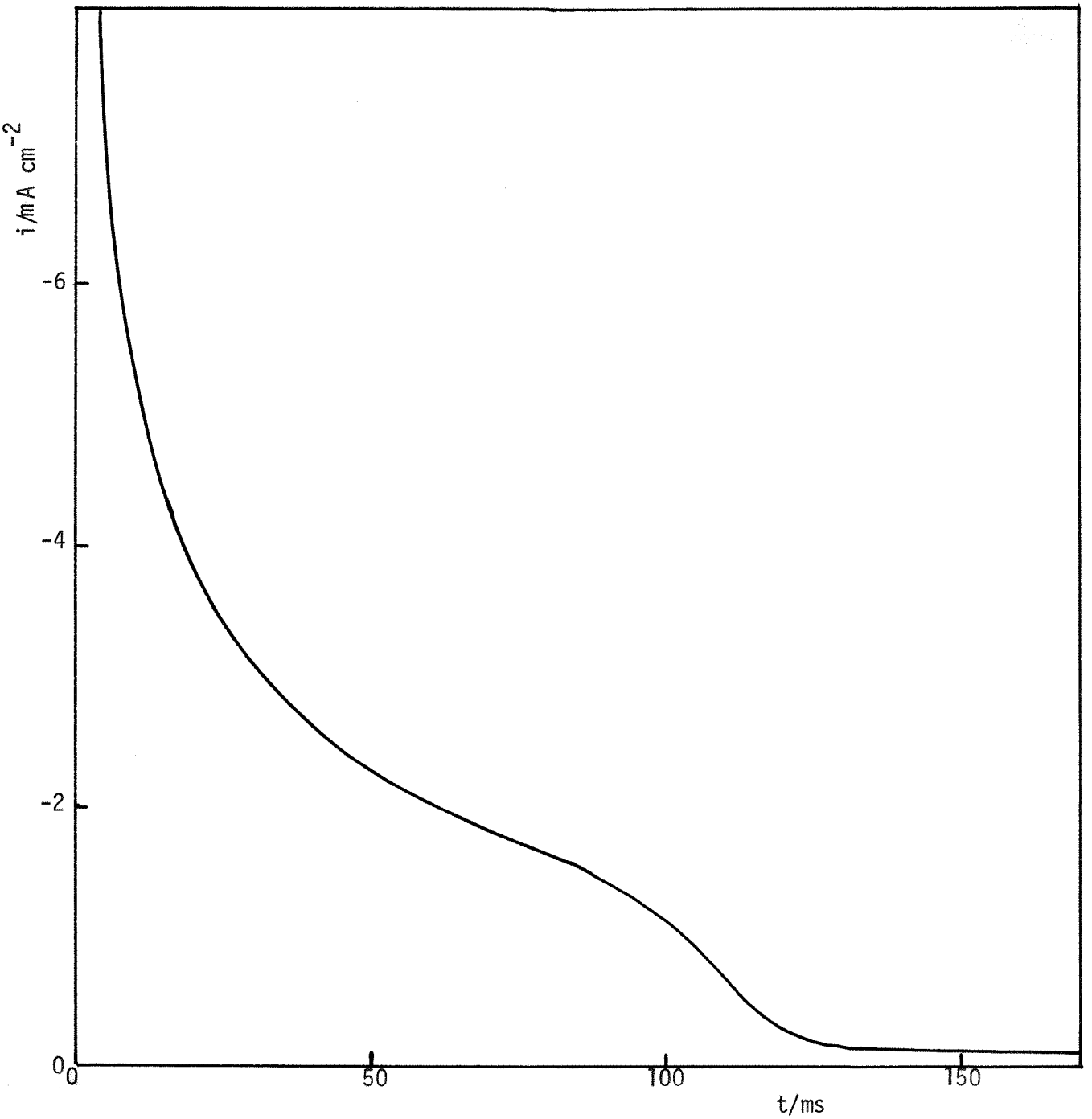

Fig. 5.5. Current-time transient for a potential step from +258mV to +8mV vs. E_r ($E_r = E_{Pb/Pb^{2+}}$), for lead deposition on the {111} face. Solution, 1mM PbO/ 0.5M $HClO_4$.

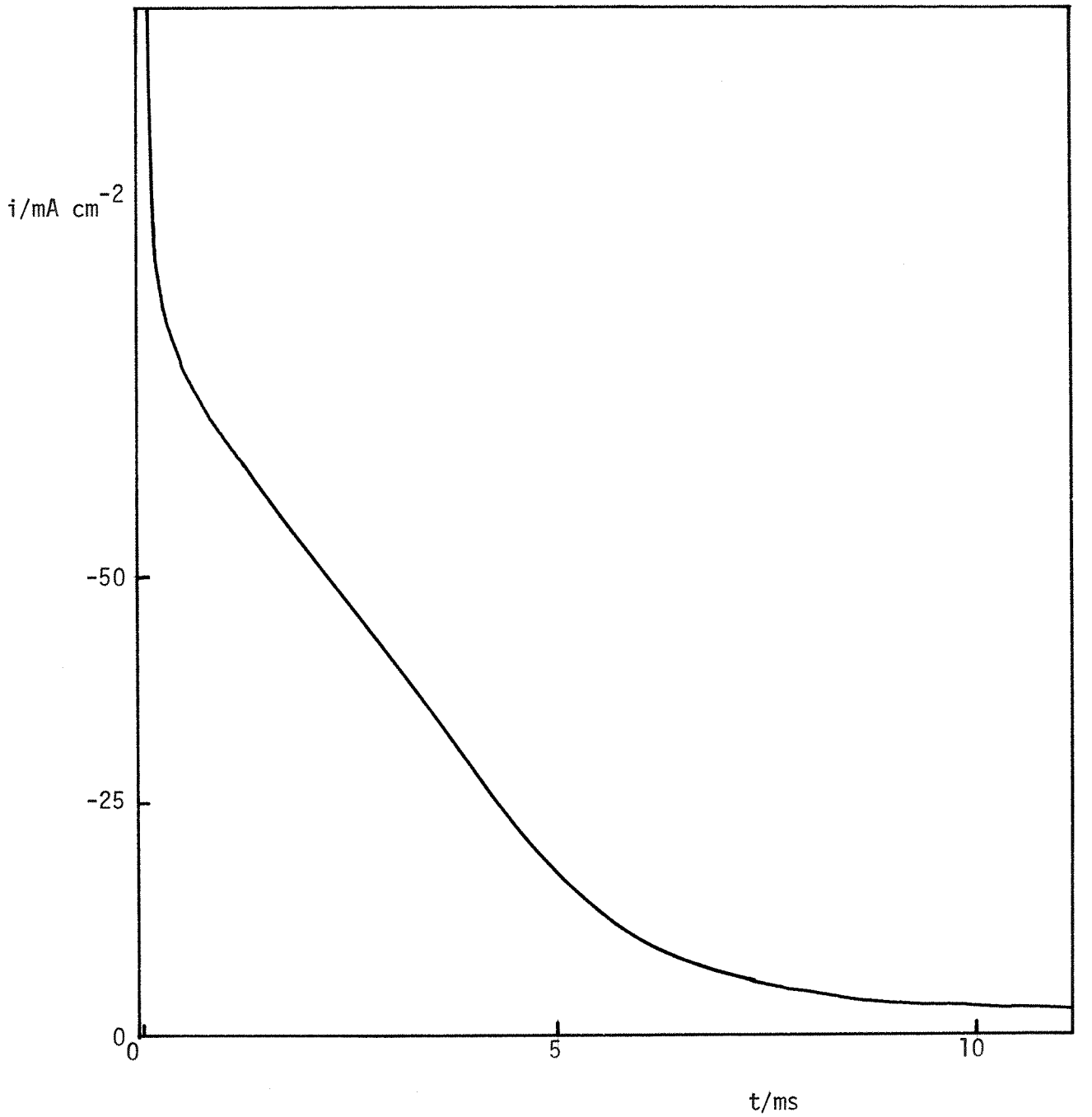

Fig. 5.6 Current-time transient for a potential step from +366mV to +107 mV vs. E_r, for lead deposition on the {111} face. Solution, 50mM PbO/ 0.6M $HClO_4$.

crystal growth region A_2, the transient develops a hump in dilute solutions, or a linear portion in more concentrated solutions.

On the {110} face, repetitive pulsing in dilute solutions (Pb^{2+} concentrations lower than 10mM), was analogous to continuous sweeping in cyclic voltammetry, i.e. complications arose. Single potential steps, or repetitive ones with a long interval in between (longer than 30s) produced transients analogous to those for thallium deposition on the same face, i.e. monotonous falling transients in the region of A_1, and transients with kinks or bulges in the region of A_2. An example for the latter region, is shown in Fig. 5.7. The results from repetitive pulse experiments are considered in section 5.10.

Although the anomalous results produced by repetitive pulsing were by far the most pronounced on the {110} plane, similar effects, but to a much lesser extent could also be observed on the {111} and {100} planes, although in these cases the anodic part of the pulse train had to be very short (only just long enough to strip off the deposit) for any effects to be seen. Under normal circumstances, the transients obtained were as described in this section.

5.4 OPTICAL EXPERIMENTS ON THE U.P.D. OF LEAD.

(a) POLYCRYSTALLINE SILVER.

Optical constants of bulk lead are available in the literature[104] for the whole of the wavelength range accessible to study with the present optical equipment (300-1000nm). This allows the experimental reflectance spectrum, associated with the deposition of a single monolayer, to be compared with that calculated from a three-layer model, using the optical constants of the bulk metal for the lead monolayer. A monolayer of lead on silver, should have optical properties which differ substantially from those of the bulk metal because of the 2-dimensional nature of the layer and the strong interaction with the band structure of the silver substrate. Even so, a comparison of the

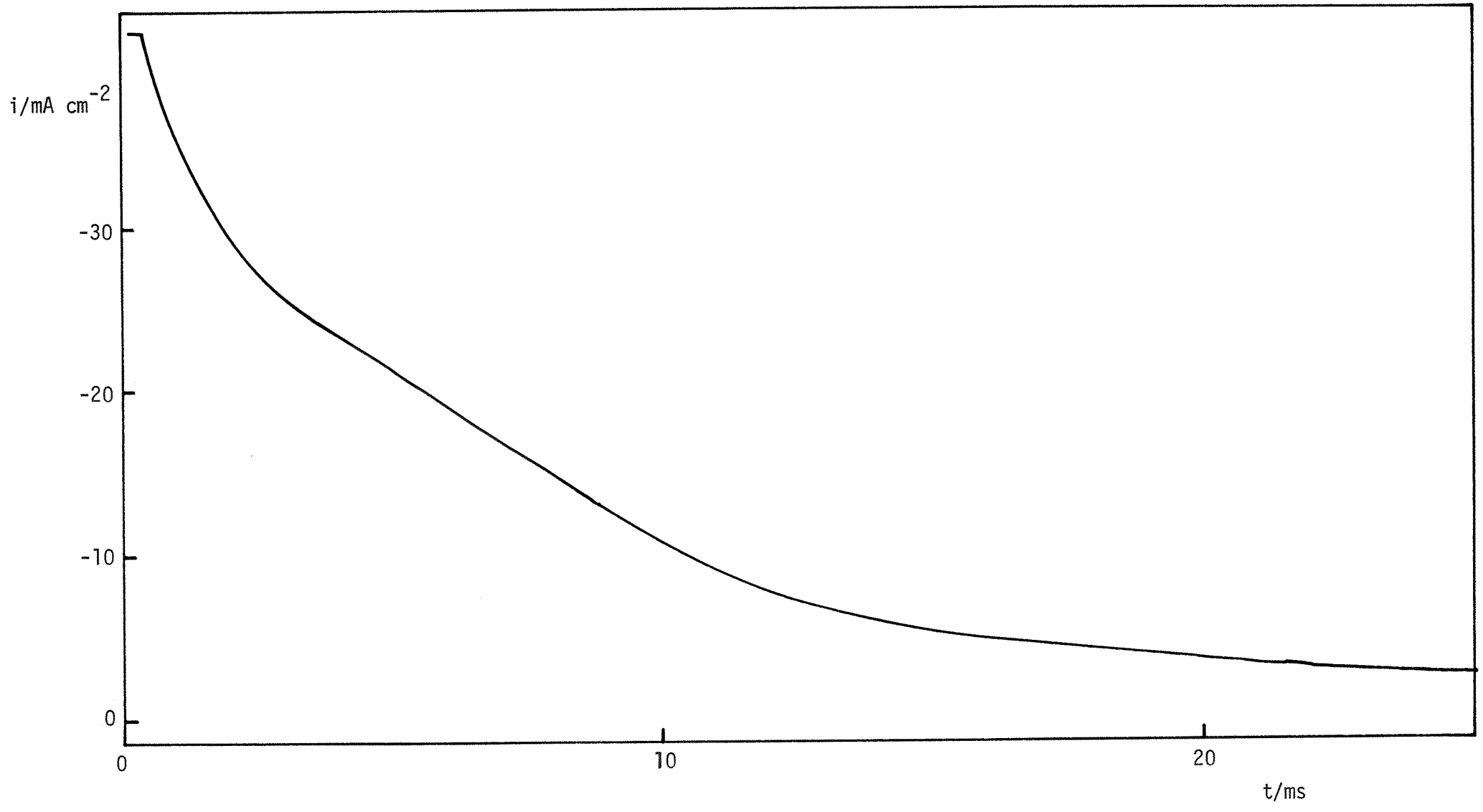

Fig. 5.7 Current-time transient for a potential step from +689mV to +79mV vs.E_r, for lead deposition on the {110} face. Solution, 50mM PbO/ 0.5M $HClO_4$.

spectra obtained experimentally, and by computation using the optical constants of bulk lead, does enable some qualitative conclusions to be made. The principles of the three-layer model and the method of calculation, together with a computer programme, are given in the appendix.

Fig. 5.8 shows both an experimental and a calculated reflectance spectrum obtained for the deposition of a monolayer of lead on chemically polished, polycrystalline silver. The experimental curve was constructed from optical transients corresponding to a potential step to a point slightly anodic to the point at which bulk deposition begins. It can be seen that the shapes of the spectra are qualitatively similar but quantitative agreement is poor. The dominating feature in both curves, is the change in sign of $\Delta R/R$ at about 320nm. This effect is caused by the interband transition in silver, where the reflectance changes dramatically. At wavelengths lower than 320nm, bulk lead is more reflecting than bulk silver and $\Delta R/R$ is positive; at longer wavelengths the reverse is true. A peak in the experimental spectrum at about 370nm is caused by surface plasmon excitation due to residual surface roughness.

Fig. 5.8 shows that, at all wavelengths, especially in the region of the interband transition the actual reflectance changes are somewhat larger than those calculated from bulk optical constants. This would imply that the optical properties of the lead monolayer are certainly not similar to those of silver as suggested by Kolb et al.[76] for their results for lead, thallium and copper deposition onto gold. If allowances were made in the computed spectrum for, say, a 10% ionic character on the monolayer atoms, the curve would be moved to less negative values of $\Delta R/R$ and hence further away from the experimental spectrum.[76] It is therefore not possible to explain the experimental results by recourse to arguments involving enhanced electroreflectance effects, and in the present case, absorption processes in the

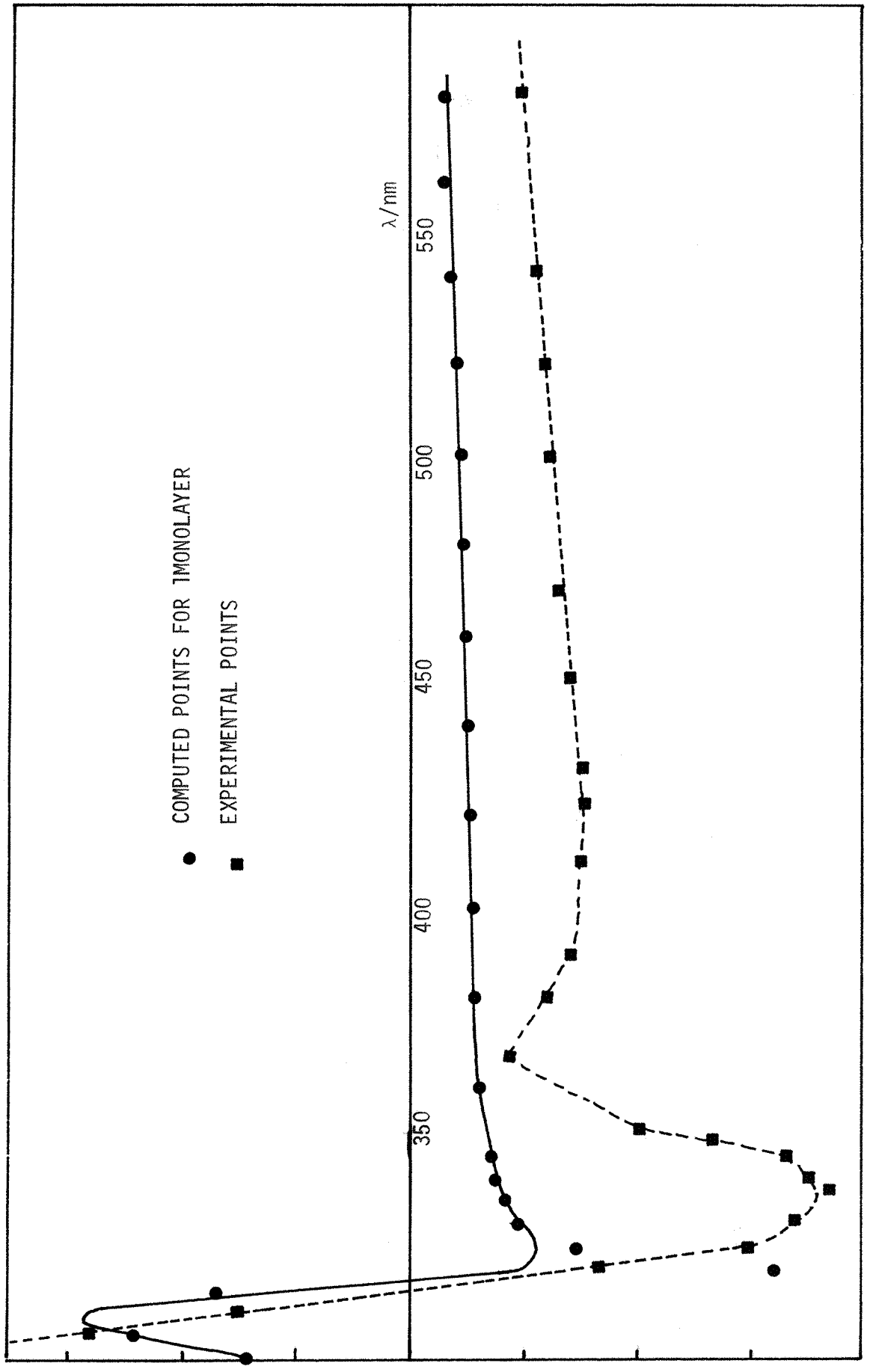

Fig. 5.8 Experimental and computed plots of $\Delta R/R$ vs. λ, for lead deposition on polycrystalline silver. Experimental points obtained from a potential step from 0 mV to -500mV vs. S.C.E. Parallel polarisation.

film itself seem to be the main factor determining the optical changes. To date, actual determinations of underpotential metal monolayer optical constants have been attempted with ellipsometric [56] and modulated reflectance spectroscopic [67,76] methods. In both cases, three-layer models were used to represent the electrode-film-solution interface [54]. In this model, the three component layers are assumed to be optically independent of each other i.e. the optical properties of the monolayer film are assumed to be totally independent from those of the substrate. As underpotential metal monolayers exist by virtue of the interaction with the electrode surface, it seems implausible that the use of such a three-layer model is valid. Kolb has suggested [76] that a four-layer model (substrate-substrate surface layer-adsorbate-solution) would be a more realistic picture. In this case, reflectance measurements at a variety of angles of incidence, with perpendicular and parallel polarised light, would be necessary to yield both the optical constants of the metal layer and the surface layer of the electrode. However, anisotropy effects are likely to prove problematical [105] in such measurements, and to date no attempts have been made in this direction.

5.4(b) OPTICAL EXPERIMENTS ON SINGLE CRYSTALS.

These were obtained in the solution, 1mM PbO/ 0.5M $HClO_4$, but only for the {111} and {100} faces. In the case of the {110} electrode, the complications caused by the continuous sweeping necessary for signal averaging cloud the basic adsorption/phase transformation/crystal growth picture. $\Delta R/R$ vs q plots for the two single crystals are shown in Fig. 5.9.

{111} FACE.

In the U.P.D. region, the optical-charge plot can be split into three components corresponding to the three peaks A_1-A_3 seen in the voltammetry. Apart from the final stage of the deposition, associated with A_3, the ad-atom formation (A_1) and crystal growth region (A_2) produce a

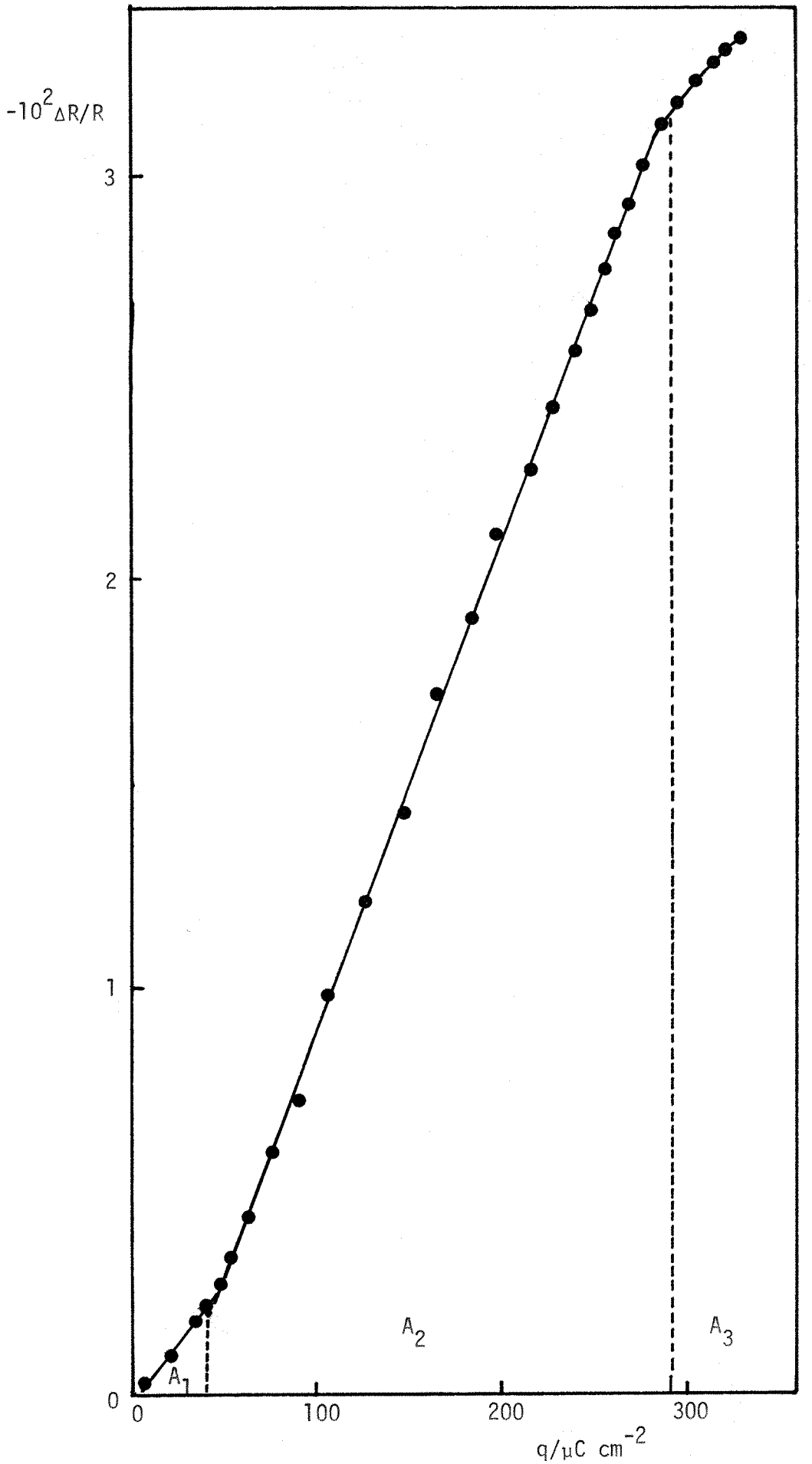

Fig. 5.9(a) Plot of $\Delta R/R$ vs. q for lead deposition on the {111} face. λ = 589nm, parallel polarisation. Solution 1mM PbO/ 0.5M $HClO_4$, sweep speed, 101mV s^{-1}.

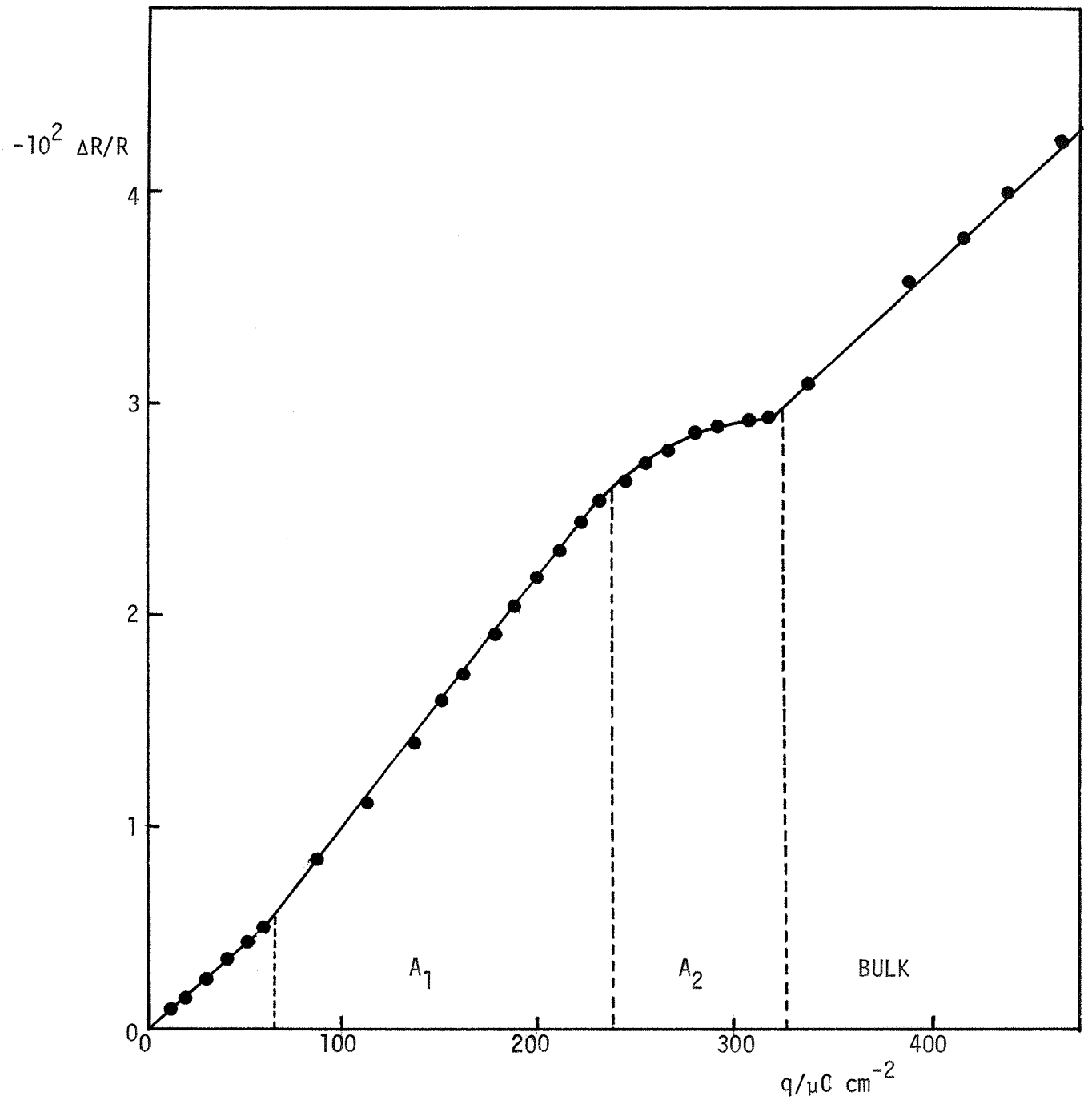

Fig. 5.9(b) Plot of ΔR/R vs. charge q for lead deposition on the {100} face. λ = 600nm, parallel polarisation. Solution, 1mM PbO/ 0.5M $HClO_4$.

linear relationship between $\Delta R/R$ and q, as was seen for thallium deposition on the same face.

{100}FACE.

The feature most apparent for the equivalent plot for thallium deposition on this face, was the plateau corresponding to the phase transformation peak, A_2. The L.S.V. for lead deposition on the {100} face, showed that the separation between the adsorption peak A_1 and the phase transformation-growth peak, A_2, was much smaller (33mV) than for thallium deposition (109mV). This results in a considerable overlap of the two peaks and a sharp resolution of the optical effects corresponding to the two separate processes of adsorption and crystal growth, would not be expected. Fig. 5.9(b) can be split into three segments in the U.P.D. region, corresponding to the features in the voltammetry. At low charge values there is a slight change in gradient of the plot, corresponding to the occupation of adsorption sites on the planar part of the electrode, rather than high co-ordination sites associated with dislocations. In the crystal growth region of coverage, the gradient is markedly less than in the adsorption region and this effect is especially pronounced with the last 50μC cm^{-2} of charge passed, where overlap with the adsorption peak would be non existent. By analogy with the thallium system, the low value of the slope in this region corresponds to the release of compensating negative charge in the ionic double layer, as the adsorbed, partially ionic lead layer, changes to a crystalline plane.

Another feature of note in Fig. 5.9(b) is the slope of the plot in the region where bulk deposition is occurring. This, as with thallium deposition on all crystal faces, is lower than that in the region corresponding to crystal growth in the underpotential region. This is probably due to both the optical and state of charge properties of the monolayer being somewhat different from bulk by virtue of the interaction with the

substrate.

$\Delta R/R$ vs. q plots obtained at wavelengths where large optical changes were taking place in the silver (375 and 320nm) [89,91] showed marked deviations from that shown in Fig. 5.9, as already illustrated for thallium deposition. In all cases the deviations were resticted to the monolayer region; the slope of the line corresponding to bulk deposition was always linear and seemingly unaffected by the factors causing the marked deviation fron linearity in the U.P.D. region (see Fig. 5.10). This illustrates dramatically that the electronic interaction between substrate and deposit, is restricted to the first monolayer (in the case of lead) or two monolayers (in the case of thallium). This point also illustrates the impossibility of using a three-layer model to determine optical constants in the region around the interband transition, as the condition of non-interacting layers is not fulfilled. Nevertheless, Kolb et al. [76] and Yeager et al. [56] have determined so-called optical constants of metal monolayers on gold at wavelengths centered around the interband transition of the metal (525nm). However, the results obtained cannot be thought of as representing the true optical constants of the monolayers in this region.

5.5 SUMMARY OF RESULTS IN 5mM PbO/ 0.5M $HClO_4$.

The results obtained from solutions of lead oxide in perchloric acid, can be summarized as follows:

1. The adsorption/phase transformation-crystal growth model, with the former process producing a superlattice structure, holds for the {110} and {100} electrodes. On the {111} face, the adsorption occurring is much less than expected from the superlattice model and must correspond to ad-atom deposition at dislocations.

2. The energy of interaction of lead atoms adsorbed at sites of different co-ordination number, varies more rapidly for lead than for thallium.

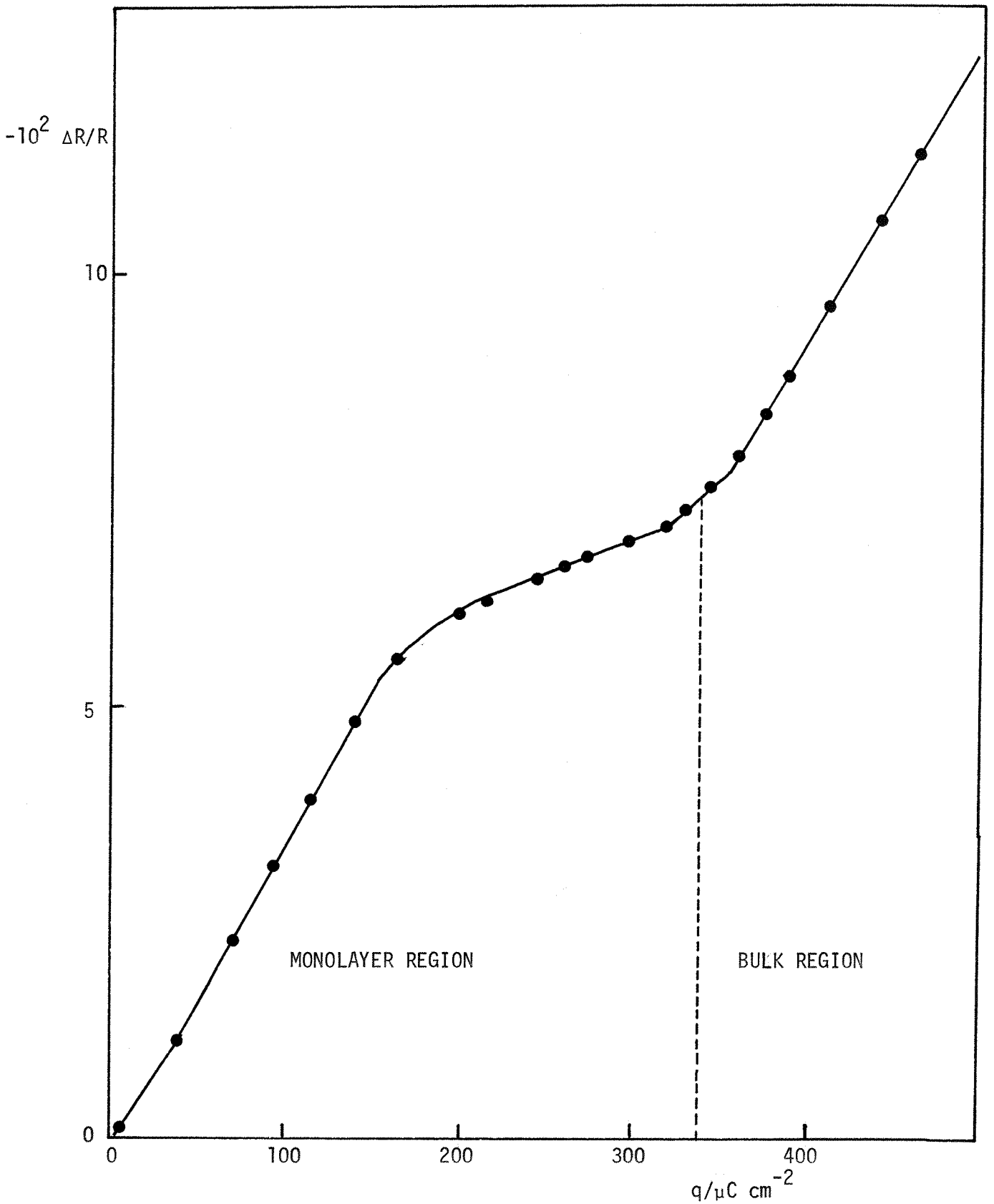

Fig. 5.10 Plot of ΔR/R vs. q for lead deposition on the {111} face at a wavelength where large optical changes are taking place in the substrate. λ = 325nm, parallel polarisation. Solution, as in Fig. 5.9(b).

3. The optical results are similar to those obtained for thallium deposition, with the various voltammetry peaks producing changes in slope of the reflectance-charge plot.

4. Potential step results are analogous to the corresponding experiments in thallium ion solutions. The rate of the charge transfer-lattice incorporation steps, in the crystal growth region, is too rapid to allow any information about nucleation and growth to be obtained.

5. Complications arise in the basic deposition pattern on the {110} electrode if the potential is swept or stepped continuously and rapidly.

Variations in the basic deposition pattern described above, will now be illustrated by varying the solution composition.

5.6 RESULTS IN 5mM $Pb(ClO_4)_2$/ 0.5M $NaClO_4$.

This solution was made up by dissolving lead oxide in an equivalent amount of perchloric acid. The resulting solution was effectively neutral (pH, 5.4). The voltammetry was identical to that obtained in 0.5M $HClO_4$ only in the case of the {100} electrode. Fig. 5.11 shows voltammograms obtained on the {111} and {110} planes. In both cases the results were independent of whether the potential was scanned continuously or not.

For the {111} face, the A_2 deposition peak is now broad. This contrasts with the behaviour in acid solutions were both deposition and stripping peaks were sharp. On the {110} face, the separation between the adsorption and phase peaks is now less well defined. However, increasing the acidity of the solutions to 1mM $HClO_4$ (i.e. a solution composition of 5mM PbO/ 11mM $HClO_4$/ 0.5M $NaClO_4$) produced voltammetry results virtually identical to those obtained in the 0.5M $HClO_4$ solutions (except in the case of the {110} orientation; the results from the 1mM $HClO_4$ solutions showed no dependence on the frequency of potential scans or steps)

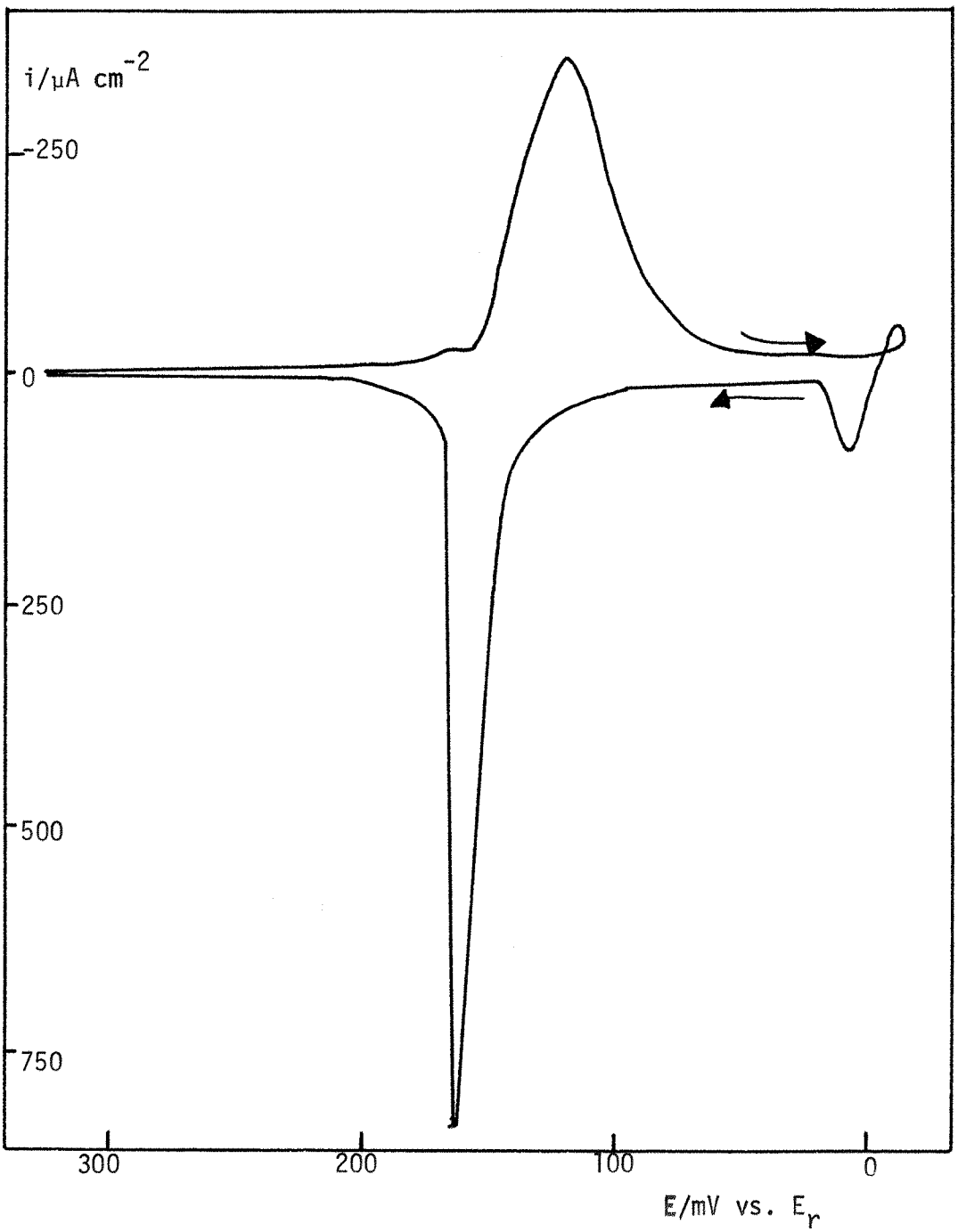

Fig. 5.11(a) L.S.V. for lead deposition on the {111} face from a neutral solution (5mM $Pb(ClO_4)_2$/ 0.5M $NaClO_4$). Sweep speed, 30 mV s^{-1}.

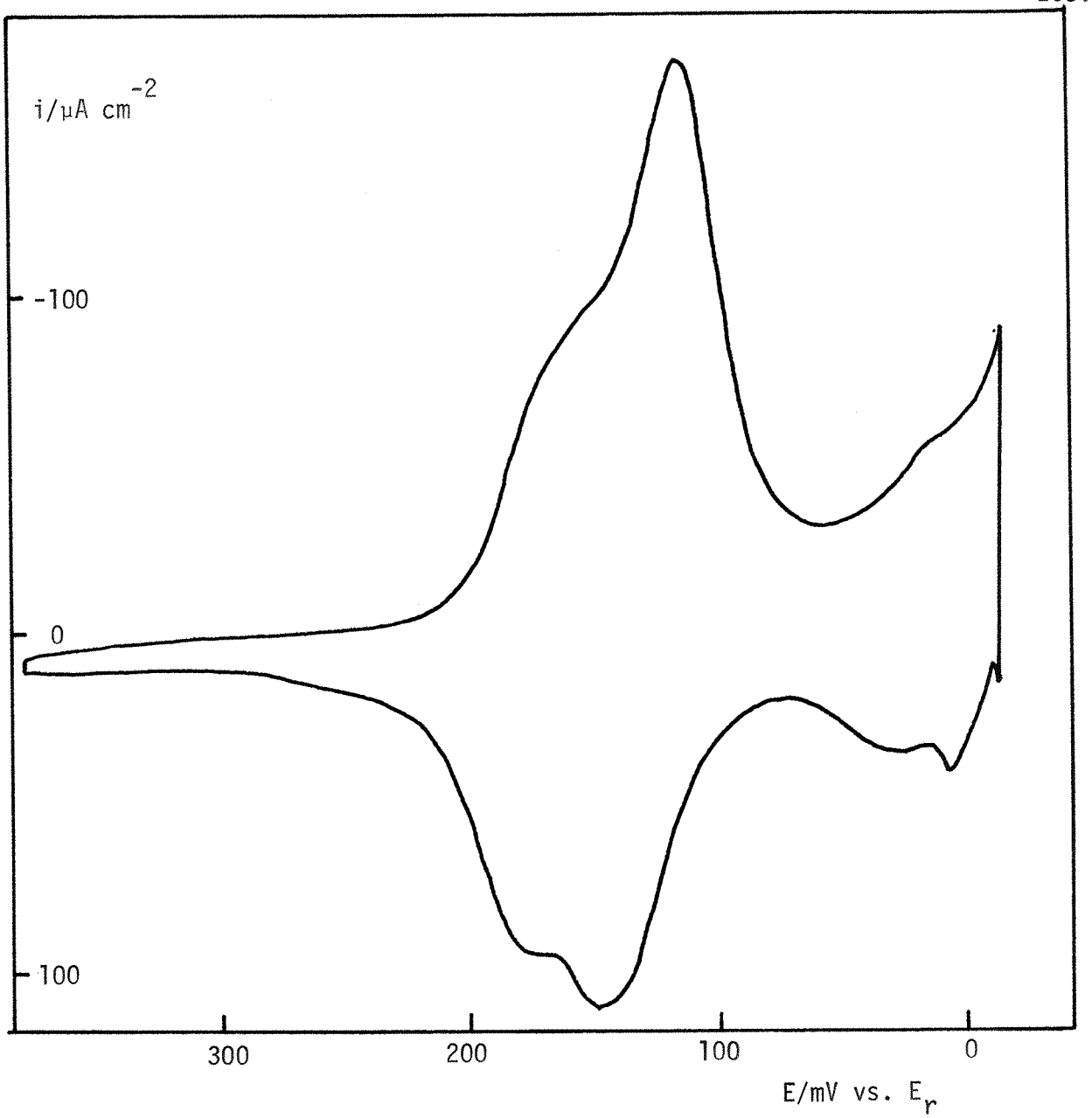

Fig. 5.11(b) L.S.V. for lead deposition on the {110} face from a neutral solution (5mM $Pb(ClO_4)_2$/ 0.5M $NaClO_4$). Sweep speed, 30mV s^{-1}.

This marked dependence of the observed behaviour on the acidity of the solution would suggest that the deposition reaction was very pH sensitive. For a metal ion reduction, involving no hydroxide complexes, the kinetics and thermodynamics of the deposition step should be independent of potential. If the reduction proceeded by a lead hydroxy complex, e.g. $PbOH^+$, [107] it would be expected that the kinetics of the charge transfer step would be pH dependent but the thermodynamics would remain unaltered. In the present case, it is evident from the results on the {111} face, that the thermodynamics of the U.P.D. process, are being affected, which implies that the nature of the deposited metal is different. It is possible that some oxidation of the monolayer film occurs in the neutral solution. This can be checked with standard electrode potential data. [106]

For the reaction,

$$PbO + H_2O + 2e^- = Pb + 2OH^- \qquad E^\circ = -819mV \text{ vs. S.C.E.}$$

therefore,

$$E = E^\circ + \frac{RT}{zF} \log_e \frac{a_{PbO} \cdot a_{H_2O}}{a_{Pb} \cdot a_{OH^-} \cdot a_{OH^-}}$$

assuming that, a_{PbO}, a_{Pb} and $a_{H_2O} = 1$, and $a_{OH^-} = [OH^-]$, then

$$E = E^\circ + \frac{RT}{zF} \log_e \frac{1}{[OH^-]^2}$$

therefore,

$$E = -819 + 29.5 \log_{10} \frac{1}{[OH^-]^2}$$

Values of E as a function of pH are shown in Table 5.3.

TABLE 5.3

pH	E/mV vs. S.C.E.
7	-406
5.4	-312
3	-170

Table showing dependence of $E_{PbO/Pb}$ on pH.

Now, $E_{r(Pb^{2+}/Pb)}$ in the solution 5mM $Pb(ClO_4)_2$/ 0.5M $xClO_4$ (where x = H or Na), is-437mV (vs. S.C.E.). The A_2 peak on the {111} face occurs 148mV positive to this value at -289mV. It can be seen from the above table that, in solutions with pH 5.4, thermodynamically, PbO is stable with respect to Pb at this potential. At pH 3 however, corresponding to an acidity of 1mM, $E_{PbO/Pb}$ is now positive to the potential where deposition starts to occur.

Presumably then, at pH 5.4 the deposition of the monolayer metal crystal plane, is hindered by incorporation of oxygen from water and this will prevent the deposition occurring over a very narrow range of potential, as in acidic solutions. The final form of the monolayer deposit however, should be a crystalline layer of lead. On the reverse scan, on the {111} plane, a single sharp stripping peak is observed occurring at the same potential as the analogous peak in acidic solutions. This would imply that no oxidation of the complete lead monolayer occurs on the reverse scan and the stripping involves oxidation of pure lead.

In the electrode potential calculation, it was assumed that the activity of the deposited lead was equal to unity. This is an approximation which is only valid when the lead patches are sufficiently large to have

achieved the activity of the bulk phase. Nevertheless, the calculated potentials should give a rough idea of the stability of the lead monolayer in the solutions of various pH.

It is interesting to consider why the {100} plane is almost totally unaffected in the neutral solution. The adsorbed layers on all crystal planes must have activity sufficiently different from bulk lead (i.e., 1) to be not susceptible to partial oxidation. The crystalline phase peak on the {110} orientation occurs, in acid solution at about 133mV positive to $E_{r(Pb^{2+}/Pb)}$ i.e. in 5mM Pb^{2+} solutions, at -304mV. At pH 5.4, this is on the borderline of the stability of PbO with respect to Pb, and some distortion of the normal two peak structure would be expected, as observed experimentally. On the {100} face, the phase peak A_2 occurs 106mV positive to $E_{r(Pb^{2+}/Pb)}$ i.e. in 5mM Pb^{2+} solutions, at -331mV. This is about 20mV more negative than the $E_{PbO/Pb}$ potential and hence should be free from oxidation effects.

No such pH dependent effects were found for thallium deposition.

$$TlOH + e = Tl + OH^- \qquad E^o = -588mV \text{ vs. S.C.E.}$$

The reduction potential[106] of TlOH is sufficiently far anodic, even in neutral solutions, to cause any problems in the thallium deposition potential range.

5.7 RESULTS IN ACETATE SOLUTIONS.

(a) VOLTAMMETRY.

The voltammetry results from acetate solutions, although showing many similarities to those from acid perchlorate solutions, also show some interesting deviations.

The reversible potential for lead in the solution 5mM $Pb(CH_3CO_2)_2$/ 0.5M $Na(CH_3CO_2)$/ 0.1M CH_3CO_2H (at -530mV vs. S.C.E.) is some 100mV more negative than the corresponding potential in perchlorate solutions of

the same total lead concentration, indicating a high degree of complexing of the lead ions by acetate ions (greater than 99%). The pH of the above solution is 5.3. Problems with oxidation of the monolayer phase were encountered at this level of acidity in perchlorate solutions but the complexing of lead in acetate solutions, [107] reduces its activity to such an extent that the deposition spectrum is moved to more negative potentials than those at which oxidation problems would be encountered. No dependence of the results on the pH of the solution, was found.

The voltammetry results for deposition on all crystal faces are shown in Fig. 5.12. On the {100} face, the result was virtually identical to that already shown for deposition from perchlorate solutions (apart from a slightly higher total charge- see later). It was noticeable however, that the shoulder on the adsorption peak attributed to deposition at defect sites, was less pronounced. Unlike the results from acid perchlorate solutions, the {110} face voltammetry was independent of whether the potential scan was repetitive or not, i.e. the first sweep was identical to subsequent sweeps in continuous cycling.

The results for each face will now be discussed separately.

{111} FACE.

The voltammetry on this plane now consists of a single sharp peak on the anodic and cathodic sweeps. If this peak is assumed to be the deposition of a crystalline phase, there is no peak corresponding to a prior adsorption step as was shown in Fig. 5.2 for perchlorate solutions. Moreover, the rearrangement peak, A_3, is also absent.

The disappearance of the adsorption peak, A_1, is almost certainly due to the blocking of these favourable sites by adsorbed acetate ions. Table 5.4 gives the peak potentials in 5mM acetate solutions and Table 5.5 gives the charge at various points.

These values can be compared with those in Table 5.1 and Table 5.2 for lead deposition from perchlorate solutions. It can be seen that in the

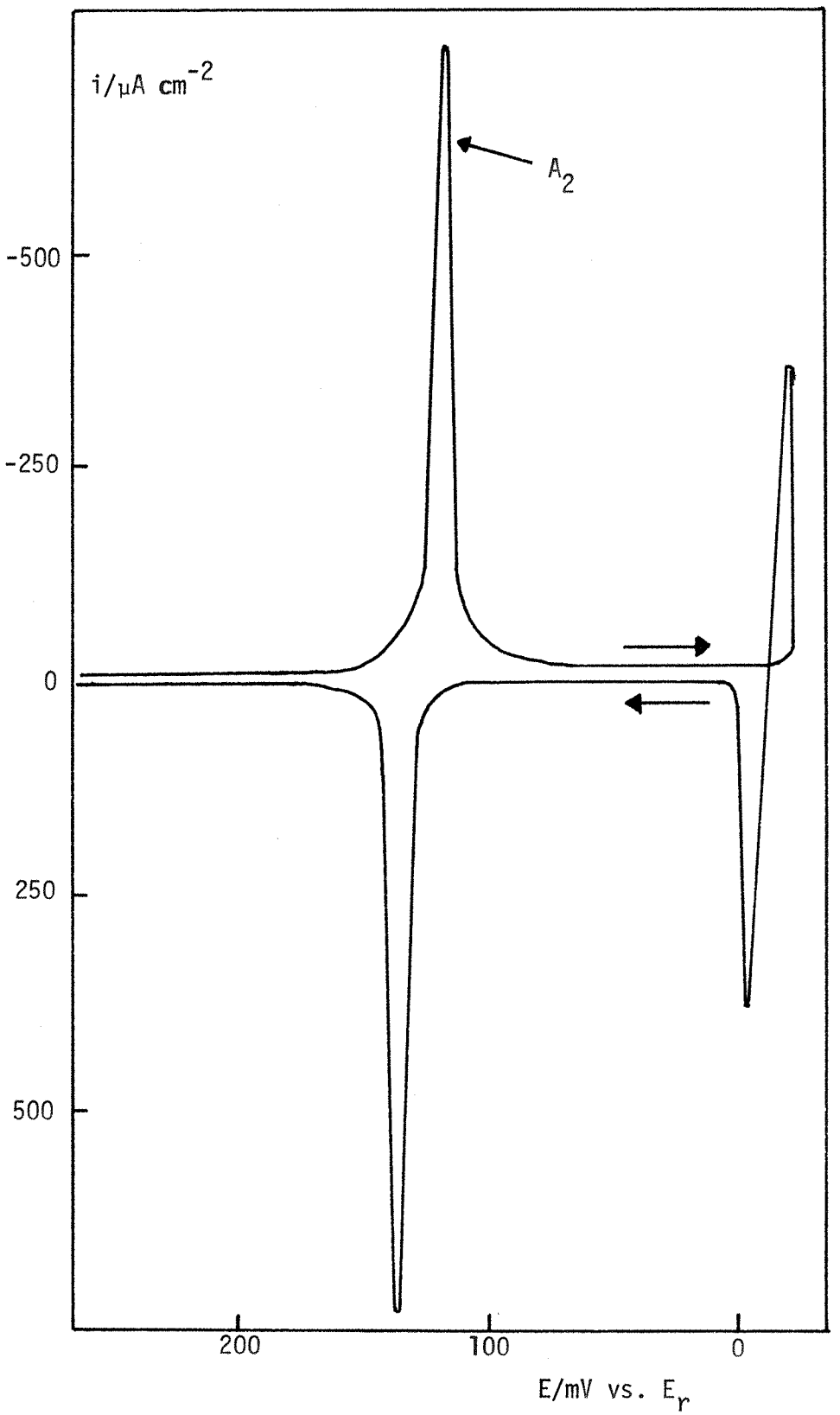

Fig. 5.12(a) L.S.V. for lead deposition on the {111} face.

Solution, 5mM $Pb(CH_3CO_2)_2$/ 0.5M $Na(CH_3CO_2)$/ 0.1M CH_3CO_2H.

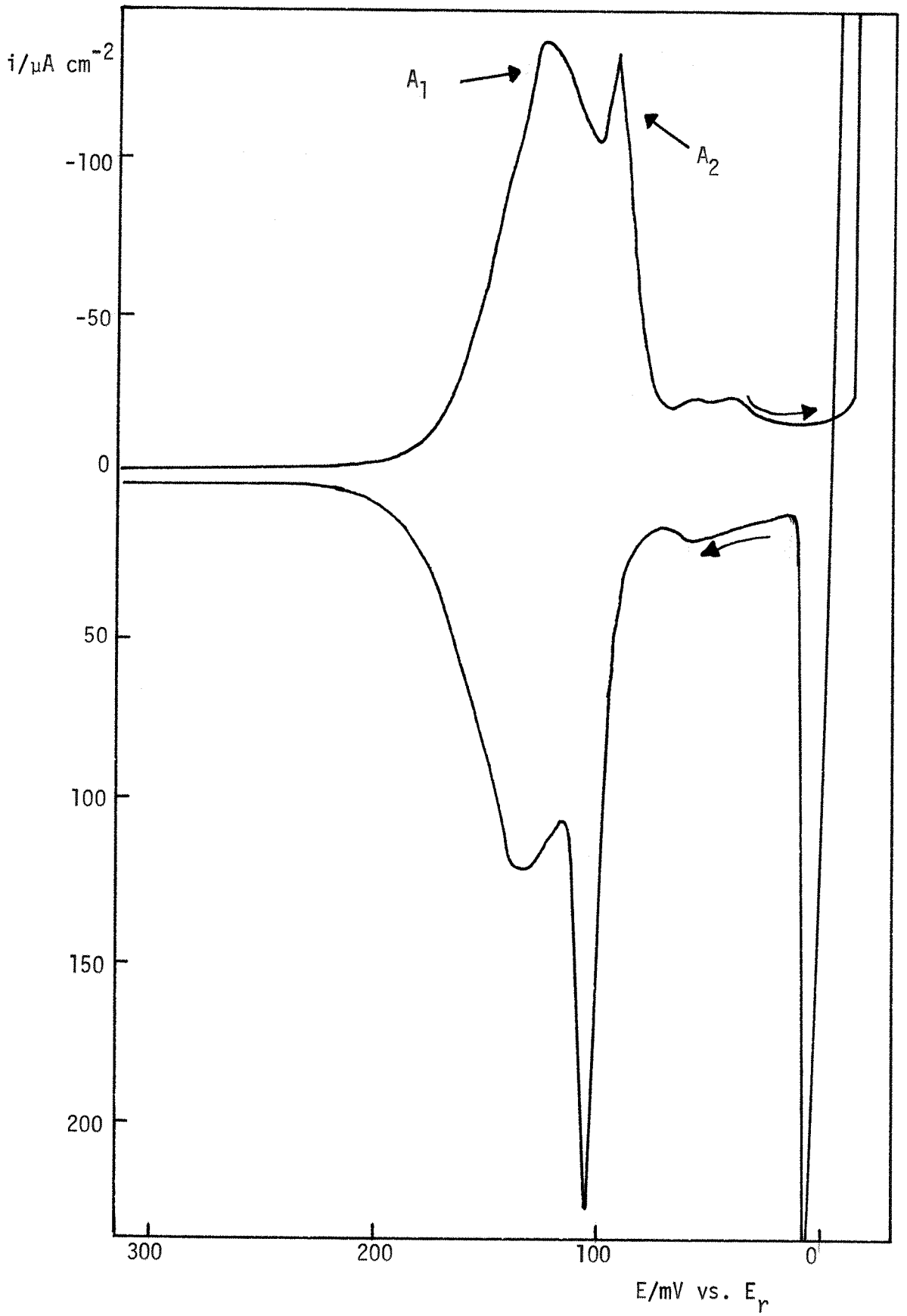

Fig. 5.12(b) L.S.V. for lead deposition on the {100}face. Solution, as in Fig. 5.12(a). Sweep speed, 30mV s^{-1}.

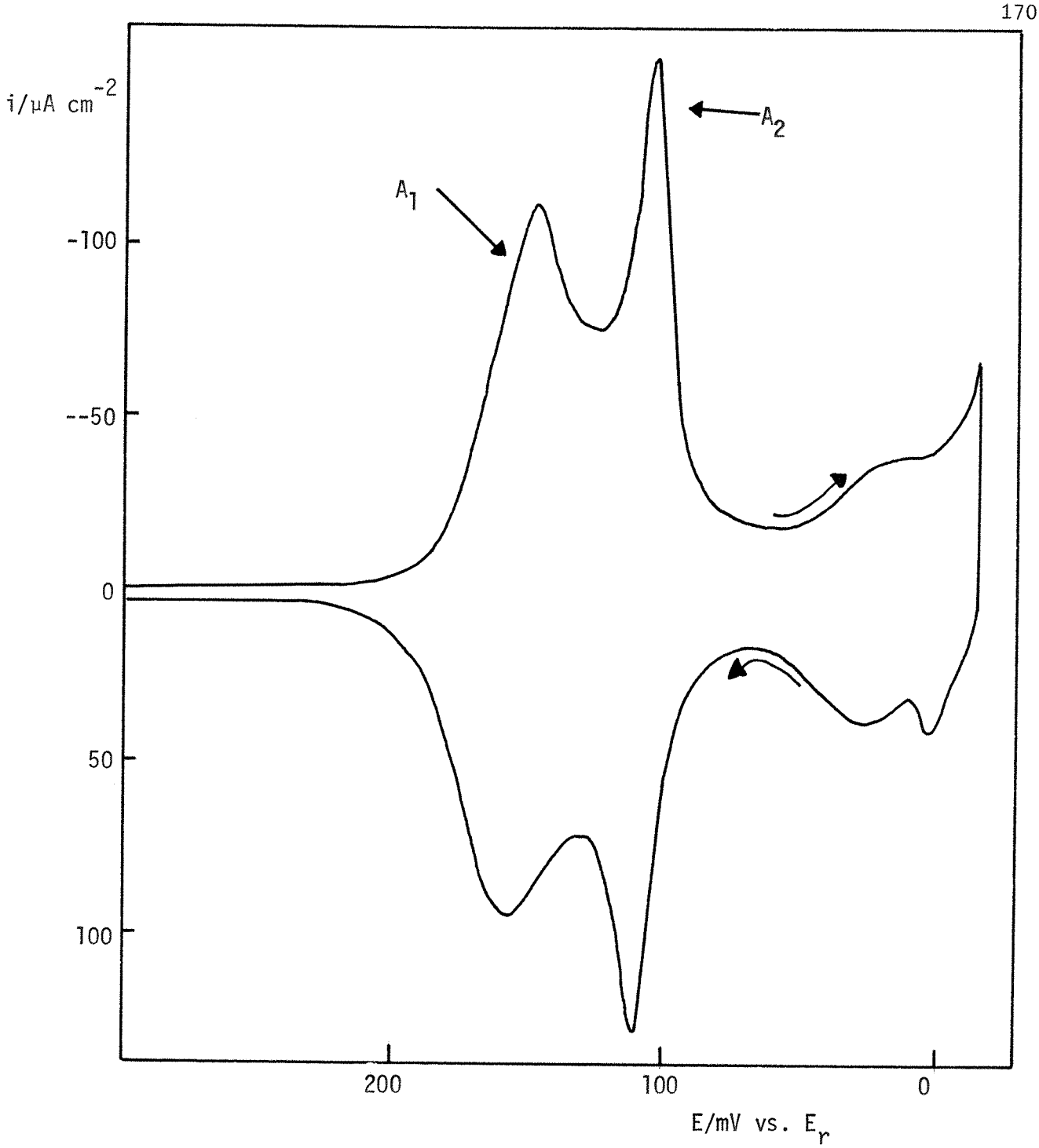

Fig. 5.12(c) L.S.V. for lead deposition on the {110} face.

Solution, 5mM $Pb(CH_3CO_2)_2$/ 0.5M $Na(CH_3CO_2)_2$/ 0.1M CH_3CO_2H. Sweep speed, 30 mV s^{-1}.

TABLE 5.4

CRYSTAL FACE	A_1/mV vs. E_r	A_2/mV vs. E_r
{110}	+149	+105
{100}	+128	+96
{111}	-	+126

Peak potentials for lead deposition on different planes of silver. Solution, 5mM $Pb(CH_3CO_2)_2$/ 0.5M $Na(CH_3CO_2)$/ 0.1M CH_3CO_2H; sweep speed 30mV s^{-1}.

TABLE 5.5

CRYSTAL FACE	'q' ASSOCIATED WITH A_1/μC cm^{-2}	TOTAL 'q' FOR MONOLAYER/μC cm^{-2}
{110}	152	394
{100}	227	369
{111}	-	362

Total monolayer charge and charge associated with peak A_1, for lead deposition on different planes of silver. Solution and sweep speed, as in Table 5.4.

above case the ΔU_p values are slightly smaller and the measured charges slightly higher than the corresponding values in perchlorate solutions. The explanation for this effect in terms of anion adsorption has already been discussed in connection with the thallium results.

The p.z.c. values of the three silver single crystals in fluoride solutions, have already been quoted[100]; these were, {111},-690mV (vs. S.C.E.); {100}, -910mV; {110}, -1010mV. These values show that at a given potential the amount of anion adsorption on the different crystal planes, would be in the sequence,

$$\{111\} < \{100\} < \{110\}$$

They also show that the defect sites on the {111} face, because of their higher co-ordinating ability, would be more favourable for the adsorption of anions than the planar sites (i.e. they would be somewhat analogous to the planar sites on the {110} face). It seems probable therefore, that the virtual absence of any adsorption step in acetate solutions, on the {111} plane, is due to the favourable sites being occupied by acetate ions. Crystal growth should take place on the planar parts of the electrode where anion adsorption is much less. The acetate ions also seem to eliminate the A_3 peak, i.e. the crystal growth part of the deposition process occurs 'smoothly' over the whole electrode and not in two separate stages, as in perchlorate solutions. Anion adsorption effects can similarly explain the less prominent shoulder in the adsorption region on the {100} face (Fig. 5.12).

Fig. 5.12(a) shows particularly well, the marked asymmetry for the deposition and stripping peaks on the {111} face, an effect which is characteristic of the nucleation overpotential in the formation and removal of crystal planes.

Optical experiments show that the relationship between reflectance and charge is substantially linear over the majority of the monolayer

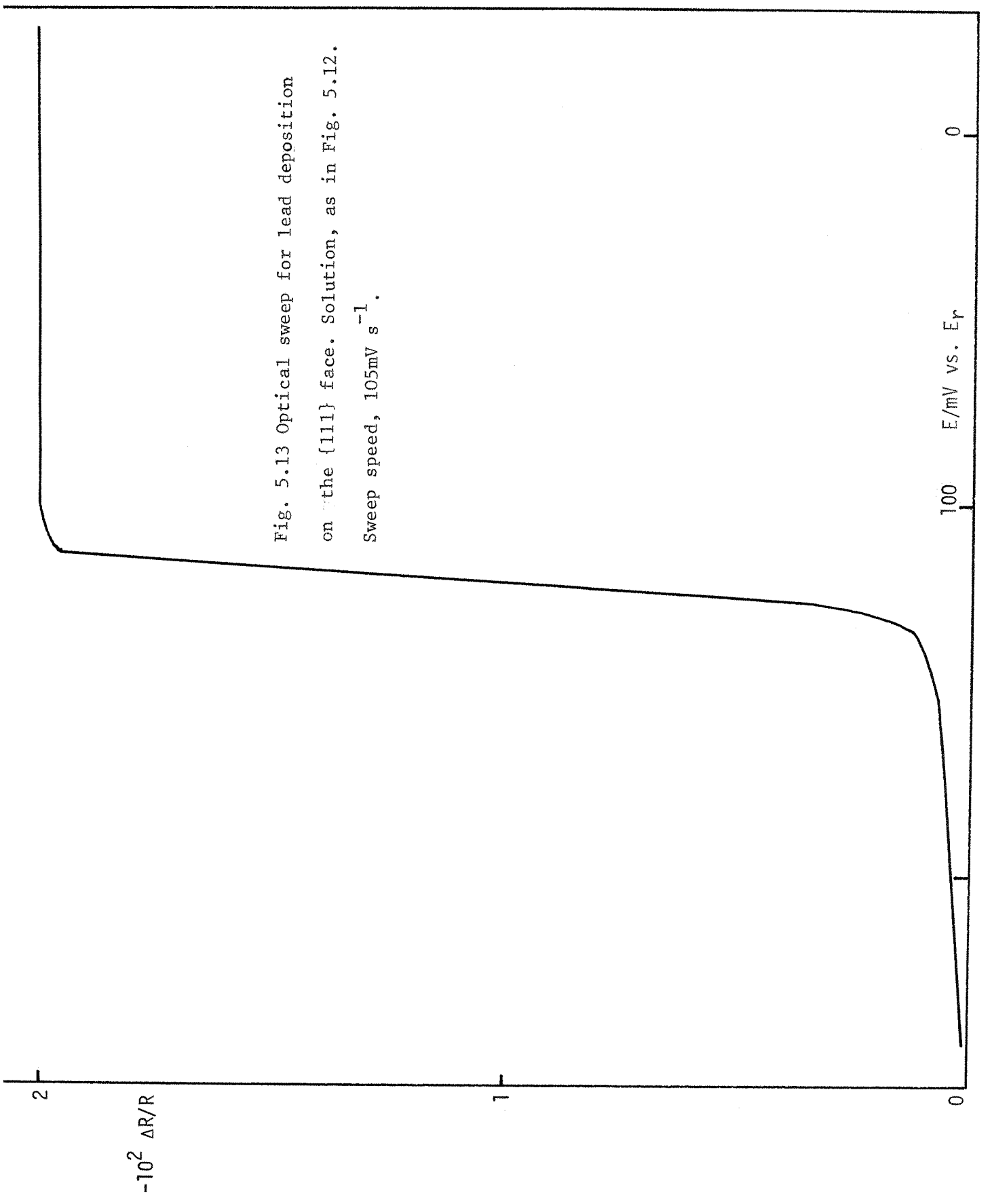

Fig. 5.13 Optical sweep for lead deposition on the {111} face. Solution, as in Fig. 5.12. Sweep speed, 105mV s^{-1}.

deposition process and consequently the reflectance-potential sweep can be used as a measure of the surface coverage-potential isotherm. An example of such a sweep is shown in Fig. 5.13. The marked discontinuity in the isotherm is typical of a crystal growth process.[108] It is indeed remarkable that such a sharp discontinuity can be observed for data from solid electrodes; in fact, the scan rate for the optical sweep shown in Fig. 5.13 (about 100mV s^{-1}) is really too high for the true equilibrium coverage isotherm to be obtained; at lower scan rates the discontinuity would be even more marked.

The growth pattern on the {111} plane in acetate solutions, seems to be the simple, one stage growth, of a two-dimensional close packed crystalline layer.

{110}FACE.

Although the voltammetry is broadly similar to that obtained in perchlorate solutions (except for the lack of any scan interval dependence) the separation between the two peaks A_1 and A_2, has increased to 44mV (34mV in perchlorate solutions) enabling a greater resolution to be obtained. The charge associated with the first peak (Table 5.5) gives reasonable agreement with the superlattice model when the roughness factor of 1.2 is used (the total charge on the {111} plane/calculated charge for a close packed layer = 1.2) and must represent occupation of all the favourable planar electrode sites. The charge associated with the second peak represents complete coverage of the surface by a close packed layer.

It is apparent that the A_2 peaks are not particularly asymmetrical, i.e. although they are associated with the formation and stripping of a close packed layer, the latter must have more the properties of an adsorbed layer than a crystalline plane. The reasons for this have already been discussed in connection with the thallium results.

A reflectance-charge plot for lead deposition on the {110} face,

from acetate solutions, is shown in Fig. 5.14. It is apparent that the deposits associated with the two voltammetry peaks, A_1 and A_2, have very similar optical characteristics, as was found for thallium deposition on this crystal face. However, the formation of the second layer produces a marked change in the gradient.

5.7(b) POTENTIAL STEP RESULTS.

These were exactly analogous to the results obtained in perchlorate solutions (except on the {110} plane, where no dependence on the frequency of pulsing was observed), i.e. the crystal growth step was sufficiently fast to allow any information about the lattice growth step to be obtained. Only one example will be given, for the {110} face. Fig. 5.15 shows transients obtained by pulsing to potentials in the A_1 and A_2 region. The A_1 transient, like its thallium equivalent, shows a linear relationship between i and $t^{-\frac{1}{2}}$ over a substantial part of the transient. In the A_2 region, the initial part of the transient again follows this relationship, but at longer times i becomes linear with t. This result emphasizes the difference in the nature of the processes occurring in the two potential regions. Evidently some influence of the crystal growth step on the charge transfer kinetics is responsible for the change in the shape of the transient.

5.7(c) POTENTIAL DECAY RESULTS.

Fig. 5.16 shows potential decay curves for the three single crystals. That associated with the {111} face is particularly noteworthy, showing that the activity of the deposited phase varies by a factor of only 1.29 as the surface coverage varies by almost 50%. It is remarkable that a surface phase formed on a single crystal plane should show such a constant activity over a wide range of coverage. This behaviour contrasts strongly with earlier assumptions concerning the nature of underpotential monolayers;

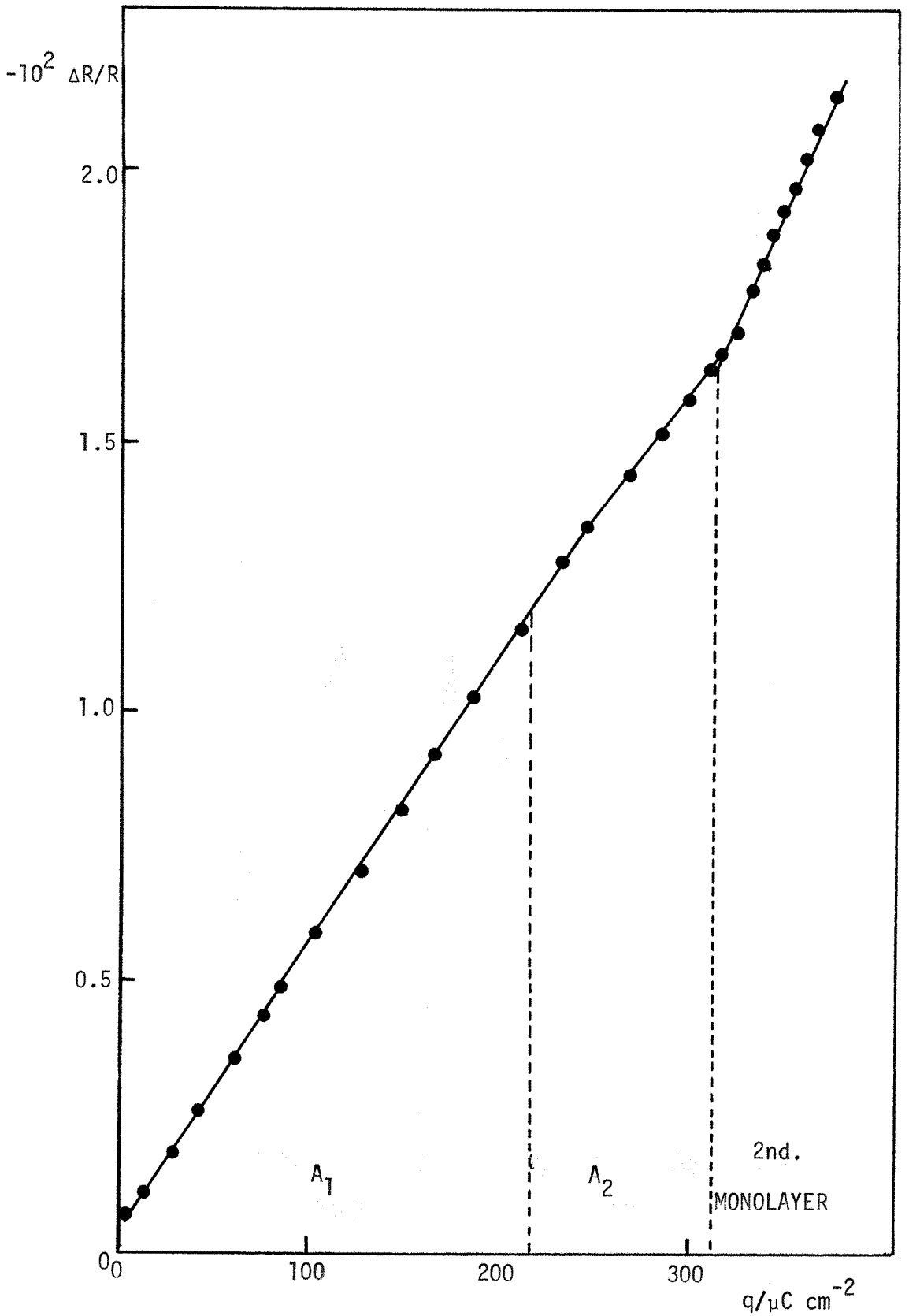

Fig. 5.14 Plot of ΔR/R vs. q for lead deposition on the {110} face λ=589nm, parallel polarisation. Solution, 5mM $Pb(CH_3CO_2)_2$/ 0.5M $Na(CH_3CO_2)_2$/ 0.1M CH_3CO_2H. Sweep speed, 105mV s^{-1}.

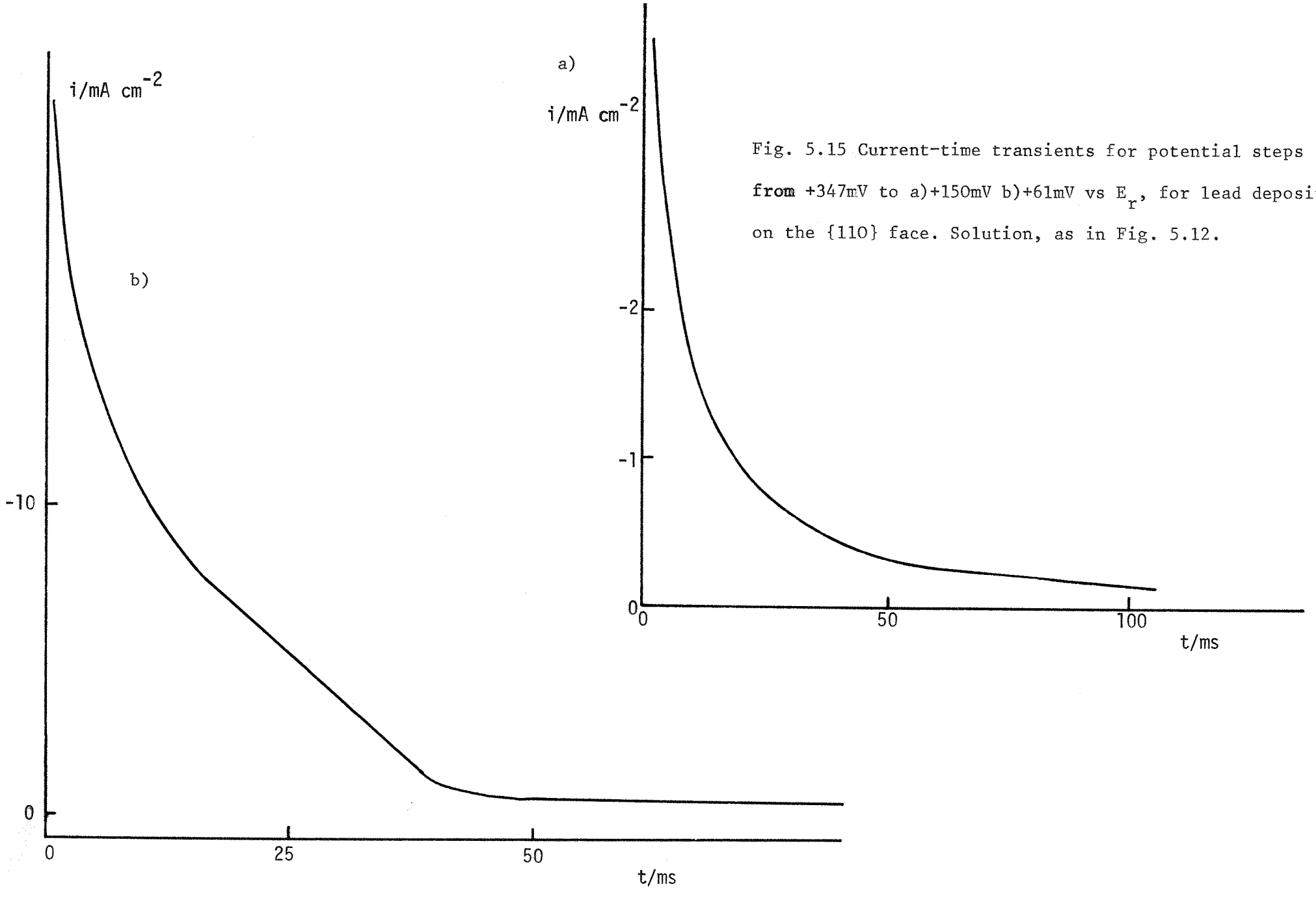

Fig. 5.15 Current-time transients for potential steps from +347mV to a)+150mV b)+61mV vs E_r, for lead deposition on the {110} face. Solution, as in Fig. 5.12.

it was assumed that these were adsorbed layers and the activity varied linearly with surface coverage.[36,109] The mean equilibrium phase potential are tabulated in Table 5.6.

TABLE 5.6

CRYSTAL FACE	LEAD PHASE POTENTIAL/mV VS. S.C.E.
{111}	-393
{100}	-433
{110}	-415

Table showing mean phase potentials for lead monolayers on silver. Solution, as in Fig. 5.12.

The mean phase potentials coincide exactly with the onset of stripping and deposition on the {111} face, indicating no overpotential for the formation of the crystalline deposit. The same arguments involving lattice distortion effects by the substrate, can be used to explain the properties of the phases formed on the different crystal planes.

5.8 THE EFFECT OF CHLORIDE ION.

The marked effect of chloride ion on the thallium deposition voltammetry, has already been illustrated. The influence of chloride ion on lead deposition will first be illustrated by making the solution 5mM PbO/0.5M $HClO_4$, 1mM with repect to chloride ion. The corresponding voltammetry on the three single crystals, is shown in Fig. 5.17.

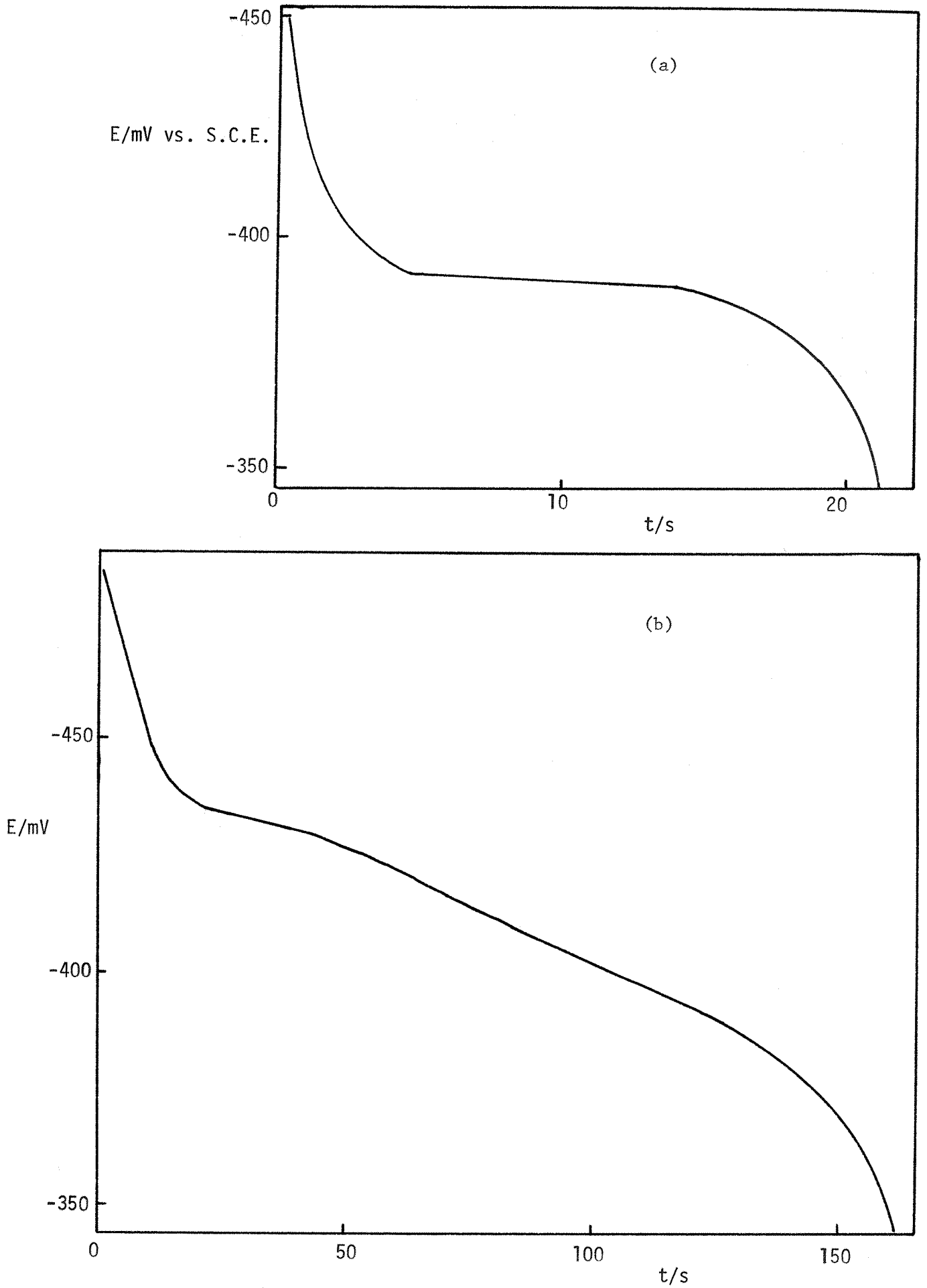

Fig. 5.16 Potential/time decay curves for lead removal from (a) the {111} and (b) the {100} planes of silver. Solution, as in Fig. 5.12.

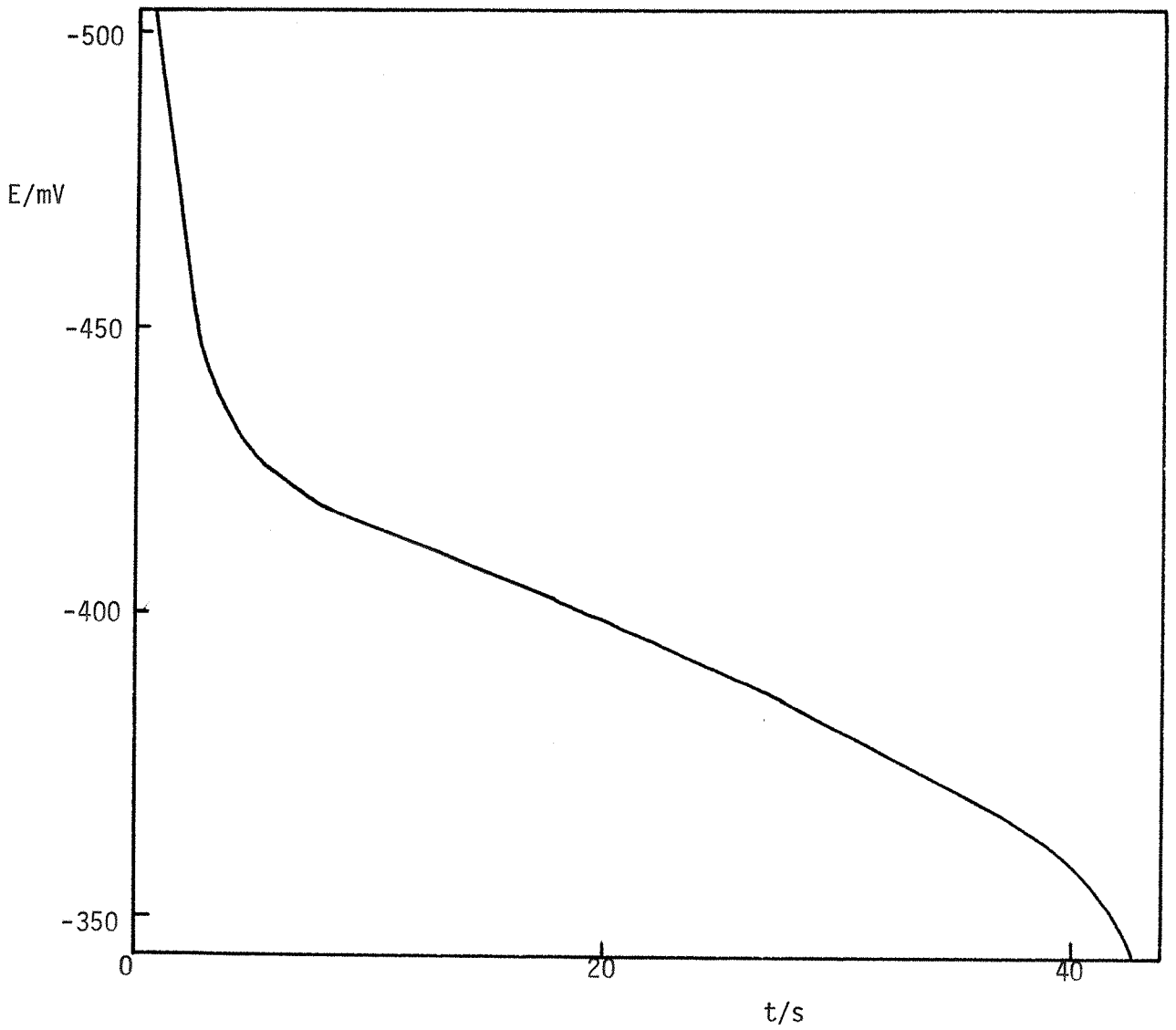

Fig. 5.16(c) Potential/time decay curve for lead removal from the {110} plane of silver. Solution, as in Fig. 5.12.

{111} FACE.

Only a single sharp peak is seen on the cathodic scan and the underpotential shift of this (see Table 5.7) is about 18mV smaller than the corresponding value in chloride free perchlorate solutions. Again, by analogy with the previous results, this must correspond to the growth of a two-dimensional crystal plane from the outset, and the disappearance of the adsorption peak A_1 is due to the blocking of the favourable adsorption sites by chloride.

{100} AND {110} FACES.

Compared to the results in chloride free perchlorate solutions, the following effects can be noted.

1. The peak potentials have moved to more negative potentials (lower underpotential shifts) (see Table 5.8). The table shows that this effect is more marked for the adsorption peak A_1, than the crystal phase peak A_2. The effect of specific adsorption on underpotential shift has already been discussed in connection with the thallium results. That such effects are more important for the adsorption process than the crystal growth step would be expected as it is the former process where competition between chloride and lead ions takes place for adsorption sites on the electrode. The crystallization process is much less dependent on the nature of the adsorption sites, and hence any occupation of them by chloride would have a smaller effect than on the adsorption process.

2.The adsorption peaks, A_1, are sharper. This effect implies that there is now a decreased difference in the adsorption energy between $\theta=0$ and $\theta=1$ (referring to superlattice coverage). Such a peak sharpening could also be described,using a Frumkin isotherm, by an increased positive interaction parameter. The E^{o} value for the reaction,

$$PbCl_2 + 2e = Pb_{(Hg)} + 2Cl^-$$

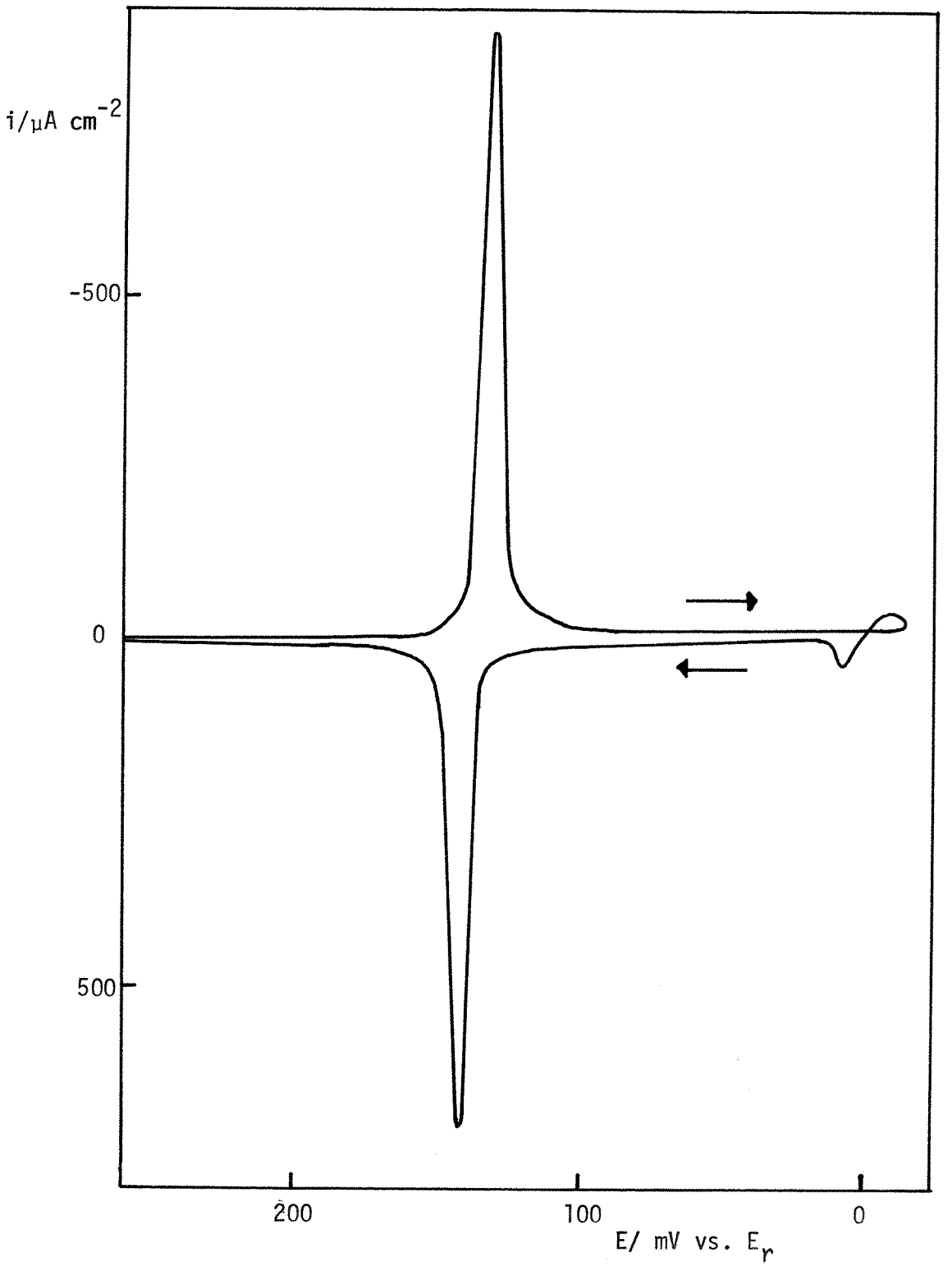

Fig. 5.17(a) L.S.V. for lead deposition on the {111} face. Solution, 5mM PbO/ 0.5M $HClO_4$/ 1mM NaCl. Sweep speed, 30mV s^{-1}.

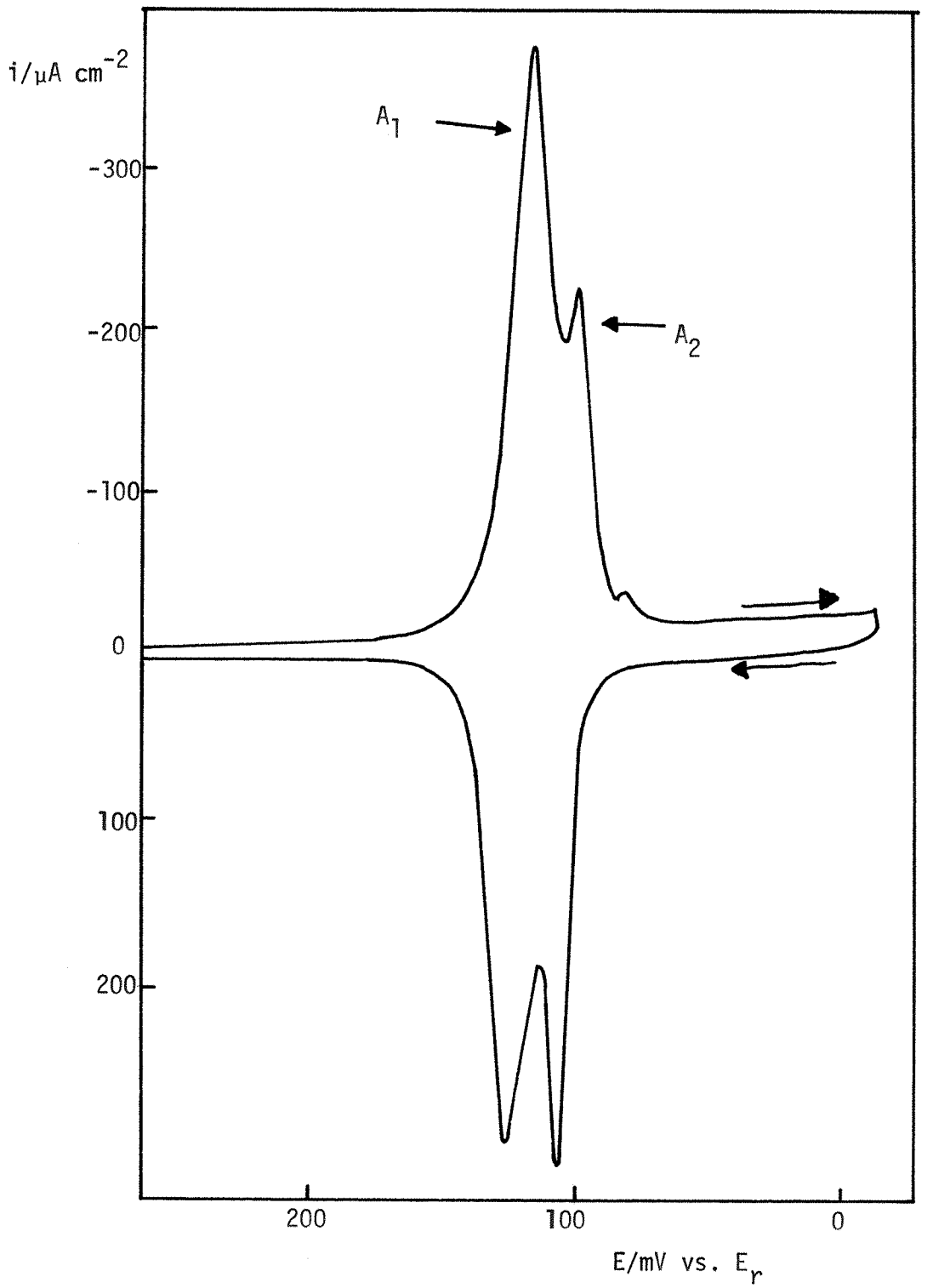

Fig. 5.17(b) L.S.V. for lead deposition on the {100} face.

Solution, 5mM PbO/ 0.5M $HClO_4$/ 1mM NaCl. Sweep speed, 30mV s^{-1}.

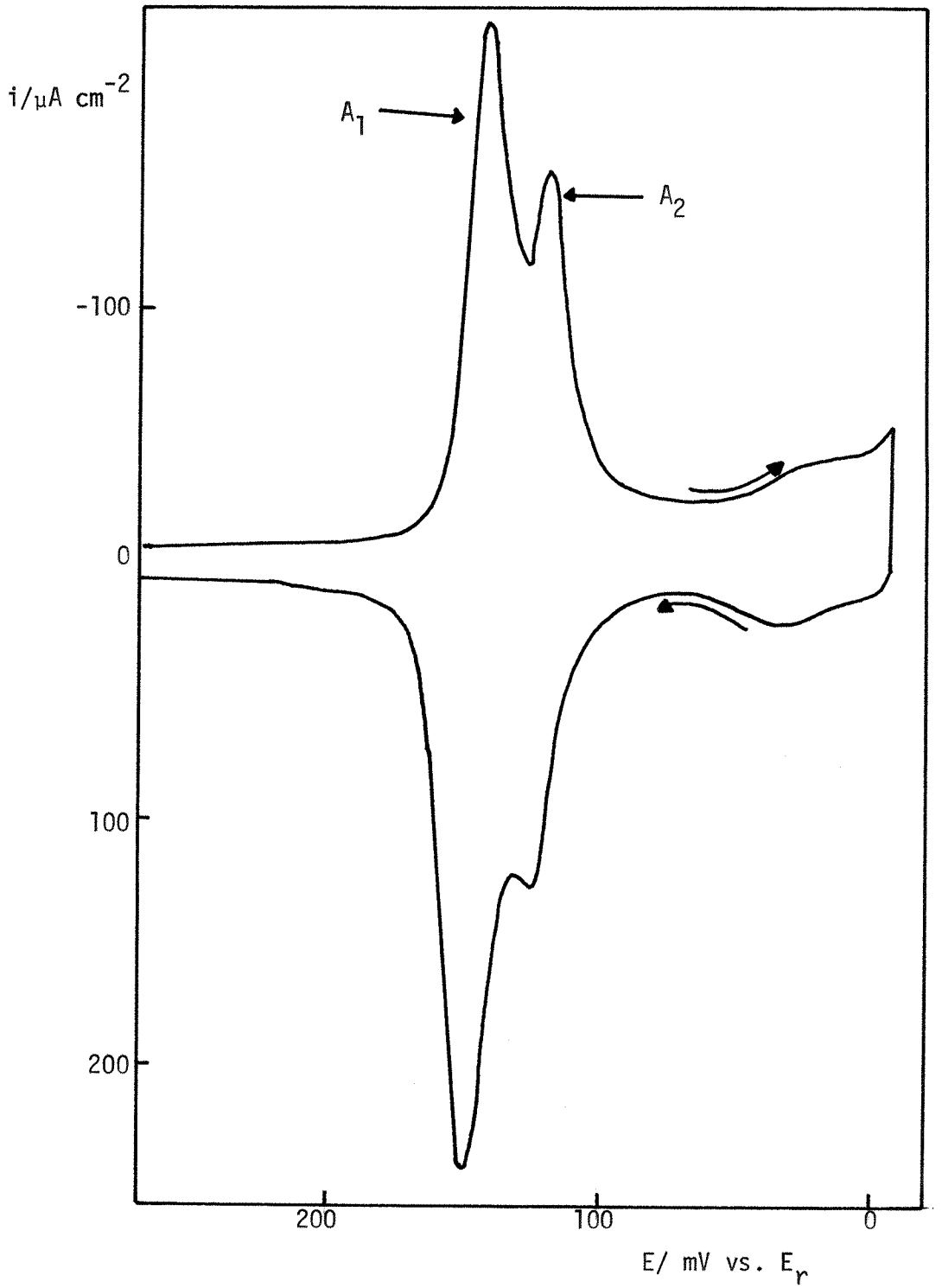

Fig. 5.17(c) L.S.V. for lead deposition on the {110} face. Solution, 5mM PbO/ 0.5M $HClO_4$/ 1mM NaCl. Sweep speed, 30mV s^{-1}.

TABLE 5.7

CRYSTAL FACE	A_1/mV vs. E_r	A_2/mV vs. E_r
{111}	-	+130
{100}	+116	+100
{110}	+139	+116

Peak potentials (vs. E_r) for lead deposition on different planes of silver. Solution, 5mM PbO/ 0.5M $HClO_4$/ 1mM NaCl; sweep speed, 30mV s^{-1}.

TABLE 5.8

CRYSTAL FACE	A_1 SHIFT/mV	A_2 SHIFT/mV
{100}	-23	-6
{110}	-28	-17

Table showing shift of peak potentials in 5mM PbO/ 0.5M $HClO_4$/ 1mM NaCl relative to those in 5mM PbO/ 0.5M $HClO_4$. Sweep speed 30mV s^{-1}.

is -505mV vs. S.C.E.. When the chloride ion concentration is 1mM, $E_{PbCl_2/Pb}$ = -328mV vs. S.C.E., which is equivalent to +109mV vs. E_r in the solution 5mM PbO/ 0.5M $HClO_4$/ 1mM NaCl. This implies that actual phase formation of $PbCl_2$ would be possible at potentials more positive than +109mV vs. E_r, although there is no evidence that this does occur. It is possible that chloride ions could act as a bridge between the lead ad-atoms and in this way, increase the interaction parameter. The results on the 111 plane, where a single sharp peak is obtained (at +130mV), do not suggest any competition between lead chloride and lead metal formation, takes place.

Schmidt's study[47] of lead deposition on polycrystalline silver has already been referred to. In the lower underpotential range, lead 'adsorption' was accompanied by chloride ion desorption, whereas at higher potentials, simultaneous 'adsorption' of lead and chloride ions took place. It seems likely that the latter process would occur when all the adsorption sites on the electrode had been occupied and crystal growth was taking place. The chloride ion could simply be adsorbed on top of the lead layer, or it could be incorporated in the two-dimensional layer itself. Certainly a complete crystalline layer of lead chloride can be ruled out, as charge measurements are not consistent with this, but it seems possible for interstitial chloride ions to be present in the final deposit.

Potential step results in this solution produced transients with the usual $i\text{-}t^{-\frac{1}{2}}$ relationship in the A_1 region, whereas in the A_2 region the lower part of the transient became linear with time.

The voltammetry results for solutions containing a much higher chloride ion concentration, 0.3M, are shown in Fig. 5.18. In each case only a single fairly sharp peak is seen in both scan directions; the potentials and total monolayer charges are tabulated in Table 5.9.

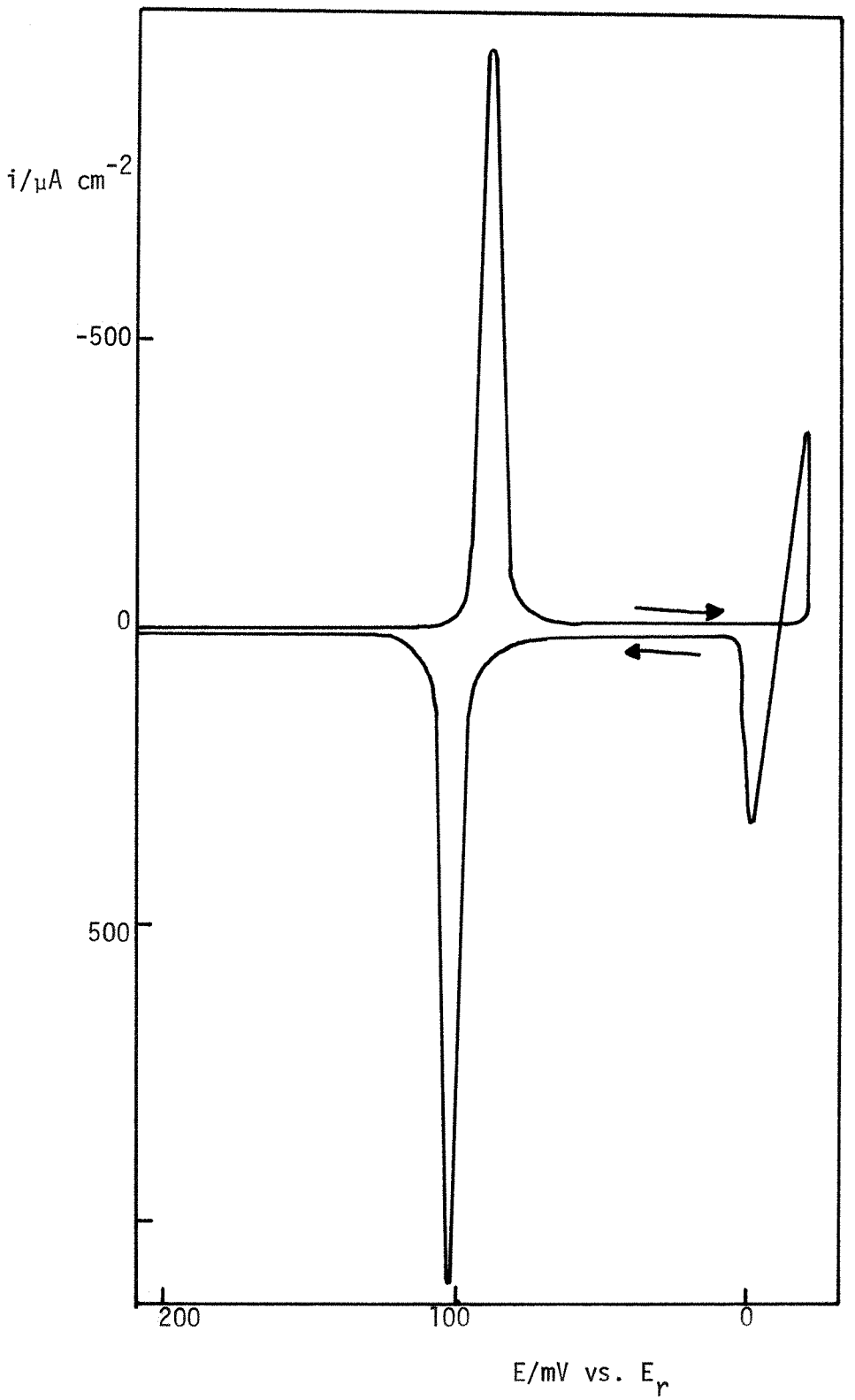

Fig. 5.18(a) L.S.V. for lead deposition on the {111} face. Solution, 1mM $Pb(ClO_4)_2$/ 0.3M KCl/ 1mM $HClO_4$. Sweep speed, 30mV s^{-1}.

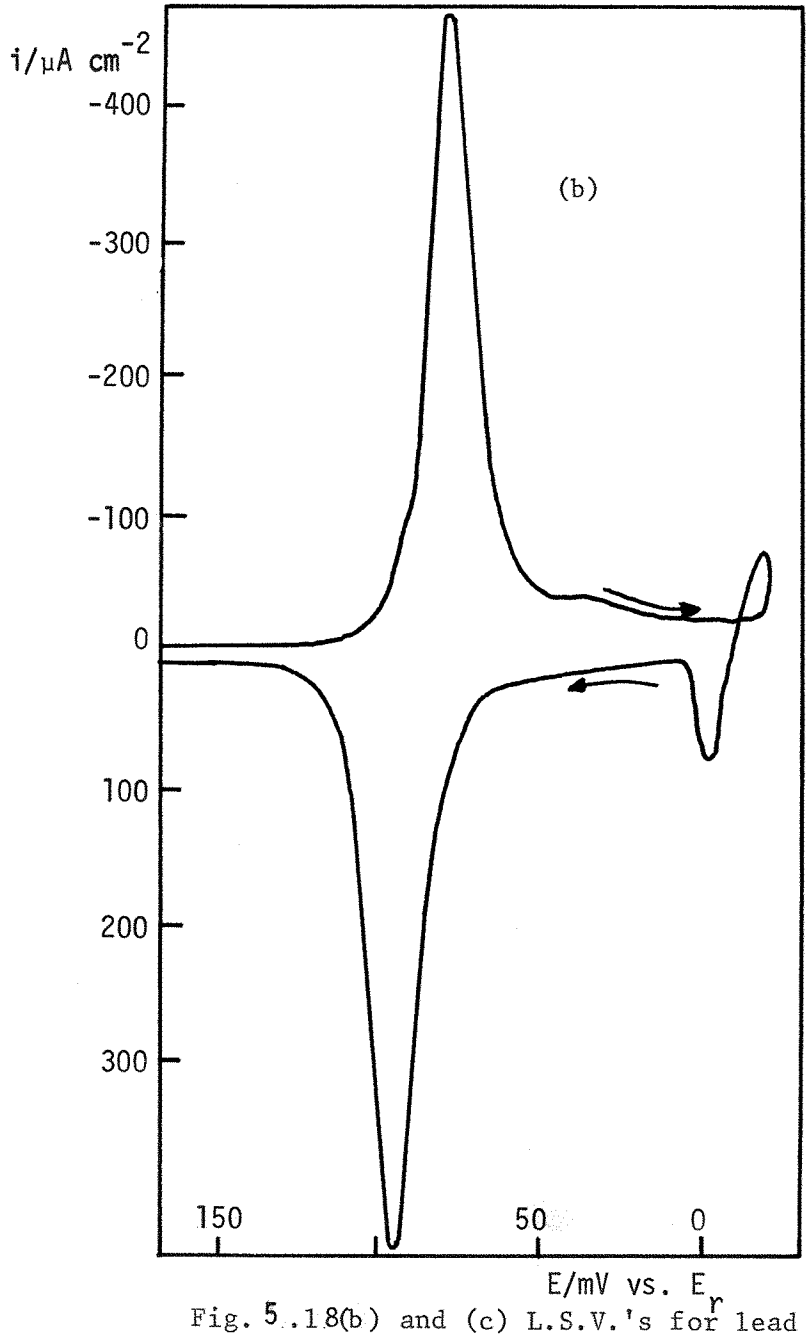

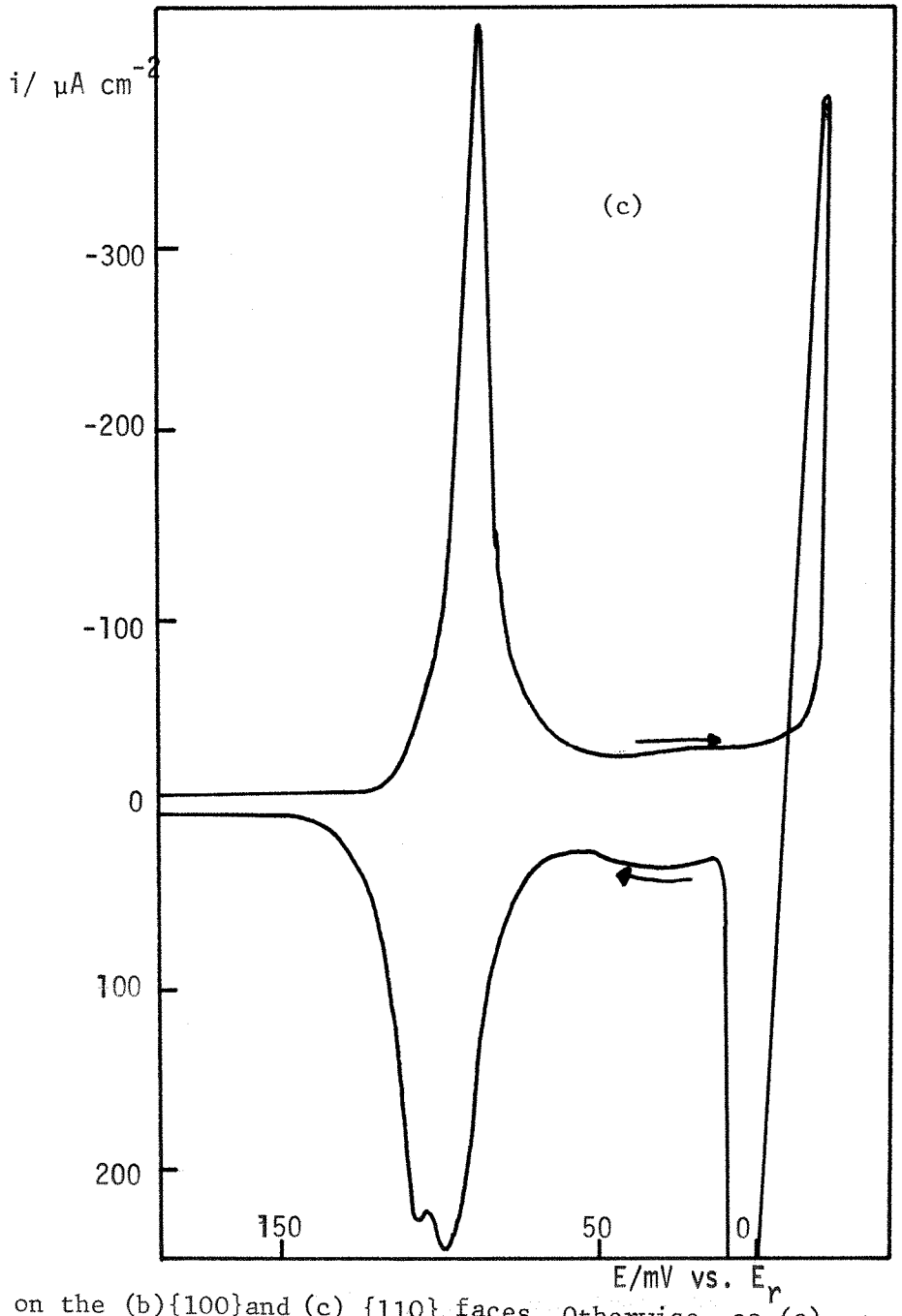

Fig. 5.18(b) and (c) L.S.V.'s for lead deposition on the (b){100}and (c) {110} faces. Otherwise, as (a).

TABLE 5.9

CRYSTAL FACE	PEAK POTENTIAL /mV vs. E_r	$q_{cathodic}$ /μC cm^{-2}
{111}	+88	358
{110}	+86	413
{100}	+78	388

Monolayer (cathodic) peak potential and charge for lead deposition on different faces of silver. Solution, 1mM $Pb(NO_3)_2$/ 0.3M KCl/ 1mM $HClO_4$. Sweep speed, 30mV s^{-1}.

The underpotential shifts are now considerably lower than the values in perchlorate solutions indicating the pronounced effect of the chloride ion; in addition the measured charge values are higher.

The explanation for the disappearance of the two peak voltammetry on the {110} and {100} faces can be seen by reference to Table 5.8. This showed that the effect of 1mM chloride ion was to reduce the underpotential shift associated with the adsorption peak by a factor of 2-3 more than the phase peak, depending on orientation. Clearly, an extrapolation of this effect to solutions of higher chloride ion concentration would result in the two peaks coalescing, as seen in the experimental results. The nature of the resulting deposit is best described by reference to the asymmetry of the cathodic and anodic peaks. The {111} face peaks as usual, show a most marked displacement with respect to each other and the associated lead deposit would be a pure two-dimensional crystalline layer.

The {100} peaks also show a marked asymmetry but in this case, the slightly wider peak width indicates that the associated monolayer phase is not as free from substrate distortion effects as the {111} electrode deposit.

The {110} face results show the least asymmetry of all, consistent with a close packed layer structure significantly distorted by the substrate.structure

These results are in exact accordance with the conclusions regarding monolayer distortion effects already derived from potential decay experiments.

5.9 RESULTS IN CITRATE SOLUTIONS.

(a) INTRODUCTION.

Potential step experiments for lead deposition from perchlorate, acetate and chloride solutions have in each case produced only falling i-t transients, with kinks or humps depending on the potential region. This

indicates that if crystal growth is taking place by a classical two-dimensional nucleation mechanism, the slowest step in the deposition process is not peripheral growth, as this would result in the current rising at least for a short portion of the transient. Certainly, in the case of acetate and chloride ion containing solutions, complexes such as $Pb(CH_3CO_2)^+$ and $PbCl^+$ exist[107] to facilitate the electron transfer process.

By complexing the deposited metal with various ligands, it is possible to vary the rate of the electron transfer step over a wide range In the present work it is desirable to reduce this rate to such a value that it becomes, to some extent, rate determining and then, if electron transfer is simultaneous with lattice incorporation, rising current-time transients, corresponding to the incresing size of the nuclei, should be obtained.

With citric acid, a number of possible complexes may be formed, e.g. PbL, PbHL, PbH_2L_2 and PbH_4L_2 (L = citric acid); the distribution depends on the concentration of citric acid and the pH.[110]

Initially the variation in the amount of lead complexing with pH was determined by adding aliquots of 1M NaOH to a solution of 0.1M citric acid, 1.5mM $Pb(NO_3)_2$ and 0.5M $NaClO_4$. The activity of lead as a function of pH was measured with a lead wire immersed in the solution together with (reference (calomel) and glass electrodes. The plot of $E_{r(Pb^{2+}/Pb)}$ vs. pH is shown in Fig. 5.19. For example at a pH of 4.4, the amount of free lead in the solution is less than 0.1%,and this pH value was chosen as being suitable for the degree of complexing required.

The solution composition used for the experiments was 3mM $Pb(CH_3CO_2)_2$/ 0.1M citric acid/ 0.2M NaOH/ 0.5M $NaClO_4$.

Voltammograms for the three single crystals in this solution are shown in Fig. 5.20. They are somewhat similar to those already reported for lead deposition from perchlorate solutions containing chloride ion, suggesting that the citrate anion, in addition to complexing with the

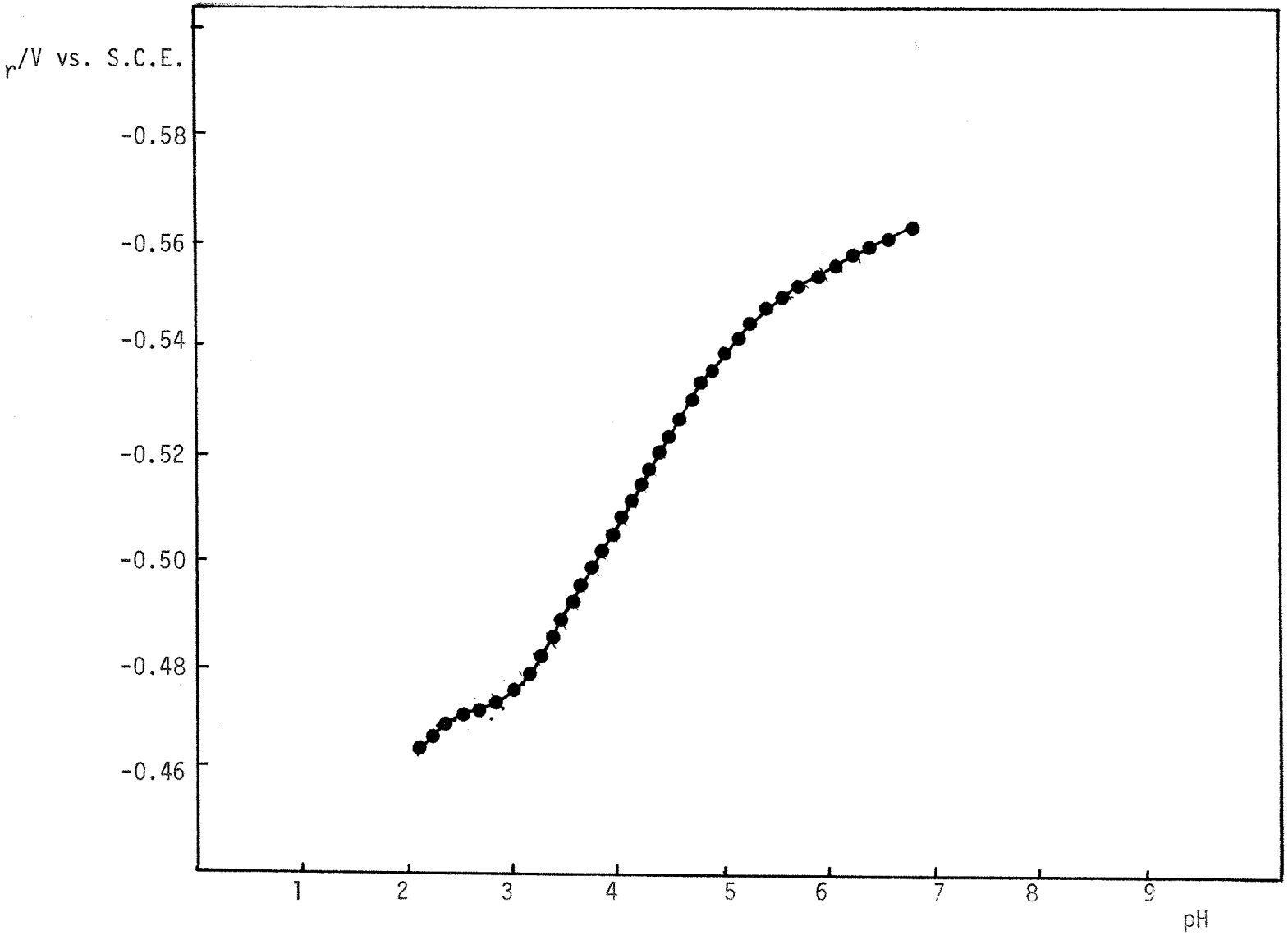

Fig. 5.19 Variation in the reversible potential with pH, for lead in the solution 1.5mM $Pb(NO_3)_2$/ 0.5M $NaClO_4$/ 0.1M citric acid + additions of NaOH.

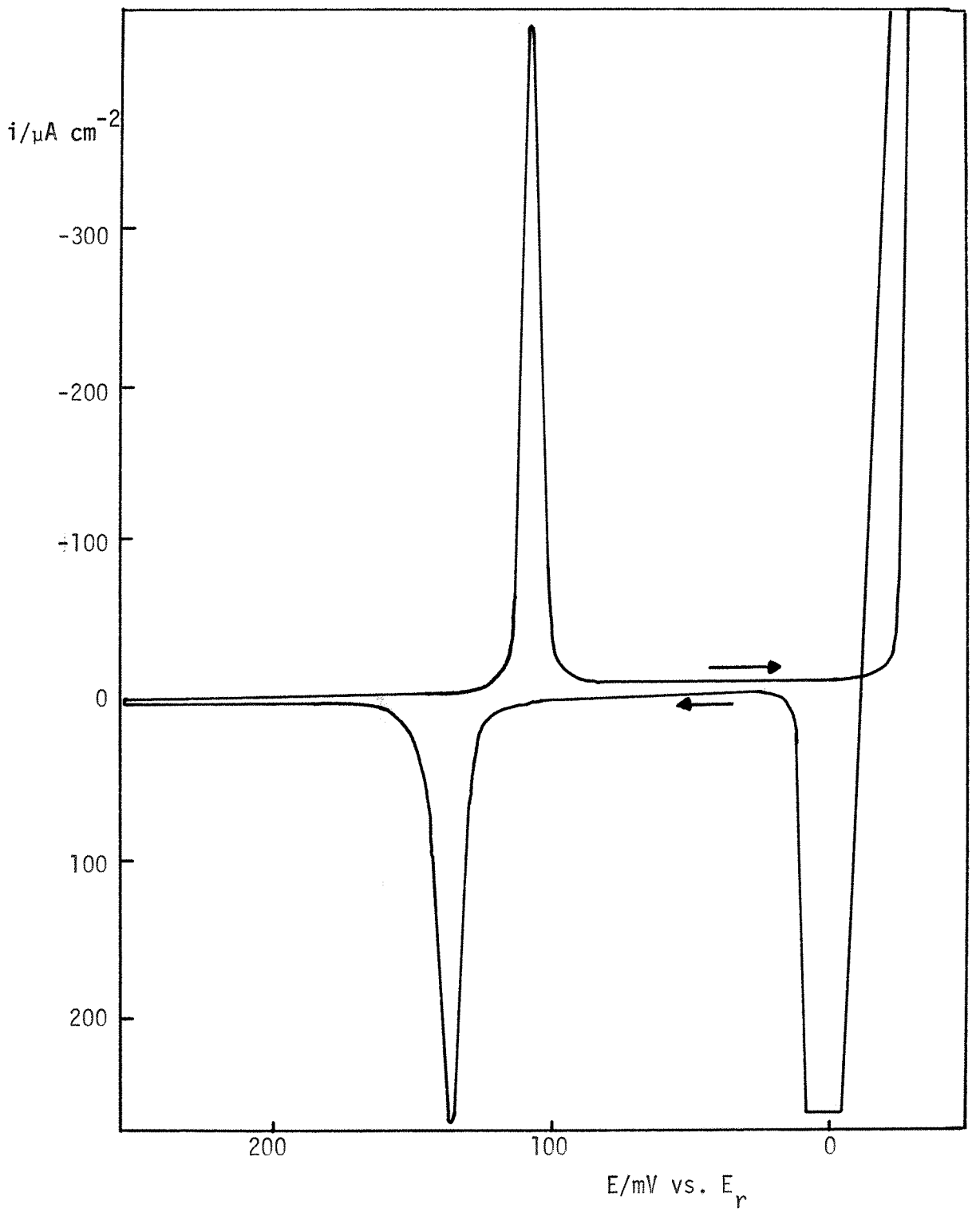

Fig. 5.20(a) L.S.V. for lead deposition on the {111} face of silver. Solution, 3mM $Pb(CH_3CO_2)_2$/ 0.1M citric acid/ 0.2M NaOH/ 0.5M $NaClO_4$; sweep speed, 10mV s^{-1}.

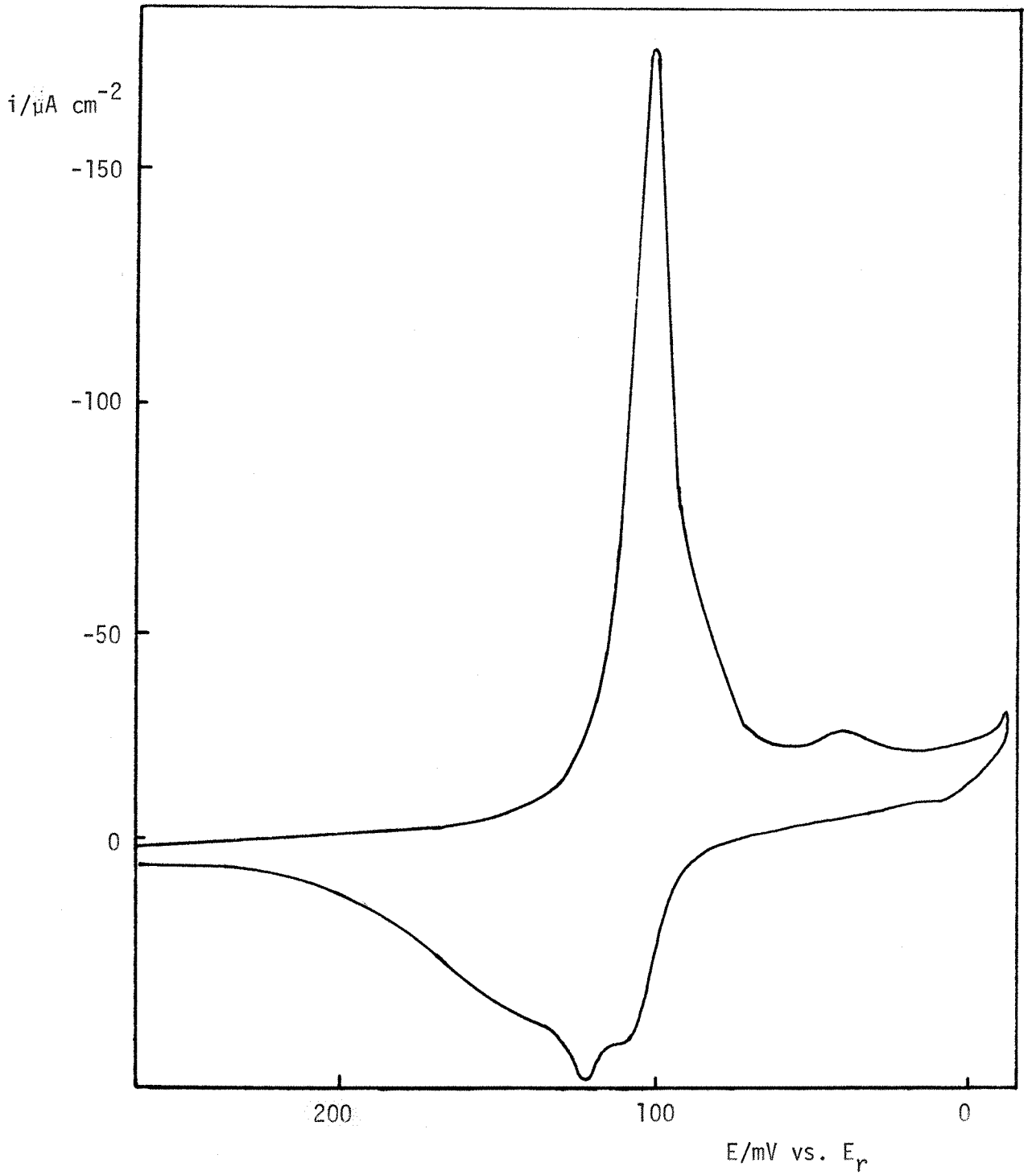

Fig. 5.20(b) L.S.V. for lead deposition on the {100} face. Solution and sweep speed, as in (a).

The slope on this L.S.V. is due to the fact that the electrode was leaking slightly in this particular experiment.

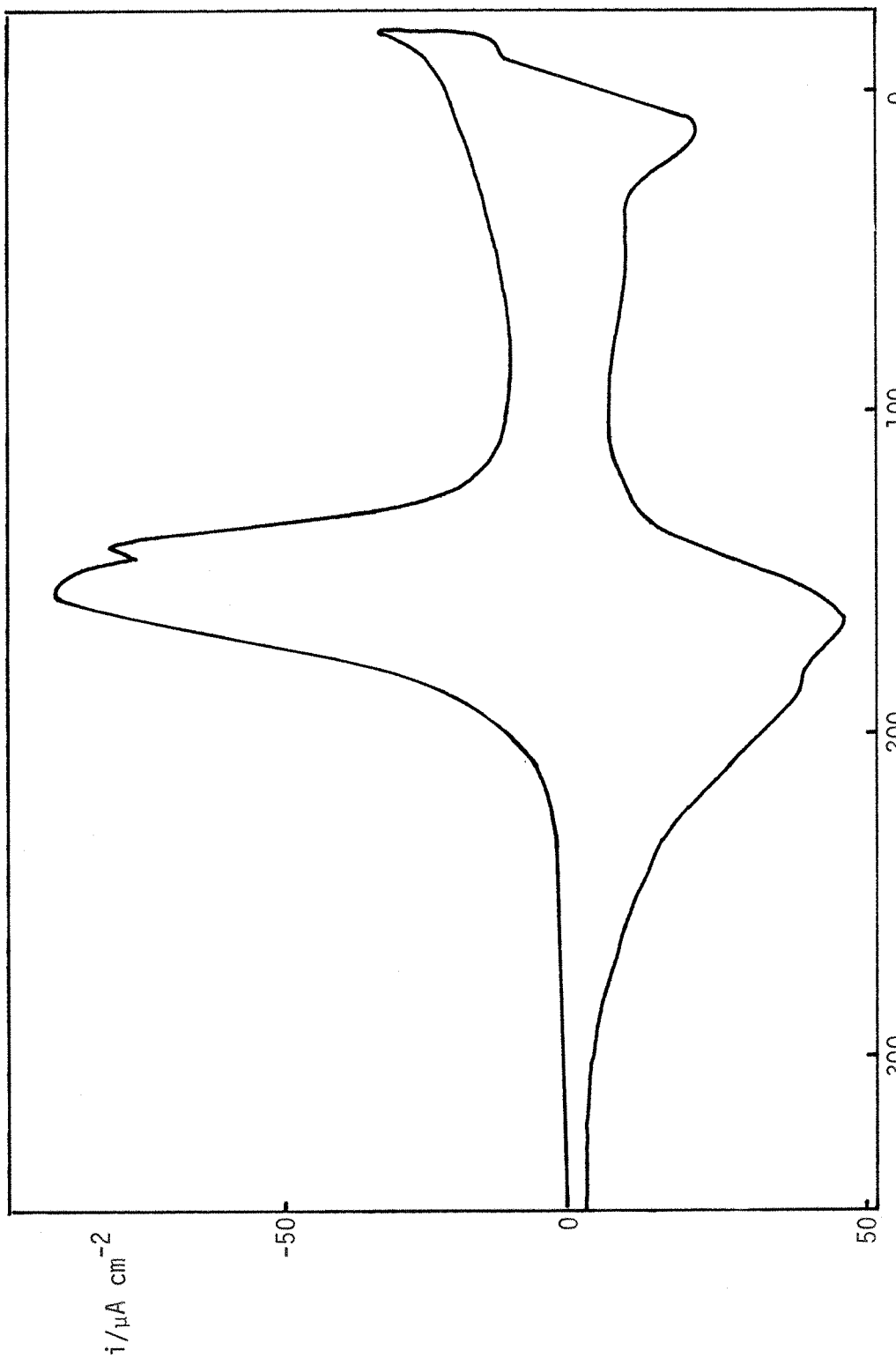

Fig. 5.20(c) L.S.V. for lead deposition on the {110} plane. Solution, as in (a), sweep speed, 10mV s^{-1}.

lead, is also slightly specifically adsorbed.

The voltammetry on the {111} plane is particularly striking because of the apparent overpotential required for the monolayer phase. This produces a marked asymmetry between the onset of stripping on the anodic scan and the onset of deposition on the cathodic scan. The mean equilibrium monolayer phase potential, as measured by a potential decay experiment, was +131-132mV vs. E_r. This coincides exactly with the onset of the rapid increase in current due to the anodic stripping of the monolayer. The potential corresponding to a rapid increase in the cathodic current due to nucleation and growth of the monolayer, is +120mV, i.e. for the formation of nuclei, an overpotential of 11-12mV relative to the monolayer phase potential, is required. The previous results for thallium and lead deposition from acetate and perchlorate solutions showed that the onset of the stripping and deposition processes occurred at virtually the same potential, which would imply a lack of any nucleation overpotential. This difference in behaviour indicates that the nucleation rate is considerably lower in the case of lead deposition from a citrate complex. If the cause of this is a reduction in the rate at which ad-atoms are incorporated into the critical nucleus, due to a lower electron transfer rate, then this result suggests that well defined, rising i-t transients could be obtained from potential step experiments.

A similar, though less marked asymmetry for the phase (A_2) peaks can be seen in the voltammetry results on the {100} plane.

5.9(b) POTENTIAL STEP RESULTS.

{111} FACE.

Pulsing into the potential region spanned by the cathodic voltammetry peak, produced transients with an initial rising portion, a peak, followed by a decay to zero. An example is shown in Fig. 5.21. The transients had the following characteristics.

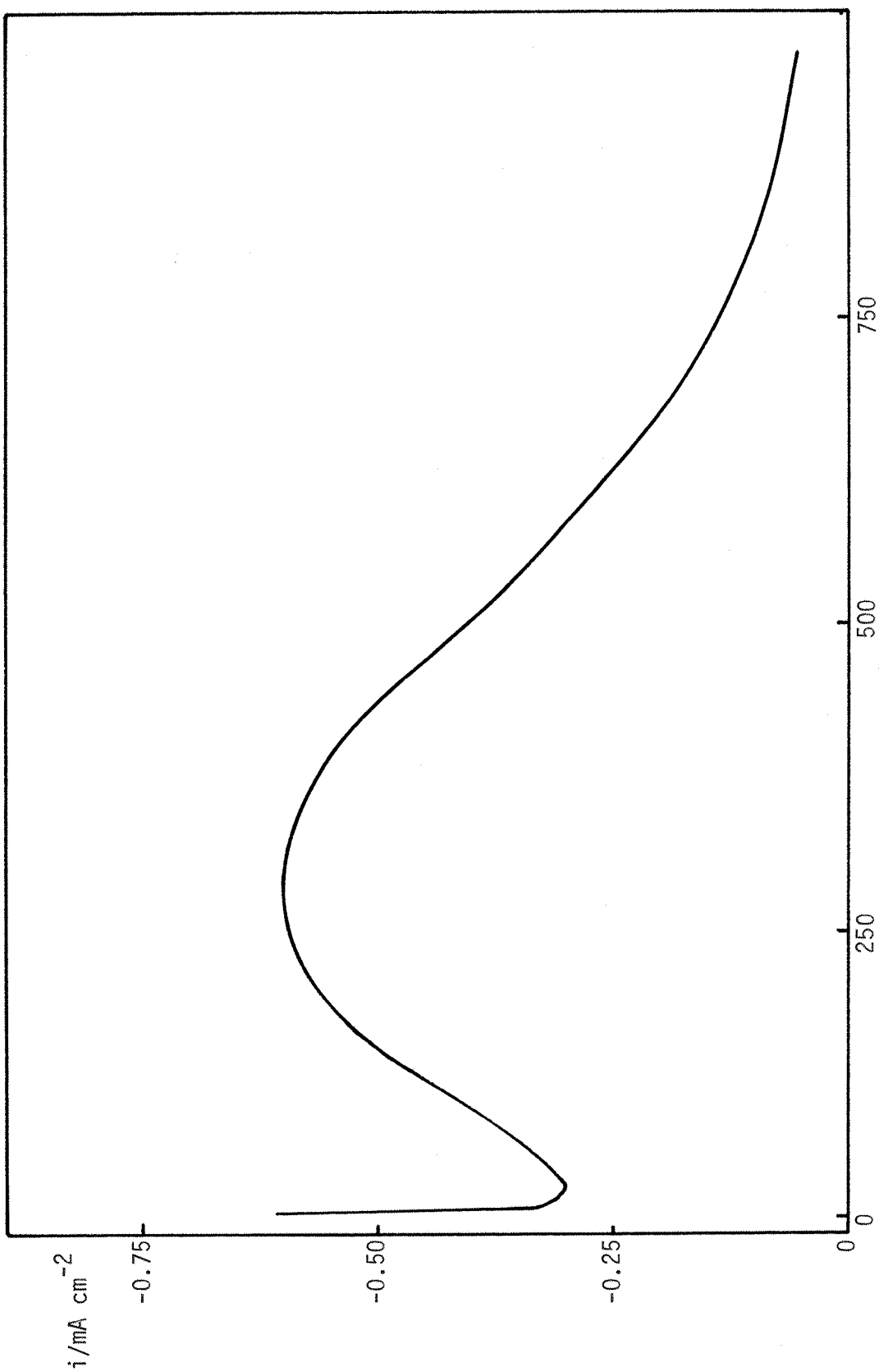

Fig. 5.21 Current-time transient for a potential step from +320mV to +107mV, for lead deposition on the {111} face. Solution, 3mM $Pb(CH_3COO)_2$/ 0.5M $NaClO_4$/ 0.1M citric acid/ 0.2M NaOH.

1. The rising portion of the transient always started at a finite current value and was preceeded (at short times) by a falling transient, even when a prepulse was employed to charge the double layer (see Fig. 5.22).

2. The initial part of the rising transient is characterized by a linear $i\text{-}t^2$ relationship (see Fig. 5.23).

3. With increasing negative potential, the peak moved to shorter times and higher current densities. Eventually the falling part of the transient comes under limiting planar diffusion control, and develops the familiar kink as monolayer saturation is approached.

4. The effect of prepulsing for a short time (1-3ms) to the reversible potential, prior to the main pulse to a lower cathodic potential, was to move the peak to shorter times; the peak current remained constant. With longer prepulses, only a falling transient was observed.

These results demonstrate the ability of the citrate anion to reduce the rate of the electron transfer/ lattice incorporation step, for lead monolayer phase formation, to such an extent that direct evidence for nucleation processes occurring in the U.P.D. region, can be obtained. It has already been shown (chapter 1) that a rising i-t transient is a consequence of the increasing peripheral growth area of a nucleus as further material is incorporated at the edges. The $i\text{-}t^2$ relationship implies progressive nucleation (equation 1.8).

At short times the transients possess a falling segment (on a longer time scale than double layer charging however) which probably corresponds to the formation of ad-atoms on the surface. Once the concentration of ad-atoms around any point has reached a critical value, nucleus formation will occur and a corresponding rise in current takes place due to that nucleus increasing in size. The fact that the rising portion of the current does not start from the current zero, but at a relatively high value, implies that the critical ad-atom concentration is

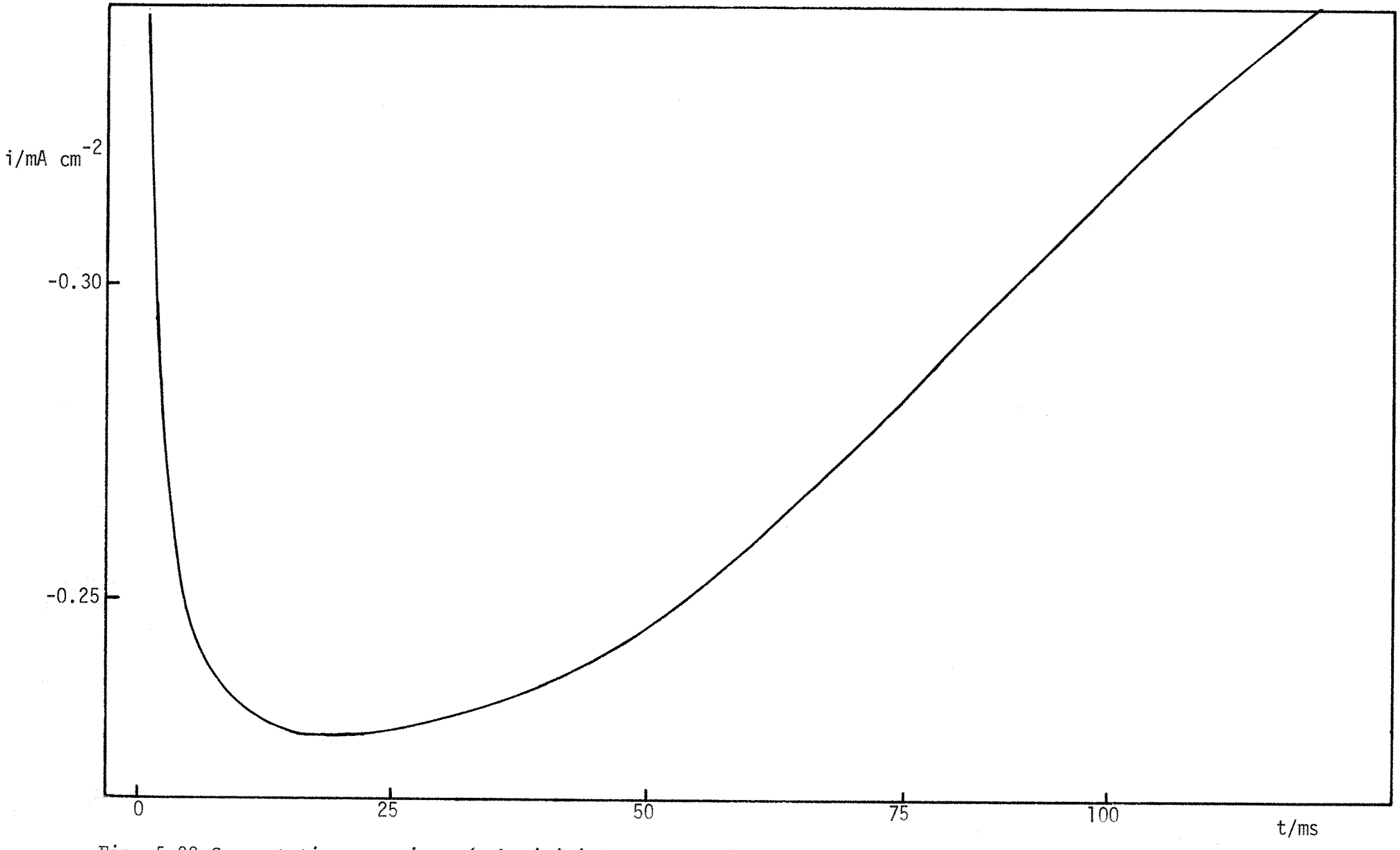

Fig. 5.22 Current-time transient (the initial part only) for a potential step from +339mV to +111mV, for lead deposition on the {111} face. Solution, as in Fig. 5.21.

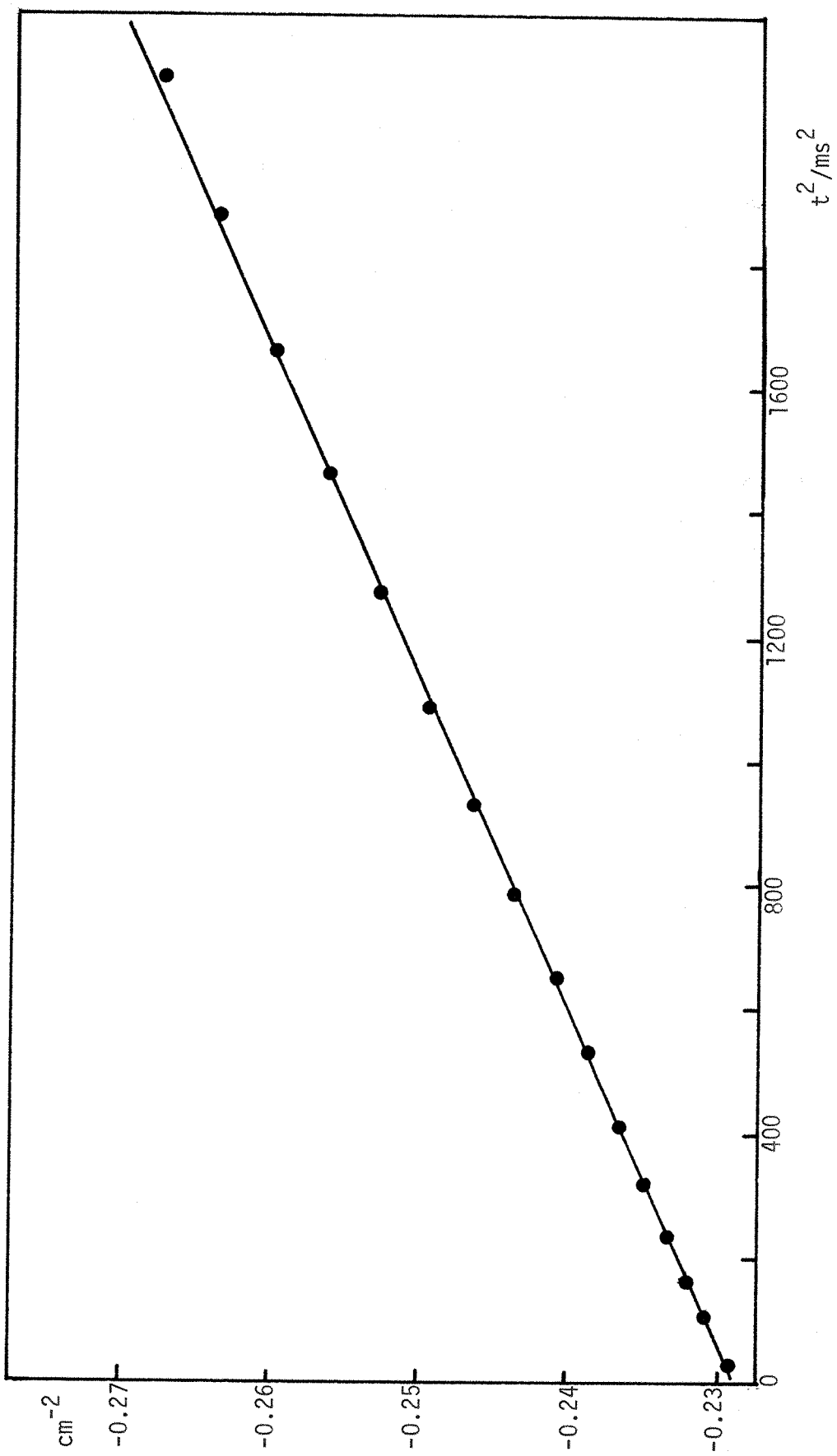

Fig. 5.23 Plot of i versus t^2 for the current-time transient of Fig. 5.22. The zero time point for this plot was the foot of the rising transient and not the actual zero.

reached before the initial falling part of the transient decays to zero.

{100} AND {110} FACES.

The voltammetry for the {100} face shows a single sharp peak on the cathodic scan. Potential steps into this region produce current-time transients with an initial rising section (similar to the one shown in Fig. 5.24 for the {110} face). This peak is much less symmetrical than than that obtained on the {111} plane, which suggests that surface diffusion is playing a more important role in the determination of the shape of the transient.

On the {110} face, the voltammetry shows two peaks. Potential steps into the region of the first peak produce only falling transients of the type shown in Fig. 5.24(a); this must correspond to an adsorption process. At more negative potentials, in the second peak region, the transients show an initial rise, as shown in Fig. 5.24(b). It is interesting to note that this rise is not preceeded by a falling transient containing an amount of charge equivalent to the first peak, i.e. phase formation can occur without the prior formation of an adsorbed layer. Again, surface diffusion is affecting the shape of the transient. This would be expected to be most pronounced on the {110} plane as interaction with the substrate is most strong.

5.10 CONTINUOUS SWEEPING AND REPETITIVE PULSING EXPERIMENTS ON THE {110} PLANE, IN A PERCHLORIC ACID MEDIUM.

(a) VOLTAMMETRY.

The results from single potential scans, or single potential step experiments, for lead deposition on the {110} face from 5mM PbO/ 0.5M $HClO_4$ solutions, have already been described and these give good agreement with the superlattice adsorption/phase transition-growth model. The effect of continuous potential scanning at a rate of 100mV s^{-1} (unless otherwise stated) will now be described.

The first sweep of a cycle to a potential just anodic to the

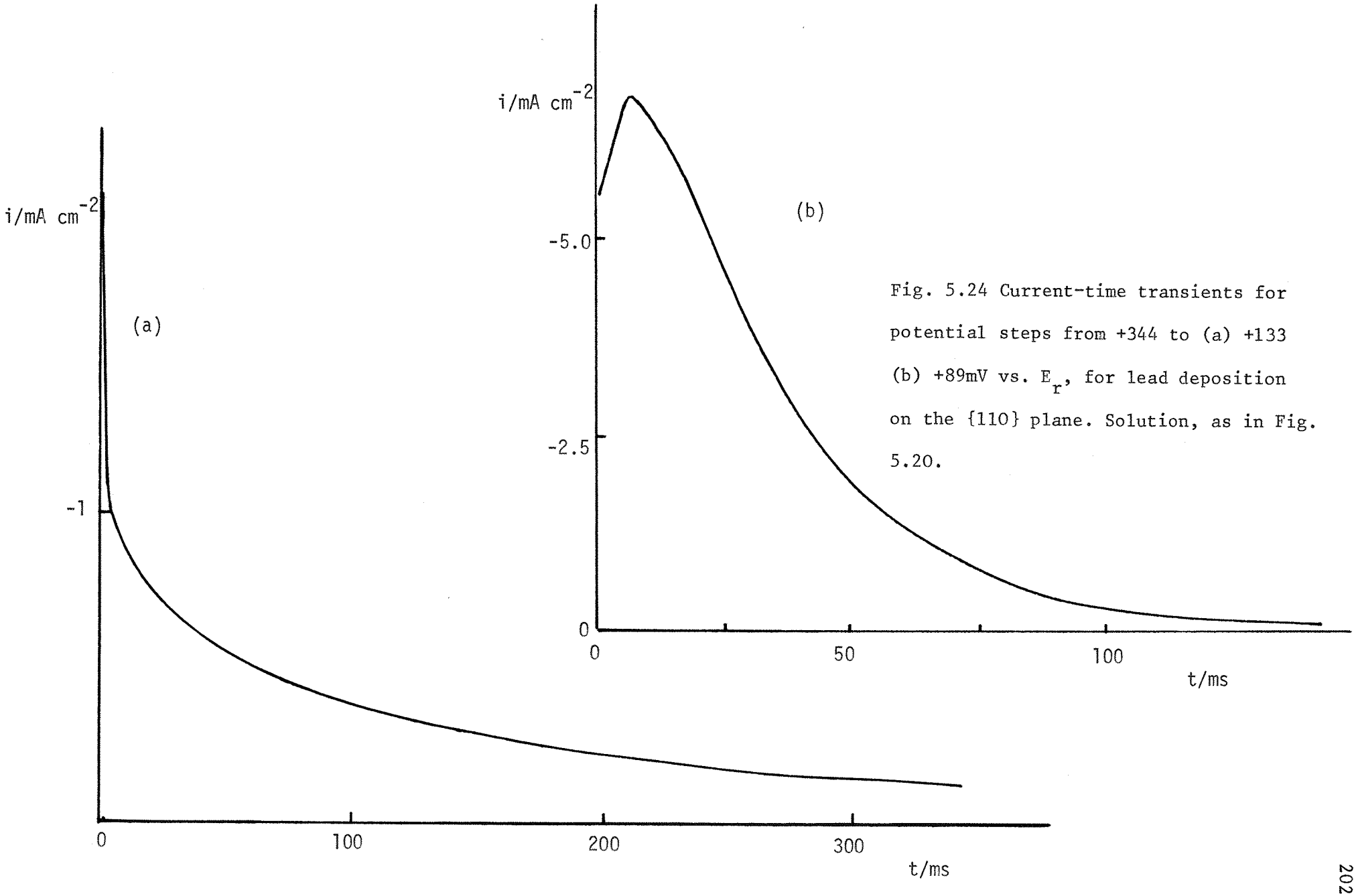

Fig. 5.24 Current-time transients for potential steps from +344 to (a) +133 (b) +89mV vs. E_r, for lead deposition on the {110} plane. Solution, as in Fig. 5.20.

point where bulk deposition began was qualitatively identical to that shown in Fig. 5.2 for a single potential sweep at 30mV s^{-1}. Each subsequent sweep showed deviations from this standard behaviour; these were;

1. After each successive sweep, the width of the adsorption peak A_1 decreased and correspondingly the peak current increased and the peak moved to more negative potentials. The peak current and potential of the phase peak remained constant.

2. The stripping peak corresponding to A_1 became more distended in the anodic direction.

3. After a certain number of sweeps 'n', no further change in the voltammetry occurred. The value of 'n' depended on a number of factors which will be described later.

4. The appearance of the voltammogram after 'n' sweeps (at 100mV s^{-1}), for a given concentration of PbO in 0.5M $HClO_4$ depended on,

   (a) the length of time the solution had been in the cell,

   (b) the batch of perchloric acid used in the solution preparation.

5. After a number of sweeps 'n', potentiostating the electrode at a potential anodic to that where U.P.D. begins, for a period of 1-5 minutes (depending on conditions), restored the original single sweep behaviour, which again on repetitive sweeping showed the same behaviour as described in 1. to 4. above. Alternatively, if the electrode was potentiostated at a potential just anodic to the onset of bulk deposition, there was little change from the behaviour after 'n' sweeps.

Fig. 5.25 shows an example of this behaviour in 1mM PbO/ 0.5M $HClO_4$. The 'n'th. sweep, i.e. that after which no further change occurred on continual sweeping, occurs in this case at the same potential as the original A_2 peak.

The figure shows the gradual increase in current density of A_1,

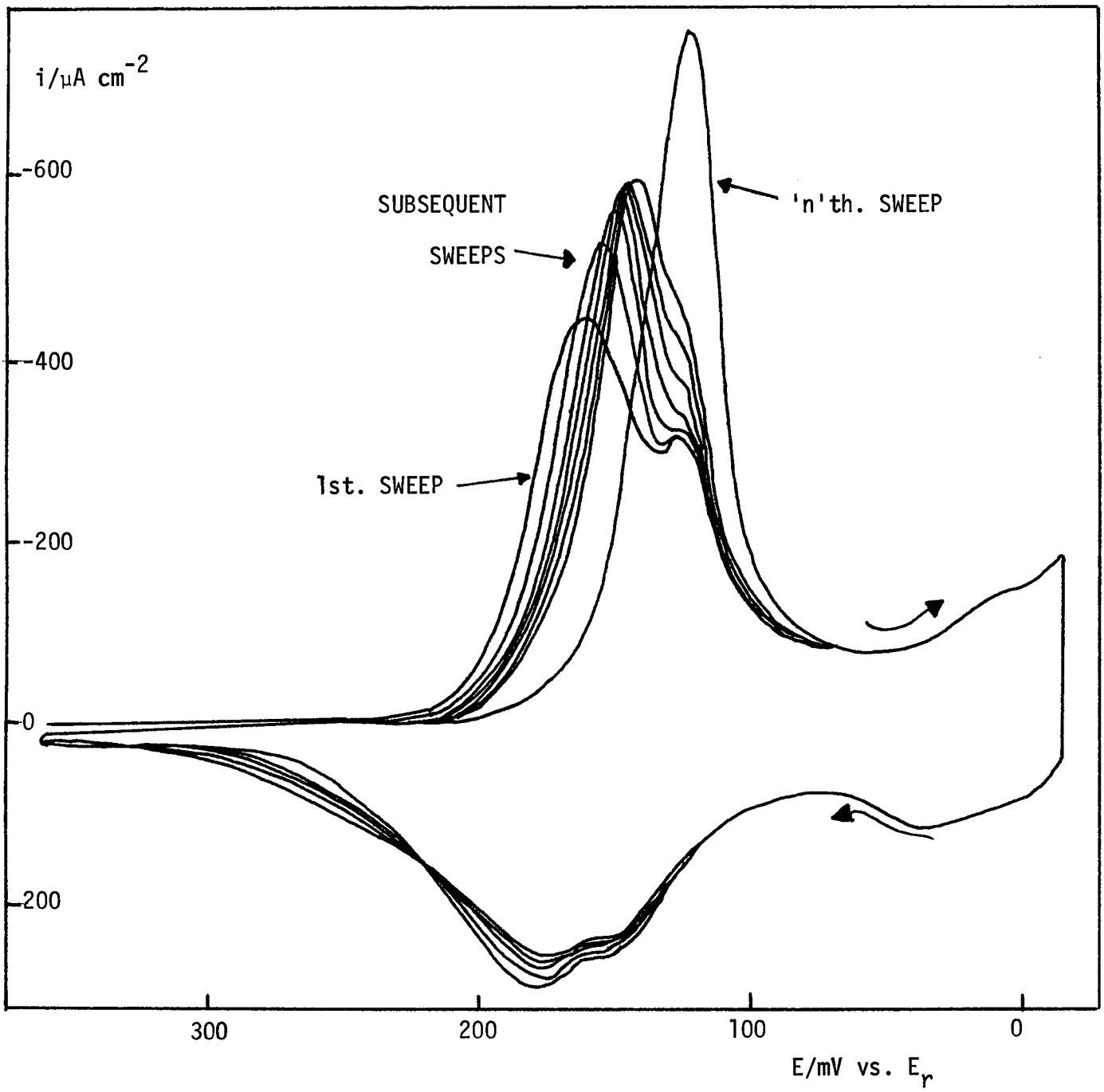

Fig. 5.25 L.S.V.'s for lead deposition on the {110} face of silver, as a function of sweep number, showing the gradual change on each successive sweep. Solution, 1mM PbO/ 0.5M $HClO_4$; sweep speed, 100mV s^{-1}.

gradual overlap with A_2 (whose position remains constant) and eventually, only a single peak is visible. Fig.5.26 shows the 'n'th. sweep at a higher sweep speed (300mV s^{-1}). In this case the underpotential shift of the cathodic peak (107mV) is considerably lower than the normal A_2 value on this face (133mV). This result shows the effect of increasing the sweep speed, which causes a gradual movement of the cathodic peak to more negative potentials. Conversely at low sweep speeds (e.g. less than 20mV s^{-1}), there was very little difference between single and repetitive sweeps. However, with increasing sweep speed, the 'n'th sweep became progressively different from the first sweep.

The effect on the stripping voltammetry is best seen from Fig. 5.27 which shows the first and 'n'th. sweeps at 100mV s^{-1} in 5mM PbO/ 0.5M $HClO_4$. The stripping curve associated with the 'n'th. cathodic sweep is extended to more positive potentials than that of the first sweep. The 300mV s^{-1} voltammogram in Fig. 5.26 shows the considerable asymmetry produced by the combined effect of the cathodic peak becoming sharper, and moving to more negative potentials, and anodic peaks merging into a single broad peak with potential identical to the original A_2 stripping peak potential (+150mV).

In all the results so far described, the cathodic potential limit has been just positive to the onset of bulk deposition. If the limit is reduced such that it is equal to a value just negative of the single sweep A_1 peak potential, and a cycle of sweeps is initiated, the difference between the first and subsequent sweeps is very small, i.e. after each sweep to this reduced cathodic limit, the peak current increases only very slightly from its value in the previous sweep, unlike the behaviour when the cathodic limit is in the low overpotential (for bulk deposition) region, when the difference between successive sweeps is much more pronounced. However if the cathodic sweep, during a cycle of scans to a limit

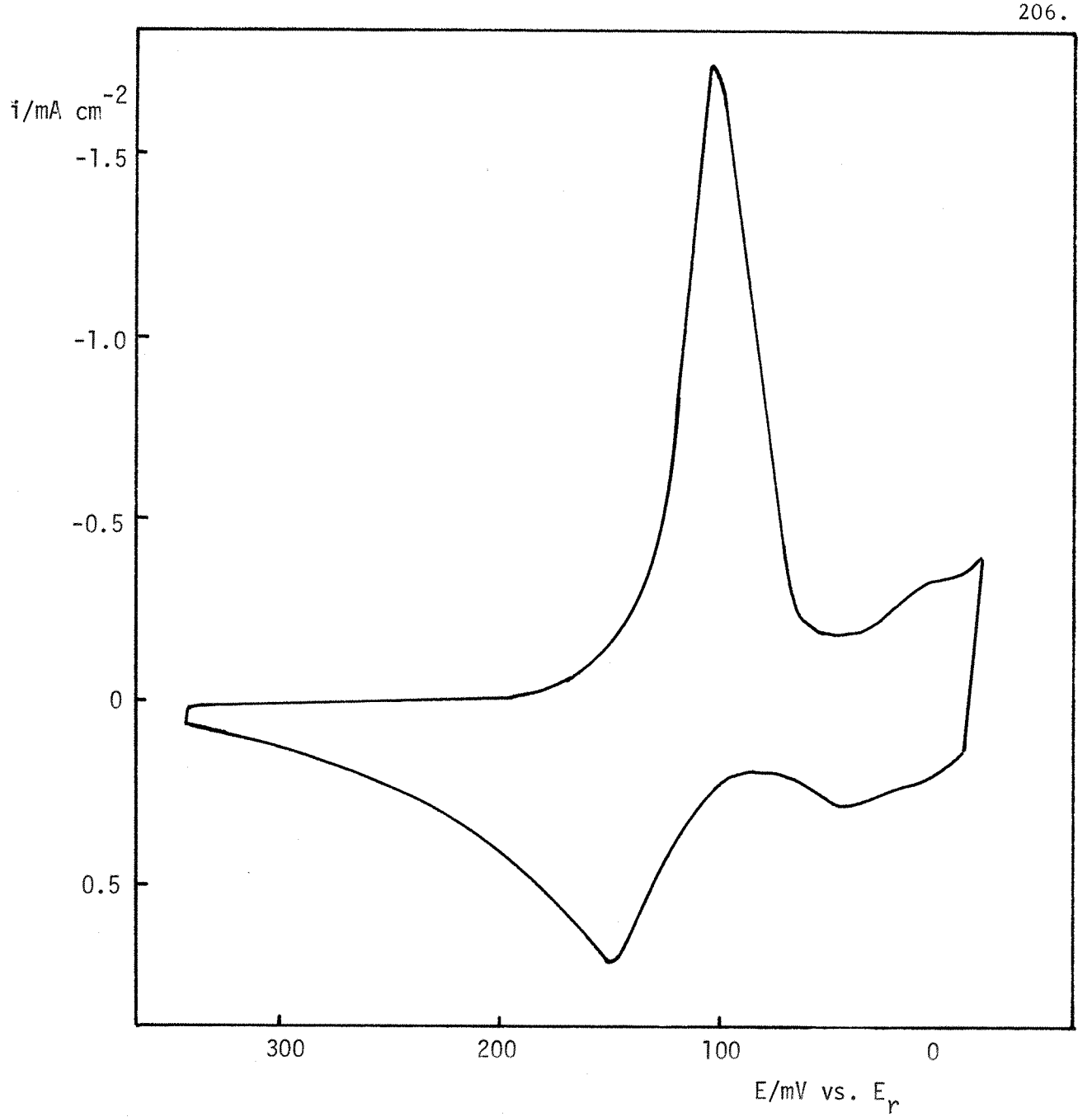

Fig. 5.26 L.S.V. for lead deposition on the {110} face. Solution, as in Fig. 5.25; sweep speed, 300 mV s^{-1}.

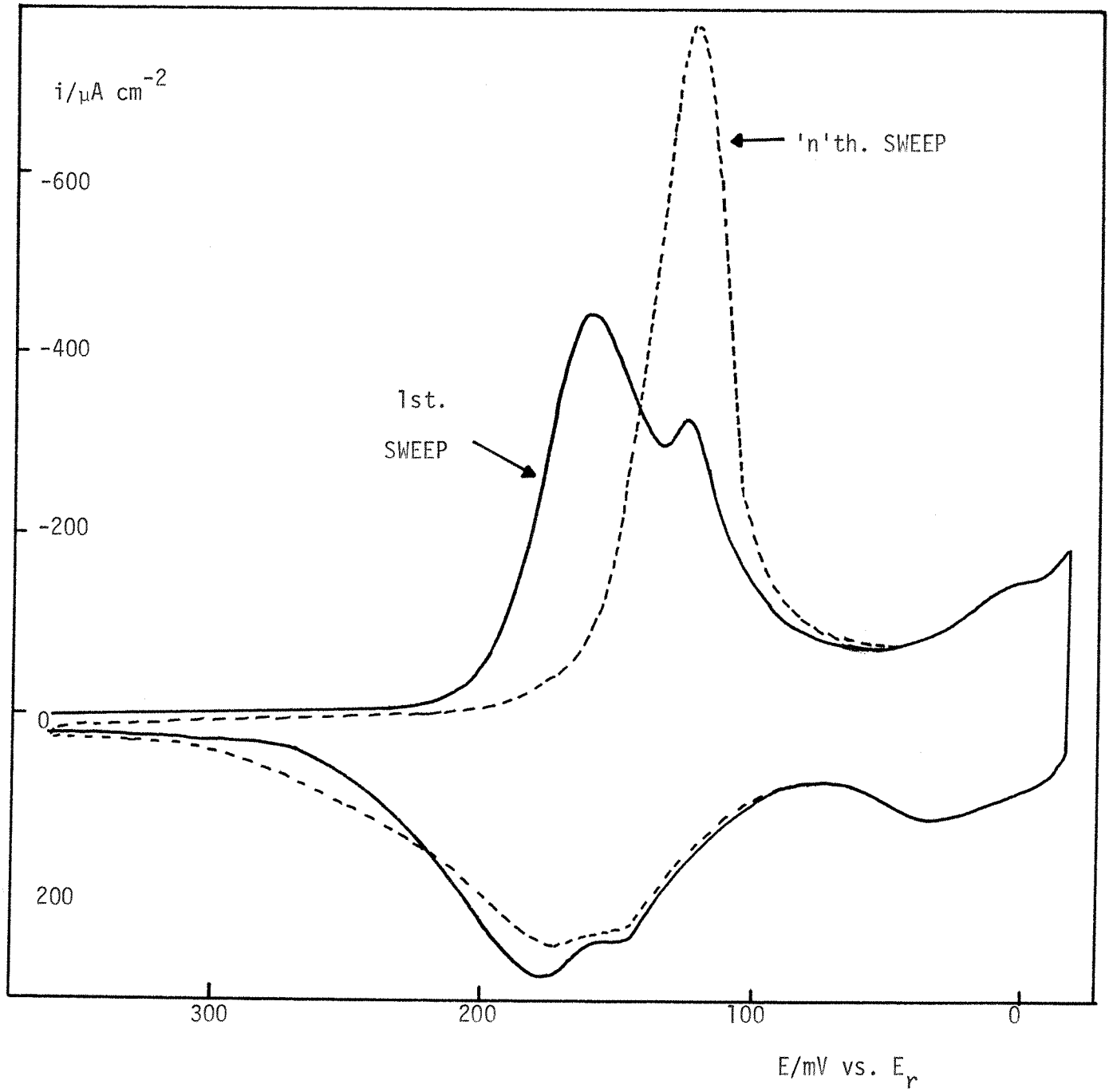

Fig. 5.27 Two L.S.V.'s for lead deposition on the 110 face; the first sweep of a cycle and the 'n'th. sweep (that after which no further change occurs); Solution and sweep speed, as in Fig. 5.25.

in the A_1 potential region, is increased suddenly to just beyond the single sweep A_2 peak, the difference between the first and subsequent sweeps to this limit is much more marked, and a single sharp peak is quite rapidly obtained.

All the effects so far described are most evident in the most dilute lead ion solutions employed (1mM). As the lead ion concentration is increased from, say, 1mM to 5mM, at a given sweep speed the coalescence of the A_1 and A_2 peaks into a single, reasonably sharp peak, becomes less marked and only partial overlap occurs. When the lead ion concentration is greater than 10mM, the difference between single and repetitive scans, at sweep speeds in the range normally employed for studying U.P.D., ($\leq$100 mV s^{-1}), are very small or zero i.e. with increasing lead concentration, a higher scan rate has to be employed before any difference between single and repetitive scans can be discerned.

Charge measurements have also been made from the cyclic voltammograms, but a discussion of these values will be deferred until the potential step results have been described.

As mentioned already, the effect of adding 1mM of chloride ion to a solution of 5mM PbO/ 0.5M $HClO_4$ was to eliminate any effect of scan rate of the type described above, i.e. the first sweep and any subsequent sweeps were identical. Also, the effect of decreasing the total acidity from 0.5M to e.g. 10mM was at a given scan rate, to diminish any dependence on the nature of the potential scan.

(b) POTENTIAL STEP EXPERIMENTS.

The results of single potential steps into the A_1 and A_2 regions have already been described. Repetitive pulsing produced very marked changes in the nature of the resulting current-time transient if the length of the anodic component was not too long compared to the cathodic pulse duration. The most marked effects in the cathodic transient were

obtained with a pulse train where the length of the anodic component was just sufficient to strip off the metal deposited in the preceeding cathodic pulse. Under such conditions, a cathodic pulse into the (single sweep) A_2 region of potential, produced well defined rising i-t transients. An example is shown in Fig. 5.28. These rising transients had the following characteristics.

1. The initial current, $i_{t=0}$, was always greater than zero and $i_{t=0}$ was a function of the length of the anodic pulse, (t_a).

As t_a increases, $i_{t=0}$ and i_{max} (current density associated with peak) increase until eventually the usual falling transient, associated with a single potential step, was observed (see Fig. 5.29).

2. Increasing the length of the cathodic pulse, t_c, (i.e. beyond the value required to effect complete deposition at that potential) whilst maintaining a constant (short) anodic pulse length, produced very little deviation from the rising transient shown in Fig. 5.28.

3. The rising transient obtained with $i_{t=0}$ at its minimum value, showed a linear $i\text{-}t^2$ relationship for a large part of the rising portion (Fig. 5.30).

4. The effect of increasing the cathodic pulse height to more negative potentials in the U.P.D. region, was to increase i_{max} and reduce t_{max}. In addition, some of the symmetry and the $i\text{-}t^2$ relationship of the transient, was lost.

5. In double pulse experiments, with an A pulse to the reversible potential for a time e.g. 1/20th. the length of the B pulse (to a potential in the A_2 region) was identical to the value with no prepulse but t_{max} was smaller.

6. If the lead ion concentration was increased, $i_{t=0}$ for any given t_a, increased, i.e. the most symmetrical rising transients were obtained with the lowest Pb^{2+} concentrations in the region of (1-5mM). For example in 1mM Pb^{2+} solutions, good rising transients could be obtained

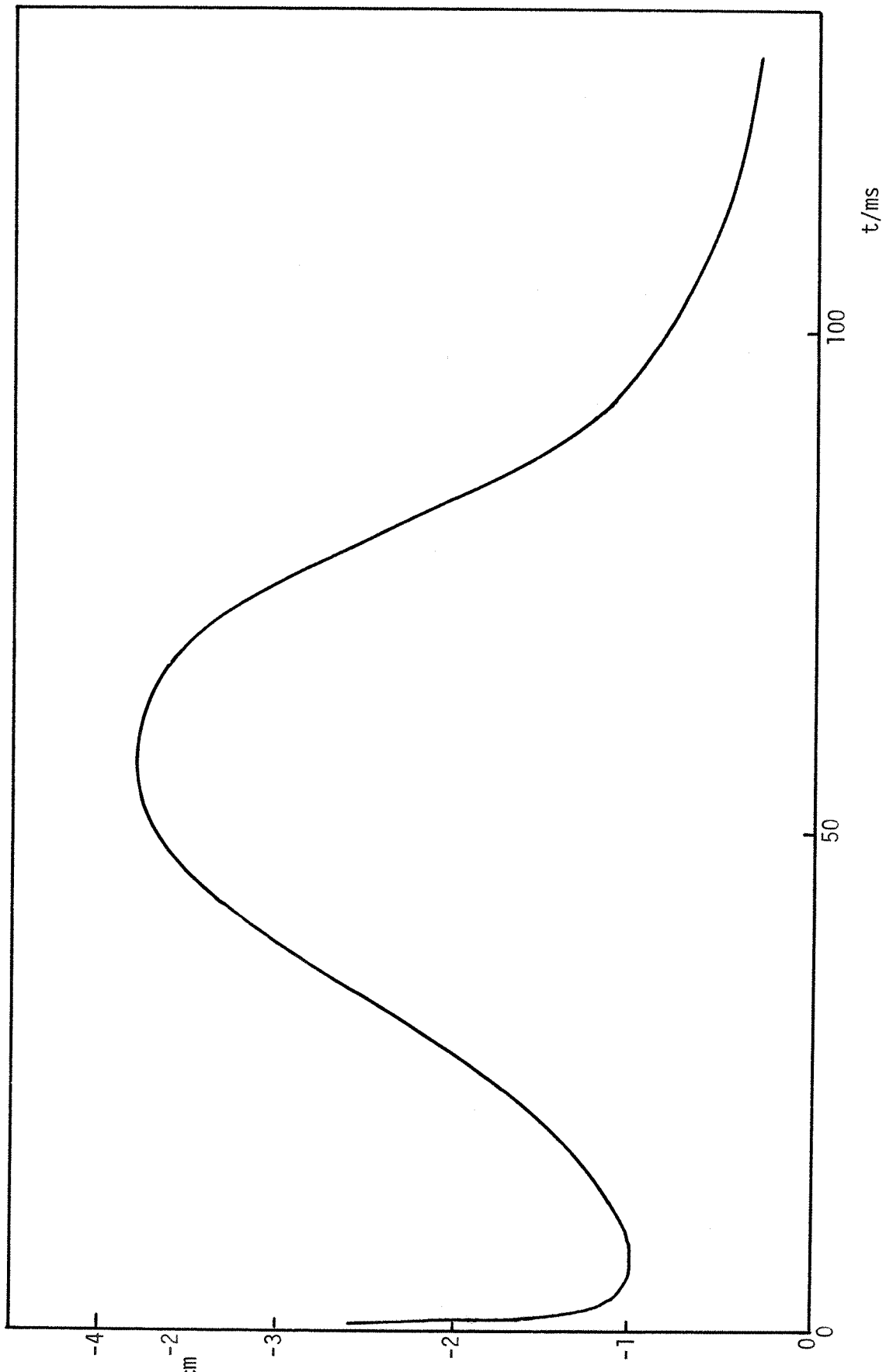

Fig. 5.28 Current-time transient for a potential step from +367mV to +115mV vs. E_r, for lead deposition on the {110} face of silver. A pulse train was employed with 1 cathodic pulse every 300ms, anodic pulse length was 150ms. Solution, 5mM PbO/ 0.5M $HClO_4$.

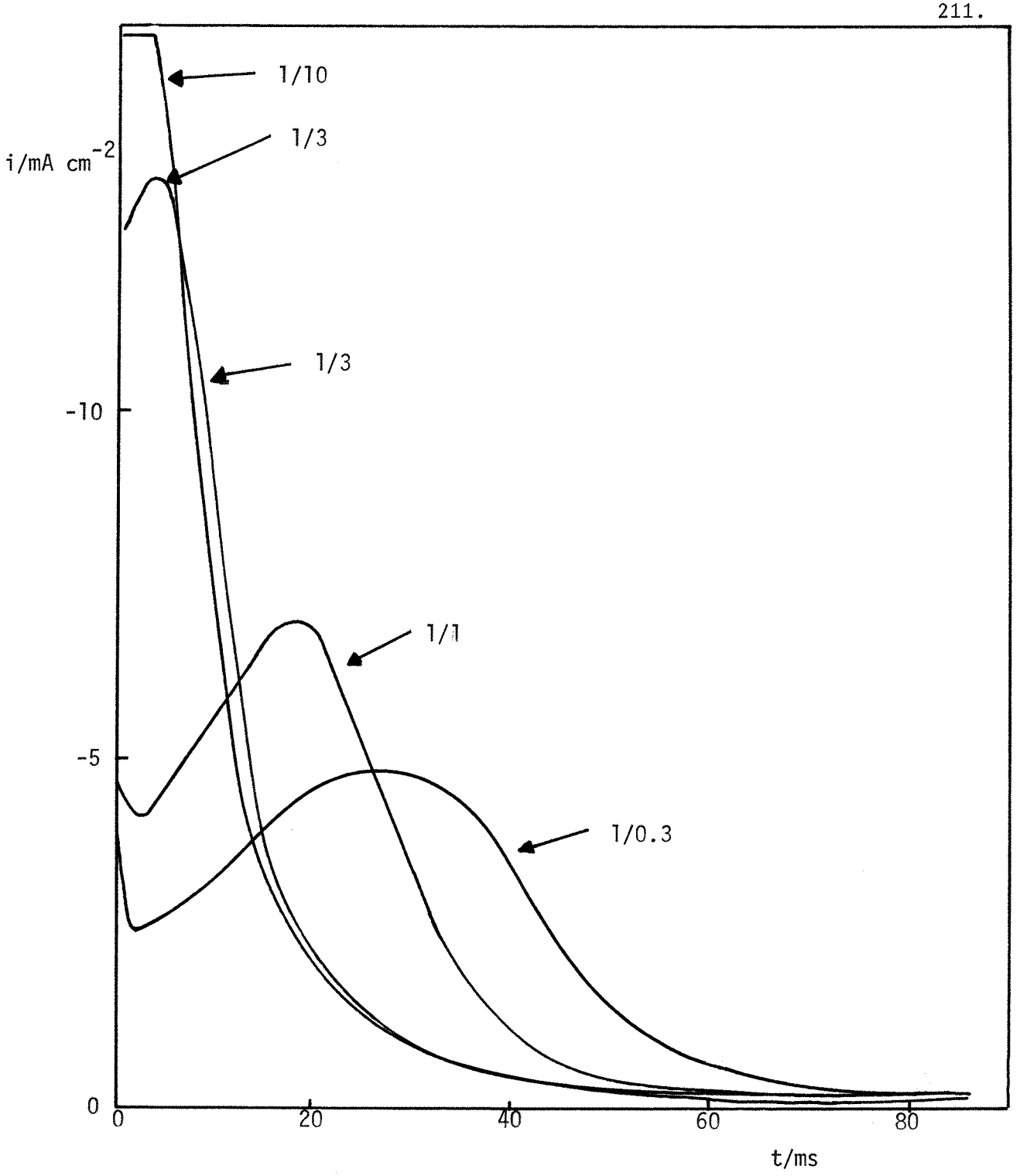

Fig. 5.29 Current-time transients for a potential step from +363mV to +113mV for lead deposition on the {110} plane, with different cathodic pulse repitition rates. Cathodic pulse length = 150ms, 1/0.3 ≡ a cathodic pulse every 0.3s, 1/10 ≡ a cathodic pulse every 10s,etc.. Solution 5mM PbO/ 0.5M $HClO_4$. A similar sequence of transients would be obtained when a pulse train was initiated, with the first pulse being equivalent to the 1/10 plot in the above figure.

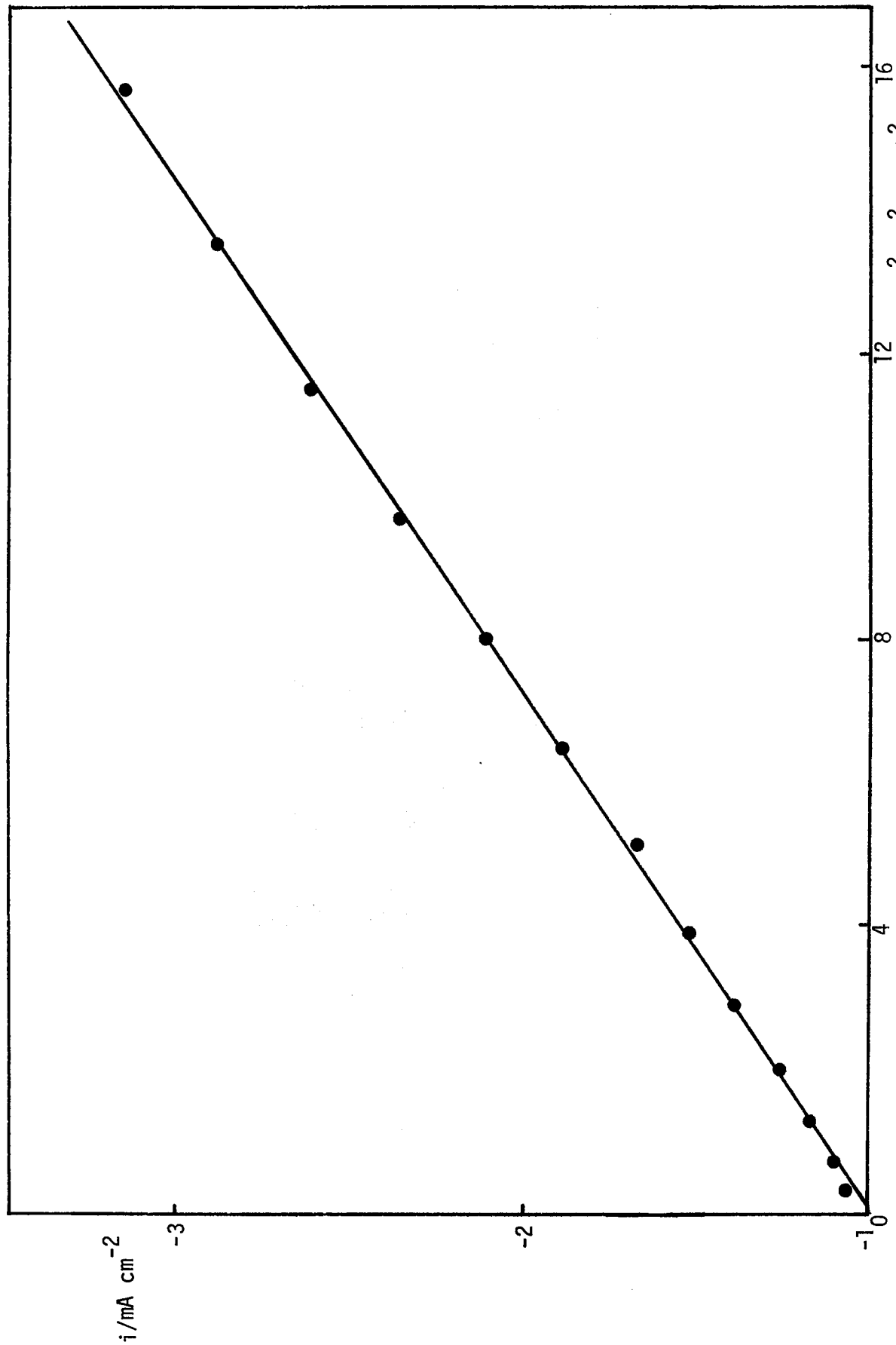

Fig. 5.30 Plot of i vs. t^2 for a potential step from +363mV to +113mV vs. E_r, in a repetitive pulsing experiment for lead deposition on the {110} face. Solution, as in Fig. 5.28.

with anodic pulse lengths of 3-5 seconds (following a cathodic pulse of say 300ms) but in 50mM Pb^{2+} solutions, rising transients were only observed with stripping transients of the order of 100ms long.

5.10(c) DISCUSSION.

The voltammetry and potential step results clearly indicate the participation of some complicating factor which is having a pronounced effect on the observed deposition and stripping behaviour. The explanation for this effect seems to be most reasonably described by postulating some catalytic reduction of the perchlorate anion, by the lead monolayer to a product which can subsequently grossly alter the charge transfer kinetics of Pb^{2+} reduction. The catalytic properties of underpotential metal monolayers have already been described. The experimental data shows that the reaction does not occur on the adsorbed lead monolayer (i.e. in the A_1 potential region) but only in the crystal growth region. The reaction would appear to be largely specific to the {110} crystal plane (the effects observed on the other crystal planes will be described later).

If a reduction reaction is taking place on the lead monolayer, a comparison of the anodic and cathodic charges should reveal a higher value associated with the latter. This comparison has been effected for both single and repetitive potential scans.

The actual charge values associated with the first cathodic sweep were slightly higher than subsequent sweep values. Table 5.10 shows the measured cathodic charge values (q_c) (corrected for double layer charging) at 100mV s^{-1} as a function of the sweep number 'N'. These values show that the first sweep was associated with charges approximately 15μC cm^{-2} higher than the steady value of 385μC cm^{-2}. The term 'first sweep' in this case, is not meant to imply the absolute first sweep taken with a freshly polished electrode, but to the first sweep of a cycle taken after a 'relaxation period' at potentials anodic

TABLE 5.10

$q_c/\mu C\ cm^{-2}$	N
398.7	1
388.8	2
386.9	3
386.2	4
385.9	5
385.7	6
385.4	7
385.3	8
385.0	9
385.0	10

Table showing cathodic charge (q_c) associated with sweep from +350mV to -10mV vs. E_r (at 100mV s^{-1}) for lead deposition on the {110} face from 1mM PbO/ 0.5M $HClO_4$, as a function of sweep number, N; the values were determined with an electronic integrator (d.l. charging subtracted).

TABLE 5.11

$\frac{(q_c - q_a)}{q_a} \times 100\%$	N
11	1
8	2
1-3	n

Table showing variation of the function$(q_c - q_a)/q_a \times 100\%$, as a function of sweep number N. Other details as in Table 5.10. The values shown are the average of five, determined by gravimetric analysis of cut out voltammograms.

to U.P.D. In practise the absolute first sweep always showed some effects of surface preparation which disappeared after a few sweeps.

A comparison between the anodic charge and cathodic charge as a function of 'N', has also been made. The value of the function,

$$\frac{(q_c - q_a)}{q_a} \times 100\%$$

where, q_c = total cathodic charge for the potential scan of Table 5.10, at 100mV s^{-1}.

q_a = ditto for anodic charge.

is tabulated in Table 5.11, as a function of 'N'.

For a normal U.P.D. process, the equality of the anodic and cathodic charges has been demonstrated many times. In this case, the initial excess of cathodic charge clearly indicates an irreversible (or not completely reversible) reduction taking place. In addition, the fact that this is most pronounced on the first sweep and the gradual relaxation of the cathodic charge values to a constant value, indicates that the reaction is inhibited by the product formed. The fact that the batch of perchloric acid used, and the length of time the solution had been in the cell, affected the observed voltammetry, also suggests that the catalytic reaction is very sensitive to the exact nature of the solution composition near the electrode, (presumably when a given solution/electrode combination has been subjected to many cycles, the build up of reaction product in the bulk of the solution is sufficient to prevent the formation of any more; in this case the voltammetry shows hardly any change between the first and subsequent sweeps).

The product of the catalytic reduction clearly has an enormous influence on both the kinetics and thermodynamics of the U.P.D. process. The effect on the cathodic voltammetry is very similar to the results obtained by adding increasing amounts of chloride ion to a perchlorate

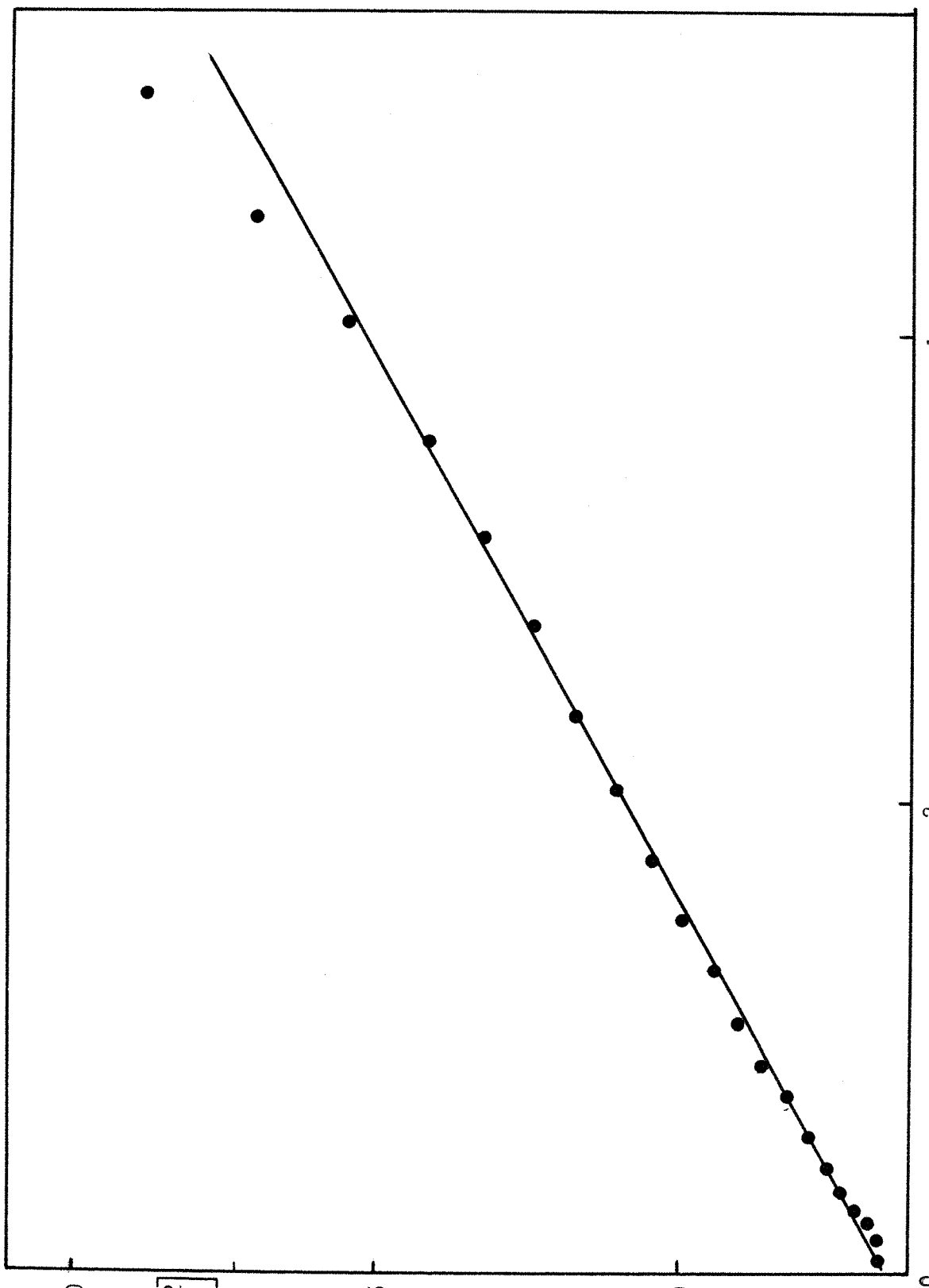

Fig. 5.30 Plot of $\log_{10}(i/t^2)$ vs. t^3 for the current-time transient of Fig. 5.27.

electrolyte (section 5.8). In the present case, the nature of the stripping voltammetry is totally different from that obtained in chloride ion containing media (where symmetry with the cathodic voltammetry peaks is observed). Moreover, only falling i-t transients could be obtained in solutions containing chloride ion. However, the fact that the addition of 1mM of chloride ion to a 5mM PbO/ 0.5M $HClO_4$ solution completely eliminated any of the anomalous behaviour described above suggests that the catalytic reaction is inhibited by the presence of this ion. It was pointed out that the reaction product also seems to inhibit the reaction. It seems likely therefore, that the species responsible for the observed behaviour is a reduction product of the perchlorate anion, but in a higher oxidation state than Cl^-. Before this discussion relating to the nature of the catalytic reaction is continued, it is interesting to consider the i-t transients obtained. These are remarkable in that they show good qualitative agreement with the transient predicted for the charge transfer controlled growth of a two-dimensional layer, with progressive nucleation (note the initial i-t^2 relationship). As mentioned already, such a situation results in an i-t relationship of the form,

$$i = \frac{zF\pi Mhk^2At^2}{\rho} \cdot \exp\left(\frac{-\pi M^2k^2At^3}{3\rho^2}\right)$$

The fit of the experimental data to this equation can be tested by plotting $\log(i/t^2)$ versus t^3. A plot of this kind for the i-t transient of Fig. 5.28 is shown in Fig. 5.31. It is seen that a linear relationship holds for greater than 80% of the charge associated with the i-t transient. This agreement with the theoretical equation for two-dimensional nucleation and growth strongly suggests that in analogy to the results from citrate solutions, the product of the catalytic reduction of the perchlorate ion has reduced the rate of the electron transfer step to such an extent that crystal growth information can be obtained.

The nature of the product generated in this catalytic reaction is most likely an uncharged species.The relatively long time effects observed in the experiments described above can only be explained by the species being adsorbed on the electrode. However, if the adsorbed species was charged, this would be detectable. No such effects are measureable, with the cathodic charge on continuous sweeping being only slightly less than the first sweep of a cycle (Table 5.10). This makes the existence of a negatively charged adsorbate unlikely, as desorption occurring when metal deposition took place would contribute an increased negative charge to the measured values (unless the product was readsorbed on the lead surface). The most plausible scheme is,

$$ClO_4^- + 2H^+ + 2e^- = ClO_3^- + H_2O \qquad E^\circ = 1.15V$$

$$ClO_3^- + 2H^+ + e^- = ClO_2 + H_2O \qquad E^\circ = 1.19V$$

(vs. N.H.E.)

This would produce the neutral ClO_2 molecules. This scheme would explain the marked pH dependence of the catalytic reaction. At the present time, no more conclusive attempt has been made to identify experimentally the nature of the catalytic product, but clearly the addition of ClO_2 to a lead ion containing solution would be a useful experiment.

The explanation for the smaller effects observed at higher lead concentrations, is probably because the ClO_2 is almost totally complexed with lead in solution, rather than adsorbed on the electrode; at higher lead ion concentrations there would always be sufficient uncomplexed lead to effect the'normal' deposition behaviour.

CHAPTER SIX: OVERPOTENTIAL DEPOSITION OF LEAD ON SILVER.

6.0 INTRODUCTION.

Studies of overpotential metal deposition in systems where underpotential metal monolayers are formed have been comparatively few in number. Although, as mentioned already, several of these studies[19] totally ignored the possible presence of an underpotential monolayer and any influence it might have on the deposition kinetics of thicker deposits.

The most relevant studies to the system in question here, i.e. lead deposition on silver, are those of Harrison et al.[28,111,112]. These workers have made a detailed study of the growth kinetics of lead and thallium deposits on polycrystalline and single crystal ({111}) silver. However, the U.P.D. voltammetry obtained indicates that the polishing methods employed for electrode preparation (a combination of mechanical and electrochemical methods) were not satisfactory in producing a well defined surface. The extent to which this affected the overpotential deposition results is not known, but a reinvestigation of these systems using carefully prepared single crystal electrodes is highly desirable.

The findings of Harrison et al. from potentiostatic pulse measurements in the overpotential region, for the growth of lead and thallium on silver, can be summarised in the following way.

1. In the initial stages of growth, rising i-t transients were obtained with a linear relationship between these two quantities.

2. The transients were extremely potential sensitive; the gradient increasing ten-fold in about 3mV.

3. Prepulsing to 200mV more cathodic than the growing potential for times ranging from 3 to 300ms, did not increase the growth currents or affect the potential dependence significantly.

4. The growth transients were independent of whether the monolayer was preformed or not.

It was thought that the nuclei grow from a Nernst diffusion layer, with the current into each nucleus being independent of the nucleus geometry. Thus the i-t dependence was explained by a progressive nucleation mechanism, with each nucleus bringing an equal increment in current. The fact that prepulsing had no effect was thought to imply that the rate of nucleation was controlled by the generation of defects in the surface of the deposited nuclei.

The results from the present investigation will now be described. A solution of 50mM $Pb(CH_3CO_2)_2$/ 0.5M $HClO_4$ was used for all experiments. At high lead concentrations such as this, the acetate salt was by far preferable to the oxide, as heavy metal impurities were present in the latter.

6.1 RESULTS.

(a) SINGLE POTENTIAL STEP AND MONOLAYER PREPULSE-GROWTH PULSE EXPERIMENTS.

On the time scale of the cathodic pulses employed (seconds), on all orientations, rising transients were obtained at overpotentials greater than 13mV. With overpotentials between 0 and 13mV, a finite current flowed, but this did not rise within the time scale of the pulse. This could correspond to nucleation at a very slow rate, or ad-atom formation.

Examples of the transients obtained for the three crystal faces, as a function of overpotential in the range 14-17mV, are shown in Fig. 6.1. The following points can be noted.

1. The transients are extremely sensitive to small changes in overpotential; e.g. for the {100} face results, an increase of 1.0mV in overpotential causes the rate (at constant time) to increase by a factor of about three.

2. The initial parts of the transients showed an $i\text{-}t^2$ relationship on the

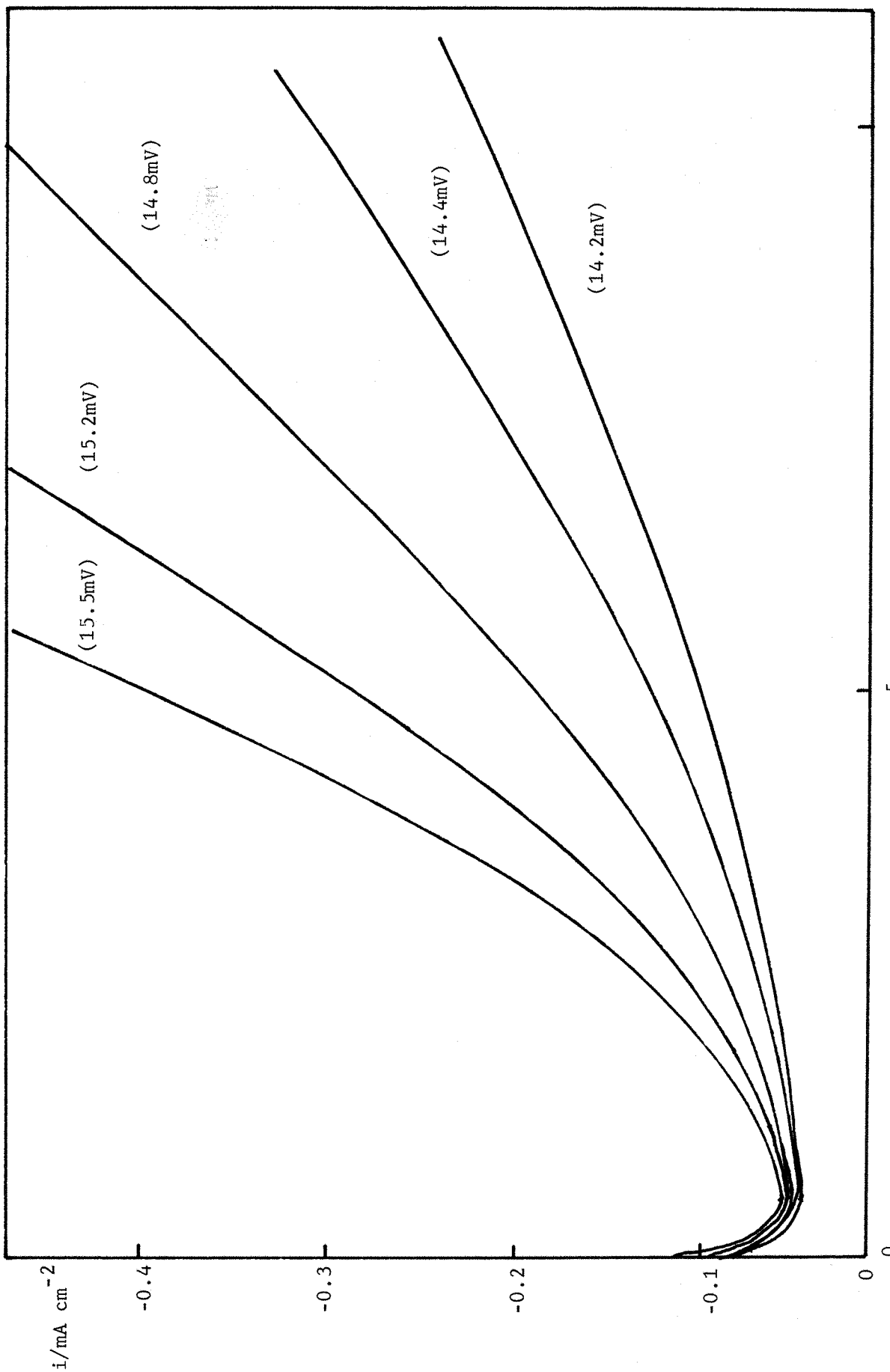

Fig. 6.1(a) Current-time transient for potential steps from +300mV to the overpotentials shown ( ), for lead deposition on the {100} face of silver. Solution, 50mM $Pb(CH_3CO_2)_2$/ 0.5M $HClO_4$.

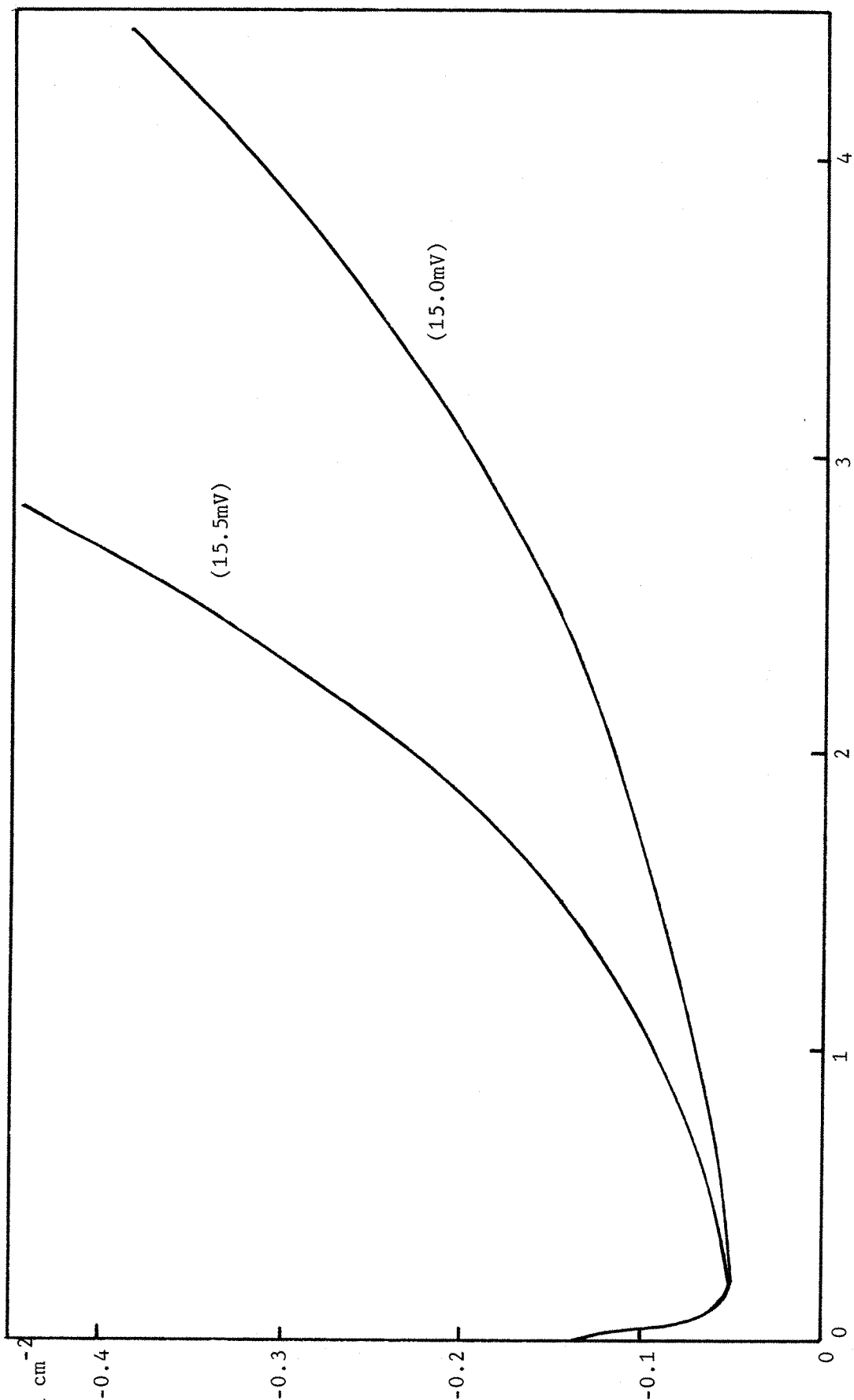

Fig. 6.1(b) Current-time transients for potential steps from +300mV to the overpotentials shown, for lead deposition on the {110} plane of silver. Solution, 50mM $Pb(CH_3CO_2)_2$/ 0.5M $HClO_4$.

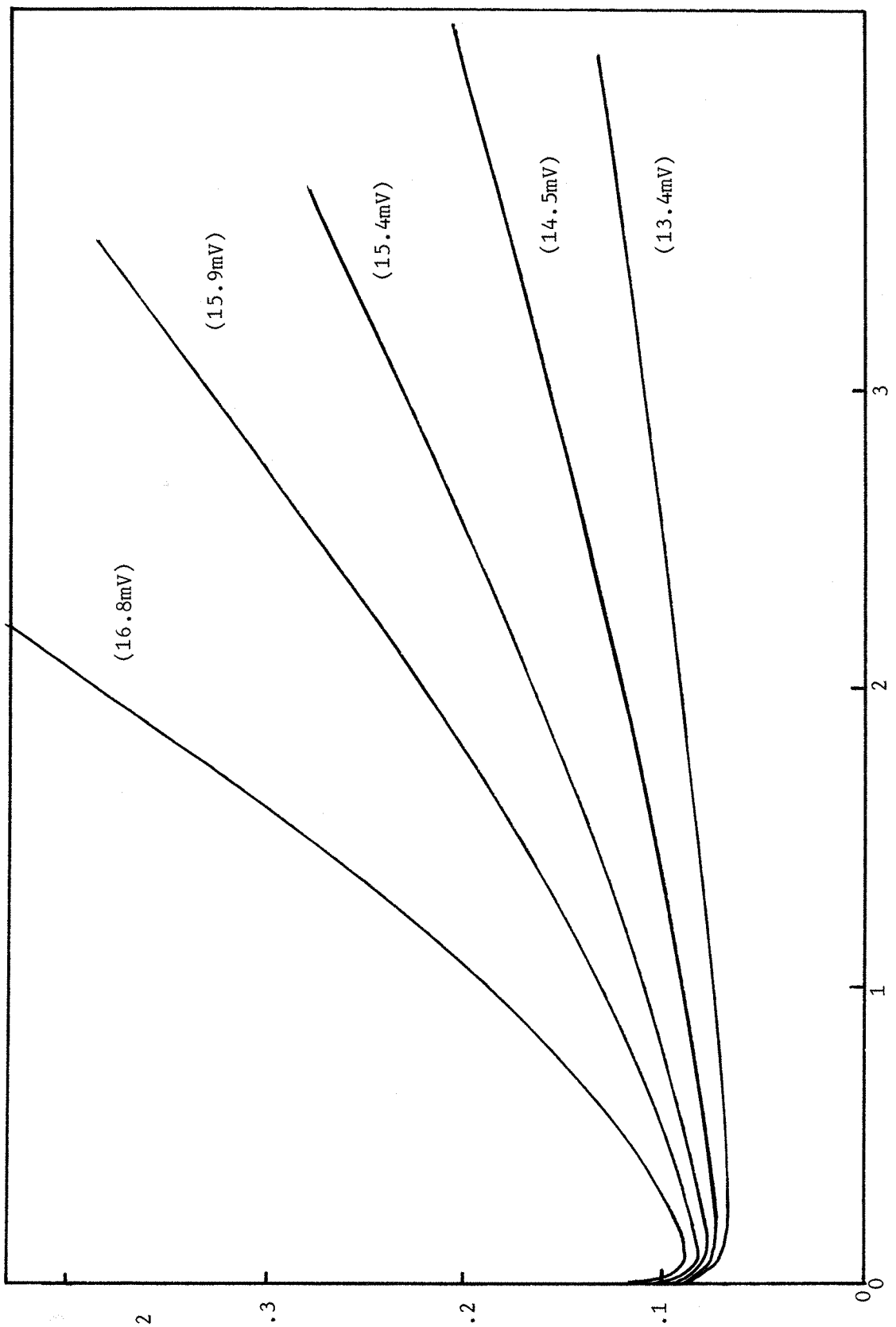

Fig. 6.1(c) Current-time transients for potential steps from +300mV to the overpotentials shown, for lead deposition on the {111} plane of silver. Solution, 50mM $Pb(CH_3CO_2)_2$/ 0.5M $HClO_4$,

{110} and {100} faces, but on the {111} face, this was i-$t^{3/2}$. Examples of i-t^2 and i-$t^{3/2}$ plots for the transients of Fig. 6.1 are shown in Fig. 6.2.

3. In experiments where a prepulse to the reversible potential was employed to form the monolayer, the nucleation and growth transient was identical to that at the same potential in single pulse experiments. The transients in Fig. 6.1 were in fact obtained from double pulse experiments, where a prepulse of 1s duration, to the reversible potential, was applied for monolayer formation.

4. At longer times, the i-t^2 or i-$t^{3/2}$ relationships were lost, and i became linear with time. Eventually the current tended to a constant, planar diffusion limited value. At high growth overpotentials (greater than 20mV) the transients pass through a maximum and decay to the planar diffusion limited value.

Before the results of double and triple potential step experiments, involving nucleation, rather than monolayer, prepulses, are described, the single potential step results will be discussed.

Harrison et al.[28,111-112] found a linear i-t relationship on both polycrystalline and {111} silver, in their experiments for lead and thallium deposition on silver. In the present case, none of the single crystals follow this relationship and the variance in behaviour must be due to the difference in pretreatment of the electrodes. As mentioned already, the voltammetry results obtained by these workers in the underpotential region, suggested that the electrode surfaces had poor crystallographic definition.

Considering first the {110} and {100} results; an i-t^2 relationship, at short times before overlap takes place, could arise from;

1. Three-dimensional growth and instantaneous nucleation,

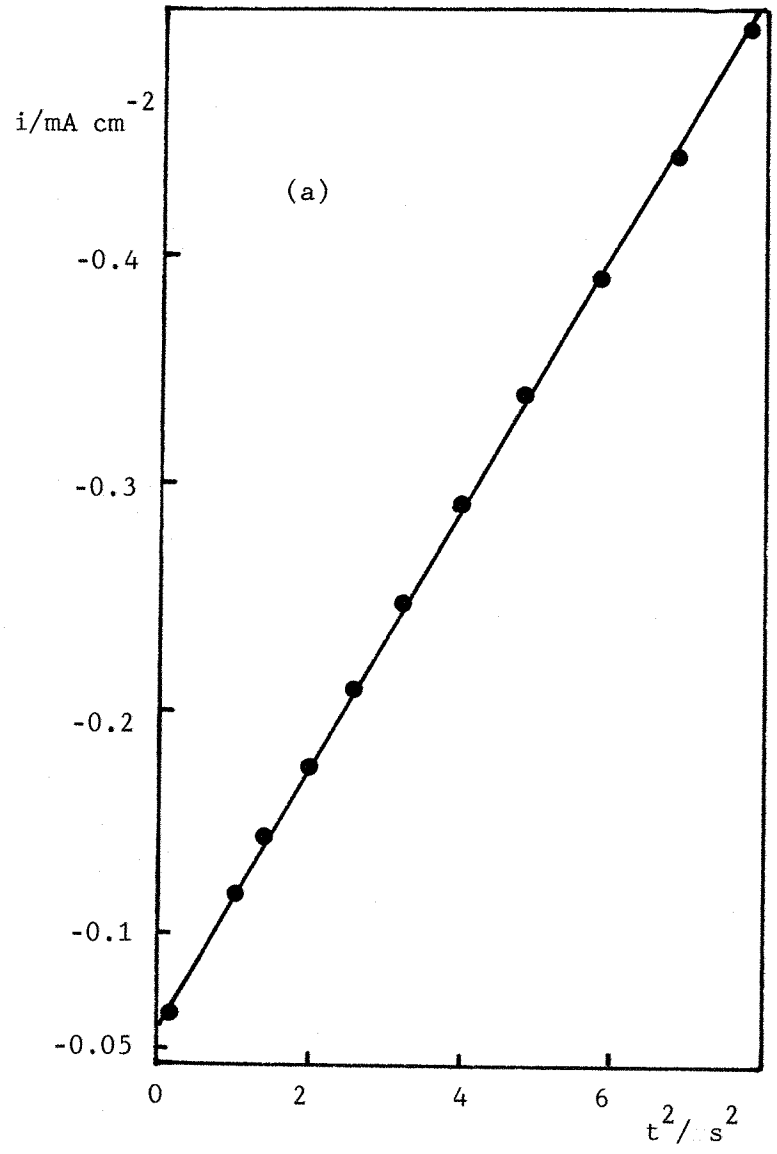

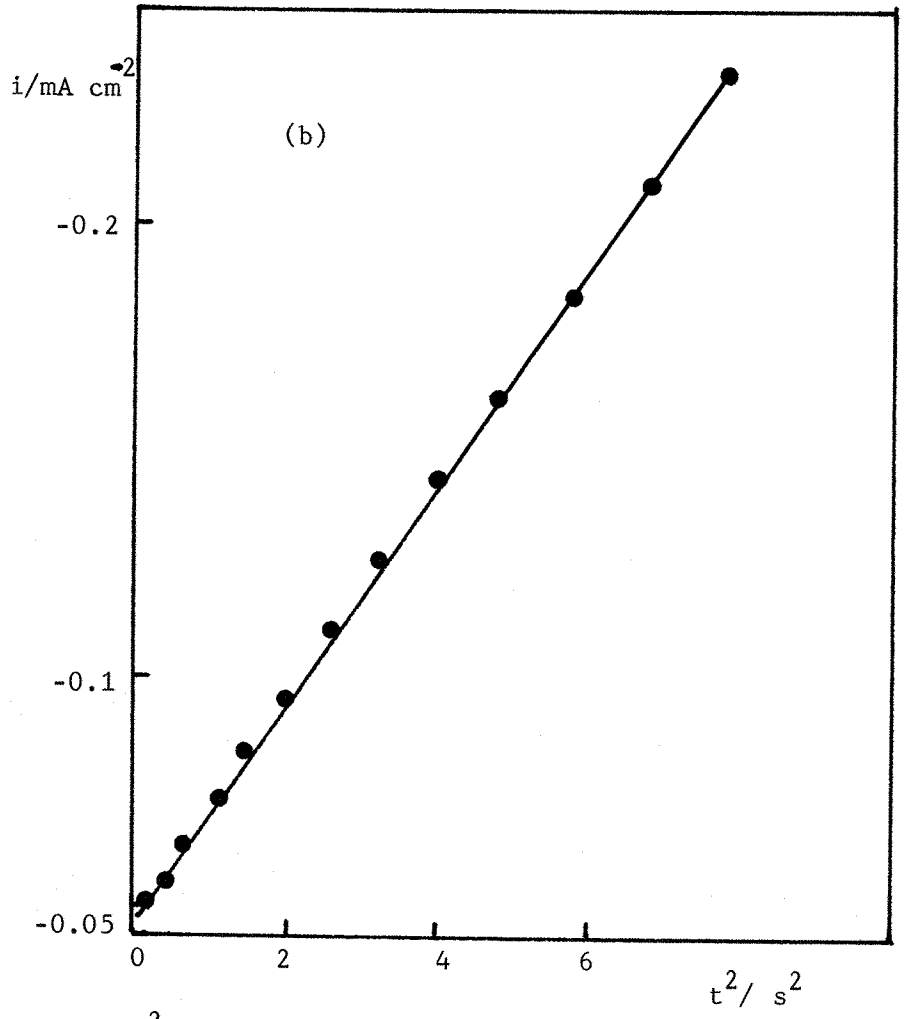

Fig. 6.2 Plots of i vs. t^2 for potential steps from +300mV to (a) -15.7mV (b) -15.3mV, for lead deposition on the {100} face. Solution, 50mM $Pb(CH_3CO_2)_2$/ 0.5M $HClO_4$. t=0 was the foot of the rise.

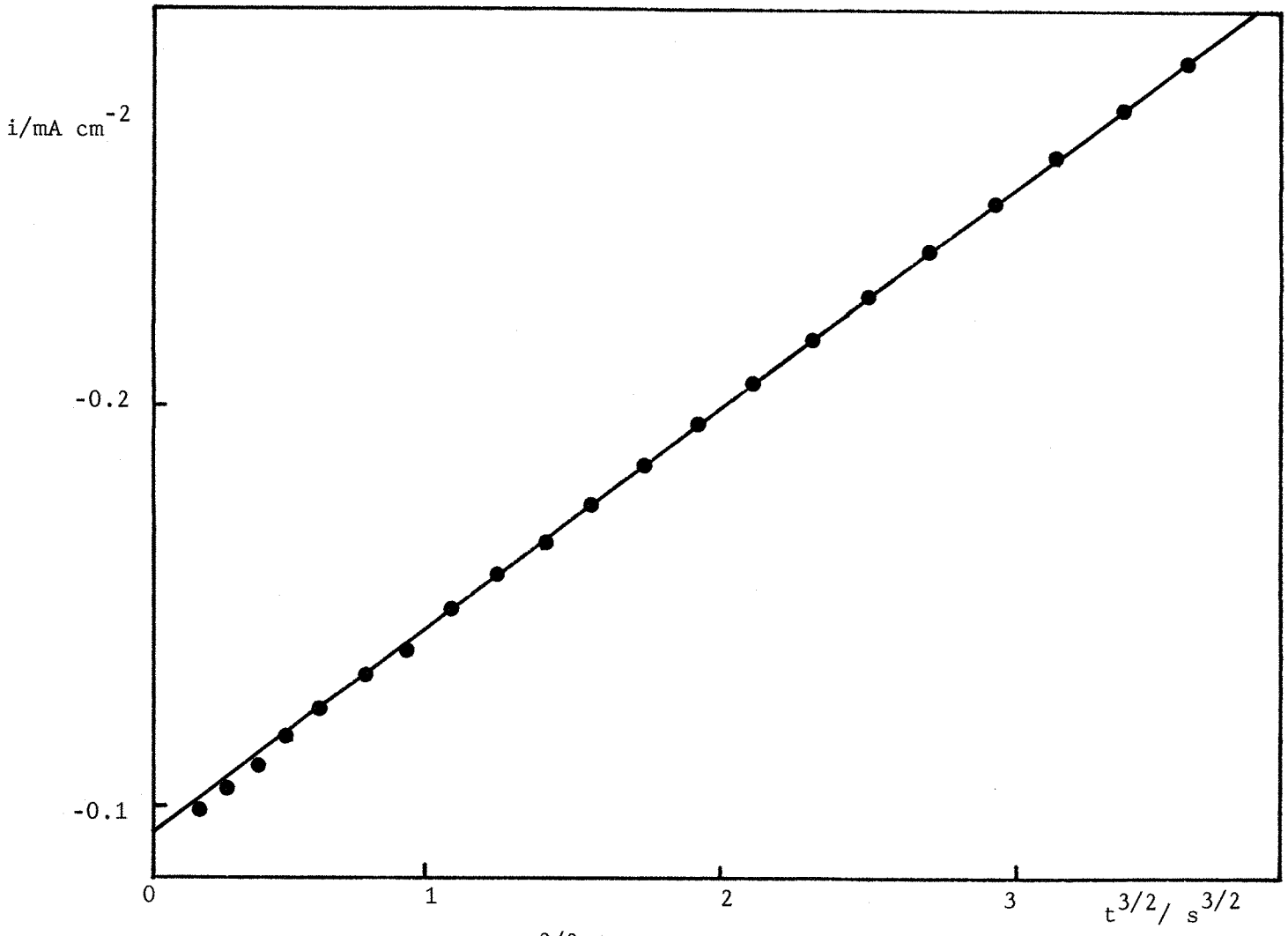

Fig. 6.2(c) Plot of i vs. $t^{3/2}$ for a potential step from +300mV to -15.9mV, for lead deposition on the {111} face. Solution 50mM $Pb(CH_3CO_2)_2$/ 0.5M $HClO_4$.

2. Two-dimensional growth and progressive nucleation.

(The rate determining step is the rate of incorporation of material at the edges of the growth centres.)

If two-dimensional nucleation and growth were taking place, one peak at least would be expected in the transients, containing approximately a monolayer amount of charge. No such effect is seen, and it must be concluded that the observed $i\text{-}t^2$ dependence at short times, corresponds to three-dimensional growth with instantaneous nucleation. The $i\text{-}t^2$ relationship for three dimensional growth, is only valid before overlap of the growing centres has taken place. At longer times, the deviation in the experimental plots from a t^2 relationship, must be due to overlap of the growing centres and ultimately, diffusion controlled growth.

The full equation relating i and t before overlap is,

$$i = \frac{2zF\pi M^2 N_o k^3 t^2}{\rho^2}$$

where,

k = lattice growth rate constant,

N_o = number of nuclei formed instantaneously.

From the gradient of the $i\text{-}t^2$ plots it is possible to determine the quantity $N_o k^3$.

In the present case, this shows an extreme potential dependence; this could arise from a highly potential dependent N_o or k or both. The variation of k with potential, for a simple electron transfer process, would be given by the relation

$$k = k_o\left\{\exp \frac{\alpha z F \eta}{RT} - \exp \frac{(\alpha-1) z F \eta}{RT}\right\}$$

Page 228 was not included in the bound thesis.

This would not predict such large potential dependencies as found experimentally, and it would seem that the variation of N_o with potential is responsible for the observed behaviour. It is interesting to consider lead deposition on a different substrate where the nucleation situation is very different. This would result in a totally different relationship between N_o and potential. Vitreous carbon is ideal for this purpose as no underpotential monolayers are formed on this substrate and three-dimensional growth occurs directly.

Fig. 6.4 shows examples of single pulse i-t transients for lead deposition from 50mM $Pb(CH_3CO_2)_2$/ 0.5M $HClO_4$ onto a polished vitreous carbon substrate. Rising transients are obtained at overpotentials slightly higher than on the silver substrate but it can be seen that the potential dependence is markedly reduced. The current is proportional to $t^{3/2}$ which corresponds to three-dimensional growth with progressive nucleation, into hemi-spherical diffusion zones (equation 1.16). The potential dependency is caused by the variation of the quantity AN_o with potential (where A is the nucleation rate constant).

These results illustrate the difference in the growth kinetics of lead on carbon and lead on {110} and {100} silver. The fact that the three-dimensional nuclei on carbon grow in diffusion zones, whereas those on {110} and {100} silver do not, suggests that the lattice incorporation step is much slower in the latter cases. In addition, the much lower potential dependencies on the carbon substrate suggest the variation in the number of nuclei and/or nucleation rate, with potential, is much smaller than with silver. This difference could be influenced by the underlying monolayer on silver and also by substrate orientation effects.

The results on the {111} silver plane are different from those on the other two faces in that the transients show initially an $i\text{-}t^{3/2}$ rather than an $i\text{-}t^{2}$ relationship. In addition it can be seen from Fig. 6.1

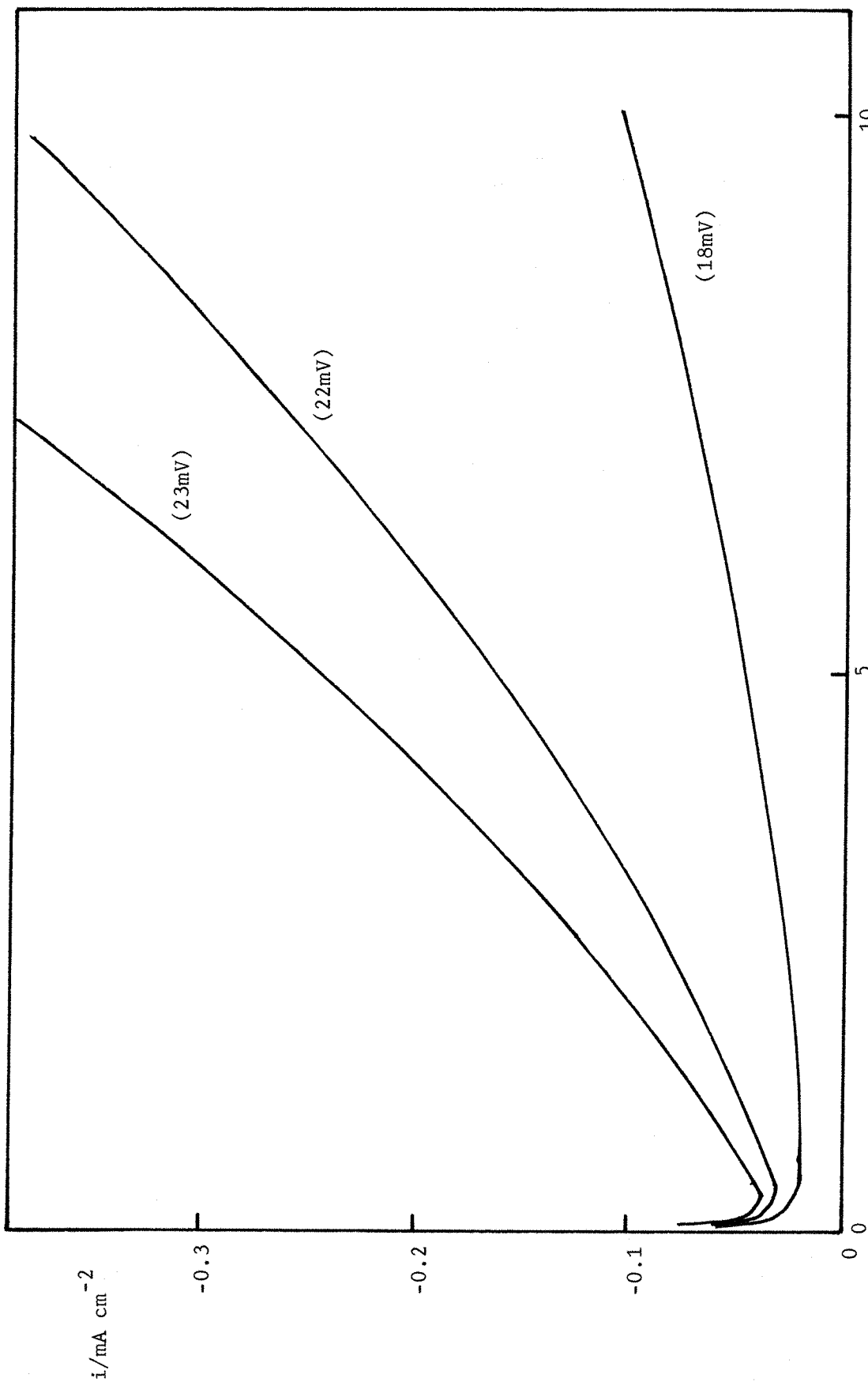

Fig. 6.4 Current-time transients for potential steps from +300mV to the overvoltages shown, for lead deposition on a vitreous carbon substrate. Solution, 50mM $Pb(CH_3CO_2)_2$/ 0.5M $HClO_4$.

that the potential dependency of the transients is somewhat reduced compared to that on the {110} and {100} faces. The i-$t^{3/2}$ relationship again suggests three-dimensional growth in hemi-spherical diffusion zones, of progressively formed nuclei. Thus both the nature of the slow step and the type of nucleation differ from those on the other planes. The difference in the potential dependencies between the {111}, and {110} and {100} planes would be expected as the potential dependent quantity in the former case is AN_o, whereas in the latter cases it is $N_o k^3$.

It has been stated many times in this Thesis that the final form of the underpotential monolayer on each plane is a close packed layer, distorted to an extent depending on the substrate structure. Clearly these distortion effects are influencing the nucleation and growth of thicker deposits. On the {111} plane, diffusion to the growing centres, formed progressively, is the slowest step in the growth process. On the {110} and {100} planes however, the lattice incorporation step is slowest. It is probable that growth in these cases is hindered by the conflict in structure between the underlying substrate and the monolayer. It is well known that the structure of electrodeposits is sensitive to the orientation of the electrode material, and it seems significant that in the case where the structure of monolayer and substrate are identical (the {111} plane), that the lattice growth step is fast. It is possible that initially, on all orientations, nuclei are orientated with the {111} plane parallel to the substrate. Subsequent growth of these into three-dimensional clusters would occur most readily on the {111} orientation, but on the {100} and {110} planes, the initially formed {111} orientated nuclei may dictate a growth form which is hindered by the influence of the substrate. In this way the variation in the nature of the slow step with orientation, could be explained. Of course, more data is required before these ideas can be substantiated. It is also possible that the surface structure on the {110} and {100} planes provides

enough favourable sites for instantaneous nucleation, whereas the relatively distortion free {111} surface does not, and nucleus formation is progressive.

More information about the nucleation processes occurring in this system can be obtained from double potential step experiments in which the prepulse is of a sufficiently high potential to form three-dimensional nuclei, e.g. an overpotential of 100mV.

6.1(b) NUCLEATION PREPULSE AND GROWTH PULSE EXPERIMENTS.

Initially, results from the {100} face will be used to illustrate the type of behaviour obtained in these experiments.

Fig. 6.5 shows that prepulses of 92.5mV for periods of time between 0 and 2.6ms, had no effect on the growth transient at 14.7mV. A prepulse of 2.8ms however, produced a marked increase in the current and a 3ms prepulse produced such a large increase in current that the transient no longer fitted on the same current axis.

Fig. 6.6 shows the results from a similar experiment over a greater range of prepulse lengths, for deposition on the {110} face. It can be seen that the size of the growth transients at the same potential are very sensitive to small changes in the length of the nucleation prepulse.

Before discussing these results, it should be pointed out that these findings also differ from those of Harrison et al. in the same system; these workers found nucleation prepulses had no effect on the growth transient. As mentioned earlier, this marked difference in results must be due to the differences in surface preparation in the two cases.

Before considering the change in shape of the growth transient produced by preformation of nuclei, it is interesting to consider why no effects are observed with prepulse lengths of less than 2.6ms. It is possible that this is the length of time needed for the nuclei to grow

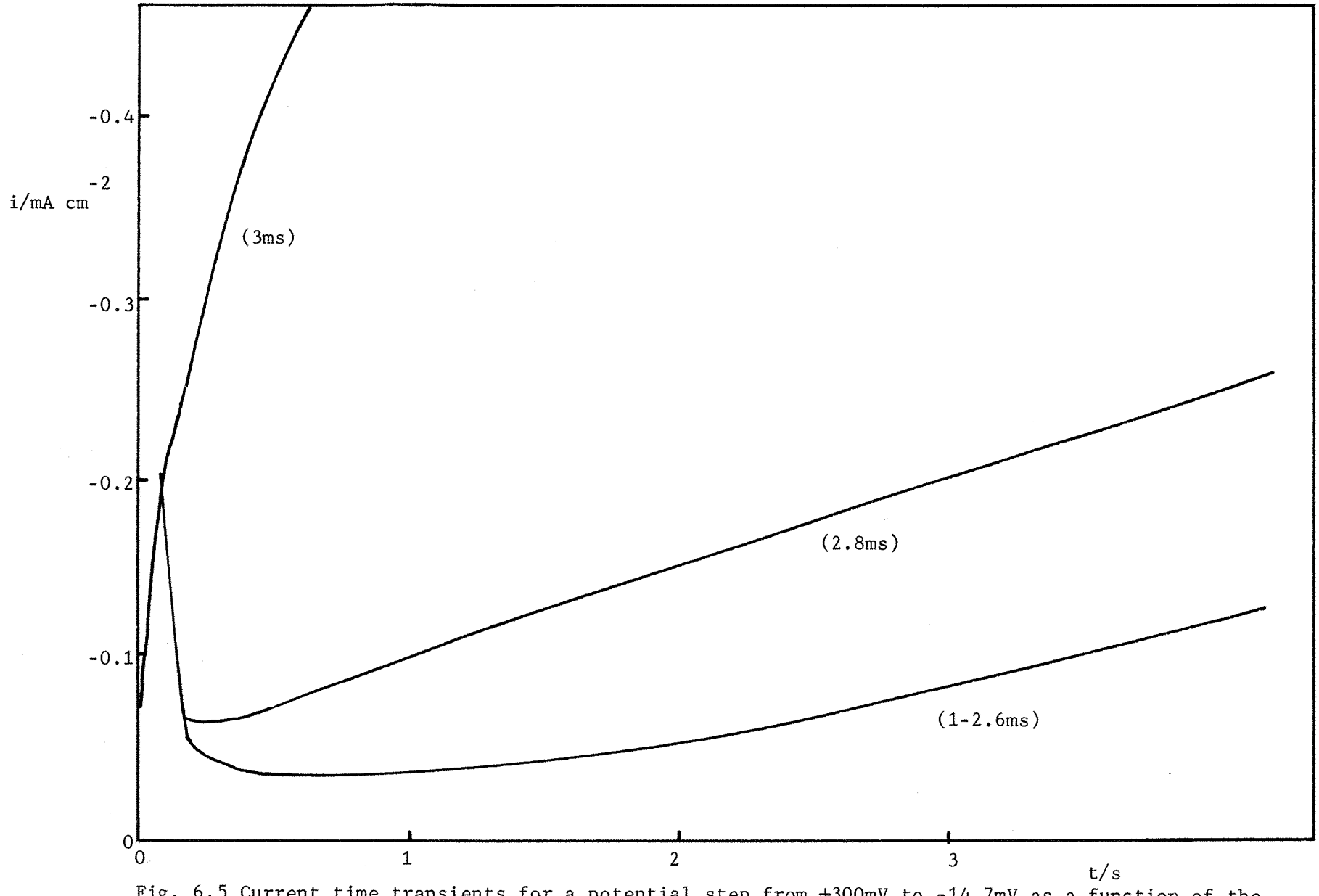

Fig. 6.5 Current time transients for a potential step from +300mV to -14.7mV as a function of the length of the nucleation prepulse (at -92.5mV), for lead deposition on the {100} face. Solution, 50mM $Pb(CH_3CO_2)_2$/ 0.5M $HClO_4$.

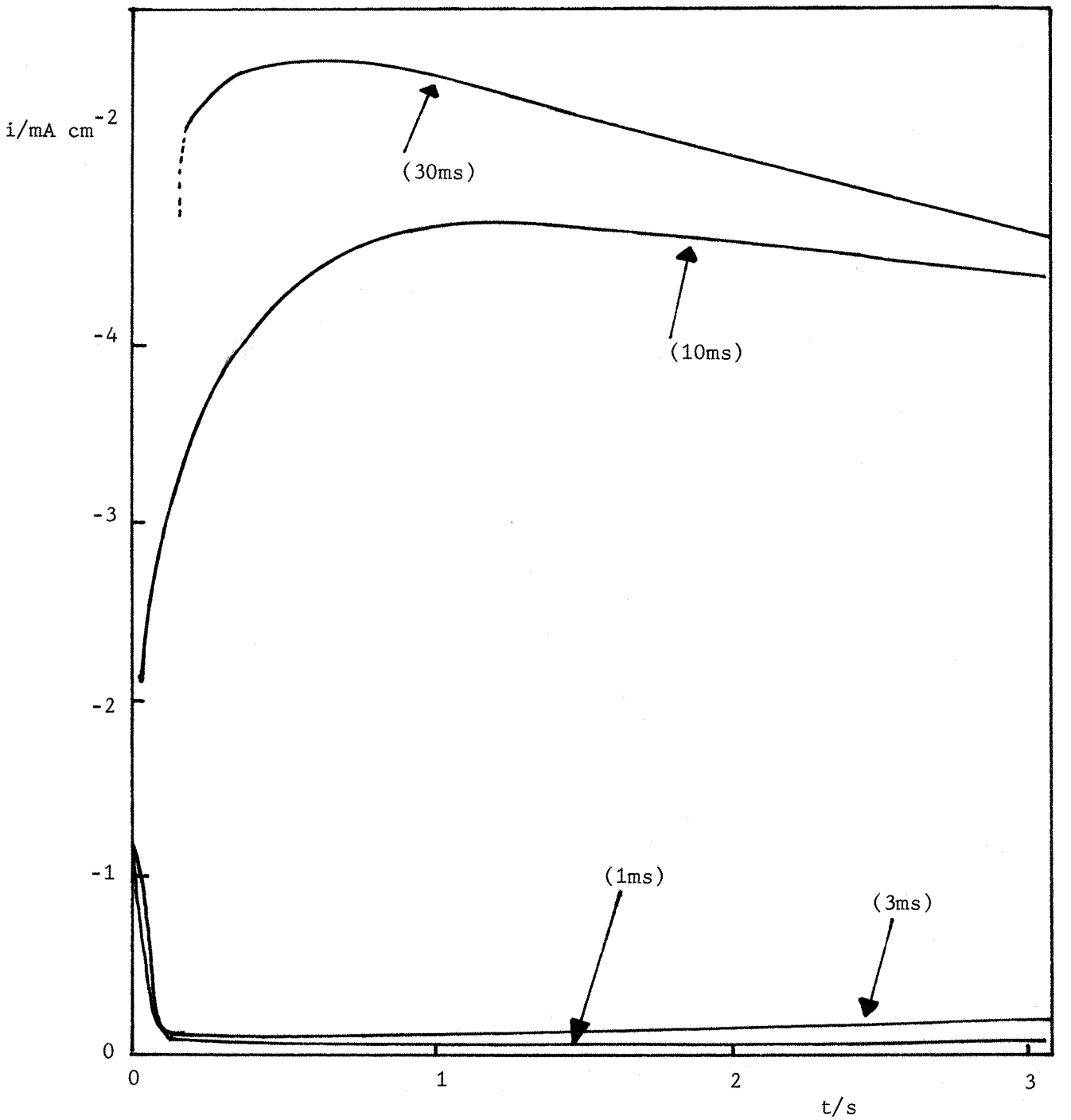

Fig. 6.6 Current-time transients for a potential step from +300mV to -14.4mV as a function of the length of the nucleation prepulse (at 92.2 mV), for lead deposition on the {110} face. Solution, 50mM $Pb(CH_3CO_2)_2$/ 0.5M $HClO_4$.

to a sufficient size to be stable at the lower growth potential, but if this were the case an anodic current corresponding to the dissolution of nuclei formed in the prepulse, should preceed the rising growth transient. With this length of prepulse, this is not observed experimentally.

The current-time behaviour in the prepulse, as a function of length, was examined. The results showed that the first process occurring was the formation of the monolayer. It has already been shown for thallium deposition that, even at overpotentials, formation of a complete monolayer occurs prior to any three- dimensional growth. The present results showed that, at nucleation overpotentials of 92.5mV, the length of time taken to complete monolayer formation was about 2.7ms, which coincides exactly with the minimum prepulse length which had any effect on the growth transient. If the length of the prepulse was less than 2.7ms there is insufficient time to complete the monolayer at this (high) nucleation overpotential, and growth is completed at the lower growth overpotential prior to the formation of any three-dimensional nuclei. In this case, no effect on the growth transient would be observed as the entire length of the prepulse is occupied with formation of the monolayer. However, if the length of the prepulse is greater than 2.7ms, there is time after completion of the monolayer, to form three-dimensional nuclei; consequently the growth transients will be modified according to the greater number of nuclei available for growth.

These results show that no appreciable three-dimensional nucleation can occur until the monolayer is complete. This cannot be explained by the relative rates of monolayer formation and three-dimensional nucleation being such that the number of nuclei formed in the time it takes to complete the monolayer is very low, as this would not result in such a sudden increase in the growth currents when the prepulse length is just sufficient to allow the complete formation of the monolayer.

More information about the rate of nucleation at the over-potentials employed in the prepulse can be obtained from triple pulse experiments, i.e. with the following pulse sequence:

A) Pulse to reversible potential for monolayer formation.

B) Nucleation pulse, for various times, to high overpotential.

C) Growth pulse at low overpotentials.

With this type of pulse train, nucleation prepulses of 92.5mV, for times longer than 0.05ms, affected the growth transient. This emphasizes the previous result, which indicated that the relative rates of monolayer formation and three-dimensional nucleation, were not responsible for the sharp transition in behaviour observed with prepulses longer than 2.7ms. The rate of three-dimensional nucleation becomes significant only when the monolayer is complete.

The shapes of the growth transients obtained in triple pulse experiments will now be discussed.

6.1(c) THE NATURE OF THE GROWTH TRANSIENT WITH NUCLEATION PREPULSES.

At a constant nucleation prepulse overpotential of 92.2mV, the nature of the growth transient was dependent on,

A) length of nucleation prepulse,

B) the overpotential in the growth pulse.

These results were essentially independent of crystal face (but see later).

CASE 1.

Nucleation prepulses longer than 7ms, growth overpotentials greater than 12mV.

In this case, only falling i-t transients could be obtained, corresponding to the growth of nuclei limited by the rate of planar diffusion.

CASE 2.

Nucleation prepulse of 3ms, growth overpotentials less than 8mV.

With the nucleation and growth conditions as above, the growth transient consisted of a negative and positive component.

At short times, the current changes from a positive to a negative value. This part of the transient is characterized by a linear $i\text{-}t^{\frac{1}{2}}$ relationship. Examples of such transients at various overpotentials are shown in Fig. 6.7. The initial cathodic current corresponds to dissolution of the nuclei formed at the prepulse overpotential, which are not of sufficient size to be stable at the growth potential (the critical radius being dependent on overpotential).

The initial $i\text{-}t^{\frac{1}{2}}$ form of the transients, in the cathodic segment, suggests the growth of three-dimensional nuclei, formed instantaneously, in hemi-spherical diffusion zones. The relationship between current and time for this situation has already been given. In full this equation is,

$$i = \frac{8N_o FM^2C^3D^{3/2}t^{\frac{1}{2}}}{\rho^2\pi^{\frac{1}{2}}}$$

where, M = Molecular weight

C = Concentration

ρ = density of material deposited

N_o = Number of nuclei formed instantaneously

It can be seen that N_o is the only potential dependent quantity in this expression and therefore any potential dependency of the growth transients must be due to the variation in N_o with growth potential (i.e. although a large number of nuclei are formed in the prepulse, the fraction of these which are allowed to grow further is dependent on the growth potential).

If the growth overpotential is increased during an actual

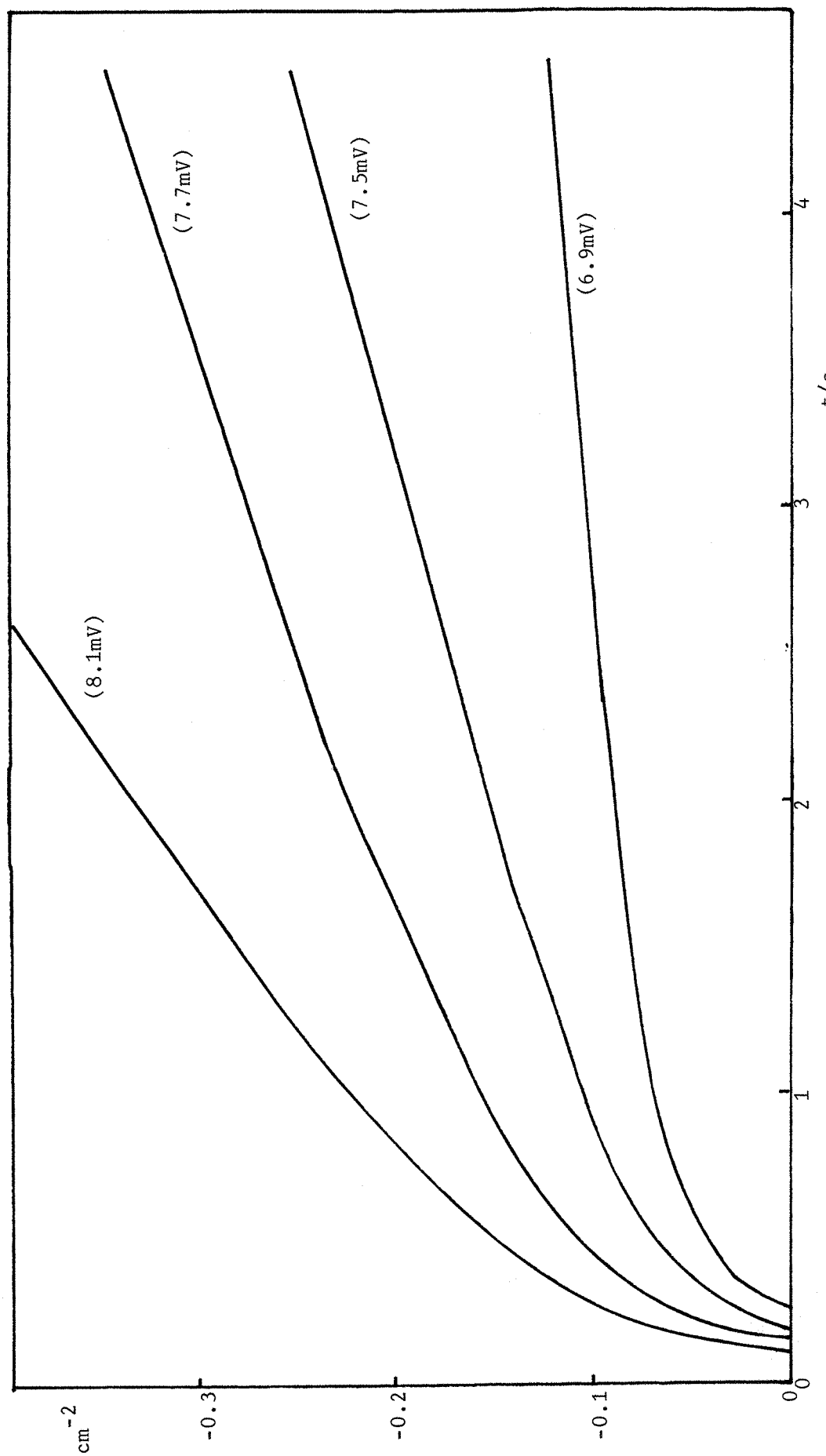

Fig. 6.7 Current-time transients for potential steps from +300mV to the overpotentials shown, following a monolayer prepulse of 1s and a nucleation prepulse of 3ms at-92.2mV, for lead deposition on the {110} plane. The anodic component is not shown. Solution, 50mM $Pb(CH_3CO_2)_2$/ 0.5M $HClO_4$.

transient, the current also increases. Again, this can only be explained on a diffusion controlled growth model if increasing the potential causes more nuclei to form on the'uncovered'parts of the electrode.

In principle, N_o at the various growth potentials could be calculated from $i\text{-}t^{\frac{1}{2}}$ plots at different potentials.

CASE 3.

Nucleation prepulse of 3ms, growth potential between 8 and 20mV.

In this case, the initial anodic current is restricted to very short times, as an increasing fraction of the preformed nuclei become stable at the growth overpotential. The initial part of the transient is described by $i \propto t^{\frac{1}{2}}$. Examples of this are shown in Fig. 6.8, (the XY recorder could not respond to the anodic dissolution current at very short times).

In some cases when nucleation prepulses were employed, the form of the growth transients was more complicated than that shown in Fig. 6.8. Fig. 6.9 shows examples of this type of transient on the {100} plane. An initial peak is followed by a rise in current. The charge associated with the peak can be seen to be far greater than a monolayer amount; e.g. for the transient at 15.0mV in Fig. 6.8, about 7mC cm^{-2}. Hence it cannot be explained by the growth of a two-dimensional layer. Unfortunately at the present time, the number of experiments performed in this area has not been sufficiently large to establish the criteria which determine whether or not this type, or the simple $i\text{-}t^{\frac{1}{2}}$ behaviour is obtained. It may be that small variations in surface pretreatment are important.

The explanation for this effect is probably related to orientation effects[113,114]. According to Pangarov, the orientation of initially formed nuclei is determined solely by the work of their formation which is a function of the overvoltage of metal deposition.

In the present case, where the experimental transients can be

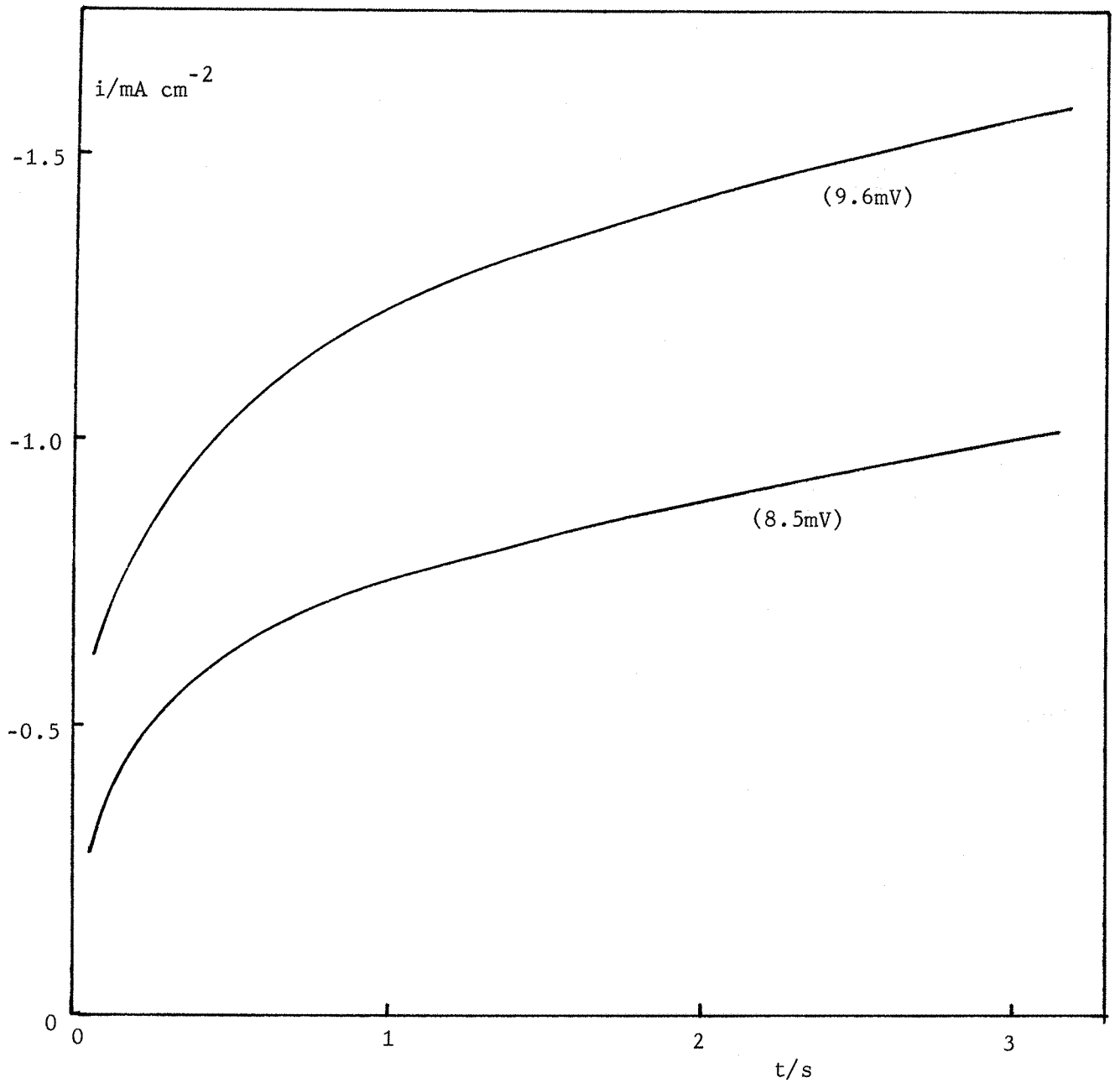

Fig. 6.8 Current-time transients for potential steps from +300mV to the overpotentials shown, following a monolayer prepulse of 1s and a nucleation prepulse of 3ms at -92.8mV, for lead deposition on the {111} plane. Solution, 50mM $Pb(CH_3CO_2)_2$/ 0.5M $HClO_4$.

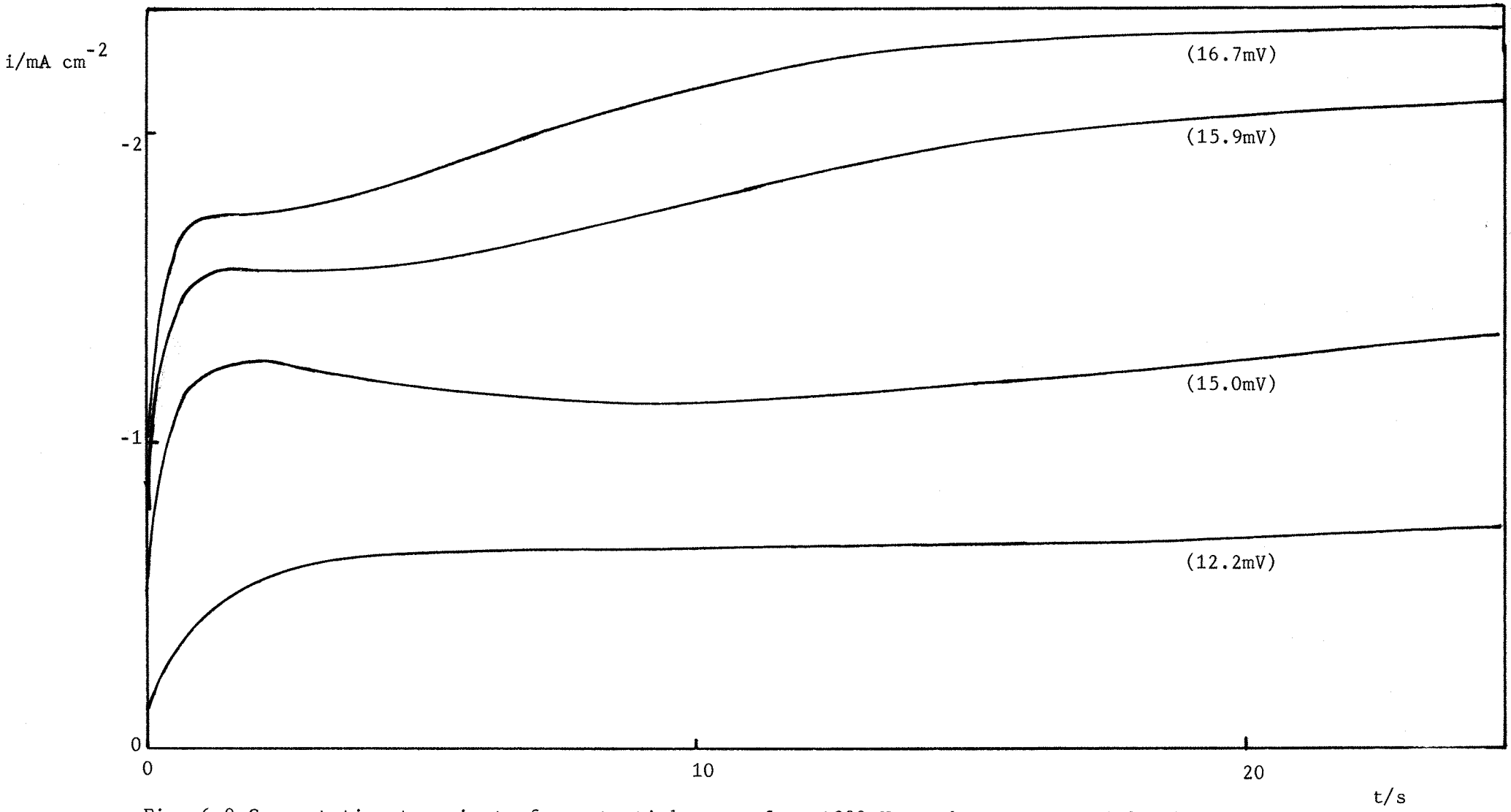

Fig. 6.9 Current-time transients for potential steps from +300mV to the overpotentials shown following a single prepulse of 92mV for 3ms, for lead deposition on the {100} plane, showing the anomalous behaviour described in the text. Solution, 50mM $Pb(CH_3CO_2)_2$/ 0.5M $HClO_4$.

divided into two sections, an initial peak or plateau followed by a rise, it is possible that the first feature corresponds to the growth of centres with orientation determined by the nucleation overpotential. If, for a given substrate, this is not the most favoured orientation at the growth overpotential, the rate of lattice growth will be slow and correspondingly the current would remain at a low value. As the centres overlap, the current will drop corresponding to the decreased area available for growth. This will produce a peak in the i-t transient. The growth potentials in Fig. 6.9 are such however, that further nucleation can occur and these centres will have the preferred orientation for growth at that potential. This second nucleation step will cause the current to rise again, corresponding to new centres formed on top of the inital layer of different orientation. To date, transients of the type shown in Fig. 6.9 have only been obtained for the $\{110\}$ and $\{100\}$ faces. It is possible that it is only in the case of the $\{111\}$ substrate that the preformed nuclei dictate a growth form at the low overpotential, which is the most stable on the $\{111\}$ face. However, further work in this area is necessary before definite conclusions can be made.

CHAPTER SEVEN: CONCLUDING REMARKS.

The work described in this Thesis has answered several of the unresolved questions pertaining to U.P.D. which were mentioned in Chapter 2. For example, there seems no doubt that the multi peak nature of the voltammetry observed on polycrystalline electrodes corresponds to deposition on the different crystal faces in the surface. In the absence of chemical polishing, such effects would be most readily discernible on the hardest of the noble metals e.g. gold and platinum, whose surfaces are most resistant to mechanical deformation from alumina polishing. Much of the previous work in U.P.D., especially on silver electrodes, is of dubious significance due to inadequate surface preparation.

There is also no doubt that the final form of the monolayer in each case, is a two-dimensional crystal plane, distorted to an extent depending on the surface structure of the substrate. In the present examples, direct evidence for nucleation, in the form of well defined rising current-time transients, could only be obtained when the rate of the electron transfer/ lattice incorporation step was reduced by complexing agents. Nevertheless the results have shown conclusively that nucleation and crystal growth processes do occur in the underpotential region.

In the present work, interaction parameters have not been determined for the surface coverage-potential relationships on the different crystal faces. An interaction parameter greater than or equal to four is usually recognised as implying crystal phase formation. It is essential however, to consider the effects of substrate structure on the properties of the monolayer phase, and the concept of a limiting interaction parameter for an adsorbed layer, derived for featureless surfaces, is of dubious significance when applied to solid surfaces. It is probable that microelectrodes would give even sharper voltammetry peaks than observed in this study, as surface heterogeneity effects would be less important. Future work in this direction should enable the effects of surface heterogeneity, and substrate distortion of the monolayer, to be resolved. It is only then that interaction parameters can be treated quantitatively and analysed in terms of the

interactions within the layer.

In conclusion it should be said that more time spent on the improvement of surface preparation procedures, plus the utilisation of monocrystalline substrates, seems essential for the study of any reaction where structural interactions with the electrode are important.

APPENDIX.

1. INTRODUCTION.

The model used to simulate the optical behaviour of a thin metal layer on a metallic substrate consists of a three phase stratified system, ambient (solution) phase/ metal layer/ substrate metal. Each phase is assumed to be homogeneous and isotropic and to have unique optical properties independent of its contact with the other phase. The optical properties of each phase can be represented by the refractive index. If the ambient phase is non absorbing, its refractive index will be real (n_1). Both the metal film and substrate metal have complex refractive indices on account of their light absorption properties, $\hat{n}_2$ and $\hat{n}_3$ respectively.

$$\hat{n}_2 = n_2 - ik_2$$
$$\hat{n}_3 = n_3 - ik_3$$

where, n_2 and n_3 are the real components of the complex refractive index,

and, i is the square root of -1,

and, k_2 and k_3 are the imaginary components of the complex refractive index.

Alternatively, the optical constants can be expressed as the dielectric constant $\hat{\epsilon}_x$,

$$\hat{\epsilon}_x = \epsilon_x^{\bullet} - i\epsilon_x^{\bullet\bullet} = \hat{n}_x^2$$

where,
$$\epsilon_x^{\bullet} = n_x^2 - k_x^2$$

$$\epsilon_x^{\bullet\bullet} = 2n_x k_x$$

2. THE REFLECTANCE EQUATIONS.

The reflectivity of any multi phase system is given by the square of the modulus of the Fresnel coefficient describing that system,

$$R = |r|^2$$

This coefficient is defined as the ratio of the complex amplitudes of the electric field vectors of the reflected and incident beams in the incident phase, and its value is a function of the polarisation state of the incident beam and of the angle of incidence in the incident phase. A multi component system[54] is treated by determining the Fresnel coefficient at each interface and from these calculating the coefficient for the total system.

For the general case of non-normal incidence, it is useful to define, for the phase j, the angular dependent quantity ξ_j, as

$$\hat{\xi}_j = \hat{n}_j \cos\theta_j = (\hat{n}_j^2 - n_1^2 \sin^2\theta_1)$$

where θ_1 is the angle of incidence in the ambient phase with refractive index n_1, whilst $\hat{n}_j$ is the complex refractive index of phase j. In the event of phase j being absorbing θ_j is a complex angle. The Fresnel coefficients for the interface between the two faces, j and k, are then given by,

$$r_{s,jk} = \frac{\mu_k \hat{\xi}_j - \mu_j \hat{\xi}_k}{\mu_k \hat{\xi}_j + \mu_j \hat{\xi}_k}$$

$$r_{p,jk} = \frac{\hat{\varepsilon}_k \hat{\xi}_j - \hat{\varepsilon}_j \hat{\xi}_k}{\hat{\varepsilon}_k \hat{\xi}_j + \hat{\varepsilon}_j \hat{\xi}_k}$$

for light polarised perpendicular (s) and parallel (p) to the plane of incidence and where μ_j, μ_k, $\hat{\varepsilon}_j$ and $\hat{\varepsilon}_k$ are the magnetic permeabilities and dielectric constants of phases j and k respectively.

For a three component system (ambient(1), thin film(2) and

absorbing substrate(3)), the Fresnel coefficients become,

$$r_{s,123} = \frac{r_{s,12} + r_{s,23}\exp\,(-2i\beta)}{1 + r_{s,12}\cdot r_{s,23}\exp\,(-2i\beta)}$$

$$r_{p,123} = \frac{r_{p,12} + r_{p,23}\exp\,(-2i\beta)}{1 + r_{p,12}\cdot r_{p,23}\exp\,(-2i\beta)}$$

where β is the phase change of the light during one traverse of the thin phase(2) and is given by,

$$\beta = \frac{2\pi n_2 d\cos\theta_2}{\lambda}$$

where d is the thickness of the thin film(2).

Now,

$$\frac{\Delta R}{R} = \frac{R_{123} - R_{13}}{R_{13}} = \frac{R_{123}}{R_{13}} - 1 = \frac{|\,r_{123}\,|^2}{|\,r_{13}\,|^2} - 1$$

$$= \frac{r_{123} \times r^*_{123}}{r_{13} \times r^*_{13}} - 1$$

where the symbol * denotes complex conjugate. An example of a typical computer programme is included.

COMPUTER PROGRAMME FOR THE THREE LAYER MODEL.

```
      MASTER DEPOSIT
C CALCULATION  OF DELTAR/R FROM EQUATIONS OF MCK AND ASPNES
      COMPLEX N1,N2,A1,A2,A3,A4,S1,S2,S3,R12,R23,B1,B2,Z,R123,
     1R13,P12,P23,P123,P13
      REAL LAMBDA
50    FORMAT(31H LAMBDA       DELTAP       DELTAS)
      WRITE(2,50)
C
C  SET DATA
C
      PI=3.141592653898
      AN1=1.534
      AK1=0.0
      N1=CMPLX(AN1,AK1)
      B=10.0*10.0**(-10)
C
75    READ(1,100)LAMBDA,AN2,AK2,EC1,EC2,
100   FORMAT(5F0.0)
      IF(LAMBDA.LT.0.0)GO TO99
      N2=CMPLX(AN2,-AK2)
      ANGLE=45.0
      A=LAMBDA*10.0**(-9)
C
C   CALCULATE REFLECTANCE
C
      THETA=(ANGLE*PI)/180.0
      A1=N1**2
      A2=N2**2
      A3=CMPLX(EC1,-EC2)
      A4=A1*((SIN(THETA))**2)
      S1=N1*COS(THETA)
      S2=CSQRT(A2-A4)
      S3=CSQRT(A3-A4)
      R12=(A2*S1-A1*S2)/(A2*S1+A1*S2)
      R23=(A3*S2-A2*S3)/(A3*S2+A2*S3)
      B1=(4.0*PI*B*S2)/A
      Y=AIMAG(B1)
      X=REAL(B1)
      B2=CMPLX(Y,-X)
      Z=CEXP(B2)
      R123=(R12+R23*Z)/(1.0+R12*R23*Z)
      R=(CABS(R123))**2
      R13=(R12+R23)/(1.0+R12*R23)
      S=(CABS(R13))**2
      DELTAP=(R-S)/S
      P12=(S1-S2)/(S1+S2)
      P23=(S2-S3)/(S2+S3)


      P123=(P12+P23*Z)/(1.0+P12*P23*Z)
      P=(CABS(P123))**2
      P13=(P12+P23)/(1.0+P12*P23)
      Q=(CABS(P13))**2
      DELTAS=(P-Q)/Q
      WRITE(2,52)LAMBDA,DELTAP,DELTAS
52    FORMAT(1H0,F7.0,2E12.4)
      GO TO 75
99    STOP
      END
```

REFERENCES.

1. M. Faraday, Phil. Trans. Roy. Soc. London, 124 (1834) 77.

2. W. Kossel, Nachr. Ges. Wiss. Gottingen, (1927) 135.

3. I.N. Stranski, Z. Phys. Chem., 136 (1928) 259.

4. H. Brandes, Z. Phys. Chem. Leipzig, A142 (1929) 97.

5. T. Erdey-Gruz & M. Volmer, ibid., A157 (1931) 165.

6. A. Bewick, PhD. Thesis (University of Durham, 1961).

7. W.K. Burton, N. Cabrera & C.F. Frank, Nature, 163 (1949) 398; Phil. Trans. Roy. Soc. London Ser. A, 123 (1951) 299.

8. M.A. Steinberg, Nature, 170 (1952) 1119.

9. H.E. Buckley, Proc. Phys. Soc., B65 (1952) 678; Z. Elektrochem, 56 (1952) 275.

10. M. Fleischmann & H.R. Thirsk, Electrochim. Acta, 1 (1959) 146.

11. A. Bewick, M. Fleischmann & H.R. Thirsk, Trans. Faraday Soc., 58 (1962) 2200.

12. B. Conway & J.O'M. Bockris, Proc. Roy. Soc. London Ser. A, 248 (1958) 394; Electrochim. Acta, 3 (1961) 340.

13. W. Mehl & J.O'M. Bockris, Can. J. Chem., 37 (1959) 190; M. Despic & J.O'M. Bockris, J. Chem. Phys., 32 (1960) 389; H. Gerischer, Z. Elektrochem, 62 (1958) 256; W. Lorenz, Z. Phys. Chem., 17 (1958) 136.

14. M. Fleischmann & J.A. Harrison, Electrochim. Acta, 11 (1966) 749; J.A. Harrison, S.K. Rangarajan & H.R. Thirsk, J. Electrochem. Soc., 113 (1966) 1120.

15. E. Budevski, V. Bostanoff, T. Witanoff, Z. Stoinoff, A. Kotzewa & R. Kaischew, Electrochim. Acta,11 (1966) 1697; V. Bostanoff & E. Budevski, J. Electrochem. Soc.,119 (1972) 1346; E. Budevski, J. Crystal Growth, 13/14 (1972) 93.

16. A.R. Despic, Croat. Chem. Acta, 42 (1970) 265.

17. T. Vitanoff, A. Popoff & E. Budevski, J. Electrochem. Soc., 121 (1974) 207; V. Bostanoff, G. Staikoff and D.K. Roe, J. Electrochem. Soc.,

122 (1975) 1301.

18. H. Fischer, Elektrolytische Abscheidung und Elektrokristallisation von Metallen, Springer-Verlag Berlin (1954); Electrochim. Acta, 2 (1960) 50; D. Postl, G. Eichkorn & H. Fischer, Z. Phys. Chem., N.F. 77 (1972) 138; 77 (1972) 149.

19. R. Kaischev & I. Gutow, Electrochim. Acta, 9 (1964) 1047 and references therein.

20. D.A. Vermilyea in Adv. in Electrochem. & Electrochem. Eng., (Ed. P. Delahay) Volume 3, Interscience, New York (1963).

21. M.F. Bell & J.A. Harrison, J. Electroanal. Chem., 41 (1973) 15; ibid., 43 (1973) 305; J.A. Harrison, ibid. 36 (1972) 71; see also ref. 30.

22. J.A. Harrison & H.R. Thirsk in Electroanal. Chem.,(Ed. A.J. Bard) Volume 5, Marcel-Dekker, New York (1967).

23. K.J. Vetter, Elektrochemische Kinetik, Springer-Verlag Berlin (1961).

24. R.D Armstrong & M.Fleischmann,J. Polarog. Soc.,11 (1965) 31; M. Fleischmann, J.A. Harrison & H.R. Thirsk, Trans Faraday Soc., 61 (1965) 2742.

25. M.Fleischmann & H.R. Thirsk in Adv. in Electrochem. & Electrochem. Eng., (Ed. P. Delahay) Volume 3, Interscience, New York (1963).

26. R.D. Armstrong & J.A. Harrison, J. Electrochem. Soc., 116 (1969) 328.

27. F.C. Frank, Proc. Roy. Soc., A201 (1950) 586.

28. D.J. Astley, J.A. Harrison & H.R. Thirsk, J. Electroanal. Chem., 19 (1968) 325.

29. M. Fleischmann, J.A. Harrison & H.R. Thirsk, Trans. Faraday Soc., 61 (1965) 2742.

30. D.J. Astley, J.A. Harrison & H.R. Thirsk, Trans. Faraday Soc., 64 (1968) 192.

31. E. Schmidt & N. Wuthrich, J. Electroanal. Chem., 40 (1972) 399.

32. M.Z. Hassan, D.F. Untereker & S. Bruckenstein, J. Electroanal. Chem. 42 (1973) 161.

33. M. Fleischmann, S.K. Rangarajan & H.R. Thirsk, Trans. Faraday Soc., 63 (1967) 1251; S.K. Rangarajan, J. Electroanal. Chem., 16 (1968) 485.

34. M.Haissinsky, J. Chim. Phys., 30 (1933) 27.

35. L.B. Rogers & A.F. Stehney, J. and Trans. Electrochem. Soc., 95 (1949)25.

36. J.T. Byrne & L.B. Rogers, J. and Trans. Electrochem. Soc., 98 (1951) 457.

37. M. Haissinsky, Experientia, 8 (1952) 125.

38. M. Haissinsky, J. Chim. Phys., 43 (1946) 21.

39. J.T. Byrne, L.B. Rogers & J.C. Griess, J. Electrochem. Soc., 98 (1951)452.

40. L.B. Rogers & A.F. Stehney, J. Electrochem. Soc.,95 (1949) 25.

41. K.F. Herzfeld, Physik Z., 13 (1913) 29.

42. T. Mills & G.M. Willis, J.Electrochem. Soc.,100 (1953) 452.

43. E. Schmidt & H.R. Gygax, Helv. Chim. Acta, 48 (1965) 1178.

44. E. Schmidt & H.R. Gygax, J. Electroanal. Chem., 12 (1966) 300.

45. For a complete review of Schmidt's papers see ref. 63.

46. E. Schmidt & H. Siegenthaler, Helv. Chim. Acta, 52 (1969) 2245.

47. E. Schmidt & N. Wuthrich, J. Electroanal. Chem., 34 (1972) 377.

48. E. Schmidt & S. Stucki, Ber. Bun. Phys. Chem. 77 (1973) 915.

49. E. Schmidt & N. Wuthrich, J. Electroanal. Chem.,28 (1970) 349.

50. G.W. Tindall & S. Bruckenstein, Anal. Chem., 40 (1968) 1051; S.H. Cadle & S. Bruckenstein, ibid.,43 (1971) 1858; G.W. Tindall & S. Bruckenstein, Electrochim. Acta, 16 (1971) 245; V.A. Vicente & S. Bruckenstein, Anal. Chem. 44 (1973) 2036; S.H. Cadle & S. Bruckenstein, J. Electrochem. Soc., 119 (1972) 1166; V.A. Vicente & S. Bruckenstein, Anal. Chem., 45 (1973) 2036.

51. J.W. Schultze, Ber. Bun. Phys. Chem., 74 (1970) 705.

52. H.D. Hermann, N. Wuthrich, W.J. Lorenz & E. Schmidt, J. Electroanal. Chem., 68 (1976) 273, 289.

53. B.J. Bowles, Electrochim. Acta, 10 (1965) 717, 731.

54. J.D.E. McIntyre in Adv. in Electrochem. and Electrochem. Eng., (Ed R.H. Muller) Volume 9, Interscience, New York (1973).

55. R.H. Muller, ibid.

56. J. Horkans, B.D. Cahan & E. Yeager, J. Electrochem. Soc., 122 (1975) 1585.

57. H. Gerischer, D.M. Kolb & M. Przasnyski, Surface Science, 43 (1974) 662; D.M. Kolb, M. Przasnyski & H. Gerischer, J. Electroanal. Chem., 54 (1974) 25.

58. A.K. Vijh, Surface Science, 46 (1974) 282; ibid.,47 (1975) 713.

59. J.W. Schultze & K.J. Vetter, J. Electroanal. Chem., 44 (1973) 63.

60. E. Schmidt, B. Beutler & W.J. Lorenz, Ber. Bun. Phys. Chem., 75 (1971) 71.

61. E. Schmidt & N. Wuthrich, J. Electrochem. Soc., 121 (1974) 1611.

62. Treatise on Solid State Chemistry, Volume 5 'Changes of State' (Ed. N.B. Hannay), Plenum Press, New York (1975).

63. W.J. Lorenz, H.D. Hermann, N. Wuthrich & F. Hilbert, J. Electrochem. Soc., 121 (1974) 1167.

64. J.W. Schultze & D. Dickertmann, Surface Science, 54 (1976) 489.

65. B.J. Bowles & T.E. Cranshaw, Phys. Lett., 17 (1965) 258; B.J. Bowles, Nature, 212 (1966) 1456.

66. R. Adzic, E. Yeager & B.D. Cahan, J. Electrochem. Soc., 121 (1974) 474.

67. D.M.Kolb, Faraday Disc. Chem. Soc., 56 (1973) 138.

68. E. Schmidt & N. Wuthrich, J. Electroanal. Chem., 40 (1972) 399.

69. E. Schmidt, J. Electroanal. Chem., 47 (1973) 441.

70. M.W. Breiter, J. Electrochem. Soc., 114 (1967) 1125.

71. F. Hilbert, C. Mayer & W.J. Lorenz, J. Electroanal. Chem., 47 (1973) 167.

72. T. Takamura, K. Takamura, W. Nippe & E. Yeager, J. Electrochem. Soc., 117 (1970) 626.

73. J.D.E. McIntyre & D.M Kolb, Symp. Faraday Soc.,4 (1970) 99.

74. T. Takamura, Y. Sato & K. Takamura, J. Electroanal. Chem.,41 (1973) 31.

75. T. Takamura & Y. Sato , J. Electroanal. Chem., 47 (1973) 245.

76. D.M. Kolb, D. Leutloff & M. Przasnyski, Surface Science, 47 (1975) 622.

77. T. Takamura, F. Watanabe & K. Takamura, Electrochim. Acta, 19 (1974) 933.

78. D.M. Kolb, Ber. Bun. Phys. Chem., 77 (1973) 891; D.M. Kolb & H. Gerischer, Electrochim. Acta, 18 (1973) 987.

79. H. Gerischer,in Physical Chemistry, (Eds. H. Eyring, D. Henderson & W. Jost) Volume 9A, Academic Press, New York (1970).

80. R. Adzic & A.R. Despic, J. Chem. Phys., 61 (1974) 3482.

81. F. Watanabe & K. Motoo, J. Electroanal. Chem., 60 (1975) 259.

82. R. Adzic, D.N. Simic, A.R. Despic & D.M. Drazic, J. Electroanal. Chem., 70 (1976) 587

83. V. Klapka, Coll. Czech. Chem. Comm., 36 (1970) 1181.

84. W.J. Lorenz, Chem Ing. Techn., 45 (1973) 175.

85. K.J. Soderberg, Trans. Electrochem. Soc., 88 (1945) 297; R. Pinner, Electroplating, (1953) 401.

86. J.A. Harrison, R.P.J. Hill & J. Thompson, J. Electroanal. Chem., 44 (1973) 445.

87. See appendix.

88. L. Samuels & J. Sanders, J. Inst. Metals, 87 (1958/59) 129.

89. D. Beaglehole & O. Hunderi, Phys. Rev. B, 2 (1970) 309.

90. T. Kurasawa, Chem. Abs., 55 (1961) 14.279(a).

91. J.K. Sass, R.K. Sen, E. Meyer & H. Gerischer, Surface Science, 44 (1974) 515.

92. R.L. Gerlach & T.N. Rhodin, Surface Science, 17 (1969) 32; J. Henrion & G.E. Rhead, ibid., 29 (1972) 20; J. Perderau & J. Szymerska, Surface Science, 32 (1972) 247.

93. J. Oudar & M. Huber, J. Crystal Growth, 31 (1975) 345.

94. W.J. Lorenz, Niederschrift der 15 Sitzung des Dechema-Arbeitsaussschusses 'Auflosung und Abscheidung von Metallen' March 1976, Frankfurt/M.

95. D.M. Kolb, Personal communication.

96. R.H. Wopschall & I. Shain, Anal. Chem., 39 (1967) 1514, 1527 & 1535.

97. A. Bewick, B.E. Conway & A.M. Tuxford, J. Electroanal. Chem. 42 (1973) App. 2; R. Garigos, R. Kofman, A. Jolivet & J. Richards, Il Nuovo Cimento, 813 (1972) 242.

98. P. Delahay & I. Trachtenberg, J. Am. Chem. Soc.,79 (1957) 2355.

99. A.U. MacRae, K. Muller, J.J. Lander & J. Morrison, Surface Science, 15 (1969) 483.

100. A. Hamelin, J. Lecoeur & G. Valette, Extended Abstacts of the 25th. Meeting of I.S.E. Brighton, England (1974), page 277.

101. P. Ruetschi & P. Delahay, J. Chem. Phys., 23 (1955) 697.

102. Films on Solid Surfaces, J.G. Dash, Academic Press, New York (1975).

103. The Chemistry of Thallium, A.G. Lee, Elsevier, Amsterdam (1971).

104. A.G. Mathewson & H.P. Myers, Physica Scripta, 4 (1971) 291.

105. J.D.E. McIntyre & D.M. Kolb, Symp. Faraday Soc., 4 (1970) 128.

106. Handbook of Chemistry and Physics,(Ed.R. Weast), 55th. Edition, Chemical Rubber Co., Cleveland (1974/75).

107. G. Sillen, Stability Constants of Metal Ion Complexes, Chem. Soc, Special Publication No. 25, (1971).

108. R.D. Armstrong & E. Barr, J. Electroanal. Chem., 20 (1969) 173.

109. K.Z. Brainina, N.F. Zakharchuk, D.P.Synkova & I.G. Yudelevich, J. Electroanal. Chem., 35 (1972) 165.

110. E. Bottari & M.Vicedomini, J. Inorg. Nucl. Che., 35 (1973) 1269, 2447; ibid., 34 (1972) 1897.

111. J.A. Harrison, J. Electroanal. Chem., 36 (1972) 71.

112. W. Davison, J.A. Harrison & J. Thompson, Faraday Disc. Chem. Soc., 56 (1973) 171.

113. N.A. Pangarov, J. Electroanal. Chem., 9 (1965) 70.

114. N.A. Pangarov & V. Velinov, Electrochim. Acta, 11 (1966) 1753.

115. C.M. Elliot & R.W. Murray, Anal. Chem., 48 (1976) 259.